40 Gb/s optical transmission systems

Buxens Azcoaga, Alvaro Juan

Publication date:
2003

Document Version
Publisher's PDF, also known as Version of record

40 Gb/s optical transmission systems

Alvaro Buxens Azcoaga

Ph.D. Thesis
Industrial Ph.D. Project EF837
October 28, 2003

Supervisors:

Palle Jeppesen, Prof. Dr. Tech.
Research Center COM
Technical University of Denmark

Dennis Olesen, Manager Engineering, Hardware
Lars Ellegård, Ph.D., Senior Staff Engineer
Tellabs Denmark

Steen Krogh Nielsen, Ph.D., Section Manager
TDC Networks

The work presented in this thesis was carried out in collaboration between Tellabs Denmark, Research Center COM at the Technical University of Denmark and with TDC TeleDenmark as a third partner in partial fulfilment of the requirements for the Ph.D. degree from the Technical University of Denmark and the Industrial Ph.D. program of the Academy for Technical Sciences, ATV, Denmark.

Abstract

This thesis investigates state of the art components and subsystems to be used in the next generation of high speed optical transmission systems at 40 Gb/s. The thesis will provide guidelines for the design and implementation of 40 Gb/s systems, investigating topics that could limit transmission; chromatic dispersion, Polarization Mode Dispersion (PMD), Self Phase Modulation (SPM) and linear or non-linear crosstalk among others.

Regarding chromatic dispersion, sufficient evidence is presented for the need in 40 Gb/s systems of either modulation formats that allow for higher tolerance than the traditional Non Return to Zero (NRZ) or use of Tunable chromatic Dispersion Compensators (TDC). Two single channel TDCs are experimentally evaluated. The first one, based on temperature changes in a chirped fiber Bragg grating, allows to reduce significantly chromatic dispersion induced penalty in a series of different standard Single Mode Fiber (SMF) spans ranging from 21.5 km to 41 km. The second one, based on the controlled stretching of a non-linearly chirped fiber Bragg grating, allows for unrepeatered transmission in standard-SMF spans ranging from 45 km to 103 km minimizing chromatic dispersion induced penalty. An optical duobinary transmitter (Tx) is implemented and its increased tolerance to chromatic dispersion is verified in a direct comparison to an NRZ transmitter.

The limitations induced by PMD in 40 Gb/s system design are investigated. It is found that even for a standardized Short haul application (maximum distance of 40 km) the maximum PMD coefficient allowed in the transmission fiber, 0.4 $ps/\sqrt{km}$, is below the values defined by actual standards, 0.5 $ps/\sqrt{km}$. The most promising PMD compensation methods are presented and their advantages and disadvantages are discussed. A PMD compensator based on a single fixed birefringent element is evaluated at 10 Gb/s and 40 Gb/s. It provides an improvement of at least a factor of two in the total PMD allowed in a link. However even when using the PMD compensator it is estimated that the maximum PMD coefficient in the fibers used in a five span link with 80 km per span is 0.25 $ps/\sqrt{km}$, still below the maximum value allowed by standards.

Return to Zero (RZ) and Carrier Suppressed RZ (CSRZ) modulation formats are found to provide a significant advantage in multi-span transmission compared to the traditional NRZ or the optical duobinary modulation formats. Using a 9 ps pulsed RZ Tx, transmission is achieved over a 400 km link consisting of 5 spans of 80 km standard-SMF with a Quality (Q) factor of 17.7 dB, while for NRZ it is reduced to 15 dB. In another experimental verification over 40 km spans of standard-SMF, we could achieve transmission over 6 spans for the aforementioned RZ Tx with a Q of 18 dB, while for NRZ, transmission over 4 spans provided a Q of 17.5 dB.

A simple analytical approach separating the limitations induced by Optical Signal to Noise Ratio (OSNR) and SPM in multi-span transmission is presented and verified in the comparison of NRZ and RZ for transmission over standard-SMF with 40 km span length.

The performance of NRZ, RZ, optical duobinary and CSRZ modulation formats in a 100 GHz channel spaced 40 Gb/s WDM system regarding linear crosstalk is investigated by means of simulations. It is found that RZ is seriously limited in 100 GHz channel spaced systems while NRZ and CSRZ provide enough tolerances to allow for practical system implementation. The optical duobinary format provides the best performance indicating the possibility of even narrower channel spaced systems using this modulation format.

Three Wavelength Division Multiplexing (WDM) experimental demonstrations are presented. The first one is a 100 GHz spaced 16 channel WDM system, using 40 Gb/s NRZ modulation over a 200 km link of standard-SMF. The second one is a 100 GHz spaced 32 channel 40 Gb/s WDM system, using CSRZ modulation over a 400 km link of standard-SMF and using Raman amplification. The third one is a 100 GHz spaced 6 channel WDM system, using NRZ as the modulation format, Semiconductor Optical Amplifiers (SOA) as the in-line amplifiers and in transmission over a 160 km link with span distances of 40 km standard-SMF, traditional target distance of metro WDM systems.

Possible practical implementation of 40 Gb/s single channel and WDM systems are proposed and described following the methodology used by international standardization bodies.

Resumé

Denne afhandling undersøger state-of-the-art komponenter og delsystemer som vil blive brugt i næste generations højhastigheds optiske transmissionssystemer ved 40 Gb/s. Afhandlingen vil give retningslinier for design og implementering af 40 Gb/s systemer samt undersøge emner som kan begrænse transmission, herunder kromatisk dispersion, Polarisation Mode Dispersion (PMD), Self Phase Modulation (SPM) samt lineær og ikke-lineær krydstale.

Vedrørende kromatisk dispersion, bliver der for 40 Gb/s systemer præsenteret tilstrækkelige beviser for nødvendigheden af enten modulations formater som tillader højere tolerancer på den kromatiske dispersion end traditionel Non Return to Zero (NRZ) eller brug af variable kromatiske dispersions kompensatorer (TDC). To enkelt kanals TDC'er bliver evalueret eksperimentelt. Den første, som er baseret på temperatur ændringer i en chirped fiber Bragg grating, medfører en betydelig reduktion i den penalty som skyldes kromatisk dispersion - dette er blevet evalueret for længder af Single Mode Fibre (SMF) fra 21.5 km til 41 km. Den anden er baseret på et kontrolleret stræk af en ikke-lineær chirped fiber Bragg grating, og denne muliggør ikke-repeteret transmission over standard SMF, på strækninger fra 45 km til 103 km med en minimeret penalty stammende fra den kromatiske dispersion. En optiske "duobinary" sender (Tx) er blevet implementeret og dens forøgede tolerance til kromatisk dispersion er blevet verificeret ved direkte sammenligning med en NRZ sender.

Begrænsningerne introduceret af PMD i 40 Gb/s system er blevet undersøgt. Det bliver konkluderet at selv for et standardiseret kort transmissions systeme (maksimal afstand er 40 km) er den tilladte PMD koefficient, 0.4 ps/$\sqrt{km}$ mindre end den tilladte standardiserede værdi på 0.5 ps/$\sqrt{km}$. De mest lovende PMD kompenserende teknikker bliver præsenteret og deres fordele og ulemper bliver diskuteret. En PMD kompensator baseret på et dobbeltbrydende element er blevet evalueret ved 10 Gb/s og ved 40 Gb/s. Den forbedrer den totale tilladelige PMD i et transmissionsspand med mindst en faktor 2. Til trods for brugen af denne PMD kompensator, bliver det vurderet at den maksimalt tilladelige PMD koefficient i et fiber transmissionsspan som består

af 5 strækninger, hver på 80 km, maksimalt må være 0.25 ps/$\sqrt{km}$, hvilket stadigvæk er mindre end den maksimalt tilladelige ifølge standarderne.

Modulationsformaterne "Return to Zero" (RZ) og "Carrier Suppressed RZ" (CSRZ) vises at have væsentlige fordele i forhold til det traditionelle "Non Return to Zero" (NRZ) format og det optiske "duobinary" format med hensyn til transmission over mange fiberstrækninger. Med en RZ sender, som frembringer 9 ps pulser, er der opnået transmission over 400 km bestående af 5 strækninger *á* 80 km standard SMF med en kvalitetsfaktor Q på 17.7 dB . En anden eksperimentel bekræftelse af fordelene ved RZ formatet er en demonstration af transmission over 6 strækninger *á* 40 km standard SMF med en Q værdi på 18 dB, mens en transmission af et NRZ signal over 4 strækninger *á* 40 km gav en Q værdi på 17.5 dB.

I afhandlingen præsenteres også en simpel analytisk model, hvor begrænsningerne sat af det optiske signal-støj forhold (OSNR) og af selv-fase modulation (SPM) behandles separat. Resultaterne herfra er i god overensstemmelse med transmissionseksperimenterne med RZ og NRZ signalerne over strækningerne *á* 40 km standard SMF.

Ved hjælp af simuleringer undersøges det, hvor gode transmissionsegenskaber af de enkelte formater (NRZ, RZ, CSRZ og optisk duobinary) er med hensyn til lineær krydstale i et 40 Gb/s "wavelength division multiplex" (WDM) system med 100 GHz kanalafstand. Det vises, at RZ formatet giver alvorlige begrænsninger i et sådant system med 100 GHz adskillelse mellem kanalerne, mens NRZ og CSRZ formaterne er tolerante nok til praktisk anvendelse. Det optiske duobinary format viser sig at have den bedste ydeevne, hvilket åbner for mulighed for endnu tættere beliggende kanaler.

Der præsenteres tre eksperimentelle WDM demonstrationer. Den første drejer sig om 16 bølgelængdekanaler adskilt med 100 GHz, hvor hver kanal bærer et 40 Gb/s data signal, og det samlede 16 gange 40 Gb/s signal transmitteres over 200 km standard SMF. Den anden demonstration handler om 32 100 GHz adskilte bølgelængdekanaler *á* 40 Gb/s med CSRZ modulationsformat og transmitteret over 400 km standard SMF, hvor der indgår distribueret Raman forstærkning i transmissionsfibrene. I den tredje demonstration bruges 6 40 Gb/s NRZ bølgelængdekanaler med 100 GHz adskillelse og med "semiconductor optical amplifiers" (SOAs) som forstærkere langs transmissionsfibrene. I dette tilfælde transmitteres der over 160 km bestående af 4 gange 40 km standard SMF strækninger, der betragtes som typiske fiberlængder i metro WDM systemer.

Mulige 40 Gb/s enkelt-kanal eller WDM systemer foreslås og beskrives i overensstemmelse med de metoder, der anvendes af de internationale standardiseringsorganisationer.

Acknowledgements

I would like to thank my supervisors Palle Jeppesen, Lars Ellegård, Dennis Olesen and Steen Krogh Nielsen for their support and good advice throughout the project.

Special thanks to Thomas Tanggaard, Brian Hermann, Rune J. Pedersen, Martin Nordal Petersen, Jesper Glar Nielsen, Leif Katsuo Oxenløwe, Anders T. Clausen, and Quang Nghi Trong Le for commenting different parts of the thesis throughout these last two specially hectic months. Jorge Seoane deserves special thanks for his time and patience dedicated to carefully reading the whole thesis and provide me with, it *seems*, wise comments even at very late hours at night.

I would like to thank former and present colleges at Tellabs Denmark for their support and help in one way or another to the project within the three last years of work there: Max Skytte Christensen, Richard Bowen, Jens Adler Nielsen, Bo Foged Jørgensen, Tobias Garde, Niels Anker Jensen, Gert Schiellerup, Bo Kristiensen, Morten Høgdal, Morten Jørgensen, Anbeth Cohn, Christian Hansen, Susanne von Daehne, Kjeld Dalgård, Lars Lindquist among others.

I would also like to thank former and present colleges at Tellabs US; Eric St. George, Estaban Draganovic, John Carrick, Glen Koste and Gheorge Sandulanche for an always friendly treatment on my visits to the Hawthorn facilities.

I appreciate sincerely the opportunity provided by AT&T Labs-Research to work in their facilities within the period of January to June of 2001. I would like to acknowledge Nick Frigo, Misha Brodsky, Martin Birk for their collaboration, good advice and intense work in the lab. I enjoyed the open atmosphere, relaxing lunch breaks and good tennis in company of Misha Borodisky, Alexandra Smiljanic, Cedric Lam, Moe Win and Bhavesh Desai.

Special thanks to Marcus and Illiana Dülk for taking very good care of Janne and me during our time in New Jersey and sharing unforgettable moments, the Long Branch court house morning just to mention one...

Christophe Peucheret, Thomas Tanggaard, Martin Nordal Petersen, Beata Zsigri, Torger Tokle, Leif Katsuo Oxenløwe, Anders T. Clausen, Jorge Seoane,

Roberto Nieves, Joan Genè and Quang Nghi Trong Le are specially acknowledged for their help in the research carried out within this project and for allowing me to keep a good contact to the Research Center COM and what goes on over there.

Thanks in general to friends and family who have put up with long working hours and have provided me with a nursing atmosphere in which I could dedicate the time needed to carry out the work presented in this thesis.

Janne thanks for your support, help, patience and smile. And little Luca, it is now time for us to play long hours...

Abbreviations

ADM/XC	Add Drop Multiplexer Cross Connect
APD	Avalanche Photodiode
ATM	Asynchronous Transfer Mode
BER	Bit Error Rate
BF	Broadening Factor
CAPEX	CApital EXpenditure
CDR	Clock and Data Recovery
CDWDM	Coarse Wavelength Division Multiplexing
CFBG	Chirped Fiber Bragg Grating
CNRZ	Chirped Non Return to Zero
CRZ	Chirped Return to Zero
CNRZ	Chirped Non Return to Zero
CSRZ	Carrier Suppressed Return to Zero
DC	Dispersion Compensation
CW	Continuous Wave
DCy	Duty Cycle
DCF	Dispersion Compensating Fiber
DC-FOM	Dispersion Compensation Figure Of Merit
DFE	Decision Feedback Equalizer
DGD	Differential Group Delay
DOP	Degree Of Polarization
DSF	Dispersion Shifted Fiber
EA	Electro Absorption
EDFA	Erbium Doped Fiber Amplifier
ETDM	Electrical Time Division Multiplexing
ER	Extinction Ratio
FBG	Fiber Bragg Grating
FEC	Forward Error Correction
FEE	Feedback Forward Equalizer
FWHM	Full Width Half Maximum
FWM	Four Wave Mixing

Gb/s	Gigabit per second
GNU	Gain Non-Uniformity
HiBi	High Birefringence
HOM	Higher Order Mode
HOP	High Order Path
IIC	Initial Installation Cost
IL	Insertion Loss
I	Intra office
IP	Internet Protocol
ISI	Inter-Symbol Interference
ITU	International Telecommunications Union
L	Long haul
LOP	Low Order Path
MA-OFA	Mid Access Optical Fiber Amplifier
MPI-S	Multiple Path Interface Sender
MPI-R	Multiple Path Interface Receiver
MSA	Multi Source Agreement
NRZ	Non Return to Zero
NZDSF	Non Zero Dispersion Shifted Fiber
OA	Optical Amplifier
OFA	Optical Fiber Amplifier
OIF	Optical Internetworking Forum
OPEX	OPerational EXpenses
OSA	Optical Spectrum Analyzer
OSC	Optical Supervisory Channel
OSNR	Optical Signal to Noise Ratio
OTN	Optical Transport Network
OTDM	Optical Time Division Multiplexing
OTDD	Optical Time Division Demultiplexing
PC	Polarization Controller
PCB	Printed Circuit Board
PDF	Probability Density Function
PIN	p-i-n photodiode
PM	Polarization Maintaining
PMD	Polarization mode dispersion
PRBS	Pseudo Random Binary Sequence
PSB	Phase Shaped Binary
PSBT	Phase Shaped Binary Transmission
PSP	Principal State of Polarization
RDS	Residual Dispersion Slope
RMS	Root Mean Square

RS	Reduced Slope
RSa	Reed Salomon
RZ	Return to Zero
SDH	Synchronous Digital Hierarchy
S	Short haul
SONET	Synchronous Optical NETwork
SMF	Single Mode Fiber
SMSR	Side Mode Suppression Ratio
SOA	Semiconductor Optical Amplifier
SPM	Self Phase Modulation
SSB	Single Side Band
STM	Synchronous Transport Module
TDC	Tunable Dispersion Compensator
TDM	Time Domain Multiplexing
TM	Transmission Media
TWRS	True Wave Reduced Slope
Tx	Transmitter
VC	Virtual Container
VCO	Voltage Controlled Oscillator
VOA	Variable Optical Attenuator
CVSEL	Vertical Cavity Surface Emitting Laser
V	Very long haul
VIPA	Virtually Imaged Phased Array
VSR	Very Short Reach
WDM	Wavelength Division Multiplex
XGM	Cross Gain Modulation
X-OR	Exclusive OR function
XPM	Cross Phase Modulation

Contents

List of Figures

List of Tables

Chapter 1

Introduction

Two ground-breaking developments in 1970 paved the way for commercial optical communication systems. Dr. Keck, Dr. Maurer and Dr. Schultz from Corning demonstrated the possibility of transmission in low loss optical fibers with an attenuation of 17 dB/km[1]. Dr. Hayashi, Dr. Panish, Dr. Foy and Dr. Sumski from Bell Telephone Laboratories demonstrated the continuous operation of GaAs semiconductor lasers at room temperature [2]. It took 18 years of research and development of these and other related technologies until the first transatlantic cable using optical transmission, the TAT-8, was installed between USA and Europe. The famous writer Isaac Asimov had the honor of dedicating the new cable and placing the first call in December 1988. Asimov said [3]: "Welcome everyone to this historic trans-Atlantic crossing, this maiden voyage across the sea on a beam of light..." He noted, "...our world has grown small, and this cable, which can carry 40,000 calls at one time is a sign of the voracious demand for communications today....."

Ten years later in 1998 the combination of a growth in the "voracious demand for communication" and technological advances such as Wavelength Division Multiplexing (WDM) [4] or the Optical Fiber Amplifier (OFA) [5, 6] pushed and allowed respectively for the installation of for example the trans-Atlantic cable AC-1. The efficiency of the technological advances are clear if we consider that the final installation cost for the AC-1 was less than three times that of the TAT-8 while it allowed for close to half a million simultaneous telephone calls between the continents.

Today optical transmission systems are widely deployed covering from submarine inter-continental transmission to metropolitan networks or even Local Area Networks (LANs). Most of telecommunications traffic is nowadays being transported one way or another through optical fibers. This thesis will focus on the high capacity optical transmission systems. These systems have tradi-

tionally been used in the long distance layer of the network but are moving closer and closer to the final users as high capacity data services are becoming broadly used.

Commercial high capacity transmission systems installed in telecommunication operator's networks are based today on 2.5 Gb/s and 10 Gb/s Electronic Time Domain Multiplexing (ETDM) technology per single wavelength. To our knowledge and even though field trials using 40 Gb/s based transmission equipment have been carried out both for single channel [7] and WDM systems [8, 9], there are not yet links in any telecommunication operator's network using this equipment for true life traffic from the network subscribers.

1.1 Motivation for the project

Historically each quadrupling of TDM rate (from 2.5 Gb/s to 10 Gb/s for example) can be achieved increasing the cost of the modules by a 2.5 factor and allowing for significant cost efficiency. If we want to achieve a total transmission capacity of 320 Gb/s between two points by using a WDM system, we can either install a 128 channel system at 2.5 Gb/s or a 32 channel system at 10 Gb/s. The following advantages are observed for the latter:

- Reduction in floor space and power consumption
- Reduction in management complexity
- Reduction in product codes and inventory

Furthermore, increasing the TDM rate per channel will allow for a higher total capacity and postpone the need to initialize transmission over a new fiber in the link.

The relation between telecommunication network operators (or service providers), equipment providers and the final users can be modelled by the spiral relation depicted in Figure 1.1. The end user is always eager to use new services especially if they provide an improvement in their life style or a reduction in their expenses. Service providers or network operators are always seeking for these new services that will attract the end user while the equipment provider working in a competitive environment will try to offer improved equipment at competitive prices.

The rate at which this spiral *turned* increased dramatically within the second half of the 90s mainly pushed by an opening of the market to competition, the popular use of mobile communications and the widespread of Internet to the public. For example the number of cellular phones in western Europe grew

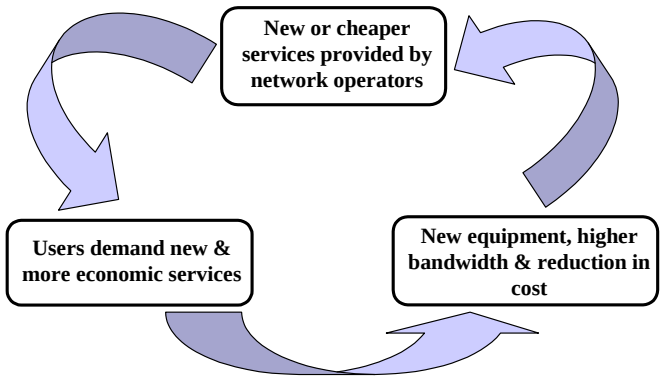

Figure 1.1: Spiral model in the telecommunications industry describing the interaction between network operators, equipment providers and final users.

from 46.9 million in 1997 to 156.9 million by the year 1999 [10]. The number of Internet hosts increased from 3.8 million in 1994 to 29.6 million by 1998 and estimates of traffic in the main U.S Internet backbones increased from 16.3 Terra-bytes (TB) per month in 1994 to over 10,000 TB per month by 1999 [11].

Following these growths in traffic, statistics predicted that a capacity exhaust could be reached in the backbone networks within a short time and that even high channel count 10 Gb/s WDM systems would be at the limit of providing the required capacity. The clear commercial option to be considered at that point in time by equipment providers was the increase in TDM rate to 40 Gb/s for their high capacity transmission products. This Ph.D. project has its origin in this context. It began in February of 2000, and at that time there was a clear feeling that by the end of 2002 a 40 Gb/s product would be needed in the market.

Unfortunately, time has proven that the traffic growth has not followed the aforementioned predictions. Instead over the last three years we have witnessed the greatest financial crash in the history of the telecommunications industry. By 2002 in Europe, only an average of 10 % of all the fiber installed to accommodate for the expected traffic was actually used for transmission, and in those fibers used, the installed systems were running only at an average 20 % of their maximum capacity [12]. Under these circumstances the demand for 40 Gb/s optical transmission systems has been delayed until there is higher demand for capacity or they can provide substantial economical advantage over 10 Gb/s systems.

1.2 Thesis overview

Challenges and limitations seem to pile-up when we consider 40 Gb/s optical transmission systems. Due to the reduced time slot, 25 ps, effects such as chromatic dispersion in the fiber or Polarization Mode Dispersion (PMD) can seriously limit transmission distances. The spectral width of a modulated signal at 40 Gb/s starts to be comparable to the desired WDM channel spacing of at least 100 GHz. Power margins are reduced compared to 10 Gb/s systems, affected both by tolerances regarding non-linear effects and optical signal to noise ratio limitations. New modulation formats such as return to zero, optical duobinary or carrier suppressed return to zero have been proposed to avoid one or another negative effect. Furthermore, the development of commercial electronic components that can work at this bit rate is extremely challenging. These effects and concepts are closely related to each other, and we can consider the investigation carried out within this project as a puzzle, see Figure 1.2, where chromatic dispersion, PMD, spectral efficiency, modulation formats and power margins are among the pieces in it.

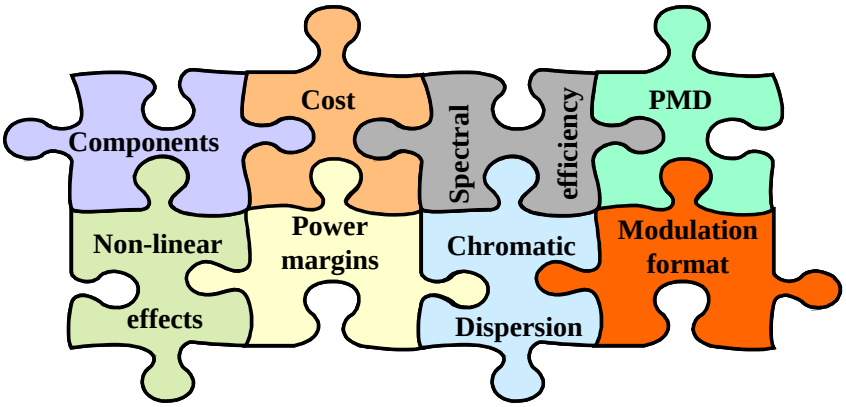

Figure 1.2: Schematic of effects and concepts that need to be handled in 40 Gb/s system design.

Since this Ph.D. project is an industrial Ph.D. project, there has been a strong emphasis on considering components, methods and systems which have strong possibilities of being used in future commercial products.

Structure of the thesis

The thesis continues in Chapter 2 with an introduction to those systems installed in a telecommunications network where there is a possible application of 40 Gb/s technology. Examples of standardized single channel and commercial 10 Gb/s WDM systems are presented in terms of their building blocks, and the main parameters to be considered in the evolution towards 40 Gb/s systems.

Chapter 3 is dedicated to the analysis of the impact of chromatic dispersion in 40 Gb/s transmission and to the evaluation of several available methods for fixed and tunable chromatic dispersion compensation. The concept of chromatic dispersion in transmission fibers is described and the limitations it induces in 40 Gb/s transmission systems are analyzed. Initially the analysis is based on the effect of chromatic dispersion on systems using Non Return to Zero (NRZ) as the modulation format, traditionally used in commercial systems. An important point in the organization of this thesis is that alternative modulation formats to NRZ; Return to Zero (RZ), optical duobinary, chirped NRZ or Carrier Suppressed RZ (CSRZ), which can provide certain advantages in 40 Gb/s transmission, will be introduced in the chapter were the topic in which they are advantageous is mentioned. Wherever the new modulation format is introduced we will review its performance with respect to other topics included previously in the thesis. Regarding chromatic dispersion we will introduce chirped NRZ and optical duobinary (also named Phase Shaped Binary Transmission or PSBT) as modulation formats with higher tolerances to chromatic dispersion effects than NRZ. Their practical implementation will be described and their performance under chromatic dispersion analyzed. Fixed chromatic dispersion compensation methods will be reviewed and their limitations in single channel and 40 Gb/s WDM transmission systems will be evaluated. The principle of operation of two methods for tunable chromatic dispersion compensation in a single channel system and one method for WDM will be presented. Furthermore, these methods will be experimentally investigated and their performance analyzed.

Chapter 4 starts out with a description of the origins of PMD in optical fiber and analyzing its effect on 40 Gb/s transmission systems. The most promising methods for PMD compensation are presented and described. One of these methods, the use of a single fixed birefringence element, has been further investigated and a prototype implemented in the Tellabs laboratories. The PMD compensator is experimentally characterized and its performance evaluated. An analysis of the tolerances the compensator allows in the system design is given. RZ is considered as a modulation format with possible increased tolerance to PMD. A description of possible implementations of an RZ transmitter is given

and its performance is evaluated in the presence of PMD and chromatic dispersion. The experimental characterization of the PMD compensator prototype has been carried out in collaboration with Thomas Tanggaard Larsen. [1]

The optical power related limitations in the design of single channel 40 Gb/s transmission systems are introduced, analyzed and investigated in Chapter 5. We will analyze the limitations in a multi-span system by means of simulations and experimental investigations. We investigate multi-span transmission by means of simulations for NRZ, RZ and optical duobinary modulation in 40 km and 80 km span set-ups for standard Single Mode Fiber (SMF) and Non Zero Dispersion Shifted Fiber (NZDSF). We investigate experimentally multi-span transmission for NRZ and RZ modulation formats in 40 km and 80 km span set-ups over standard-SMF. These experimental investigations were carried out at AT&T Labs-Research in collaboration with Misha Brodsky and Martin Birk. Finally, simple design rules based on analytical approximations of the simulated results are proposed.

Chapter 6 is dedicated entirely to the design of 40 Gb/s WDM systems and the experimental implementation and characterization of several practical examples. We will analyze the limitations induced by linear crosstalk in a 100 GHz channel spaced WDM system for NRZ, RZ and optical duobinary modulation. We introduce CSRZ as a new modulation format, describe its implementation and analyze its performance regarding linear crosstalk in a 100 GHz channel spaced WDM system. Furthermore, we review the performance of CSRZ under chromatic dispersion and in a multi-span single channel system to allow for comparison with NRZ, RZ or optical duobinary modulation formats. We will also introduce and analyze the effect of two non-linear effects characteristic in WDM systems; Cross Phase Modulation (XPM) and Four Wave Mixing (FWM). Experimental work includes a 32 channel WDM system allowing for transmission over a 400 km fiber link consisting of five spans of 80 km standard-SMF. Finally we investigate the use of Semiconductor Optical Amplifiers (SOA) in a low channel count WDM system aiming at distances characteristic of a metro network. Some of the experimental investigation in WDM systems has been done in collaboration with Quang Nghi Trong Le (with OFS Fitel & COM). The experimental investigation regarding transmission with SOAs was carried out at AT&T Labs-Research in collaboration with Misha Brodsky and Martin Birk.

Chapter 7 is initiated by presenting a comparison of the performance of the different modulation formats investigated throughout the thesis: NRZ, optical duobinary, RZ and CSRZ. Different proposals for the implementation of 40 Gb/s single channel and WDM systems are presented. We will closely follow

[1] Now with the Research Center COM.

the method presented in standards from the International Telecommunications Union, Telecommunications sector (ITU-T) and define several application codes both for single channel and WDM systems. The system implementations proposed have taken into consideration the results and conclusions presented in the previous chapters. Furthermore we evaluate the availability of the components needed for the different proposed implementations .

The work is summarized and the thesis concluded in Chapter 8.

Chapter 2

Application of 40 Gb/s transmission systems in a telecommunications network architecture

This chapter will introduce those systems installed in a telecommunications network where there is a possible application for 40 Gb/s technology. We will present the main building blocks of these systems, and analyze the topics that need to be considered in the evolution from actual state of the art products at 10 Gb/s. For clarity we will focus on network functionality and applications codes described in standards available. Mainly on Synchronous Digital Hierarchy (SDH) [13, 14] and Optical Transport Network (OTN) [15, 16] from the Telecommunications standardization section of the International Telecommunications Union (ITU-T) or other recognized standards, the Optical Internetworking Forum (OIF) for example.

The objective of this chapter is to introduce the main design considerations and unknown parameters foreseen in the evolution from 10 Gb/s towards 40 Gb/s optical transmission systems. We will initiate the chapter by providing a very general picture of a telecommunications network in Section 2.1 and indicating where 40 Gb/s optical transmission technology is expected to be implemented. Section 2.2 will be dedicated to present the different application codes defined for single wavelength system, covering from Very Short Reach (VSR) to Very long haul (V). Wavelength Division Multiplexing (WDM) systems will be presented in Section 2.3. In this section we will analyze the typical limitations in WDM technology to the number of channels being used and the transmission distance covered before electronic regeneration is needed. The

main characteristics of metro WDM networks and differences from traditional WDM systems will be introduced in Section 2.4. The chapter ends with a brief summary.

2.1 High capacity transmission systems in a telecommunications network

The goal of this section is not to describe a telecommunications network in its full complexity but to point out where in this network high capacity transmission systems and high speed optical modules (2.5 Gb/s and above) will be used. We can present a telecommunications networks as a layered network. This means that we can describe each of these layers separately and by adding adaptation functions between the different layers (transmission rate adaptation, multiplexing, aligning and pointer justification in SDH, quality of service control etc) we can provide a detailed consistent description of the network. In SDH for example three main layers are defined [17]. The Low Order Path (LOP) layer deals with multiplexing and switching signals ranging from the VC-12 level (2240 kbit/s) to the VC-3 level (48960 kbit/s). The Higher Order Path (HOP) layer deals with the multiplexing of LOP layer signals into VC-4 (150336 kbit/s) and switching these signals in the network. Finally the Transmission Media (TM) layer deals with the physical transmission of high capacity signals within the network, see Table 2.1 for a relation of typical specified signals and their capacity in SDH/SONET.

SONET	SDH	Capacity (Mbit/s)
OC-3	STM-1	155.520
OC-12	STM-4	622.080
OC-48	STM-16	2488.320
OC-192	STM-64	9953.280
OC-768	STM-256	39813.120

Table 2.1: Terms used in SDH and SONET to define the different signals included in the transmission layer and capacity they can accommodate. STM: Synchronous Transport Module.

An example of the interconnection between different transmission and switching systems in a TM layer is presented in Figure 2.1. A short explanation follows: The "low order" cross connects,which refer also to electrical add-drop multiplexers, aggregate traffic from the LOP of the network and provide STM-1 level signals to the "high order" cross connects. These are able to receive a full range of signals from STM-1 to STM-64 and switch at VC-4 level the infor-

mation within the signal according to the output destination in the network intended for each container. They are also able to form new transport units again ranging from STM-1 to STM-64, which will be connected to either other "low order" cross connects, "high order" cross connects or to dedicated high capacity transmission systems. Until now all transmission has been done by dedicated single wavelength over a single fiber for each direction of transmission (Duplex). According to the distance between the two points connected, the links are named VSR ($< 600m$), Intra Office (I) ($< 2km$), Short haul (S) ($< 40km$), Long haul (L) ($< 80km$) and very long haul ($< 120km$) [13], values in parenthesis indicating traditional SDH target distances.

Several STM-16 to STM-64 signals from different "high order" cross connects can be joined in a dedicated WDM transmission system over a single fiber in each direction to provide a more cost effective solution. In general, the signals which are multiplexed could originate in other networks using different protocol structures than SDH, e.g. Asynchronous Transfer Mode (ATM) or Internet Protocol (IP) based data signals. We consider a "WDM transmission system" as a multi-protocol transmission system transparent to the information content for each wavelength. Several application codes fall within these kind of systems [15]. They are referred to as unrepeatered or repeatered systems depending on the presence of succeeding fibre spans concatenated using optical amplifiers. The length of each span in a repeatered system follows the single wavelength definition for short, long and very long haul. Finally depending on the total length reached, the system can be considered long haul (usually up to a 640 km total distance [15]) or ultra long haul (higher than 640 km), which in its extremes can reach transoceanic lengths for submarine systems. As these systems are responsible for the transmission of an enormous amount of information protection and reliability issues are of maximum importance. In general WDM systems will have a protection path in a $1 + 1$ configuration allowing for complete signal recovery in the case of a fiber cut. In relation to this observe the double connection between multiplexer and demultiplexer in WDM systems of Figure 2.1.

The last application included in the example is a "metro WDM network", which has attracted a lot of attention within the last years [18, 19, 20, 21]. Traditional SDH metro networks are based on optical to electrical conversion at each node of all signals reaching a node even though those with another destination in the network could just pass through. WDM networks make use of wavelength group allocation to allow for those wavelengths to pass through the node optically, leading to a reduced number of transmitter-receiver modules and reduced system cost. Only those wavelengths leaving the WDM network at a node will be translated to standard single wavelength application codes to reach their origin/destination at an Add-Drop Multiplexer Cross Connect

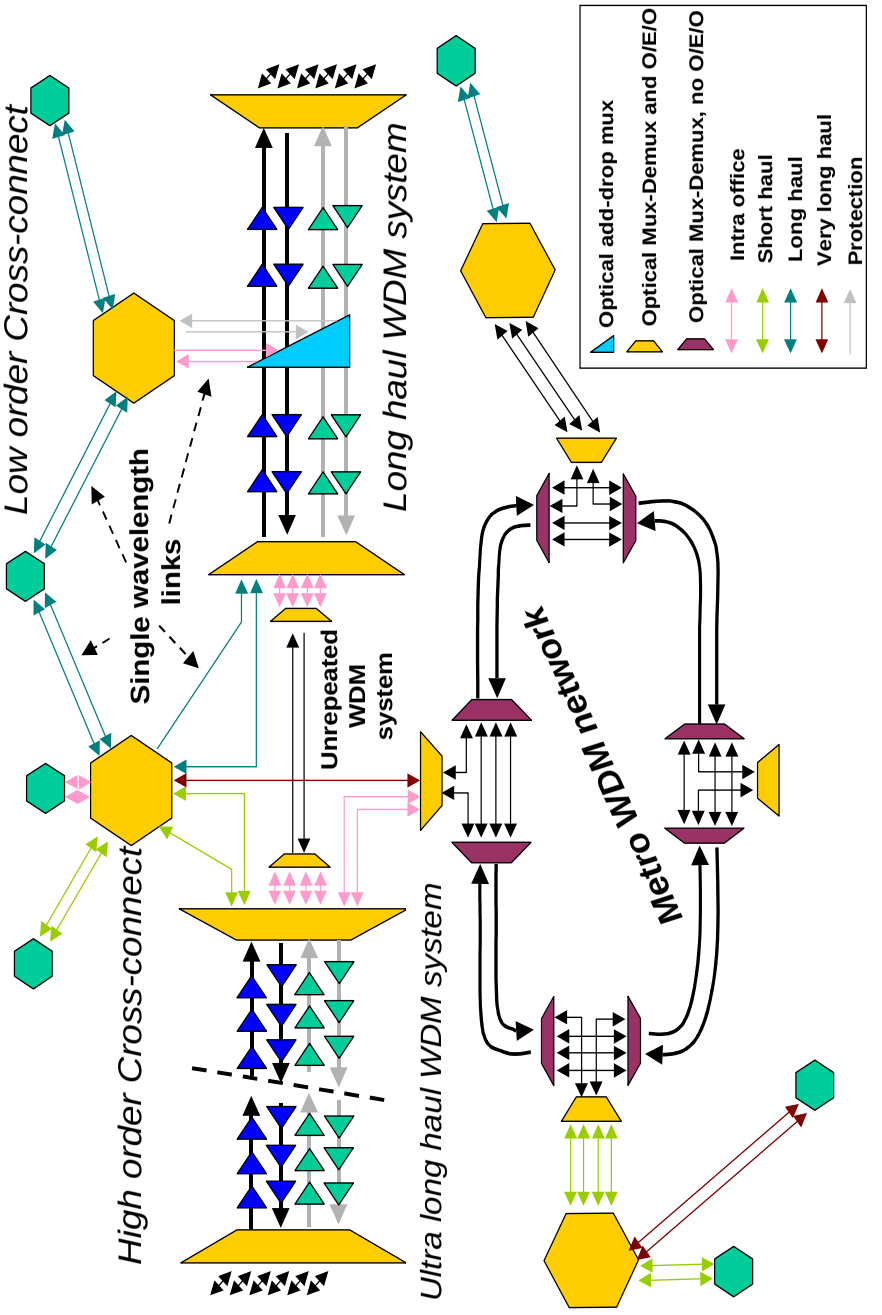

Figure 2.1: Example of the high capacity transport layers in telecommunications network architecture.

(ADM/XC), a WDM link or another WDM network. A second advantage of WDM based networks is their transparency to the protocol used per wavelength which can eliminate the need of having a network for each protocol.

Example of commercial equipment that covers the applications described can be taken from actual Tellabs products. The Tellabs 6350 Switch Node [22] is an SDH, ADM/XC with capability for a 768 port VC-4 cross connect matrix with STM-1 to STM-64 interfaces and the possibility to be configured as a low order cross-connect. Tellabs 7200 Optical Transport System [23] is a 32 channel STM-16 or STM-64 WDM system with capability for transmission over six Long haul spans and optical add-drop feasibility. Finally Tellabs 7100 Optical Transport System (Metro WDM) [24] is a 32 wavelength STM-16 or STM-64 WDM metro system with wavelength grouping capability.

2.2 Single wavelength optical transmission systems

We divide this section into two parts. The first one dedicated to very short reach and intra-office applications. The second part will be dedicated to short, long and very long haul applications.

2.2.1 Very Short Reach and Intra-office applications

Traditionally interconnection between equipment placed in a service providers office (intra office communication) is done using the same kind of transceivers as were used for transmission over longer distances (inter office communication) or electrical connections. This approach is economically inappropriate at high bit rates, as the performance needed in an intra office application is considerably lower than that of an inter office or short reach (40 km) application. Both ITU-T and OIF have standardized cost effective very short reach or intra office application codes for 2.5 Gb/s (STM-16) and 10 Gb/s (STM-64) single wavelength links [13, 15, 25]. Traditionally the VSR will cover up to 600 m and the Intra Office will cover up to 2 km of transmission. OIF has proposed up to 5 different solutions for VSR OC-192 [25]. For example parallel optics over multi-mode fibers (12 fibers at 1.24 Gbps), using Vertical Cavity Surface Emitting Lasers (VCSELs) as transmitters at 850 nm and *p-i-n* photodiode (PIN) array at the receiver side [26].

Evolution of the standards towards 40 Gb/s (OC-768 or STM-256) has been rather slow, even though STM-256 application codes are defined in [27] no implementation methods are described. The OIF has presented a standard [28] defining 3 methods for implementation of an OC-768 VSR link. The first method is the use of parallel optics (12 fibers at 3.3 Gb/s) transmitters in the

850 nm region over multi mode fiber and a PIN diode array [29]. The second method is by using Coarse Wavelength Division Multiplexing (CWDM) of four channels in the 1310 nm region over standard fiber. The final method is a single wavelength serial 40 Gb transmitter-receiver over standard fiber either in the 1310 nm or 1550 nm region. This last method seems to go against the original intention of defining VSR and Intra Office applications, namely reduction of cost compared to transponder type solutions. However single wavelength has been the choice considered in the Multi Source Agreement (MSA) for a 40 Gb transponder for example [30] where the VSR application code has been specified for a 1310 nm and 1550 nm solution.

2.2.2 Single wavelength short, long and very long haul applications

Single wavelength transmission modules will be generally transmitter / receiver modules (line cards) of an ADM/XC, or the client side of a WDM system. These modules can support the different application codes defined in standards [13, 14]. In this section we focus on application codes for STM-64 [13] from which future application codes for STM-256 might evolve. At the point in time of writing this thesis the only parameters included in the standards for STM-256 are the target distances for the short and long application codes, which are identical to those defined for STM-64. In all the application codes included in this section we have assumed that standard Single Mode Fiber (SMF) has been used, other fiber types will be introduced in Section 3.1.1. In all the application codes we will consider that the induced Differential Group Delay (DGD) of the transmission link is below the required limits. We will look into DGD induced limitations in the system in Chapter 4 dedicated to Polarization Mode Dispersion (PMD).

The main building blocks of the Short, Long and Very Long haul application codes are presented in Figure 2.2 while Figure 2.3 presents the definition of the main optical parameters used to define the application codes. Table 2.2 finally shows the typical limits for the optical parameters specified by ITU-T in [13].

Short reach STM-64 application is based on a straight forward link design, it requires moderate transmitter powers, sensitivity levels, which can be handled by available PIN receivers [31, 32] and no dispersion compensation, see Section 3.1 for details on origins and effects of dispersion.

Long haul applications are severely affected by dispersion and need some sort of dispersion compensation. Most practical compensation methods are based on changes at the optical transmitter, e.g. induced pre-chirp in the modulator [33, 34], or passive dispersion compensation [35]. These methods will be described

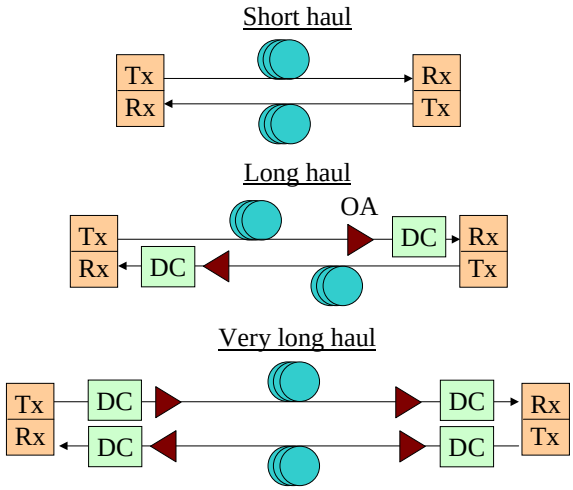

Figure 2.2: Examples of short, long and very long haul application codes following [13]. DC: Dispersion Compensation module, OA: Optical Amplifier. The DC and OA modules are included as an example of the application code configuration.

in more detail in Section 3.2. A main difference between these methods is the extra attenuation induced by the passive dispersion compensation module (in the order of 6 dB for a module required in the long haul application), which requires the use of an optical amplifier, severely increasing the cost of the module. On the other hand, the pre-chirping technique can be implemented together with state of the art Avalanche Photodiode (APD) based receivers [36] avoiding the need for optical amplifiers and allowing for cost and complexity reduction in the module.

The dispersion induced in a very long haul application overcomes the pre-chirp correction capability and there is a need to use passive dispersion compensation modules. Generally the insertion loss of these modules adds enough attenuation for the system to need an optical amplifier. There are several combinations possible depending on whether optical amplifier and the DC module are placed at the transmitter, at the receiver or in both ends as shown in Figure 2.2. The choice will be a compromise between cost and performance. It is important to notice the increased output power from the transmitter used for this application. Power levels in the 13 dBm order are close to the Self Phase Modulation (SPM) transmission induced limit for some fiber types at 10 Gb/s and could be a strong limitation for 40 Gb/s transmission, see Chapter 5.

Evolution of the described single wavelength application codes from STM-64 to STM-256 (and in general from any 10 Gb/s to 40 Gb/s transmission module)

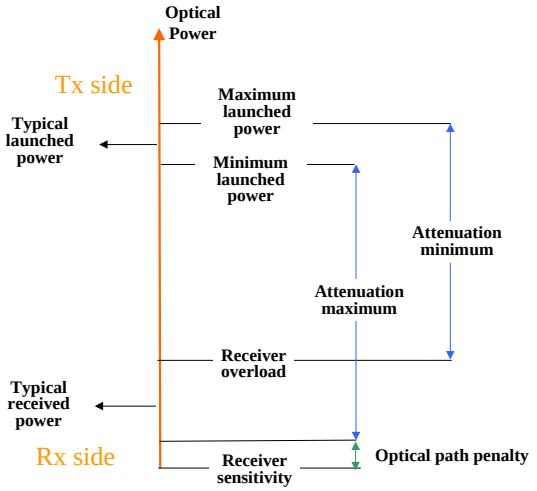

Figure 2.3: Relation between the optical parameters used in the description of the application codes following [13].

Application	Short	Long	Very long
Example of application code	S-64.2b	L-64.2c	V-64.2a
Operating wavelength [nm]	Any between 1530 and 1565		
Fiber type	Standard fiber G.652		
Mean launched power [dBm]	$-1 < P < 2$	$-2 < P < 2$	$10 < P < 13$
Minimum ER [dB]	8.2	10	10
Minimum SMSR [dB]	30	30	30
Attenuation [dB]	$3 < A < 11$	$11 < A < 22$	$22 < A < 33$
Chromatic dispersion [ps/nm]	< 800	< 1600	$800 < D < 2400$
Maximum DGD [ps]	30	30	30
Minimum sensitivity[1] [dBm]	-14	-26	-25
Minimum overload [dBm]	-1	-9	-9
Path penalty	2	2	2

Table 2.2: Main optical parameters that specify the short, long and very long application codes [13] for STM-64 signals. ER: Extinction Ratio, SMSR: Side Mode Suppression Ratio, BER: Bit Error Rate. [1] Sensitivity penalty considered for BER at 10^{-12} and end of life of the system.

should be done after careful consideration of the following questions:

- What is the dispersion induced transmission limit for 40 Gb/s?

- What are the dispersion margins in a practical system and what kind of granularity of the dispersion compensation modules is required?

- What are the sensitivity limits in practical 40 Gb/s receivers?

- What are the maximum launched power limits at 40 Gb/s?

2.3 WDM transmission systems

In its simplest description a WDM system is a combination of N wavelength channels (at a predetermined channel grid [15]) that are transmitted over a number of spans, M where the spans fall within specific single wavelength application code (length of span L). An example of the main building blocks characteristic of a WDM system is presented in Figure 2.4. An important difference from the single channel applications is the need for signal and system performance control in multi-span WDM systems. Traditionally two methods are generally used. The first one is to use an Optical Supervisory Channel (OSC) communicating between amplifier stations which can be used to locate faults and to communicate alarms to the end terminals. The second one is an Optical Channel Performance Monitor (OCPM), which is based on a spectrum analysis [37] and can provide information on laser or optical amplifier degradation. Communication from the OCPM to the end terminals could be done via the OSC.

WDM systems are used to overcome fiber shortage and to maximize throughput on a fiber reducing cost per transmitted bit over a certain distance. Installing a WDM system requires a high Initial Installation Cost (IIC) mainly because of two reasons. First due to the need of investment in full system requirements (e.g. multiplexer-demultiplexer equipment, optical amplifiers). Second as we need *field stations* to physically accommodate for the optical amplifiers. A longer span length will reduce the number of field stations needed reducing the overall IIC. The IIC will be shared however between the number of channels to be installed and the overall cost per channel will drop as a function of the number of channels used. The ideal WDM system will then be one allowing for higher channel count and longer span length with lowest IIC while allowing for cost efficient channel upgrades.

Unfortunately WDM systems are limited both in the number of channels and the span length (as a function of the total system length). We dedicate a subsection to each of these limitations. We will focus on limitations observed in WDM systems with STM-64 transmitter-receiver modules.

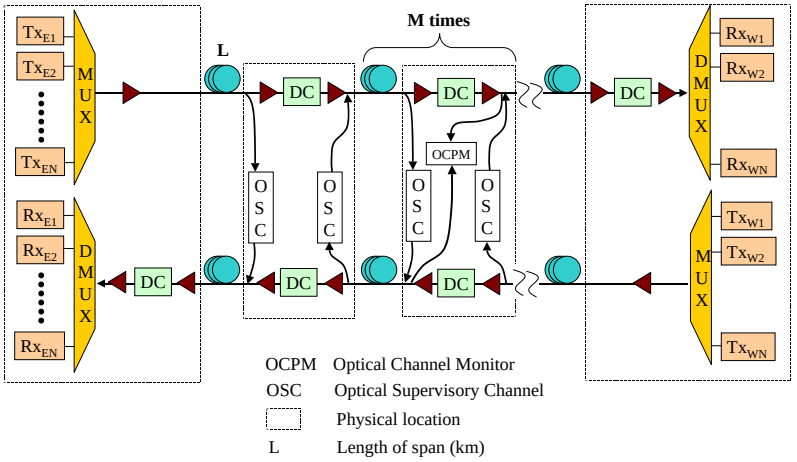

Figure 2.4: Building blocks of a WDM system without protection. Main parameters are the number of transmitter-receivers, N, the length of span, L, and the number of spans, M.

2.3.1 Limitations to the number of channels in a WDM system

The number of channels is mainly limited by two factors, the optical bandwidth allowed by the optical amplifiers and the frequency spacing between channels. The first limitation is induced by the inherent properties of Erbium Doped Fiber Amplifiers (EDFAs), traditional optical amplifier used in WDM systems. We will keep the discussion centered on applications in the C band (1530 nm to 1565 nm) even though the L band (1570 nm to 1610 nm) has attracted a lot of attention both in the scientific community and within the system manufactures over the last years [38, 39]. Intrinsically C-band EDFAs have a non-flat limited gain over more than 30 nm, from which only around 18 nm is useful for a WDM multi-span system . The "non-flatness" is characterized by the Gain Non-Uniformity (GNU) and determines the effective bandwidth of the amplifier in a multi span system. Even though research groups have focused on optimizing the gain bandwidth by changes in the materials used in the fabrication of the Erbium fiber [40] it seems that the preferred commercial solution is to use gain-flattening filters which can provide amplifiers with 40 nm optical bandwidth and less than 1 dB GNU at moderate gain values [41].

The frequency spacing is inherently limited by the optical bandwidth of each channel (determined by the rise/fall time of the optical pulses and contents of information in the signal) and the filtering characteristics of the multiplexers and demultiplexer used in the system. It is important to note at this point

that it is not the amplitude frequency response of the demultiplexer, which will determine the crosstalk induced between channels, but the effective bandwidth including dispersion within the bandpass range that determines the filter's effectiveness. Generally, in STM-64 WDM systems where filters are only used at the transmitter and receiver this is not a dominant factor. However, and due to the limitations imposed by dispersion at 40 Gb/s, see Section 3.1.2, we should consider which kind of filters should be used in a 40 Gb/s WDM system and their dispersive effects [42, 43, 44]. Finally when considering the filter characteristics we have to take into account that the transmitter might induce some center frequency variations originating in the laser and we must allow for these by proper design tolerance. However the introduction of wavelength lockers has reduced wavelength variations from the transmitter to the order of 2 *pm* [45] relaxing filter tolerances considerably.

Actual WDM standards have defined a frequency grid [15] to place the channels at a fixed frequency spacing of 200 GHz, 100 GHz and 50 GHz allowing for 16, 32 and 64 general cases of maximum channel count respectively [1]. Even though WDM systems with 25 GHz channel spacing have been demonstrated [46] they include tight restrictions in the system design and have not been included at this point of time in the standards.

2.3.2 Limitations to the span length and total system distance in a WDM system

The optical amplifiers included in the transmission introduce a certain level of noise that can be considered to accumulate linearly. The level of noise from the OA is directly dependent on the gain (see Section A.3.1 for details) and the gain is dependent on the span loss (usually directly related to the span length). As an example [47] if we use an amplifier for a 150 km span we will introduce around 100 times more noise than when using an amplifier for a 50 km span. If we want to reach the same total distance, the need of 3 times more amplifiers in a 50 km span system settles the relation to 33 times more noise in the 150 km span system than the 50 km span system. Of course the final best solution is a compromise between cost and performance.

A way of representing the relation is shown in Figure 2.5 by plotting the Quality factor, Q, as a function of the span number for different number of span attenuations. The system considered, refer to Section A.3 for further details, is of bit rate 10 Gb/s, 1 mW launched average power into the fiber, and extinction ratio of 10 dB in the transmitter, a sensitivity of the receiver

[1] Alternatively unequal channel spacing can be used. However, in transmission over G.653 dispersion shifted fiber also included in ITU-T WDM standard G.692.

(PIN diode) of -16 dBm and a noise figure of the amplifiers of 6 dB. It is clearly observed that increasing the span attenuation reduces significantly the number of spans that can be covered. For example if we assume a 22 dB span loss for an 80 km span and a 33 dB for a 120 km span, we reduce the ideal total transmission length from over 2000 km down to 360 km, (we require Q better than 17 dB (BER below 10^{-12} for a successful system).

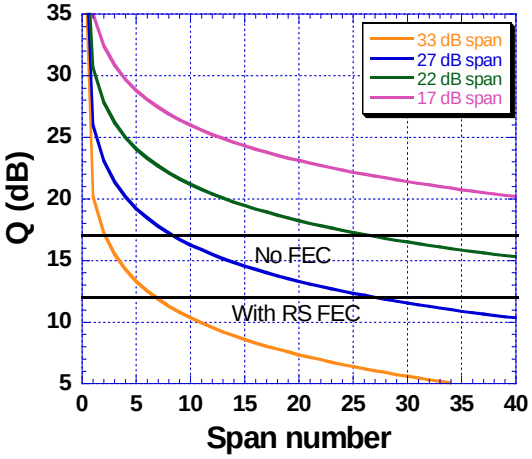

Figure 2.5: Relation between Q and the span attenuation as a function of the number of spans in a repeatered system. The lines indicate an accepted limit in the Q level without and with Reed-Salomon forward error correction.

A main point to consider is that the Q factor is directly related to the average power launched per span, see Equation A.12 for more details. A 3 dB increase in launched power will improve Q by 3 dB. However it is important to remember that at high power levels non-linear effects can distort the transmitted signal. The simple model for a repeatered system shown previously can be upgraded to include two new factors. First, the double stage amplifiers with dispersion compensation modules in the middle stage, see Figure 2.4. Second, the effect of GNU mentioned in 2.3.1, which emulates closely an actual system. GNU will reduce the launched power for those channels which experience lower gain reducing their Q factor as a function of the span number. On the other hand, it will increase the launched power for those channels falling in the high gain, which even though increases in theory their Q factor, might reach levels able to trigger non-linear effects.

An example of a 22 dB attenuation per span case, with a dispersion compensation module introducing an extra attenuation of 10.4 dB, $G1$ of 16 dB, $G2$ of

16.4 dB, $F1$ and $F2$ of 6 dB and a GNU per amplifier stage of ± 0.3 dB is shown in Figure 2.6. Where G1 and F1 are the gain and noise figure of the first section of the amplifier and G2 and F2 characterize the second amplifier section. The drastic reduction of Q for those channels that fall within the low power gain of the amplifier can be clearly observed in the figure. The example shows a worst case situation where all amplifiers have an equal gain profile. This will however not be the case in real life were there are small fluctuations in the production process of gain flattening filters or a second filter can be placed every N spans to correct for the effect of worst case accumulation.

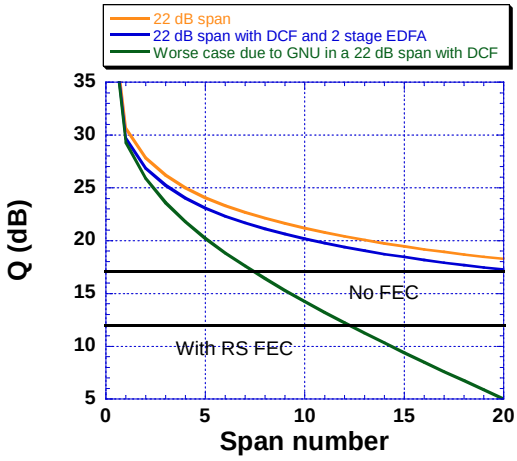

Figure 2.6: Calculated effect of the inclusion of a two stage amplifier and DCF in a repeatered span and of the effect of the gain non-uniformity. The example is based on a 22 dB span with 10.4 dB attenuation in DCF, 0 dBm launched power into transmission fiber and -6 dBm into the DCF modules, the noise figure of the amplifiers is 6 dB and the GNU is 0.3 dB per amplifier stage.

Even though they were originally used in submarine ultra long haul applications, Forward Error Correction (FEC) techniques [48, 49] are now being used in moderate length WDM systems to increase the margins against noise and pulse distortion. We will not go into details regarding FEC methods[2]. However, in some sections throughout the thesis we will indicate for a specific application the coding gain obtained when using typical FEC methods. The coding gain is defined as reduction in the Q level needed for a certain BER and usually expressed directly in decibels. As an example we have included both in Figures

[2]The reader is suggested to look into reference [50] for a complete presentation of error-control coding methods.

2.5 and 2.6 the Q required for a BER of 10^{-12} in the system when we are using a standard Reed-Salomon (RSa) FEC [51, 52] which provides an approximate 5 dB coding gain. It is clear from these examples that the use of FEC allows for considerably relaxed system tolerances, or to provide extra transmission distance.

2.3.3 Evolution towards an STM-256 WDM system

An important question in the evolution of WDM systems using STM-256 transmitter-receivers is whether it is possible to use actual commercial systems designed for STM-64 or we would need to redesign the whole system to allow for STM-256 signals. The last option will provide the best performance but will be an over-priced and extra complex system if it carries only STM-64 signals. However to understand this evolution it is required that we are able to answer among others the following questions

- What is the practical channel spacing we can set for an STM-256 WDM system?
- What power levels will allow us to avoid non-linear effects in transmission?
- What are the span lengths and total system distance that can be covered for an STM-256?
- Are there any methods to increase these distances if they fall short of actual standards?
- Are we limited by factors (for example Polarization Mode Dispersion or the residual dispersion from optical components), which were not limiting an STM-64 WDM system?
- Which is the most effective method to ensure proper dispersion compensation of all WDM channels?

2.4 Metro WDM networks

It is not the intention of this section to provide a detailed study of metro WDM networks [3], but to point out the topics that need more careful consideration if a metro WDM network should support STM-256 signals. We consider a metro

[3]The reader is suggested to look into reference [18] for a complete description of Metropolitan Optical Networks.

optical network following the structure in Figure 2.1 where designated wavelengths (channels) can be dropped and added at each node, the network having a number of nodes. A channel added at a specific node will pass through a series of nodes in the network before reaching its destination. Similar to the WDM repeatered system described in Section 2.3.2 the metro network will be limited in the maximum number of nodes that an optical channel can travel before there is a need of electronic regeneration. However, this is seldom the final limitation as total distances in metro networks are usually below the 200 km and the maximum span length is typically less than 50 km. It is important to consider that there are serious attenuations to include in the system budget from each node introduced by the optical filtering of the channels in the demultiplexing-multiplexing process (or in the optical cross-connects if they are used).

An important limitation in metro networks can be the effect of concatenation of a series of filters, as mentioned in Section 2.3.1: not only the amplitude but also the dispersion induced by the filters has to be taken into account. Finally we have to consider that signals in the transmission fibers will travel along different optical paths and can be exposed to different total dispersion. Furthermore, dispersion margins for STM-64 might allow placing dispersion compensation every two spans. This will not be adequate for an STM-256 channel, see Section 3.1.2 for further details on dispersion margins.

As mentioned previously there are two scenarios to consider for an STM-256 based metro network. In the first one we want to use a metro WDM network designed for STM-64 to transfer STM-256 signals. In the second scenario we design the network with an STM-256 approach which will ensure usability at STM-64 but perhaps the design will not provide the most cost effective architecture if few STM-256 are used. Mainly the questions that need to be looked into for the design of a metro WDM network are similar to those presented in Section 2.3.3. We will add those regarding the node concatenation

- How many nodes can an optical channel go through before need of electrical regeneration?
- What are the requirements for the components situated in the nodes to ensure optimum performance?

2.5 Summary

We have introduced in this chapter the optical transmission systems where application of 40 Gb/s technology can be foreseen in the future. We have described the main building blocks of single wavelength applications, WDM

repeatered systems and metro WDM networks. For each of these systems we have suggested a series of questions which need to be analyzed in order to be able to design an upgrade scenario for the use of 40 Gb/s transmission modules. We will provide answers to these questions throughout the remaining chapters of this thesis.

Chapter 3

Chromatic dispersion and its compensation in 40 Gb/s transmission systems

Fiber induced chromatic dispersion is an effect which clearly distinguishes the design of 10 Gb/s optical transmission systems from previous 2.5 Gb/s generation. Whereas in 2.5 Gb/s externally modulated systems dispersion limited transmission is not reached before 900 km in standard single mode fiber, the margin is reduced down to 60 km in a 10 Gb/s system. Following the trend we will expect 40 Gb/s systems to be limited to 4 km of transmission in standard single mode fiber. This fact points out the importance of correct treatment of chromatic dispersion compensation in future 40 Gb/s systems. This chapter is intended to provide a realistic approach to the design of 40 Gb/s optical transmission systems with regards to dispersion. We will do this by understanding the limitations of fixed dispersion compensation and investigating the feasibility of tunable dispersion compensation methods or alternative modulation schemes.

We initiate the chapter by an introduction in Section 3.1 to dispersion in the various optical fibers used for high capacity transmission and presenting the transmission tolerance of 40 Gb/s Non Return to Zero (NRZ) optical signals in the presence of dispersion. Section 3.2 will be dedicated to present the different fixed dispersion compensation methods and to describe design limitations in future 40 Gb/s systems. Examples of tunable dispersion compensators for single channel and for WDM systems will be introduced in Section 3.3. We will describe their working mechanism and characteristic parameters. Furthermore, we will investigate experimentally their performance in independent characterization set-ups. Alternative modulation formats such as chirped-NRZ or optical

duobinary might provide higher margins to chromatic dispersion than the traditional NRZ used in most of the commercial systems. These modulation formats are described and investigated in Section 3.4 providing their tolerance margins to chromatic dispersion. The chapter finalizes with a Summary.

3.1 Chromatic dispersion, origin and effects

Dispersion is an effect characteristic in the propagation of electromagnetic waves. In any medium other than vacuum or in any waveguide structure electromagnetic waves of different frequencies will propagate at different speeds. An optical pulse has a more or less wide spectral content, each frequency of the spectra will propagate at different speed in the fiber creating a delay for the different frequency components after travelling a distance over the fiber. The pulse experiences a broadening in the time domain induced by the difference in the time delays observed by the spectral components of the pulse. Following [53] the time delay difference, $\Delta\tau$, observed after a transmission length L for a pulse with spectral width $\Delta\omega$ is related to the *Dispersion parameter*, D by

$$\Delta\tau = L \cdot D \cdot \Delta\lambda \tag{3.1}$$

where the wavelength width $\Delta\lambda$ is related to the frequency width of the optical signal $\Delta\omega$ by

$$\Delta\omega = (-\frac{2\pi c}{\lambda^2}) \cdot \Delta\lambda \tag{3.2}$$

In optical fibers D is directly related to the second derivative of the propagation constant, β_2 and the wavelength considered, λ by

$$D = -\frac{2\pi c}{\lambda^2} \cdot \beta_2 \tag{3.3}$$

And it is measured traditionally in $ps/nm \cdot km$.

3.1.1 Dispersion in transmission fibers

The dispersion parameter in optical fibers, usually referred as *Chromatic Dispersion*, has its origin in the frequency dependence of the refractive index of the glass used in the fiber, the *Material dispersion*, and the waveguide structure, the *Waveguide dispersion*. In a standard single mode fiber, the later contribution has a negative slope as a function of wavelength while the former has a positive slope cancelling each other out at the *Zero dispersion wavelength*, λ_{ZD}. In a standard Single Mode Fiber (SMF) dispersion will be zero within the 1300 to 1324 nm wavelength range [54]. The Waveguide and Material dispersion

contributions do not cancel out for all other wavelengths but λ_{ZD}, phenomena represented by the dispersion slope, S, and related to the chromatic dispersion by

$$S = \frac{dD}{d\lambda} \tag{3.4}$$

and measured in units of $ps/nm^2 \cdot km$. For standard single mode fiber the slope is positive and defined at λ_{ZD} to be less than 0.093 $ps/nm^2 \cdot km$ [54].

Changes in the waveguide structure can affect the waveguide dispersion inducing a shift in the zero dispersion and the dispersion slope. Small changes induced in the manufacturing process can induce small statistical variations of the dispersion and the dispersion slope within several samples of the same commercial standard single mode fiber. This phenomena is shown in Figure 3.1, where dispersion has been measured for 22 spools of 40 km and 20 km standard-SMF. Regarding the dispersion it can be observed that measurements at any specific wavelength are spread over a 1 $ps/nm \cdot km$ while the slope of dispersion measured at 1550 nm varies from a minimum of 0.057 to a maximum of 0.068 $ps/nm^2 \cdot km$. The maximum dispersion margin is obtained using the maximum dispersion at 1530 nm allowed by [54] and an average slope from the data obtained.

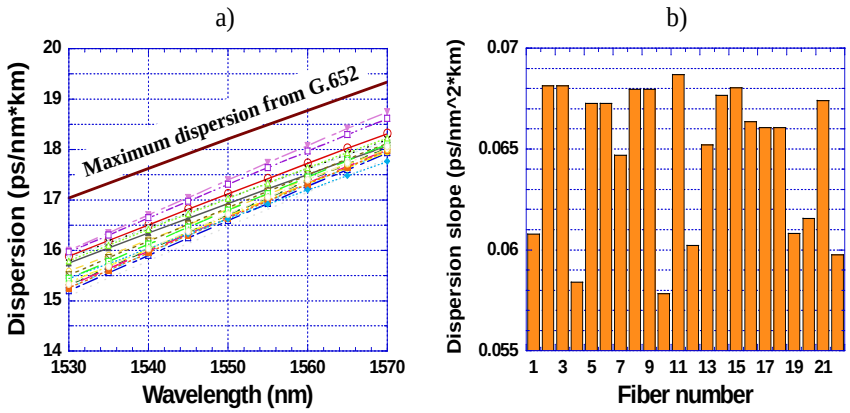

Figure 3.1: Characterization of 22 samples of 40 km and 20 km standard single mode fibers a) Measured dispersion in the 1530 to 1570 nm wavelength range, b) slope of dispersion at 1550 nm.

On the other hand, controlled changes in the waveguide structure allowed fiber designers to manufacture transmission fibers with zero dispersion shifted towards the low attenuation region, in the 1550 nm window, Dispersion Shifted Fibers (DSF) [55], which optimized single wavelength transmission. However

the need for high capacity and cost effectiveness provided by WDM systems was limited in this kind of fibers [56],[57]. Fiber dispersion values close to zero increase the walk-off length, which determines the duration over which nonlinear effects dependent on phase matching such as Cross Phase Modulation (XPM) or Four Wave mixing (FWM) are induced, see Section 6.2 for further details on this topic. As an example, the effect of FWM in a fixed channel spaced WDM system is to create a new wavelength component situated at the frequency allocated for one of the WDM channels. The crosstalk level seen by a transmitted signal can be increased by more than 30 dB when using DSF compared to standard-SMF [56].

Optimization of fiber design for WDM systems has lead to the development of Non Zero Dispersion Shifted Fiber (NZDSF). These fibers have enough dispersion to reduce non-linear effects to an acceptable level compared to DSF while inducing lower dispersion than standard-SMF fibers. The dispersion and mode field diameter limits specified in the standard G.655 [58] provide flexible margins in the design and each manufacturer has proposed different fiber types, see Table 3.1 ranging different dispersion, dispersion slope and effective area (influential value in the non-linear effects).

G.655 Fiber	**EA** $[\mu m^2]$	**Attenuation** $[dB/km]$ 1530-1565 nm	**Dispersion** $[ps/(nm \cdot km)]$ 1530-1565 nm	**Dispersion slope** $[ps/(nm^2 \cdot km]$ at 1550 nm
$TrueWave^{®}$[59]	53	≤0.25	2.6 to 6	≤0.05
$Corning^{®} Leaf^{®}$ [60]	72	≤0.25	2 to 6	typ 0.08
$TeraLight^{TM}$ [61]	63	≤0.3	5.5 to 10	Typ 0.052
$PureGuide^{TM}$ [62]	63	≤0.22	5.5 to 10	≤0.063

Table 3.1: Basic fiber parameters of several commercial G.655 fibers. Data is extracted from available datasheets on January 2003. EA: Effective Area.

The values of dispersion and dispersion slope specified in Table 3.1 provide enough margins for uncontrolled changes in the waveguide structure. Figure 3.2 shows the measured dispersion and slope of dispersion for 31 pieces of 25 km True Wave Reduced Slope (TWRS). Regarding the dispersion it can be observed that measurements at any specific wavelength are spread over 1.3 $ps/nm \cdot km$, while the slope of dispersion measured at 1550 nm varies from a minimum of 0.044 to a maximum of 0.049 $ps/nm^2 \cdot km$. These changes will have an influence in dispersion compensation considerations which will be looked into in Section 3.2. The maximum and minimum dispersion margins are calculated taking the maximum allowed dispersion at 1570 nm and minimum at 1530 nm from [58] and an average slope from measurements.

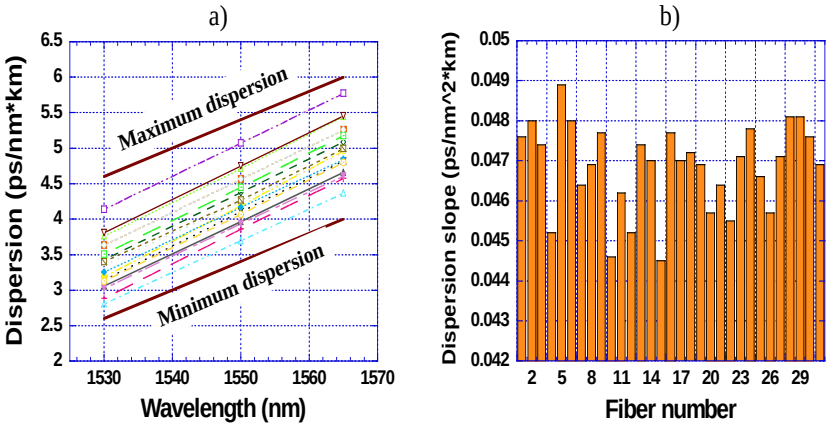

Figure 3.2: Characterization of 31 samples of 25 km True Wave RS fiber. a) Measured dispersion in the 1530 to 1565 nm wavelength range, b) slope of dispersion at 1550. The "maximum dispersion" line in a) is calculated by taken a minimum slope of 0.04 $ps/(nm^2 \cdot km)$ and a dispersion at 1565 nm of 6 $ps/(nm \cdot km)$. The "minimum dispersion" is calculated with minimum slope of 0.04 $ps/(nm^2 \cdot km)$ and a dispersion at 1530 nm of 2.6 $ps/(nm \cdot km)$.

Temperature induced dispersion fluctuations

Temperature related variations in the dispersion of a fiber are induced mainly by material dispersion variation [63, 64]. If we consider that dispersion at a given wavelength, λ, can be calculated from Equation 3.5 [54, 64] in the 1550 nm region, where S_{ZD} is the slope of dispersion at λ_{ZD}

$$D = \frac{S_{ZD}}{4} \cdot (\lambda - \frac{\lambda_{ZD}^4}{\lambda^3}) \tag{3.5}$$

the variation of dispersion with temperature is obtained by differentiating 3.5 with respect to temperature taking into account that both the λ_{ZD} and the S_{ZD} are temperature dependent [63, 64], leaving

$$\frac{dD}{dT} = \frac{1}{4} \cdot (\lambda - \frac{\lambda_{ZD}^4}{\lambda^3}) \cdot \frac{dS_{ZD}}{dT} - \frac{S_{ZD} \cdot \lambda_{ZD}^3}{\lambda^3} \cdot \frac{d\lambda_{ZD}}{dT} \tag{3.6}$$

By measuring the variations of λ_{ZD} and S_{ZD} with temperature we can obtain the temperature dependence of the dispersion of the fiber. Furthermore, it has been discovered that there is a linear relation between the slope of dispersion and the temperature dependence of dispersion [65]. Experimental results show [65, 63, 66] a similar dependence for standard-SMF and True Wave RS NZDSF fiber with a coefficient value of -0.0025 $(ps/(nm \cdot km)/^oC)$ while a value of

-0.0038 $(ps/(nm \cdot km)/^oC)$ for Leaf NZDSF fiber is explained by the higher dispersion slope of this type of fiber.

3.1.2 Dispersion induced limitations in 40 Gb/s transmission systems

As it was introduced in Section 3.1.1 the main effect of dispersion is the broadening of the optical pulses travelling in the fiber as a function of the distance travelled and the actual dispersion of the fiber. As in communication systems we are interested in the transmission of information signals at a bit rate B and not single pulses, we will introduce a magnitude which can quantify when the broadening of one bit of information is affecting the neighboring bit. The *Dispersion Limited Distance*, D_{ld} is the distance at which the pulse broadening is equal to the bit period, P, where $P = \frac{1}{B}$. Using Equation 3.1 we can write

$$\frac{1}{B} = D_{ld} \cdot D \cdot \Delta\lambda \tag{3.7}$$

and D_{ld} is given by

$$D_{ld} = \frac{1}{D \cdot \Delta\lambda \cdot B} \tag{3.8}$$

If we consider a normalized equal pulse shape for any bit rate considered we can estimate $\Delta\lambda$ to be proportional to B, $\Delta\lambda = k \cdot B$ and D_{ld} will be given by

$$D_{ld} = \frac{1}{D \cdot kB \cdot B} \tag{3.9}$$

This indicates that an increase in bit rate by four, from 10 Gb/s to 40 Gb/s for example will induce a 16 time reduction in D_{ld}. This squared reduction of the dispersion limitations is induced by a two fold effect of linear increase of the spectral width and linear decrease of the bit period as a function of the bit rate. As an example and following [53] we show in Figure 3.3 the dispersion observed in the transmission of a 40 ps and a 10 ps Full Width Half Maximum (FWHM) Gaussian pulse over a fiber with dispersion 17 $ps/(nm \cdot km)$. The pulse widths are scaled relative to a 10 Gb and a 40 Gb bit period. It is clear when comparing a) and b) in Figure 3.3 that even though the represented transmission length is reduced by more than four times the broadening of the 10 ps pulses is significantly higher than for the 40 ps pulses.

Receiver sensitivity can be defined as the optical power needed at the input of the receiver to ensure a certain signal quality. Usually we will provide a value for the receiver sensitivity which ensures a specific BER, for example 10^{-12}. We will call *back-to-back sensitivity* the receiver sensitivity measured when no component or fiber is situated between transmitter and receiver and

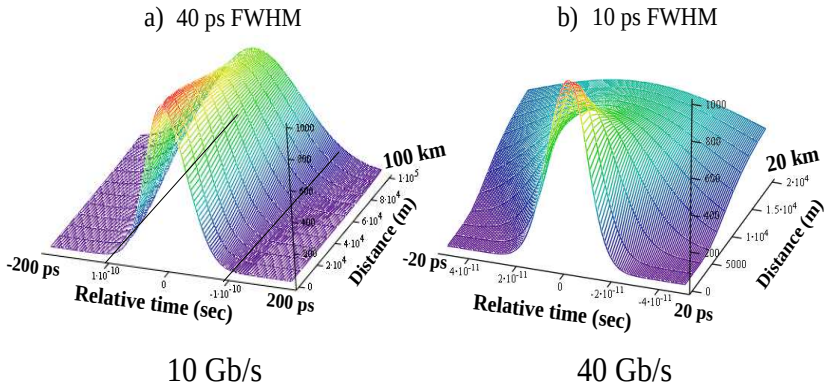

Figure 3.3: Evolution of Gaussian pulses in a dispersive fiber, 17 $(ps/(nm \cdot km))$. a) 40 ps FWHM pulse over a 100 km distance observed in a 400 ps time window. b) 10 ps FWHM pulse over a 20 km distance observed in a 100 ps time window. Vertical axis are in arbitrary units.

no distortions are affecting the performance. When a signal is slightly distorted we might be able to observe the same BER but for a higher input power to the receiver. The difference between this power and the back-to-back sensitivity is defined as the *sensitivity penalty*. Finally we define *dispersion tolerance* as the maximum and minimum dispersion we can allow in a system to ensure a certain sensitivity penalty in a transmitter/receiver module.

The effect of dispersion in a communication channel is more complex than the effect observed for a single pulse. In the following example, shown in Figure 3.4, we evaluate the sensitivity penalty induced by accumulated dispersion on a 10 Gb/s and 40 Gb/s Non Return to Zero (NRZ) Pseudo Random Binary Sequence (PRBS) signal.

The sensitivity penalty should be considered as a reference line, but will be dependent on chirp, rise/fall time and shape of the pulses and on the receiver used for estimating the penalties. The accumulated dispersion allowed for a 1 dB penalty is 1200 ps/nm for a 10 Gb/s signal while only 70 ps/nm for the 40 Gb/s case [1]. This indicates that transmission at 40 Gb/s for NRZ is limited to a distance of 4 km in standard-SMF (consider 17 $ps/nm \cdot km$) or in the order of 17 km in NZDSF (using a typical value of 4 $ps/nm \cdot km$). Experimental investigation of the dispersion margin for NRZ is shown in Section 3.3.1.

In order to increase the dispersion limits characteristic of NRZ modulation

[1]We consider 1 dB penalty for a PIN based receiver and a 2 dB penalty for a signal dependent receiver, EDFA or APD. These are traditionally margins allowed in standards [13]

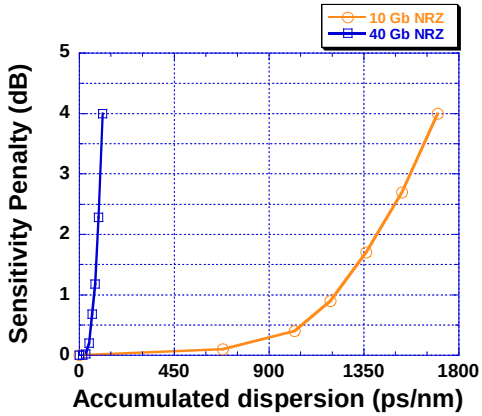

Figure 3.4: Comparison of sensitivity penalty as a function of accumulated dispersion for 10 Gb/s and 40 Gb/s. Results are obtained by means of simulation, details on parameters used are found on B.1.

format, several alternative modulation formats have been proposed and investigated [67, 68, 69, 70, 71] at 10 Gb/s and 40 Gb/s. We will look into the Phase Shaped Binary Transmission (PSBT) method in Section 3.4.2.

In the following sections we will concentrate on NRZ as the modulation format since it has been employed traditionally in systems such as those described in Chapter 2. This will provide an understanding of the dispersion limitations imposed in system design when upgrading bit rate from 10 Gb/s to 40 Gb/s.

3.2 Fixed passive dispersion compensation

To center the discussion on dispersion compensation methods with commercial application we will concentrate on passive methods. These differentiate from the active methods, for example optical phase conjugation [72] by FWM in Semiconductor Optical Amplifiers (SOAs) [73] or highly non-linear fiber, in the fact that we do not need any active component (e.g.,pump laser) to provide the compensation effect. We will look into the available methods for fixed passive compensation in the next subsection trying to highlight their system related characteristics. We dedicate the last part of this section to look into system implications of using fixed dispersion compensation in 40 Gb/s systems, single wavelength and WDM application.

3.2.1 Methods for fixed passive dispersion compensation

There are basically three commercial methods for fixed dispersion compensation, Dispersion Compensating Fiber (DCF), Higher Order Mode (HOM) DCF and Chirped Fiber Bragg gratings (CFBG). We will provide a brief introduction to these methods. Other techniques which are dispersion tunable such as the Virtually Imaged Phased Array (VIPA) could also be used as fixed compensators and will be discussed in a dedicated Section 3.3.

Dispersion compensating fiber

Making use of the ability to design complex refractive index profiles in fibers, it is possible to reverse the positive slope of the fiber and obtain a negative slope and dispersion in the 1550 nm region. The negative dispersion inverts the effect induced by a positive dispersion in the transmission fiber compressing the pulses back into their original shape. Initially the design of DCF modules restricted dispersion compensation to a narrow optical bandwidth, due to the slope difference between transmission and compensating fibers. The design of modules were slope compensation was also achieved over the full C and L band for all kinds of transmission fibers [74, 75, 76] has been a breakthrough in fiber transmission. DCF modules however suffer from some weak points. They are highly non-linear (due to their considerably small effective area , 15 to 20 μm^2) requiring low input powers to be launched into the modules, and have a high insertion loss (due to high attenuation in the fiber and splicing loss). These two characteristic force system designers to place DCF modules in specific points of the transmission link and to even design complex double stage EDFAs where DCF modules are placed in the middle section. We introduce here two concepts used in dispersion compensation. The Relative Dispersion Slope (RDS) is a parameter independent of fiber length which allows to compare directly how a transmission fiber and a DCF module fit each other. It is defined as the dispersion slope divided by the dispersion of the fiber

$$RDS = \frac{S}{D} \tag{3.10}$$

with units of nm^{-1}.

Two fibers with equal RDS can provide broadband dispersion compensation. The second concept is a Dispersion Compensation Figure Of Merit (DC-FOM) defined as the dispersion of the module divided by the Insertion Loss, IL

$$FOM = \frac{D}{IL} \tag{3.11}$$

The FOM of DCF is not constant as a function of fiber length in the module due to the fixed splicing loss. The FOM of DCFs is higher for high dispersion DCF modules, reaching values of 160 for a commercial module [77] designed to compensate for 80 km of standard-SMF.

High Order Mode DCF

HOM dispersion compensating modules are designed to allow for the propagation of the high order mode LP_{01} where dispersion is high ($< -200ps/(nm{\cdot}km)$) and fiber can be designed with high effective area ($78\mu m^2$) [78]. The modules are designed with mode converters at input and output with the HOM fiber placed in between. The high effective area raises the non-linear threshold allowing for high power levels to be launched into the modules [78]. Even though loss in the high order mode transmission are higher per unit length and we need to include the insertion loss of mode converters, the high dispersion per unit length allows to use less fiber length. Relatively high FOM values, 230 for a -2300 ps/nm module can be obtained for high dispersion modules [79]. As in traditional DCF modules, dispersion slope can be tailored to match the transmission fiber slope [80] and modules are designed for WDM multi-span systems. A drawback of the HOM DCF modules is however the mode leakage observed from the mode converters. It is important for the designers to reduce the mode crosstalk allowed in the mode converters to levels where it will not affect a repeatered system performance using several concatenated modules.

Chirped Fiber Bragg gratings

Fiber gratings[2] have their origin in the photosensitivity of optical fiber to ultraviolet light at wavelengths around 242 nm. This photosensitivity creates refractive index changes in the waveguide core of the fiber. The optical properties of a fiber grating are determined by the variation of the induced index change δn_{eff} along the fiber (in the path of light direction). The main effect of an uniform index change is the coupling between two modes, how this coupling occurs defines the type of grating. *Bragg gratings* are those where the coupling occurs between modes travelling in opposite direction, on the contrary in the *transmission gratings* coupling occurs between modes travelling in the same direction. Bragg gratings act as optical filters with a stop band centered at the Bragg reflection wavelength, λ_b related to the refractive index n_{eff} and the period of the grating Λ by

$$\lambda_b = 2 \cdot n_{eff} \cdot \Lambda \tag{3.12}$$

[2]The reader is suggested to look into references [81, 82] for a complete description of Fiber Bragg Gratings and their applications

Traditional uniform-period based Bragg gratings are generally limited by a narrow stop-band. If we induce a linear change in $n_{eff} \cdot \Lambda$ over the length of the fibers (inducing a phase change as a function of length in the refractive index modulation function) we will satisfy the Bragg condition for different wavelengths along the fiber and obtain a broad reflection. However we will also induce a delay between the different wavelength components as they travel different distances in the fiber grating. This effect is exactly what we are looking for in a dispersion compensating device.

The principle of pulse compression in a CFBG is sketched in Figure 3.5 and has been demonstrated in single wavelength transmission compensating the dispersion of more than 500 km standard-SMF using two CFBG devices [83]. The Figure shows a pulse dispersed in standard-SMF fiber, positive dispersion, where the lower frequency components of the pulse (red) travel slower than the high frequency components (violet). A longer period grating is created at the beginning of the CFBG reflecting the longer wavelengths (red) first while shorter and shorter period gratings are created towards the end of the CFBG reflecting progressively the rest of the frequency components with increasing delay for lower wavelengths. The pulse at the output of the CFBG has ideally the original shape of the pulse with only an amplitude variation.

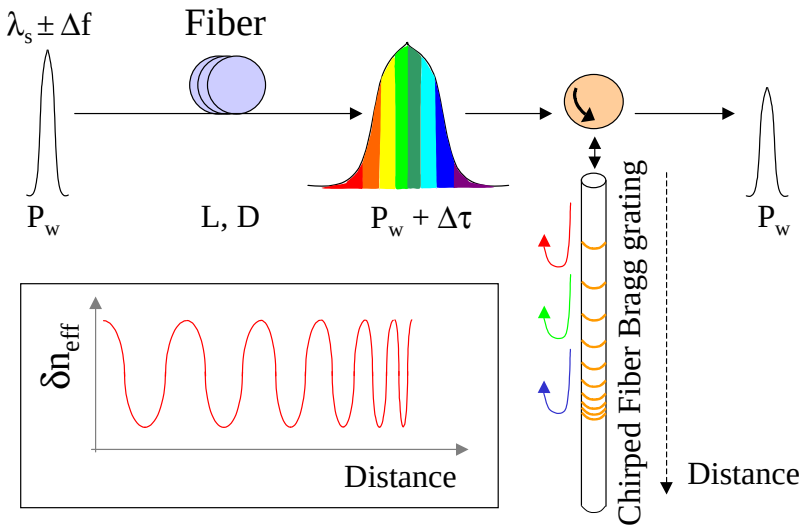

Figure 3.5: Principle of operation of a chirped fiber Bragg grating used for dispersion compensation.

Initial evolution of single channel CFBG to devices that could handle a series

of WDM channels was done by writing long gratings in the fiber [84], this technique presents serious manufacturing challenges, but devices have been shown to cover the full C-band [85]. Other approaches to WDM devices are to create a repetitive Bragg condition by inducing a complex sampling function in the refractive index [86] or create superimposed refractive index functions, one for each desired channel, [87]. This last approach has the great advantage of allowing to include a dispersion slope profile in the device. Advantages of CFBG are their low insertion loss and that their threshold to non-linear effects is comparable to those found in standard-SMF fibers [88]. The insertion loss is mainly induced by the circulator needed to separate transmitted and reflected signals and not by the grating itself. FOM values higher than 900 have been obtained for CFBG [83].

A main disadvantage of the CFBG in a fixed dispersion application is their temperature dependence. This is induced by the dependence of the refractive index on temperature, which provides a change in the Bragg wavelength with temperature in the order of 0.01 to 0.02 $nm/^oC$. The effect will be a shift of the center wavelength while keeping the same dispersion characteristics in the pass-band. The temperature dependence can be avoided however with careful thermal compensation packages. Another disadvantage is the amplitude and group delay ripples obtained in the grating process, influence of group delay ripple in system performance has been analyzed in [89, 90].

3.2.2 Compensation for single wavelength 40 Gb/s systems

If we follow the standardized application codes described in Section 2.2.2, for example the Short reach application, a 40 Gb/s system should be designed so that it is possible to be installed in any span length from 0 to 40 km. If we consider the $\pm 70 ps/nm$ dispersion margin estimated in Section 3.1.2 we can easily observe that dispersion compensation needs to be extremely precise to allow for effective transmission.

Lets present a possible practical scenario, we will call it Scenario A.

- A system provider receives an order for a 40 Gb/s system from a telecommunications operator installing a new network. The operator knows the exact measured length of the link and type of fiber used, knowing a maximum-minimum dispersion for the wavelength of the system to be installed as in Figures 3.1 or 3.2.
- The system provider has an agreement with the manufacturer of dispersion compensation modules, let us suppose DCF as data is available in data-sheets [77, 91] from where dispersion compensation tolerances for the modules can be obtained.

- We consider temperature fluctuations only in the transmission fiber following the coefficients of Section 3.1.1. Even though some studies have shown the temperature dependence cancellation for a positive-negative slope span [65] in a real system the DCF will be placed in a concealed environment and will not be affected by extreme temperature fluctuations. We consider temperature variations affecting the transmission fiber between -10 and 50 ^oC and consider that the dispersion data has been taken at 20 ^oC.

We consider the cases of a short and long haul applications for standard-SMF and Leaf fiber. The values considered for dispersion of transmission fiber, $Max-Min\ D$, dispersion of DCF module, $Max-Min\ D\ (DCF)$, and temperature coefficient, $Temp.\ Coeff.$ are shown in Table 3.2 together with the total dispersion, $Max-Min\ Dtotal$ expected in the link. It is clear that the long haul application falls out of the dispersion margin for standard-SMF and Leaf and it indicates that the system provider is not able to provide a commercial solution. If all the requirements described above are satisfied correctly the short haul application could be provided as maximum and minimum dispersion fall below the dispersion margin both for standard-SMF and Leaf.

Fiber type	Distance $[km]$	Max-Min D $[ps/(nm \cdot km)]$	T.C.[1]	Max-Min D (DCF) $[ps/(nm \cdot km)]$	Max-Min D total $[ps/nm]$
SMF	40	16.5 to 17.5	-0.0025	-701 to -659	-44 to 44
	80			-1401 to -1319	-87 to 87
Leaf	40	3.25 to 4.25	-0.0038	-164 to -142	-38 to 32
	80			-326 to -285	-75 to 64

Table 3.2: Dispersion values considered and dispersion margins to be expected following Scenario A in a short and long haul application for standard-SMF and Leaf fibers including temperature fluctuations and DCF tolerances. [1] TC: Temperature Coefficient measured in $[(ps/(nm \cdot km)/^oC)]$.

Let us consider a second situation Scenario B ,which only differs from Scenario A in the first condition, now the telecommunications network operator has not only measured the length, but also has measured the dispersion of the link to an accuracy[3] of 0.1 $ps/(nm \cdot km)$. Under these circumstances where only accuracy of the dispersion measurement, temperature fluctuations and DCF module tolerances we consider the worst case situation. For a long haul transmission over standard-SMF the maximum-minimum dispersion is reduced

[3]Typical accuracy of a commercial chromatic dispersion measurement system, see for example [92]

now to -55 to 55 $ps/(nm \cdot km)$ allowing to consider it as a possible system but with very tight margins.

3.2.3 Compensation in 40 Gb/s WDM systems

When we evolve from single channel to a WDM system the main consideration regarding dispersion is; How do the slopes of transmission fiber and DCF modules fit with each other? If we could match the slopes ideally we would obtain a perfect dispersion compensation for all the wavelengths at the same time. However slope compensation is rarely 100% allowing for residual slope to accumulate with increasing number of span count. In Figure 3.6 we present an ideal case where only the ratio of slope compensation has been considered. The span length is of 80 km and the fiber used is standard-SMF, we do not take into account temperature variations, tolerances or accuracy of dispersion measurements. We can observe that if we want to ensure transmission at 40 Gb/s for all wavelengths over a six span system we need to have a slope compensation higher than 85% for all spans.

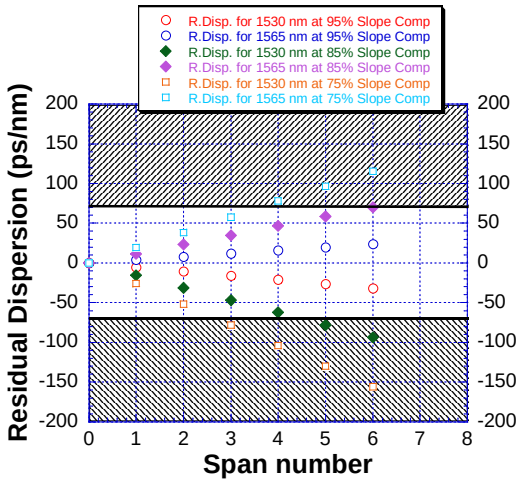

Figure 3.6: Residual dispersion as a function of span number for a 80 km span WDM system as a function of the slope compensation ratio of the DCF modules.

Let us consider now a more realistic example following Scenario B described in the previous Section for a multi-span WDM system with standard-SMF and 80 km spans. In addition to the conditions previously described, the network operator has also measured the dispersion slope at a specific wavelength, 0.065 $ps/nm^2 \cdot km$ at 1550 nm, and with an accuracy of 0.001 $ps/nm^2 \cdot km$.

Considering the dispersion accuracy, the slope accuracy and the temperature fluctuations we can obtain the relation of possible dispersion values expected for highest and lowest wavelength. If finally we consider an RDS for the slope compensating fiber of $0.0036 \pm 20\%(nm^{-1})$ [77] and the tolerances of DCF from Table 3.2 we can deduce that the worst case residual dispersion in a single long haul span will provide 60 $ps/(nm \cdot km)$ for 1530 nm while -68 $ps/(nm \cdot km)$ for 1565 nm. These values indicate that even a single span 40 Gb/s WDM link over standard-SMF could be a serious challenge using available fixed dispersion compensation modules.

3.3 Tunable dispersion compensation

We have shown in the previous Section the challenges to consider for dispersion compensation in 40 Gb/s commercial systems. It has been demonstrated that for example a Long haul application could be provided under a series of conditions: the first one, *the network operator has measured dispersion of the links*, is a costly process. The second one, *the dispersion compensation module provider has available the exact match to the dispersion*, is an approach that reduces the economics of scale obtained by the standardization of distances for transmission systems. An alternative is to consider tunable dispersion compensation techniques which either alone, in single wavelength systems, or in combination with fixed dispersion compensation modules, in multi-span WDM systems, can reduce considerably the complexity of 40 Gb/s system design. We focus in the following two sections on the demonstration of practical use of two tunable dispersion compensation techniques for single channel and one technique for WDM 40 Gb systems. For a wider analysis of dynamic dispersion compensation techniques the reader could refer to [35].

3.3.1 Tunable dispersion compensation for single wavelength systems

For single wavelength applications we have investigated Tunable Dispersion Compensators (TDCs) based on CFBG. The first technique we will describe uses the mentioned dependence of CFBG on temperature to provide the tuning mechanism by inducing a temperature gradient [93] and has been applied to a short reach application over standard-SMF. The second technique uses changes in the stretching applied to a non-linear CFBG as the tuning mechanism [94] and has been investigated in a long haul application over standard-SMF.

TDC using temperature gradient as the tuning mechanism

As mentioned in Section 3.2.1 the reflected wavelength at a fixed point in the CFBG will change with temperature, if the same change in temperature is applied to all the points of the CFBG we will obtain a shift in the center wavelength. On the other hand if we apply a gradient in temperature while keeping the center point of the grating stable with temperature, see Figure 3.7, we will shift towards higher wavelengths the reflections for heated areas while towards lower wavelengths in cooled areas (always with respect to the temperature of the center of the device). This will induce a spectral broadening or narrowing (dependent on the sign of the gradient) of the reflectivity spectra while keeping the relative delays constant (the grating has the same length). The same differential delay over a broader bandwidth provides lower dispersion, while over narrower bandwidth it will provide higher dispersion.

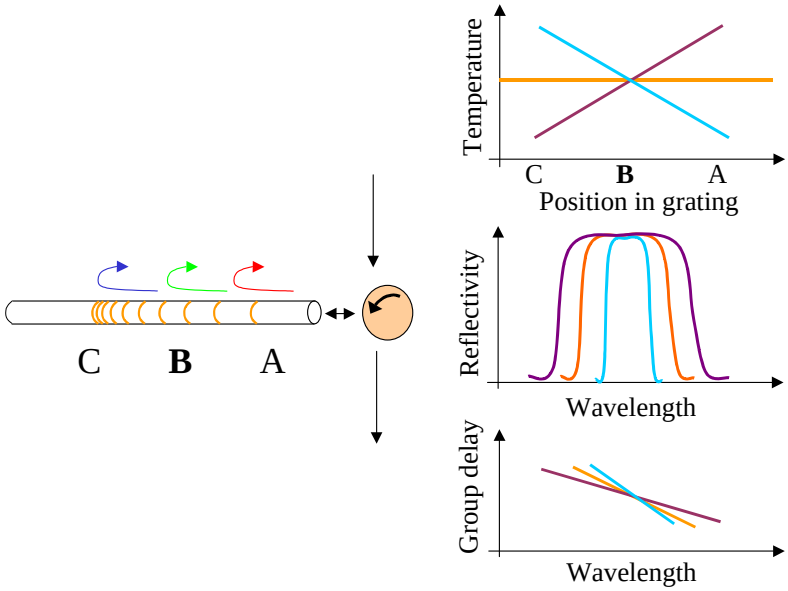

Figure 3.7: Schematic of the principle behind the tunable dispersion in CFBG by changes in the temperature gradient.

The main properties of the tested device are presented in Table 3.3, values are obtained from measurements and datasheet [95]. The device uses three temperature controllers (positions A, B and C in Figure 3.7) to create the appropriate temperature gradient, the temperature for controllers A and C is changed while keeping the temperature at position B constant. A look up table for the relation between temperature settings and dispersion has been provided

by the manufacturer.

Parameter	Value	Units
Wavelength	1555.47	[nm]
Insertion loss[1]	5	[dB]
Center dispersion	-500	$[ps/nm]$
Dispersion tunable range	-300 to -700	$[ps/nm]$
Group delay ripple	± 5	[ps]
Operating temperature	-5 to 70	$[^oC]$
Minimum optical bandwidth[2]	85	[GHz]
PMD	0.5	[ps]
Dimensions[3]	17x12x150	[mm]
FOM[4]	60 to 140	

Table 3.3: Main parameters of tunable dispersion CFBG based on temperature gradient changes.
[1] Including circulator. [2] For a tuning to -700 ps/nm . [3] Temperature control modules are not included. [4] For maximum-minimum dispersion.

A schematic of the experimental set-up used for testing the tunable dispersion compensator is shown in Figure 3.8. The set-up uses a 40 Gb/s NRZ electrical time domain multiplexing (four channels at 10 Gb/s) based transmitter and an Optical Time Domain Demultiplexer (OTDD), which allows only one 10 Gb/s channel to reach the receiver, for further details on the set-up the reader should refer to Appendix C [4]. One variation from the general set-up described in this Appendix is that the wavelength used for the clock will not pass through the transmission line as the device is narrow band and is passed by directly to the receiver. This introduces a time drift at the receiver, which restricts the evaluation to short periods, however penalties could still be measured with sufficient confidence for a BER of 10^{-10}. As an example, in Figure 3.8 we can observe the effect of de-tuning dispersion compensation by -110 ps/nm from the optimum value in the measured eye diagrams. All eye diagrams are measured with a time scale of 12.5 ps/division.

The device has been initially used to investigate the dispersion margin for a 40 Gb/s system in a 21.53 km standard-SMF fiber (dispersion 368 ps/nm) by de-tuning dispersion away from the optimum point of performance in both directions. Results of this evaluation are shown in Figure 3.9. We have initially

[4]We use an OTDD receiver in all the experimental measurements presented throughout the thesis. No test-set was available for direct evaluation of penalties at 40 Gb/s. This is a temporal solution and should not be used when a commercial 40 Gb/s test-set is available.

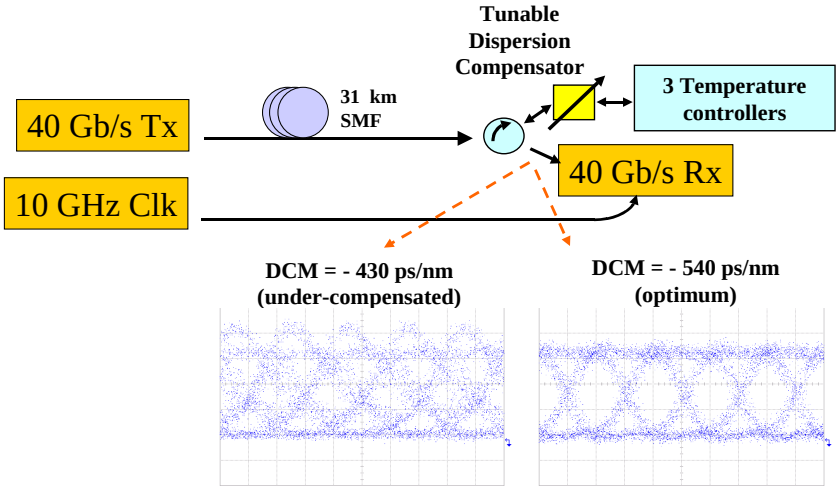

Figure 3.8: Schematic of experimental set-up used for measurement of performance of a TDC based on temperature gradient change. Horizontal scale in eye diagrams 12.5 ps/div. Vertical scale 150 μW/div.

measured the back to back sensitivity for a BER of 10^{-10} to be -16 dBm using the OTDD receiver, this value is used as the basis for the sensitivity penalty calculation. We observe a slight de-tuning of the penalty curve towards lower dispersion believed to be induced by a small residual chirp in the modulator scheme. The second observation is that clearly the dispersion margin for 1 dB penalty is reduced to ± 45 ps/nm (from optimum performance) compared to the expected ± 70 ps/nm. This is believed to be directly a measurement error induced by the OTDD receiver set-up and has been verified by means of simulations, please refer to Appendix D for more details and results. Eye diagrams are shown for best dispersion tuning and for the 2 dB penalty operation points.

Finally we demonstrate the tunability of the device over the expected range by changing the standard-SMF fiber span from 21.5 km to 41 km. We evaluate sensitivity penalty at the following intermediate standard-SMF span lengths: for 24.7 km, 31.5 km, 33.3 km and 37.8 km. Sensitivity penalty results are shown in Figure 3.10 together with eye diagrams for optimum setting of the TDC. A maximum penalty of 0.8 dB was observed for the longest fiber length of 41 km at maximum tuning of the device. However the performance shows the ability for the device to be used in a short haul application over standard-SMF for any span length included in the dispersion tuning range, from 18 km to 41 km.

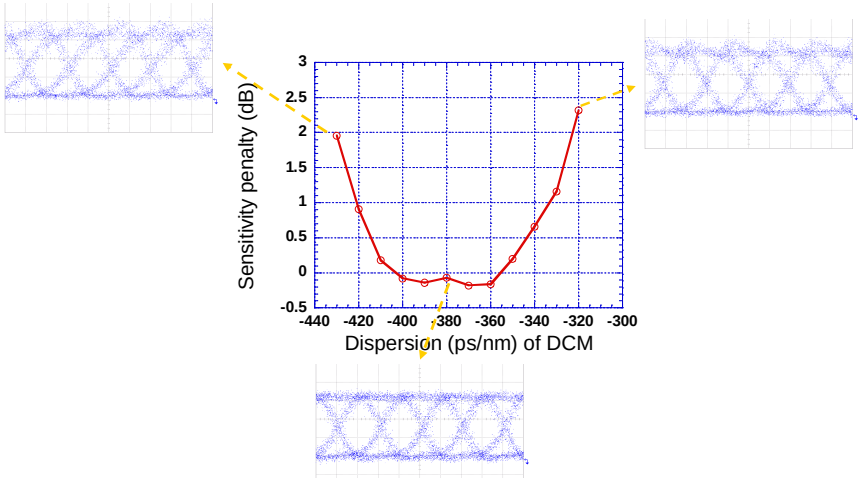

Figure 3.9: Experimental measurement of the dispersion margin measured in a 21.53 km of standard-SMF span where chromatic dispersion has been compensated for by a TDC CFBG based on temperature gradient change. Penalties measured at 10 Gb/s after OTDD from a 40 Gb/s signal. Horizontal scale in eye diagrams 12.5 ps/div. Vertical scale 150 μW/div.

From a practical point of view it would be ideal to integrate the heating capability into the device reducing the complexity of the set-up. This has been achieved in a very interesting approach [96] where a thin-film heater is deposited onto the outer surface of the fiber directly. The thickness of the heater is varied along the fiber grating providing the desired temperature gradient. These devices have proven their efficiency even compensating for dispersion in single wavelength transmission at 160 Gb/s [97].

TDC using stretching in a nonlinear CFBG

If we apply stretching between the ends of a CFBG we will increase equally the periods of the grating throughout the fiber moving the reflection towards longer wavelengths but without inducing any change in the slope of the group delay, case a) in Figure 3.11. The dispersion seen by a signal within the reflectivity bandwidth before and after the stretching will be the same. On the other hand if we apply a stretching function to the grating, which increases gradually the stretching towards the end of the fiber (seen from the circulator) we will induce a change in the chirp rate inducing a change in the slope of the group delay and a change in dispersion [98], case b) in Figure 3.11. Finally, if we induce a non-linear chirp in the fabrication of the grating we will obtain a non-linear group

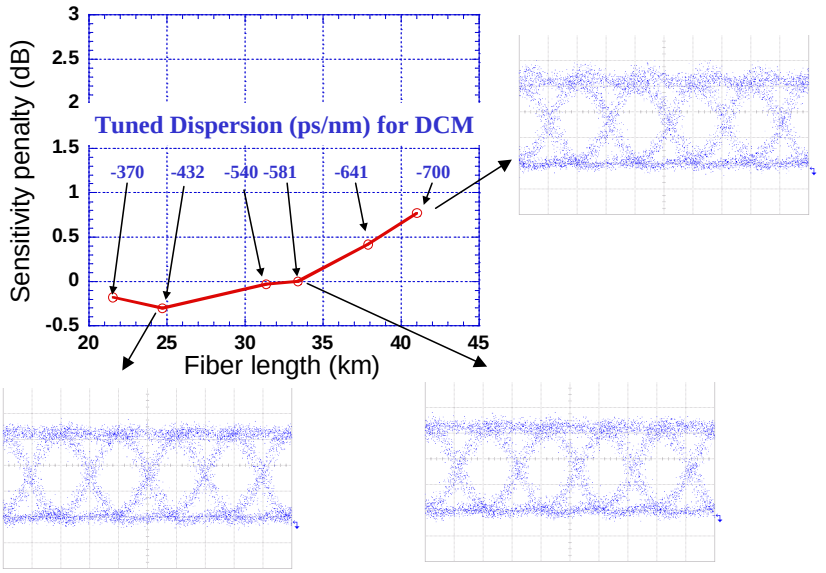

Figure 3.10: Sensitivity penalty evaluation as a function of span length for an optimum tuning of the TDC CFBG based on tuning by changing the gradient of temperature The TDC is tested in a 21.5 km, 24.7 km, 31.5 km, 33.3 km, 37.8 km and 41 km standard-SMF span. Penalty measured at 10 Gb/s after OTDD from a 40 Gb/s signal. Horizontal scale in eye diagrams 12.5 ps/div. Vertical scale 150 μW/div.

delay function, the slope of the function at a given wavelength provides the dispersion. If we apply stretching between the ends of the non-linear CFBG we will move the group delay to higher wavelengths while the center wavelength of the signal will observe a different slope of group delay and a different dispersion, case c) in Figure 3.11. The results presented in this section are based on a TDC using the latter described principle [94]. It can be observed that in case c) of Figure 3.11 the slope of the dispersion will also change within the signal bandwidth inducing a degradation in the signal dependent on the tuning of the device. However this can be avoided [99] if we use a double grating with opposite curvature in the group delay shape. The device tested has included this last improvement allowing for high dispersion tuning. The main properties of the device are presented in Table 3.4 and are obtained from measurements or specifications provided [100].

The dispersion tuning capability of the device makes it ideal for a long haul application. The initial test conducted uses the TDC to compensate dispersion for an 82 km span length of standard-SMF. A schematic of the experimental set-up is depicted in Figure 3.12 together with eye diagrams in back to back

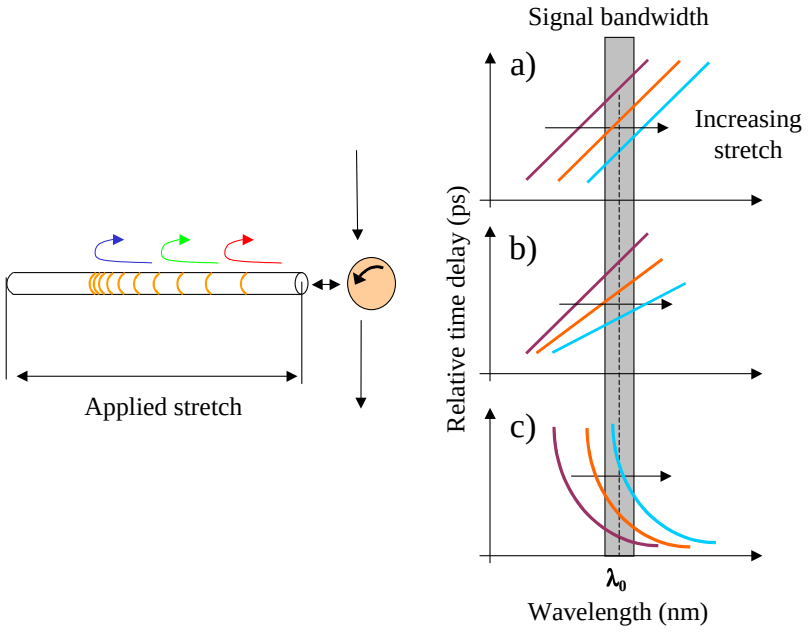

Figure 3.11: Schematic showing some of the possible effects of stress on CFBG. a) Linearly chirped FBG with applied stress only in the ends of fiber grating, b) Linearly chirped FBG with linearly increasing stress along the fiber and c) Non-linearly chirped FBG with applied stress only in the ends of fiber grating

situation, after 22 km of standard-SMF with no compensation and after 82 km of standard-SMF using the TDC. Due to the long path difference between clock and signal, sensitivity penalties were now limited to measurements for a BER of 10^{-9}. Close to 1 dB penalty was observed after the 82 km transmission and compensation with the TDC. The penalty is induced by OSNR degradation and confirmed by setting attenuators emulating the insertion loss of the standard-SMF and the TDC in their place. When we compared to using a fiber based dispersion compensation module instead of the TDC we observed also similar results. However, the power into the DCF had to be reduced to -3 dBm while for the TDC we could increase it up to 6 dBm (limited by amplifier gain) without noticing any penalty increase.

In order to test the device in the long haul application the following standard-SMF span lengths have been used: 45.8 km, 50.9 km, 56.0 km, 62.4 km, 67.6 km, 72.7 km, 77.8 km and 82.0 km. We kept insertion loss of the span fixed to 16.2 dB by tuning an optical attenuator to ensure same OSNR observed at the receiver. Sensitivity penalty for these measurements compared to the back

Parameter	Value	Units
Wavelength	1551.72	[nm]
Insertion loss[1]	4.2	[dB]
Center dispersion	-1486	$[ps/nm]$
Dispersion tunable range	-786 to -2186	$[ps/nm]$
Maximum optical input power	13	dBm
Group delay ripple	± 9	[ps]
Operating temperature	-5 to 70	$[^oC]$
Minimum optical bandwidth[2]	65	[GHz]
PMD	0.3	[ps]
Dimensions[3]	200x54x18.5	[mm]
Tuning speed	250	[ps/nm/sec]
FOM[4]	187 to 493	

Table 3.4: Main parameters of tunable dispersion compensator based on stretching of a non-linearly chirped FBG.
[1] Including circulator. [2] For a given fixed center wavelength at ITU-T grid, reached for maximum and minimum dispersion settings. [3] Including stretching mechanism. [4] For minimum and maximum tuning of dispersion.

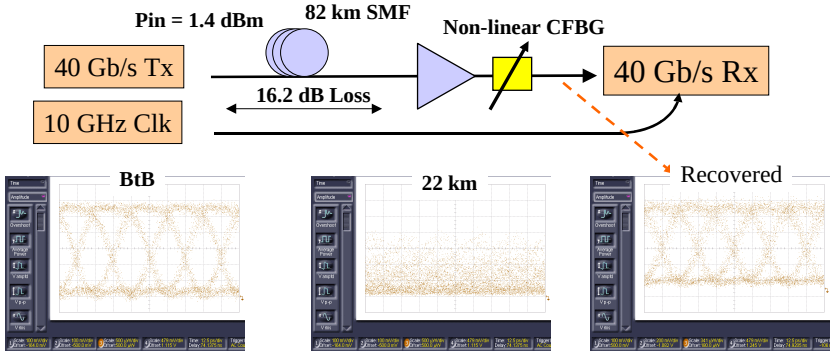

Figure 3.12: Schematic for the experimental set-up used in the characterization of the non-linearly chirped FBG. Eye diagrams shown for back to back performance, after 22 km and after 82 km of standard SMF with the TDC recovering the signal

to back situation are shown in Figure 3.13. For all tested spans the penalty was kept below 1.2 dB. The device has been moreover tested in an extended long haul application for 92.2 km and 103.8 km of still unrepeatered spans

with increased insertion loss of 18.4 dB and 20.8 dB respectively. Sensitivity penalties are believed to be induced by the higher span loss. However the device could compensate up to a 122 km span of standard-SMF with an extra 1.5 dB penalty where the transmission fiber was now separated into an 82 km and a 40 km spans. The penalty is believed to be induced mainly by OSNR degradation. In this case the TDC might not be situated optimally at the receiver and we could gain from placing the device at the transmitter while increasing launched power into it, up to a level where the output power will not induce nonlinear effects in the transmission fiber.

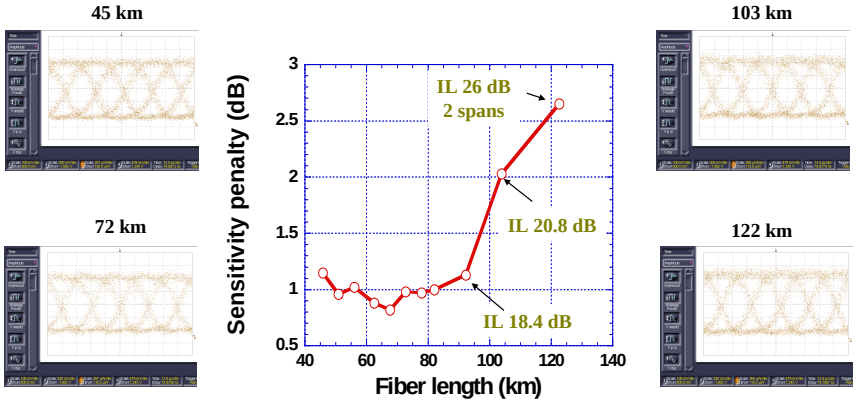

Figure 3.13: Sensitivity penalty evaluation as a function of span length for an optimum tuning of the non-linearly chirped FBG in a long haul application. The device has been tested for the following standard-SMF span lengths : 45.83 km, 50.91 km, 56.0 km, 62.4 km, 67.6 km, 72.7 km, 77.8 km, 82.0 km, 92.2 km 103.8 km and 122 km

3.3.2 Tunable dispersion compensation in WDM systems

Unfortunately we have not been able to test any CFBG based WDM tunable dispersion compensator. We have focused for WDM application on another type of technology, the virtually imaged phased array (VIPA) based dispersion compensator [101]. The VIPA technology is originally intended to provide large angular dispersion of a WDM signal, changing the output angle as a function of wavelength, a property used in a wavelength multiplexer/demultiplexer for example [102]. By combining the VIPA with a moving mirror we can create different relative delays between the wavelength components inducing dispersion [102]. We can also integrate a 3 dimensional mirror (the curvature of the mirror changes from concave to convex) moving in the direction perpendicular to the light. Moving the mirror allows to compensate for positive and negative values

of dispersion [103]. VIPA based dispersion compensators have been used in 10 Gb/s WDM transmission experiments [104] and recently in a multi-band WDM demonstration at 40 Gb/s used as a tuning device for dispersion per channel at the receiver [105]. The main parameters that describe the device which has been tested at Tellabs are presented in Table 3.5. The main limitation to the number of channels and the free spectral range of the device is the level of crosstalk allowed between neighboring channels.

Parameter	Value	Units
Free spectral range	200	[GHz]
Maximum number of channels	25	
Insertion loss	10	[dB]
Center dispersion	0	$[ps/nm]$
Dispersion tunable range[1]	-400 to 400	$[ps/nm]$
Dispersion resolution	1	[ps/nm]
Maximum optical input power	23	dBm
Group delay ripple	± 5	[ps]
Operating temperature	0 to 65	$[^oC]$
Minimum optical bandwidth[2]	65	[GHz]
PMD	0.5	[ps]
Dimensions	192x95x29	[mm]
Tuning speed	50	[ps/nm/sec]
FOM	< 40	

Table 3.5: Main parameters of WDM tunable dispersion compensator based on VIPA and 3D mirror.
[1] Suggested to avoid slope compensation issues.

In Figure 3.14 we show experimental results from testing the VIPA in a 40 Gb/s 22 km set-up for a single channel at 1550 nm. The effect of high power (13 dBm) being launched into the transmission (standard-SMF) fiber can be observed in the eye diagram in Figure 3.14 a). In b) we invert the order of the set-up, the same optical power is launched now into the VIPA with no signs of eye degradation. In c) we evaluate the dispersion margin to de-tuning of the device. As in the results obtained in Section 3.3.1 we observe both a smaller margin ($\pm 35 ps/nm$) than expected and a shift towards negative dispersion of the optimum dispersion compensation (accumulated dispersion of the fiber at 1550 nm is 355 ps/nm).

We evaluate the device now as a function of wavelength by using a tunable laser at the transmitter. We keep the same set-up as shown previously where

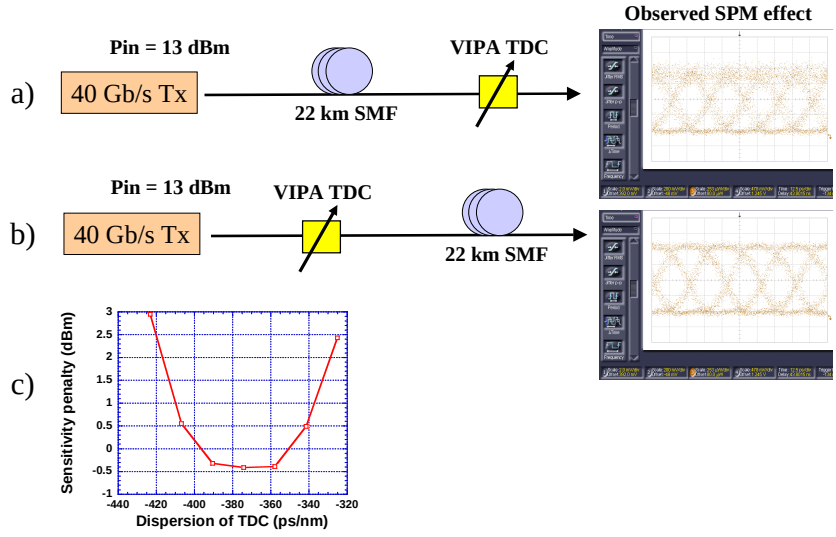

Figure 3.14: Schematic for the experimental set-up used in the characterization of the VIPA based TDC device. a) 13 dBm optical power launched into standard-SMF, b) 13 dBm launched into VIPA based TDC, c) dispersion de-tuning margin for single wavelength. Penalties measured at 10 Gb/s after OTDD from a 40 Gb/s signal. Horizontal scale in eye diagrams 12.5 ps/div. Vertical scale 253 μW/div.

the VIPA is placed before the transmission fiber. Due to the limited optical bandwidth of the receiver for BER measurements, see Appendix C for further details, we evaluate the sensitivity only for 1545 nm, 1550 nm and 1560 nm. The back to back sensitivity measurement included the VIPA device tuned to zero dispersion. Sensitivity measurements are shown in Figure 3.15 for the back to back case, for a 22 km and a 41 km of standard-SMF span length. There is no penalty observed for the 22 km case but in the 41 km case we observe a high penalty for the 1560 nm wavelength. The explanation for this penalty is found in the fact that we tune the device for best performance at 1545 nm (where no penalty is observed) and keep those settings to measure the other WDM channels. The VIPA based TDC does not include slope compensation and a fixed negative dispersion applies to all channels. Unfortunately as we increase transmission distance we obtain a higher spreading of the dispersion for the different channels, compensation with the VIPA still provides a residual dispersion as no slope compensation is provided. This residual dispersion has been calculated to be + 50 ps/nm for the 1560 nm wavelength and 41 km span for the settings of the VIPA at the moment of measuring the sensitivity penalty. If we observe the dispersion margin evaluation of Figure 3.14 we can

estimate that the penalty for a + 50 ps/nm de-tuning can be well above the 2 dB. This was further confirmed by re-tuning the device for best performance at 1560 nm with no signs of sensitivity penalty. Eye diagrams in Figure 3.15 are shown also for the compensation of a 62 km span using standard-SMF, where we can clearly observe the effects of no slope compensation in the device. We will expect future versions of the device to incorporate slope compensation as in [103].

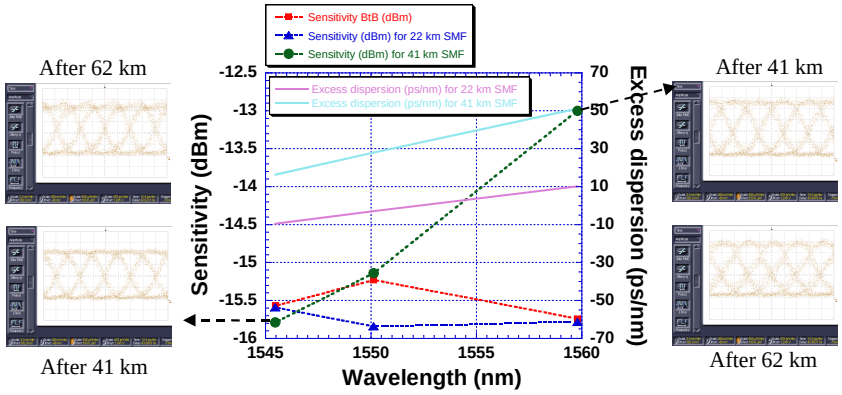

Figure 3.15: Characterization of the VIPA based TDC as a function of wavelength for a 22 km and a 41 km of standard-SMF transmission span. Eye diagrams are shown for the 41 km case and for a 62 km case at 1545 nm and 1560 nm. Penalties are measured at 10 Gb/s after OTDD from a 40 Gb/s signal. Horizontal scale in eye diagrams 12.5 ps/div. Vertical scale 500 μW/div.

3.3.3 Application of tunable dispersion compensation methods to practical systems

It is clear that including tunable dispersion compensation will induce changes in the system design. At first we have to consider how these devices will be tuned to provide best quality for transmission. If dispersion values are available from the network operator for the link a presetting of the TDC might be able to be done at the factory avoiding need for tuning in the field. A more friendly system should however be able to tune itself to the appropriate value of dispersion according to the span characteristics allowing for reduction in OPeration EXpenses (OPEX) for the network operator. Several methods have been investigated to provide dispersion monitoring integrated in a transmitter-receiver module, an overview of these methods is presented in Section 3.3.4. An important issue is where in the system we place the TDC unit. Due to the high

tolerance to high power levels of CFBG or the VIPA based tunable dispersion compensators we are able to situate them at points in the system where high power is available and increase the OSNR. This could mean that we place the TDC at the transmitter while the tuning information might be obtained at the receiver side. We need to ensure a feedback communication channel from receiver to transmitter to allow for the tuning. This channel might be the OSC in a WDM system, see Section 2.3, but for a single wavelength system we will need to add it to the framing structure of the returning signal.

It seems clear that for a single wavelength application the CFBG can be efficiently used. For a WDM multi-span system we could use a VIPA based TDC to final tune the dispersion of the link and DCF modules as span to span compensation. Still this requires that we have a very close to perfect slope compensation by means of fine tuning the DCF at the other links reducing considerably the tolerance of the system to dispersion. Moreover, as the free spectral range of the VIPA is 200 GHz we will need two devices for a 100 GHz spacing increasing system cost and complexity. It is clear that further work needs to be done in WDM dispersion compensation to provide an effective solution for dispersion and slope of dispersion compensation simultaneously for all WDM channels. A promising approach which allows for slope compensation is the use of all-pass filters using ring resonators [106, 107] or cavity filters [108, 109, 110]. To provide a complete picture of the dispersion of the WDM signal we might need to integrate a dispersion monitoring mechanism in the lowest and highest wavelength which could provide a value of the dispersion slope remaining to be compensated for. For application of TDC in a Metro WDM network we have two great advantages compared to WDM multi-span systems, first distances are shorter and reduce the dispersion slope de-tuning, second we use wavelength grouping to route channels from node to node. We might need only the tunable compensator at a node for the wavelength group leaving/entering the network while other channels will pass through a passive compensation. TDCs with reduced number of channels are possible to fabricate with CFBG technology [111] and are promising candidates for a metro WDM network application.

A very important parameter to consider from a TDC is the stability of the dispersion setting to external influences, e.g. temperature, vibrations or variations in the driving mechanism over time. It is important that component providers of TDC provide long term measurements of dispersion settings of the device.

We have looked in this section into optical dispersion compensators. However there is also an optional approach by using electronic dispersion compensation [112, 113] which is increasingly attracting more attention as available products

enter the market for 10 Gb/s modules [114]. Electronic compensation could reduce considerably complexity of the optical system design and reduce insertion loss budget of the system.

3.3.4 Dispersion monitoring for active compensation

Methods suggested in literature for the monitoring of dispersion which could be integrated in a transmitter-receiver module are: Phase to amplitude modulation induced in the transmitted signal [115], fading of in -band subcarrier tone [116], clock regeneration in NRZ and clock fading in RZ [117] and finally phase comparison of filtered clocks by vestigial-sideband filtering [118]. A comparison of some of the main properties of these methods is presented in Table 3.6. Data for the four first methods is based on an investigation by means of simulations and experimental work at 10 Gb/s carried out within a Master Thesis project (collaboration between Tellabs and the Research Center COM) by Martin N. Petersen [119]. Data for the last method is obtained from [118]. Scalability of all these methods should be possible into a 40 Gb/s system, and has been demonstrated for example in [120, 121].

	PM-AM conversion	Subcarrier in-band	Clock regenerator	Clock fading	PC of filtered clock
Equipment at Tx	Yes	Yes	No	No	No
Equipment at Rx	Yes	Yes	Yes	Yes	Yes
Induced penalty[1]	None	$< 0.5dB$	None	None	None
Max dispersion[5]	2000[2]	1500[3]	900[4]	700[4]	>1700
Influence of PMD	Low	Yes	Yes	Expected	No
Influenced by nonlinear effects	Low	Yes	Yes	Expected	Not described
Limited to modulation format	No	No	NRZ	RZ	No

Table 3.6: Main parameters of the most practical techniques of dispersion monitoring that could be implemented in a transmitter-receiver module. The four first methods have been investigated at 10 Gb/s in [119] while the last method is presented in [118]. PM-AM: Phase modulation to amplitude modulation. PC: Phase comparison. [1] For dispersion fully compensated in the link. [2] Dependent on phase modulation frequency and index of modulation. [3] Dependent on frequency of the carrier used. [4] When using only first part of power & dispersion curve to avoid possible double points. [5] Maximum dispersion for 10 Gb/s [ps/nm].

3.4 Dispersion tolerant modulation formats

As we mentioned in Section 3.1.2 attention within the research community has been directed to implement modulation formats, which can provide higher dispersion margins than those of NRZ modulation. This effort was originally intended for 10 Gb/s systems, but has evolved into 40 Gb/s systems. Modulation formats, which can increase dispersion tolerance compared to a traditional NRZ modulation are mainly: Single Side Band (SSB) modulation [69, 70], multilevel signalling [122], PSBT (also referred to as optical duobinary) [67, 68, 123] or chirped NRZ [33, 34]. The two first methods aim at the reduction of the optical bandwidth of the signal, which according to Equation 3.1 will reduce directly the maximum delay between components of the fiber induced by the dispersion. The chirping technique relies on inducing a frequency shift in the leading-trailing edges of the transmitted pulse, which counteracts the broadening induced by the dispersion of the fiber. The PSBT technique relies on both a bandwidth reduction, and also on creating a phase induced correction to the pulse broadening [67]. We focus in this Section on the last two methods due to their reduced complexity and promising results.

3.4.1 Pre-chirped NRZ modulation

Pre-chirp in NRZ modulation is a well established technique defined as a dispersion accommodation method for STM-64 transmission in ITU-T standards [13]. It generally requires the use of a dual drive Mach-Zehnder based modulator [33] where chirp can be adjusted by careful control of the amplitude of the signals applied. Advances in the design of modulators has allowed to predefine a chirp in single drive modulators (generally X-cut Lithium Niobate modulators) relaxing the matching requirements needed in a dual drive. The chirp parameter α relates the phase variations at the modulator output with the normalized power variations and is defined as [124]

$$\alpha = \frac{\left(\frac{d\theta}{dt}\right)}{\left(\frac{1}{2 \cdot P}\right) \cdot \left(\frac{dP}{dt}\right)} \tag{3.13}$$

Where θ is the phase and P is the optical power of the modulated pulses.

We evaluate the performance of chirped NRZ under dispersion by means of simulations both for a PIN and a preamplified receiver. We evaluate the effects of dispersion only by turning off all non-linear effects. Results of the dispersion margin comparing the sensitivity penalty induced for chirped NRZ with unchirped NRZ are shown in Figure 3.16, main parameters of the simulation are presented in Table B.2. We observe that it is true that we obtain a higher

margin for chirped NRZ for positive dispersion, but the margin towards negative dispersion is reduced to -17 ps/nm, is equivalent to 1 km of standard-SMF. Simply, the dispersion margin curve obtained for NRZ is shifted towards positive dispersion values. Simulated optical eye diagrams are shown for a dispersion of 80 ps/nm for comparison. The penalty for chirped NRZ is shown for a preamplified receiver, penalties are higher due to the signal dependent noise of this kind of receivers and the influence of ISI [125].

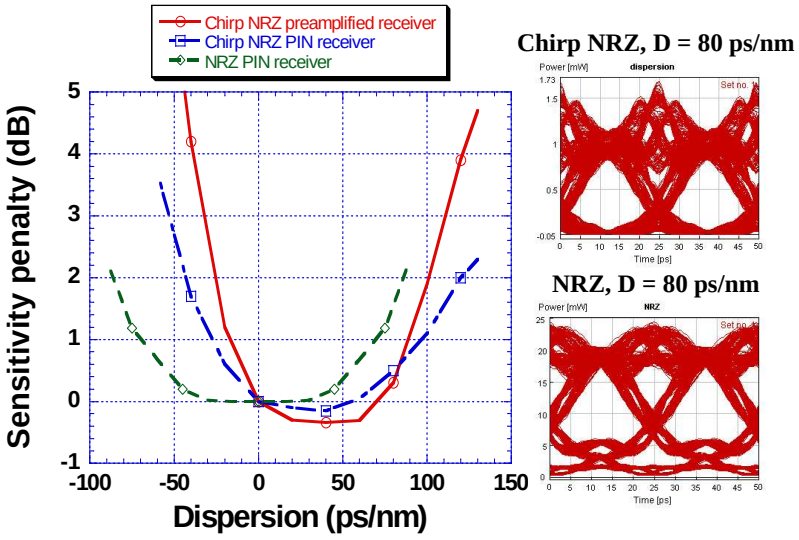

Figure 3.16: Simulated effect of dispersion in a chirped NRZ signal. The sensitivity penalty is shown as a function of the dispersion both for a PIN and EDFA preamplified receiver. For comparison results are shown for NRZ modulation and PIN based receiver. Eye diagrams for a dispersion of 80 ps/nm are shown both for chirped NRZ and NRZ.

If we consider transmission over NZDSF fiber and a dispersion margin for chirped NRZ modulation up to $+100ps/nm$ we could transmit maximally over 25 km of fiber. This will not be enough to cover the long haul application and we would in any case need dispersion compensation fiber. On the other hand if we use dispersion compensation fiber for a 40 km span the use of chirped NRZ will increase the effect of fiber tolerances for over compensation while relaxing those of under compensation. These kind of asymmetric performance is not desired in a system design. It is interesting to observe that if we have control of the chirp at the transmitter and can vary its sign keeping the same α value we will obtain a completely symmetric dispersion margin curve, but now the increased margin is obtained both for under- and over-compensation. This method has been shown for chirped RZ modulation in [126]. Controlling the

sign of the chirp we could obtain a dispersion margin of $\pm 100 ps/nm$ relaxing tolerances in the system design.

3.4.2 Optical duobinary or phase shaped binary modulation

Background and implementation

The PSBT or optical duobinary modulation has its origins in the modulation known as "duobinary" in communication theory [127], we will name it "traditional duobinary". This modulation is based on correlative coding, which tries to increase noise immunity of a transmitted signal by introducing a controlled level of Inter-Symbol Interference (ISI) between adjacent pulses. The building blocks of a theoretical optical duobinary transmitter based on the traditional duobinary method are presented in Figure 3.17. Duobinary modulation requires coding at the transmitter to create a two level signal. Moreover and in order to avoid error concatenation a pre-coder is introduced (usually a exclusive-OR gate). The three level electrical signal obtained as a traditional duobinary modulation is now applied to a Mach-Zehnder modulator setting the middle level at the lowest point of the transfer function while the first and third level will see the peaks. The optical signal will be a two level signal however the ones will carry information in the phase, where a π phase shift will be observed between a one originated from the first and the third level of the traditional duobinary electrical signal. An example of duobinary coding is shown in Figure 3.17 for clarity.

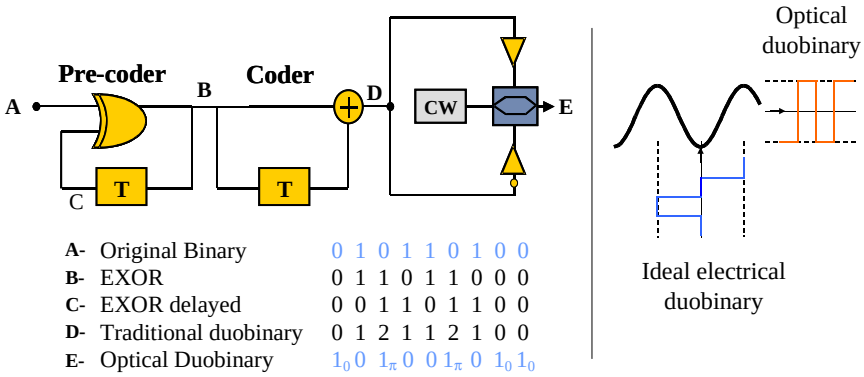

Figure 3.17: Schematic of the principle of optical duobinary or PSBT, building blocks and electrical to optical conversion in a Mach-Zehnder modulator.

The optical duobinary signal is an inverted copy of the original signal with a phase change in the ones when there is an odd number of zeros since the

last one transmitted. The phase information is not used at the receiver as the original data appears in the amplitude of the signal. Traditionally a dual drive modulator has been used at the transmitter to avoid chirp, which imposes even tighter restrictions than for NRZ in the symmetry requirements for the driving signals [128]. The complexity can be reduced substantially if we use a single drive chirp free Mach-Zehnder modulator [129]. No changes have to be introduced in a traditional receiver module to support optical duobinary modulation, only notice that the signal received is inverted.

A possible practical implementation of an optical duobinary transmitter is presented in Figure 3.18. Pre-coders using an X-OR gate have been demonstrated working up to 40 Gb/s [130]. A Bessel filter substitutes the coder and creates the three level signal. This substitution has shown to provide increased performance compared to the delay based coding [131, 132], an explanation following [67] is presented. The three level electrical signal can be observed in Figure 3.18 to be a fluctuating signal, which applied to the modulator creates zeros with a certain power level in the optical signal. When the *ones* try to broaden due to dispersion into the bit period where a *zero* travels they observe a signal with a π phase difference which cancels part of the broadening and keeps the *ones* from inducing a high ISI level.

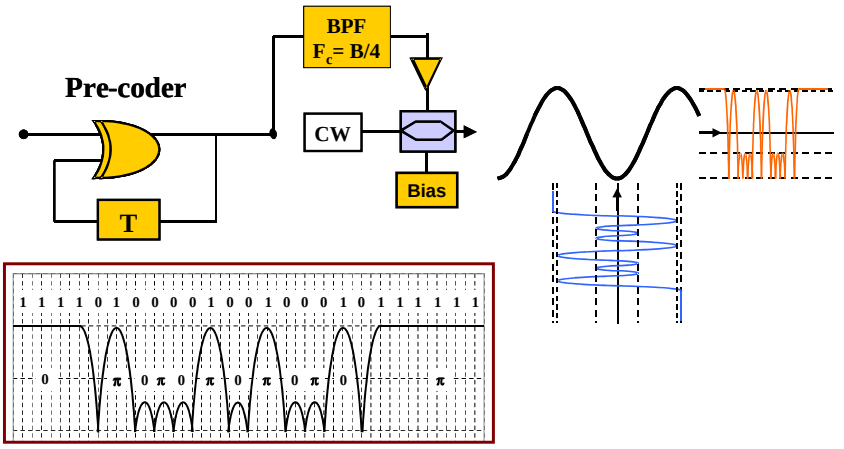

Figure 3.18: Practical implementation of the optical duobinary or PSBT modulation using a chirp free single drive modulator and a X-OR based pre-coder.

Dispersion tolerance

We have investigated the expected dispersion margins for optical duobinary modulation using a dual drive Mach-Zehnder modulator and a 11.2 GHz fifth order Bessel filter for a PIN and EDFA preamplified receiver. The sensitivity penalty as a function of dispersion can be observed in Figure 3.19. Please notice that we plot sensitivity penalty compared to the back to back of each case (modulation and receiver setting) and that for NRZ and PIN diode we obtain a sensitivity of -12.48 dBm compared to -11.6 dBm of optical duobinary, details on simulation parameters are shown in Table B.2. Simulated optical eye diagrams are shown for 90 ps/nm dispersion in NRZ compared to 150 ps/nm of optical duobinary. We can observe a symmetric dispersion margin of $\pm 200 ps/nm$, which nearly triples the NRZ dispersion margin.

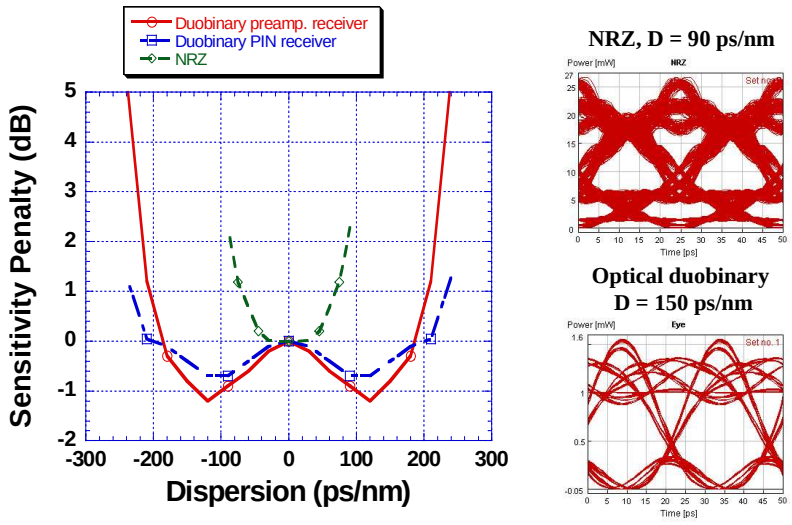

Figure 3.19: Simulated effect of dispersion in an optical duobinary signal. The sensitivity penalty is shown as a function of the dispersion both for a PIN and EDFA preamplified receiver. For comparison results are shown for NRZ modulation and PIN based receiver (0.9 dB better sensitivity than PIN receiver for duobinary). Eye diagrams are shown for 90 ps/nm NRZ and 150 ps/nm optical duobinary.

Unfortunately the OTDD based receiver requires very low zero levels to allow for BER measurements after demultiplexing. This has restricted the evaluation of optical duobinary dispersion margins to inspection of eye diagrams. We have built an optical duobinary transmitter set-up, see Figure 3.20, using an X-cut Mach-Zehnder Lithium Niobate modulator with a V_π of 5 V . The applied electrical signal is only equivalent to V_π and not twice as required, however

the reduced extinction ratio does not seem to affect the optical duobinary performance in terms of dispersion tolerance [133]. We can clearly observe how the optical duobinary eye diagrams after 12 km (204 ps/nm) are clear and opened, while already after 8 km NRZ eyes are completely closed. Experimental demonstration of a $\pm 190 ps/nm$ dispersion margin has been presented in [123] for example. It is important to mention that the back to back sensitivity degradation observed for duobinary compared to NRZ modulation can be greatly reduced with the correct receiver design [134].

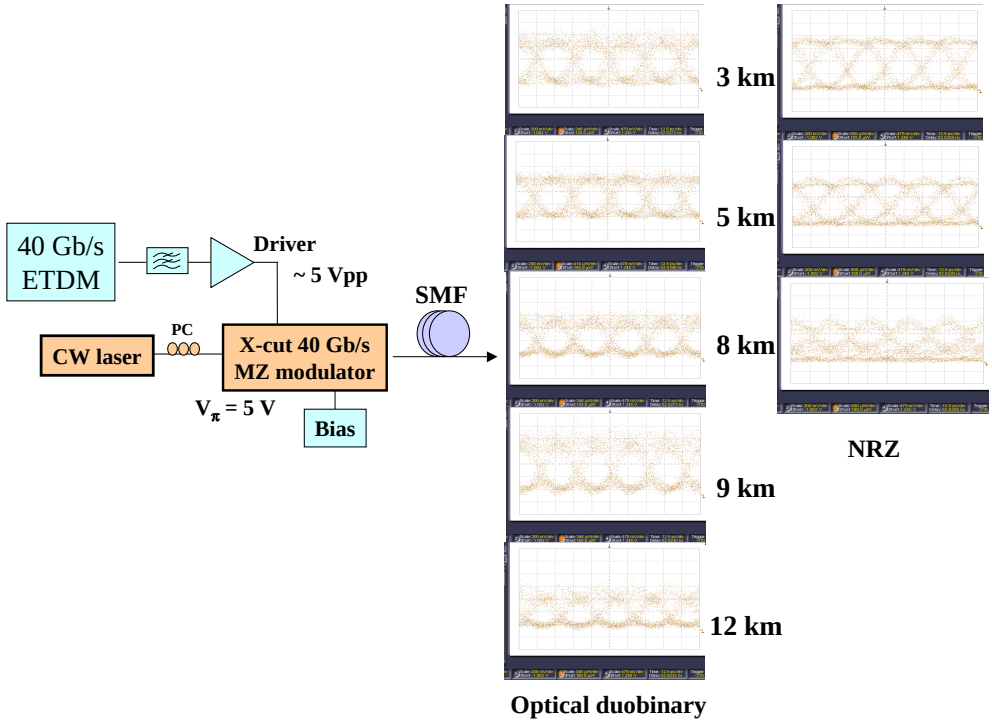

Figure 3.20: Experimental verification of the improvement of dispersion margin for optical duobinary modulation compared to NRZ. Eye diagrams are shown after 3 km, 5 km, 8 km, 9 km and 12 km of standard-SMF fiber. The amplitude of the electrical driving signal is 50% of V_π.Penalties measured at 10 Gb/s after OTDD from a 40 Gb/s signal. Horizontal scale in eye diagrams 12.5 ps/div. Vertical scale 500 μW/div for NRZ, 348 μW/div for NRZ.

We would like finally to sum up the advantages and disadvantages of optical duobinary comparing it to NRZ modulation. A clear advantage is that the increased dispersion margin will relax fiber and system design tolerances, moreover a short haul application over NZDSF fiber could be supported using

optical duobinary transmission. A second advantage is that even though we need to double the driving voltage the bandwidth of drivers can be fitted to the filtered signal and relax speed of electronic equipment at the transmitter. A third advantage, not presented previously, is the significant increased threshold to Stimulated Brillouin Scattering (SBS) as a carrier-less modulation [135]. A first disadvantage is clearly the reduction in sensitivity. A second disadvantage is the cost, complexity and Printed Circuit Board (PCB) space added by the pre-coder and filter to the transmitter design. We will consider again optical duobinary modulation in Chapter 6, where we investigate WDM systems and spectral efficiency.

3.5 Summary

In this chapter we have introduced the concept of chromatic dispersion in optical fibers and presented the main characteristics of the different transmission fibers that are available in the market. We have evaluated possible variations of dispersion in the fiber induced by the fabrication process or by temperature. The dispersion margin for a traditional NRZ modulated signal at 40 Gb/s has been evaluated to be as low as $\pm 70 ps/nm$, which requires careful tuning of dispersion compensation in any kind of link above the very short reach application. The different techniques used traditionally for fixed dispersion compensation: DCF modules, fiber Bragg grating based dispersion compensators or HOM DCF modules, have been presented and analyzed from a system design perspective.

The combination of the low dispersion margins allowed at 40 Gb/s, the dispersion variations induced by temperature and the tolerances needed to quote dispersion values of commercial fiber modules constrain considerably the design of commercial 40 Gb/s transmission systems. We find that a tunable dispersion compensator can be a necessary element for a 40 Gb/s commercial system.

The performance of two different methods of single wavelength tunable dispersion compensators based on chirped fiber Bragg gratings have been investigated experimentally. The first method uses control over the temperature gradient induced on grating to tune the dispersion. We could tune the device to minimize system penalty in a series of different transmission spans ranging from 21.5 km to 41 km of standard-SMF fiber. Tuning within this range provided a maximum sensitivity penalty of 0.8 dB. The second method uses controlled stretching of a non linearly chirped fiber Bragg grating as the dispersion tuning mechanism. We evaluated the performance of the device in a series of unrepeatered transmission spans ranging from 45.8 km to 103.8 km with a maximum sensitivity penalty of 2 dB, observed for the longest span.

We have tested a tunable dispersion compensator intended for WDM applica-

tion. The device is based on a combination of a VIPA and a three dimensional mirror which allows to tune dispersion within $\pm 700 ps/nm$ for 25 WDM channels spaced 200 GHz. The performance of the device is mainly limited by the lack of slope compensation which can clearly be observed if the residual dispersion overcomes the dispersion margin. Tunability of the dispersion slope is clearly a necessary function of a WDM tunable dispersion compensator if it wants to compete against a channel by channel compensator technique. To include dispersion monitoring in a transmitter-receiver module will allow for a stable self regulating control of the tunable dispersion compensation that could allow for long term stability of the system. The dispersion monitoring techniques that could be implemented in a transmitter-receiver module have been reviewed.

Finally alternative modulation formats that could relax the strict dispersion margin observed for NRZ have been reviewed. Two methods, the pre-chirped NRZ and the optical duobinary have been analyzed. It has been shown that even though we obtain an improvement of the positive dispersion margin to $100 ps/nm$ with the pre-chirp technique, the asymmetric shape of the dispersion margin curve limits the practical application in a commercial system if no chirp sign control is available. The optical duobinary modulation format allows to increase the dispersion margin up to $\pm 200 ps/nm$ improving considerably the system tolerances. However the complexity of the practical implementation for the optical duobinary transmitter should be carefully considered.

Chapter 4

Polarization mode dispersion and its compensation in 40 Gb/s systems

The purpose of this chapter is to analyze the limitations imposed by Polarization Mode Dispersion (PMD) in 40 Gb/s system design. Chromatic dispersion in a transmission link can be considered constant over time under small temperature changes. PMD on the contrary, is a randomly varying effect which needs to be treated statistically. These random variations can be observed not only in the time but also in the frequency domain. A link that today seems to be working under healthy conditions might perform tomorrow below the required quality due to worsened PMD situation in the link. PMD has been described as one of the main limiting effects for practical implementation of commercial 40 Gb/s optical transmission systems [136].

We initiate the Chapter by an introduction in Section 4.1 to PMD and the main concepts needed for a practical understanding of its characterization and influence in system performance. In Section 4.2 we analyze the penalty induced by PMD on a 40 Gb/s NRZ modulated signal and provide recommendations to single wavelength, WDM and metro system design. The main methods of PMD compensation are analyzed in Section 4.3, where we present the implementation and testing of a PMD compensator build at Tellabs. Section 4.4 provides an overview of PMD tolerant modulation formats focusing on RZ modulation. The Chapter finalizes with a summary.

4.1 Origins of polarization mode dispersion

In this section we will introduce the concepts of Polarization Mode Dispersion (PMD), Differential Group Delay (DGD) and Principal State of Polarization (PSP). We will review the main statistical properties of PMD to be considered in the practical implementation of high speed transmission systems and introduce the concepts of first- and second-order PMD. A more detailed description of PMD can be found in [137], for example.

4.1.1 PMD in optical fibers

A single mode fiber supports two degenerate modes of polarization. Any plane-polarized wave considered is composed of the linear combination of these two orthogonal degenerate modes. In principle, single mode fibers should be perfectly cylindrical and both modes should travel at the same speed. However, in a real fiber the core has an elliptical shape, which introduces a slight phase velocity difference between the modes, *birefringence*, acting as a two channel medium with the input data pulses being split and differentially delayed. Moreover, as the light travels along the fiber it encounters non-circular symmetric stresses such as bends and inhomogeneities that affect both polarizations differently; light can be coupled from one polarization mode to the other. The coupling is not constant in time once a fiber is installed. It is affected by random variations of stress introduced in the fiber by temperature variations or other environmental changes. Figure 4.1 illustrates the birefringence and the mode coupling in a fiber represented as a concatenation of birefringent sections. The pulse broadening induced in the pulse due to the delay between the polarization modes and affected by the mode coupling is commonly known as Polarization Mode Dispersion. In optical communication systems, transmission performance is seriously degraded when the pulse broadening induced by PMD becomes comparable to the bit period.

An important property of any transmission fiber is that we can always find two orthogonal states of polarization at the input of the fiber at which the optical pulses will appear undistorted at the output of the fiber. Formally, we define a Principal State of Polarization (PSP) as an input polarization for which the output state of polarization is independent of frequency to first order [138]. An important point to remember is that a pulse launched at a PSP will see distortion throughout the fiber but will be reshaped back to the original shape if observed at the output of the fiber. The orthogonality of the PSP makes them ideal to be defined as the polarization basis in which to decompose any polarization. PMD is usually quantified by the instantaneous Differential Group Delay (DGD) observed between the two PSP modes at the receiver end

of the fiber, $\Delta\tau$ usually expressed in picoseconds.

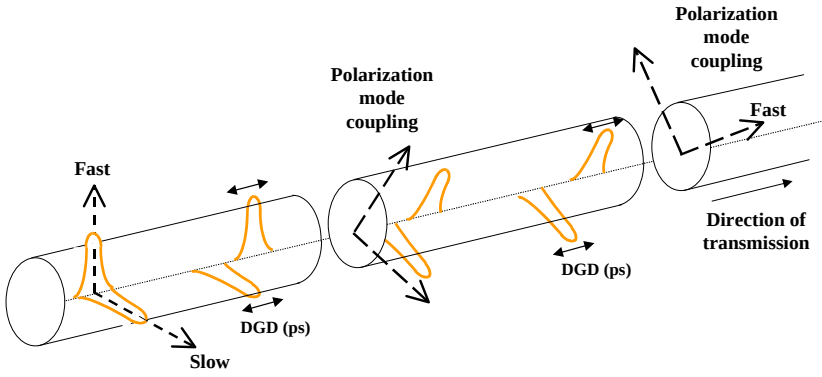

Figure 4.1: Illustration of the birefringence and mode coupling observed in a fiber.

The final pulse broadening is highly dependent on the amount of mode coupling existing in a particular fiber. We can difference two types of mode coupling [139]; weak mode coupling and strong mode coupling. Weak mode coupling is characteristic of Polarization Maintaining (PM) fibers and the mean DGD, $\overline{\Delta\tau}$, will increase linearly with the fiber length. Strong coupling is characteristic of transmission fibers with relatively long length ($>$ 1 km for cabled fiber) were the mean DGD increases with the square root of the length of the fiber.

The PMD of a fiber is traditionally specified by the square root dependence using the *PMD coefficient*, which we will represent by PMD_c, and is measured in $ps/\sqrt{km}$. Specified PMD coefficient in ITU-T standards set the maximum PMD coefficient of cabled fiber to be 0.5 $ps/\sqrt{km}$ [54]. This value is extremely conservative if we consider values specified in transmission fiber specifications. All fibers presented in Table 3.1 have a PMD coefficient below 0.2 $ps/\sqrt{km}$ and most transmission fibers sold today can be specified with a PMD_c below 0.1 $ps/\sqrt{km}$. Changes in PMD_c when the fiber is cabled can nowadays be kept very low. For example, maximum variations of 0.15 $ps/\sqrt{km}$ with low probability were observed in 45 dispersion shifted fibers of 20 km when the fiber spools where cabled [140]. The maximum PMD_c observed in this case for cabled fibers was below 0.25 $ps/\sqrt{km}$.

If we observe the instantaneous DGD of a fiber over time we will measure random variations. Statistically they follow a Maxwellian Probability Density Function (PDF) dependent only on the average DGD [141, 13] where the probability of obtaining an instantaneous DGD, $\Delta\tau$, for a certain average DGD is

given by

$$P(\Delta\tau, \overline{\Delta\tau}) = 32 \cdot \frac{\Delta\tau^2}{\pi^2 \cdot \overline{\Delta\tau^3}} \cdot \exp - \left(\frac{4 \cdot \Delta\tau^2}{\pi \cdot \overline{\Delta\tau^2}} \right) \tag{4.1}$$

As an example, we can see the PDF for a fiber with an average DGD of 6 ps in Figure 4.2 a). The accumulative probability of the PDF can be represented as a function of the average DGD providing a direct probability value of the instantaneous DGD being a certain number of times higher than the average DGD, see Figure 4.2 b). This accumulative probability is used in the design of optical transmission systems following ITU-T standards [13] and we will refer to it later.

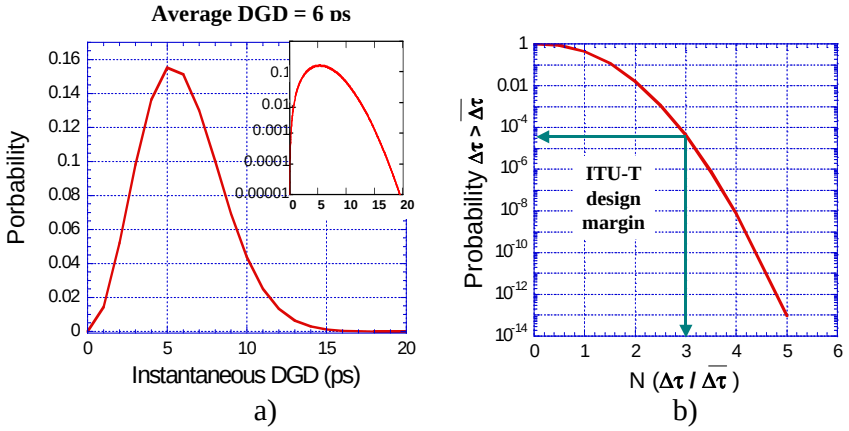

Figure 4.2: a) Example of Maxwellian probability density function observed for a fiber with an average DGD of 6 ps. The inset shows the logarithmic representation which is useful to appreciate the low order probabilities. b) Accumulative probability of the instantaneous DGD being N times higher than the average DGD.

The fastest fluctuations of PMD have been described to occur in the millisecond regime [142], however these fast changes can be followed by long periods of stability. They are presumed to be provoked by human induced variations on the position of fibers situated in the offices where the equipment is installed or induced vibrations in specific locations of the cable, for example cables situated close to railway paths. There is an observed difference in the fluctuations for an underground and an aerial cable, seeing faster variations for the last one [143], which can for example be induced by wind.

The fast variations are usually added to a slow variation, which follows temperature changes in surroundings of the cable [144]. Temperature variations have recently been suggested to be the dominant influence in very low PMD

fibers [145]. Fibers situated in the same physical path will follow similar temporal variations. This has been verified by measurement of the instantaneous DGD of two different fibers situated in the same cable over a 36 days observation [144]. The main conclusion from these investigations is that enough data exists to define the order of magnitude of time changes to be expected in the instantaneous DGD of installed cable links, which well might be an individual parameter for each situation.

4.1.2 First- order and second-order PMD

Observing the DGD of a fiber over a certain wavelength range shows a clear variation of the instantaneous DGD over wavelength. This wavelength/frequency variation of the DGD is also time dependent following a complex pattern [144]. If we study the statistic distribution of instantaneous DGDs for the different wavelengths and enough samples are taken, we will also observe a Maxwellian distribution. Consideration presented in the previous section of the variations of the DGD over time are included in the first-order PMD. Second-order PMD will include the frequency dependence of the DGD and the PSPs. Furthermore, this dependence can also be observed to be varying over time and second-order PMD should also be treated with a statistical approach. The PMD vector is defined as [146]

$$\overrightarrow{\Omega} = \Delta\tau \cdot \overrightarrow{q} \tag{4.2}$$

and defines first order PMD where $\overrightarrow{q}$ is the unity Stokes vector aligned with the fast PSP and $\Delta\tau$ as defined previously and following a Maxwellian PDF.

The second order PMD vector can be evaluated by direct derivation of the first order PMD with frequency

$$\overrightarrow{\Omega_w} = \Delta\tau_w \cdot \overrightarrow{q} + \Delta\tau \cdot \overrightarrow{q}_\omega \tag{4.3}$$

with the subscript w indicating differentiation with frequency. The main relation between the different terms of the second order PMD vector are shown for reference in Figure 4.3. Where $\overrightarrow{\Omega_{\omega II}}$ and $\overrightarrow{\Omega_{w\perp}}$ represent the parallel and perpendicular components of the second order PMD vector.

The first component in Equation 4.3 is parallel to the PMD vector and induces polarization-dependent pulse compression and broadening, which can be described by a change of the chromatic dispersion $D \cdot L$ (dispersion times the transmission length) of the fiber to an effective dispersion $(D \cdot L)_{eff}$ defined as

$$(D \cdot L)_{eff} = D \cdot L \pm \tau_\lambda \tag{4.4}$$

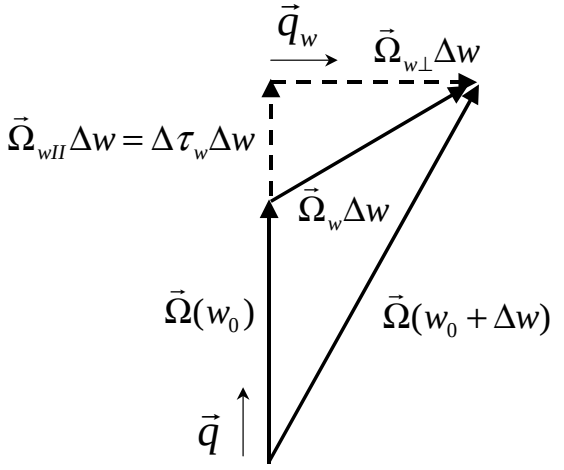

Figure 4.3: . Schematic diagram of the PMD vector, and the second-order PMD components showing their frequency dependence.

where τ_λ is related to $\Delta\tau_\omega$ by

$$\tau_\lambda = -(\frac{\pi \cdot c}{\lambda^2}) \cdot \Delta\tau_w \tag{4.5}$$

The second term in Equation 4.3 causes depolarization as a result of a rotation of the principal states of polarization with frequency, characterized by a rotation rate k defined as

$$2k = |\overrightarrow{q}_w| \tag{4.6}$$

and measured in ps equivalent to $mrad/GHz$.

The statistical characteristics of the different terms of the second order PMD vector have been carefully analyzed and measured in [146, 147, 148, 149, 150]. We will present here the main conclusions. The effect of the parallel term, which affects the chromatic dispersion is rather low, we will need to have a fiber with more than 12 ps average DGD to induce a dispersion of ± 50 ps/nm, which could be affecting a 40 Gb/s system. This would correspond to a 600 km fiber link with the highest allowed PMD coefficient of 0.5 $ps/\sqrt{km}$. The second order PMD vector is mostly influenced by the depolarization term [146]. The depolarization term is statistically related to the instantaneous DGD, high instantaneous DGD values will induce low rotation values of the PSPs, while high rotations can be observed for low DGD values [146, 149, 150]. A positive conclusion of the last effect is that there is a low probability of observing a high

instantaneous DGD and a high rotation of the PSPs[1].

An important property of the statistics of the second order terms is their scaling with the mean DGD [146]. The chromatic dispersion induced by the parallel term scales with the square of the mean DGD, while the depolarization scales linearly with the mean DGD.

Finally, an important concept to consider for WDM systems is the bandwidth of the principal states, $\Delta\omega_{PSP}$. It provides an approximate value of the frequency range over which the PMD vector can be considered constant and can be related to the average DGD in the 1550 nm region by the simple expression [137].

$$\Delta\omega_{PSP} = \frac{\pi}{4} \cdot \frac{1}{\overline{\Delta\tau}} \tag{4.7}$$

The bandwidth of the PSP for a system with an average DGD of 5 ps will for example be 25 GHz, which indicates that in a traditional 100 GHz spacing we can not consider the same variations of the PMD vector in two neighboring channels.

4.2 Effect of PMD on 40 Gb/s transmission systems

In this section we will first analyze the penalties induced by first- order and second-order PMD on an NRZ based 40 Gb/s signal. Secondly, we will try to provide a working frame for the system designer on the accumulated PMD on a multi-span system.

4.2.1 Analysis of penalty induced by PMD on a 40 Gb/s signal

First-order PMD can be easily emulated using polarization beam splitters to divide the input signal into two orthogonal polarizations and a variable time delay to induce the DGD. In order to induce a worst case situation, power should be equally distributed in both polarizations by control of a polarization controller, see schematic set-up in Figure 4.4. This set-up has been implemented both in a simulated and an experimental set-up at 40 Gb/s for NRZ modulation. Please notice that due to the time scaling of PMD, an average DGD of 16 ps will induce the same influence in a 10 Gb/s system as an average DGD of 4 ps in a 40 Gb/s system if we keep same pulse shape and relative rise-fall times. The horizontal axis is in this way independent of the bit rate if we consider it in relation to the bit period of the signal treated.

[1]For a complete study of the statistics of first- and second-order PMD the reader is highly recommended reference [137]

Results of the investigation are shown in Figure 4.4. Simulations have been carried out for a PIN and a EDFA preamplified receiver, see Table B.2 for details on parameters. Penalties are measured at a BER of 10^{-10}. The higher penalty observed when using the preamplified receiver is induced by the signal dependent noise of this kind of receivers, and has been analyzed in [151] as a function of the electrical filtering at the receiver. The experimental penalty observed is extremely high, but can be explained by the use of an OTDD receiver, which has been verified by simulating the OTDD receiver in Appendix D. Eye diagrams observed for 12 ps are opened and do not indicate the high penalty observed in the measurements. We have in addition verified this point by repeating the measurements for a 10 Gb/s transmitter/PIN receiver and applying the scaling principle, results are shown for comparison also in Figure 4.4. ITU-T recommendation [13] specifies an expected penalty induced by a DGD equivalent to 30% of the bit period of 0.5 dB for a PIN receiver and 1 dB for a noise dependent receiver.

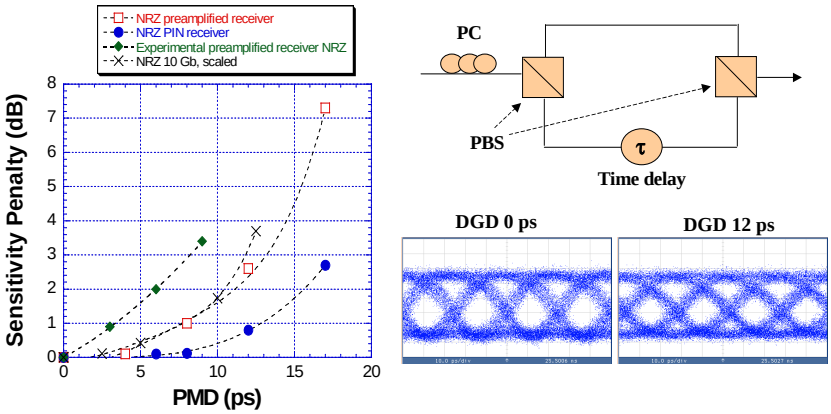

Figure 4.4: Analysis of penalty induced by first order PMD on a 40 Gb/s NRZ signal and schematic of 1st order PMD emulator. Sensitivity values are obtained for a BER of 10^{-10}. Optical eye diagrams are obtained from experimental investigation (time scale 10 ps/div).

Emulation of second order PMD is a complex issue whether it is by means of simulations or experimentally. The most common way of emulating the effect of PMD is by following its origins, mode coupling and birefringence. We model the fiber as a concatenation of birefringent sections, where each has a random differential group delay, which follows a Gaussian distribution with a mean value and a standard deviation. The coupling between each slice is affected by a random angle orientation of the birefringence axis following a white noise

distribution $(0..2\pi)$ [152, 153, 154]. This is the approach used in the commercial simulator used to generate the results in this chapter [155]. Experimentally we can emulate PMD the same way by for example concatenation of Polarization Maintaining (PM) fibers with certain DGD and an arbitrary angle in between them. There is a need of high count of PM fiber sections (> 15) and suggestions that the angle of rotation should be randomly set in order to emulate accurately PMD [156]. Throughout the rest of this section all results will be based on simulation of PMD in fiber by the described method.

The main effect of second order PMD is a statistical spreading of the pulse width broadening observed for a given set of equal instantaneous DGD samples. We present this phenomena by simulating transmission of a 40 Gb/s NRZ signal over a fiber with 9 ps average DGD, 1000 different PMD random settings of the fiber and evaluating the BER with the same noise included at the receiver in all cases. We compare the spreading of BER observed to the expected BER for an instantaneous DGD when emulating only first order PMD. Results can be observed in Figure 4.5 including optical eye diagrams observed for the same instantaneous DGD with different influences of second order PMD. Without any PMD the system is performing at a BER of 10^{-12}.

An interesting way of representing these BER spreading results is by means of the PDF of the BER. This method can also be applied to the Q factor [157]. The PDF will provide the probability of a system to be performing below a desired Q or exceeding a minimum BER when having into consideration both orders of PMD. Figure 4.6 shows in a) PDFs of the logarithm of the BER for 4 ps, 8 ps and 12 ps of emulated average DGD in the fiber when we force the system, by setting an attenuator at the receiver, to be working at the limit of sensitivity, providing a BER of 10^{-12}. The broadening of the PDF can be observed as a function of average DGD that induces probabilities in the 0.2 % order for a system under 8 ps PMD to have a BER of 10^{-4} instead of the expected 10^{-12}. In case b) we evaluate the effect of introducing a 3 dB power margin at the receiver before reaching the power which induces a BER of 10^{-12}. We can observe that for 4 ps average DGD in the fiber we do not observe any cases were the BER has been in the 10^{-12} area. However, for 8 ps average DGD it seems that there is a 0.2 % probability of providing a BER close to the 10^{-12}. For the 12 ps case it is clear that the 3 dB margin does not alter the probability of providing bit error rates in the 10^{-2} area. The accuracy of the results and the probability level that can be observed are limited by the number of repeated iterations applied in the simulations.

In previous simulated results we have considered an ideal receiver model where the best sampling point and threshold can be chosen for each received signal. However, this is not the configuration of a typical receiver were threshold

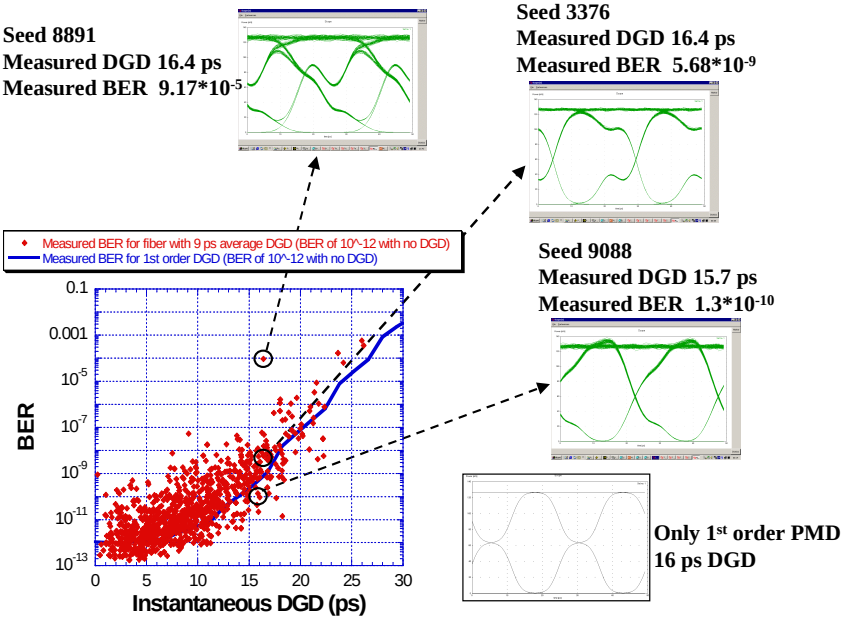

Figure 4.5: Example of the influence of second order PMD from a simulation of a 40 km standard-SMF fiber with an average DGD of 9 ps in a 40 Gb/s systems. The effect of first order is shown as a reference and eye diagrams at approximately same instantaneous DGD affected differently by second order PMD effects. We plot BER for the sample considered for 1000 different cases of the simulated fiber where the receiver is kept to provide same noise characteristics in all simulations. The general parameters used in the simulations can be found in Appendix B, Figure B.3.

is generally preset in factory and sampling time generally is set to the mid point of the bit period. We have investigated the effect of using a fixed sampling and threshold at the receiver and compared it to the ideal case. Results are presented in Figure 4.7 for four possible cases: optimum threshold and sampling, optimum timing and fixed threshold to best performance without PMD, fixed timing at 1/2 bit period and optimized threshold, and fixed timing at 1/2 bit period and fixed threshold to best performance without PMD. It would be ideal that the timing would be optimized for each situation, this has been suggested to occur automatically induced by the clock recovery circuit [158]. We would be left with a dynamical fine tuning of the threshold level which would provide best performance.

Unfortunately in a real situation we will have other factors affecting transmission at the same time as PMD. For example uncompensated residual chromatic dispersion. In [138] this effect was analyzed by means of the broadening factor.

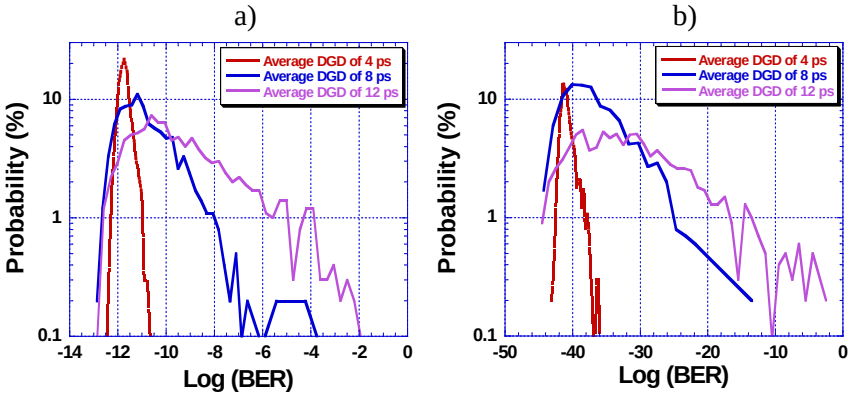

Figure 4.6: Probability density functions observed for a 40 Gb/s NRZ transmission over fiber with 4 ps, 8 ps and 12 ps of average DGD. a) When system is working in the limit of the receiver sensitivity for BER of 10^{-12}. b) When we allow a 3 dB margin in power budget for receiver working below sensitivity. The general parameters used in the simulations can be found in Appendix B, Figure B.3.

Evaluation of the Broadening Factor (BF) is another way of estimating the influence of PMD. It is defined as the relation between the Root Mean Square (RMS) of the pulse with PMD, σ and without PMD, σ_0 [154]:

$$BF = \frac{\sigma}{\sigma_0} \tag{4.8}$$

In Figure 4.8 we can observe how not only the average BF increases as a function of residual chromatic dispersion but also the distribution of samples broadens affected by second order PMD. The example is based on a fiber with average PMD of 5 ps and a pulse corresponding to a 40 Gb/s NRZ signal. This results point out that a system with not perfect dispersion compensation will suffer more from effects induced by second order PMD. The straight lines shows the BF for emulation of only first order PMD.

4.2.2 40 Gb/s system design taking PMD into account

PMD will affect transmission performance in a commercial system if it induces *out of service* (or *outage*) situations for the network operator. As it was described in previous sections, these situations are difficult to predict due to the statistical nature of PMD. The goal of the system designer is to minimize the probability that an out of service situation is observed in the system. ITU-T defines in [13] that a system should have a probability below $4 \cdot 10^{-5}$ to observe a 0.5 dB sensitivity penalty induced by PMD using a PIN based receiver or

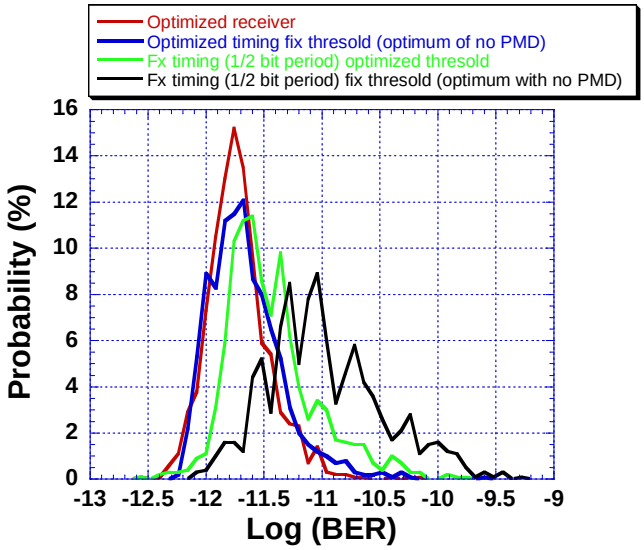

Figure 4.7: Probability density functions observed for a 40 Gb/s NRZ transmission over 40 km standard-SMF with 4 ps average DGD under different receiver configurations. Red trace: Optimum threshold and sampling; Blue trace: Optimum timing and fixed threshold to best performance without PMD; Green trace: Fixed timing at 1/2 bit period and optimized threshold, Black trace: fixed timing at 1/2 bit period and fixed threshold to best performance without PMD.

1 dB if a preamplified noise dependent receiver is used (e.g. EDFA or APD). These probabilities and penalties are interrelated by the statistics of PMD (only first order is considered), see Figure 4.2, and the expected penalty curves, see Figure 4.4. A penalty of 1 dB will appear in a preamplified receiver for an instantaneous DGD in the order of 8 ps and if it is required to observe this situation with a probability below $4 \cdot 10^{-5}$ we will need to ensure an average DGD three times lower than the instantaneous DGD. These considerations provide a higher margin to the total average DGD that can be observed in a link, in the order of 2.5 ps for a 40 Gb/s system using NRZ as the modulation format. The public acceptance of the $4 \cdot 10^{-5}$ margin is related to the debate regarding the time constant in the changes of PMD observed in a fiber or a system, Section 4.1.1. Furthermore, this approach considers that we are always in a worst situation regarding the PSP while this is not the case of a real system. If intervals between PMD changes in the order of one day are considered, only once every 70 years we will have an out of service induced by PMD (much higher than a normal life time of a system). On the other hand, if the fiber is for example aerial, changes might take place every minute [143] and as an average once ev-

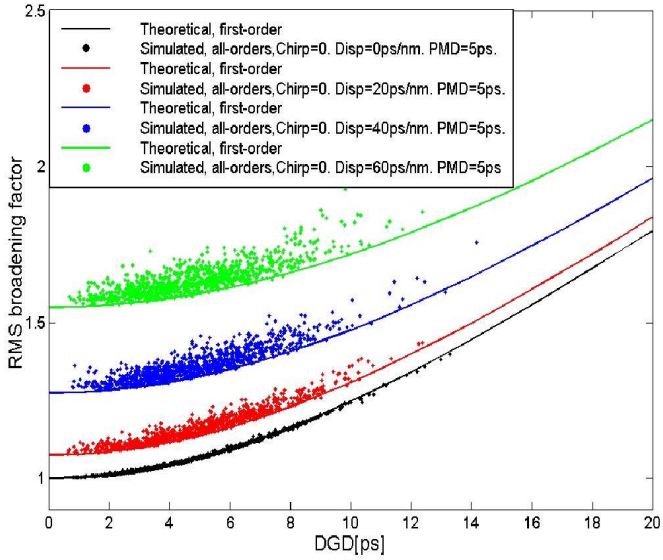

Figure 4.8: Influence of chromatic dispersion on the broadening factor induced by PMD. Residual chromatic dispersion considered 0 to 60 ps/nm, PMD considered in the link is 5 ps. Results appear courtesy of Thomas Tanggaard Larsen [138].

ery 17 days we will have an out of service situation induced by PMD. As the duration of the out of service situation are significantly different in both cases, one day against one minute, we will express the outage by using *minutes per year* or *minutes per life time*.

The average DGD observed from a fiber is known for a given *PMD coefficient* and fiber length, see Section 4.1.1. Average DGD observed for a concatenation of fibers can be calculated by quadratic summation [159]. However, other components have to be considered in a general optical transmission system, e.g. dispersion compensation modules, demultiplexers or optical amplifiers. The way in which the addition of the influence of PMD from different components has to be realized is an open topic and depends on the mode coupling we consider between components. We use in the following calculations the quadratic summation approach independently of the components included on the system. This will provide at least an order of magnitude for the limitations in the system design.

Let us look first at a single wavelength system in a very long haul application (120 km fiber). We would expect to have PMD contributions from the fiber, a tunable dispersion compensation (TDC) and an optical amplifier (EDFA). We

can write the total average DGD as:

$$DGD_{link} = \sqrt{(\sqrt{L} \cdot PMD_c(Fiber))^2 + PMD(EDFA)^2 + PMD(TDC)^2} \tag{4.9}$$

We can consider a typical average DGD from an EDFA to be in the order of 0.5 ps [160] and from a TDC 0.5 ps, see Section 3.3.1. For these values the maximum PMD coefficient allowed for the fiber would be 0.22 $ps/\sqrt{km}$, which is below the allowed 0.5 $ps/\sqrt{km}$. Even in a short haul application (40 km fiber) we will be limited to a maximum PMD coefficient in the fiber of 0.4 $ps/\sqrt{km}$ still below the allowed 0.5 $ps/\sqrt{km}$. However, as mentioned previously, the maximum allowed PMD coefficient in the fiber might not be a realistic value considering the actual state of the art in fiber design. Another approach is that the network provider has a detailed record of PMD for all fibers in the links where 40 Gb/s systems are to be installed. The fibers which are below the limits described above could be chosen to ensure good system performance.

A WDM system will be modelled as a concatenation of spans each including a transmission fiber of 80 km, an EDFA with average DGD of 0.5 ps and a fiber based compensation module (DCF) for 80 km with 0.9 ps average DGD [77]. We do not consider the influence of PMD in the multiplexer and demultiplexer as these components are not repeated in the system and due to their traditionally low values will not influence the results presented here. We do not consider the need of tunable dispersion compensation as we are aiming to provide a design frame. The average DGD of a full multi-span link is given by

$$DGD_{link} = \sqrt{N \cdot [(\sqrt{80} \cdot PMD_c(Fiber))^2 + PMD(EDFA)^2 + PMD(FDC)^2]} \tag{4.10}$$

where N represents the number of spans considered. This relation is represented in Figure 4.9 providing the maximum fiber PMD coefficient allowed for a number of spans considered given the maximum total average DGD of 2.5 ps. It is clear from this figure that serious limitations are induced by PMD in a multi-span link, in order to be able to transmit over 4 spans all the installed fiber should have a coefficient below 0.1 $ps/\sqrt{km}$.

Finally, we consider a metro network with 40 km span length between nodes. At each node we have an optical multiplexer and a demultiplexer,(Mx) each with 0.1 ps average DGD, an EDFA and a dispersion compensation module with 0.65 ps average DGD [77]. The average DGD of a full multi-span link is given now by

$$DGD_{link} = \sqrt{N \cdot [(\sqrt{40} \cdot PMD_c(Fiber))^2 + PMD(EDFA)^2 + PMD(FDC)^2 + 2 \cdot PMD(MX)^2]} \tag{4.11}$$

Results are presented in Figure 4.10 We can observe that the situation has improved slightly from the WDM design case as span length is reduced to 40

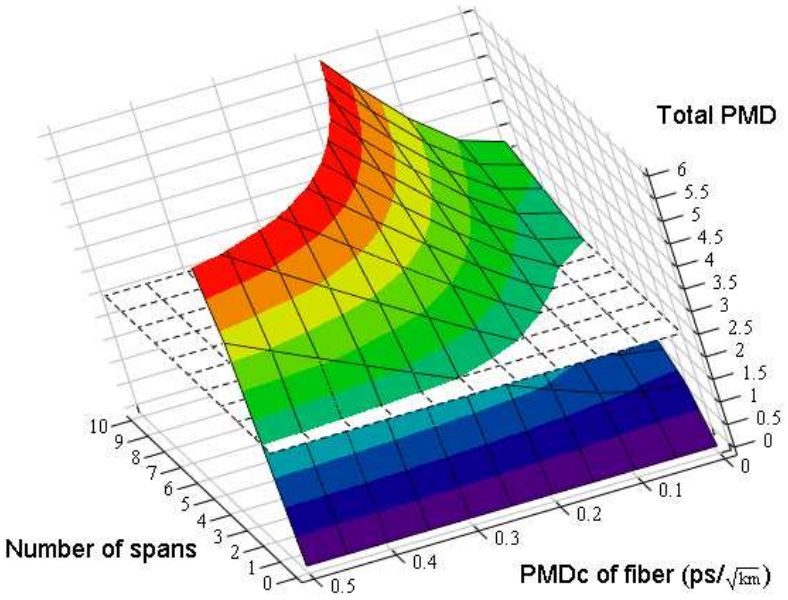

Figure 4.9: Design limitations induced by PMD in a 40 Gb/s WDM multi-span system design. We consider an average DGD in the EDFA of 0.5 ps and of 0.9 in the fiber based dispersion compensation modules. Span length is 80 km.

km. However, we still need a fiber PMD coefficient below 0.15 $ps/\sqrt{km}$ if we want to design a network where signals can be routed optically through four nodes or below the 0.1 $ps/\sqrt{km}$ through six nodes. These are still very tight margins for fiber PMD coefficient in a series of installed links.

It is important to notice that in a WDM system, not all channels will observe the same instantaneous DGD due to it statistical distribution. In the case of a WDM system designed out of the required PMD margins mentioned previously the probability that we observe an outage situation for all channels simultaneously is very small [161] . This is induced by the wavelength de-correlation of the PSP and the Maxwellian distribution observed for the instantaneous DGD in the different channels.

4.3 Compensation of PMD

Compensation of PMD seems necessary if we want to overcome the PMD limits in system design reviewed in the previous section. We review in this section the most promising methods for compensation and present the implementation

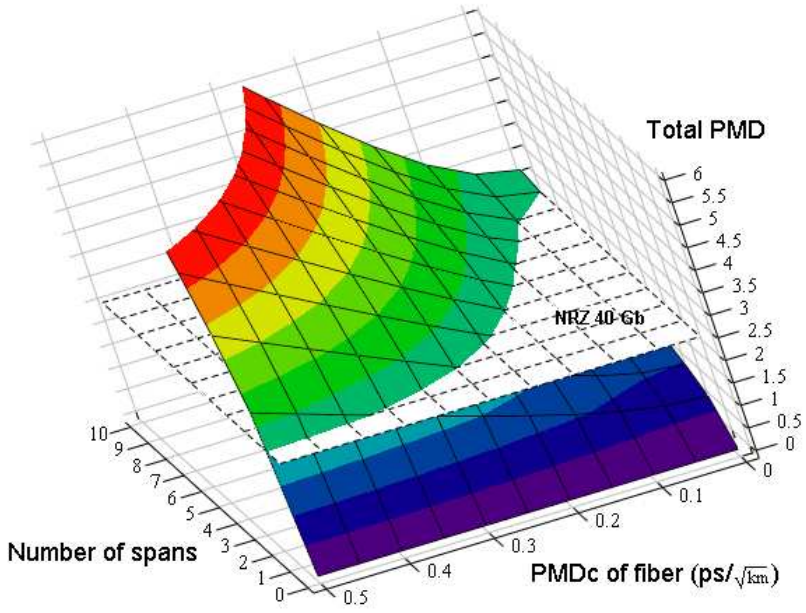

Figure 4.10: Design limitations induced by PMD in a WDM metro system design. We consider an average DGD in the EDFA of 0.5 ps, an average DGD in each multiplexer or demultiplexer of 0.1 ps and of 0.65 ps in the fiber based dispersion compensation modules. The span length is 40 km.

and characterization of an optical PMD compensator designed at Tellabs.

4.3.1 Overview of methods for PMD compensation

The methods which have been investigated to allow for PMD compensation can be separated into two main groups: optical PMD compensation methods and electrical PMD compensation methods.

Optical PMD compensation methods

An illustration of the most common optical PMD compensation methods is shown in Figure 4.11. The *PSP method* [162] uses a feedback channel to provide information from the receiver side on the PMD observed to tune a polarization controller at the transmitter in order to launch the signal into the actual PSP of the fiber.

The *fixed DGD* method [163, 164, 165] uses a High Birefringence (HiBi) element, usually a PM fiber, to compensate the observed instantaneous DGD

by setting an opposite fixed delay in the HiBi element. Control is needed to align the input state of polarization to the HiBi element with the fast-slow axis in order to obtain the desired delay. For an observed average DGD in the fiber link there is an optimum delay in the HiBi element for best performance of the compensator[138]. Actually, the fixed DGD method is usually operated in a second mode for fiber DGD values below the DGD of the compensating element [138, 166]. In this second mode the input polarization to the HiBi element is tuned in such a way that the PSPs of the grouping of the transmission fiber and compensator are aligned with the input state of polarization to the transmission fiber.

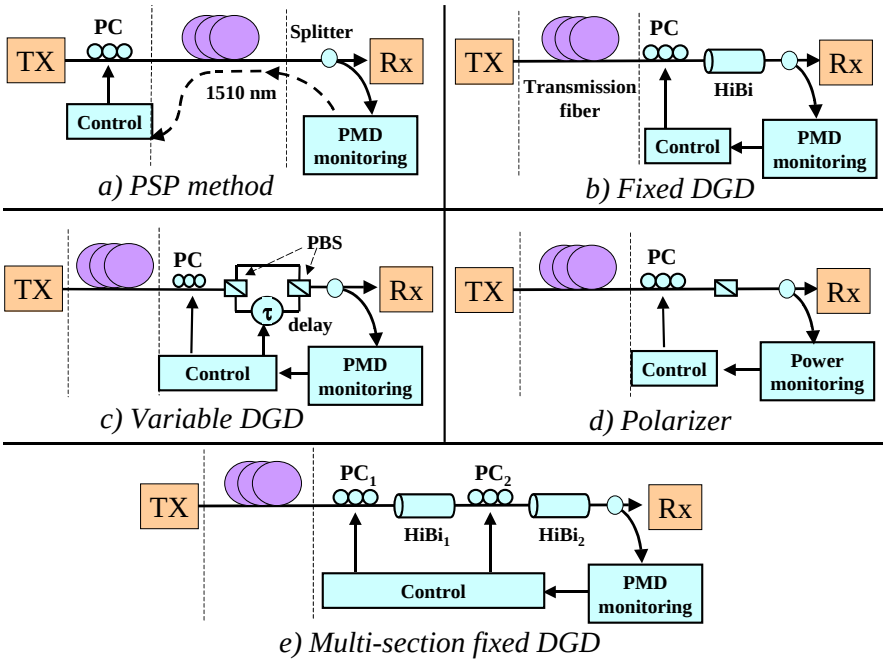

Figure 4.11: Illustration of the most common optical PMD compensation methods. Components characteristic of the compensation method are highlighted in blue. a) Principal state of polarization method, b) Fixed differential group delay (DGD) method, c) Variable DGD method, d) Polarizer method, e) Extension of method "b)" to a multi-section fixed DGD. PBS: Polarization Beam Splitter, HiBi: High Birefringence, PC: Polarization Controller.

The *variable DGD* method [167] uses a tunable delay line and allows to always set the compensator to invert the delay induced by the DGD in the fiber. There is a need to control two elements as the input polarization to the first polarization beam splitter has to be tuned also to allow for a correct splitting of the signal.

The *polarizer method* has been proposed in [168] as a simple method as it allows to control the polarization controller by a maximum power condition after compensation.

Finally, repetition of polarization controller and HiBi sections leads to the *multi-section fixed DGD method* [169, 170], which allows higher freedom to compensate over a broader fiber DGD range by optimum combination of the delays in the different HiBi elements. The drawback is the need for a more complex algorithm to control all the polarization controllers and the increase in the insertion loss with the number of elements.

PMD monitoring methods, which can be used in a practical system to control the different active elements of the compensator are mainly reduced to three: measurement of the Degree Of Polarization (DOP) of the received signal [166], measurement of the power in certain frequency components of the signal [169] and the use of a polarimetric error signal [171].

The basic characteristics of the optical PMD compensation methods mentioned above are presented in Table 4.1.[2] The tolerable average DGD in the link is obtained considering the tolerable average DGD after compensation to be a 10 % of the bit period and using the RMS of broadening factor of a pulse corresponding to an NRZ modulation in 1000 simulated samples as the success criteria [138]. The insertion loss is an estimate considering tolerances of available commercial components .

	PSP	Fixed DGD	Variable DGD	Polarizer	Two-section fixed DGD
Tolerable average DGD^1	25 %	25 %	26.5 %	21 %	27.5 %
Insertion loss $[dB]^2$	< 2	< 3	< 4	< 4.5	< 5
Number of elements to control	1	1	2	1	2
Need of feedback to Tx	Yes	No	No	No	No

Table 4.1: Basic characteristics of optical PMD compensators. [1] Tolerable average DGD of the link considering a tolerable average DGD observed after compensation of 10 %. Values are presented in a % mode relative to the bit period. [2] Insertion loss is an estimate taking into account commercial components.

[2][168, 172, 167] provide a detailed comparison of the methods presented and some experimental verification.

Electronic PMD compensation methods

The most extended technique in electronic PMD compensator is the use of Feed Forward Equalizers (FFE) and Decision Feedback Equalizers (DFE) [173, 174]. The FFE delays copies of the received signal and adds the copies with a specific weight for each sample optimizing the received signal quality. The DFE takes into account already made decisions to eliminate ISI in future bits arriving at the decision circuit. These mechanisms are the base for a commercial electronic dispersion and PMD compensator [113, 114].

The use of Forward Error Correction (FEC) as a way of increasing the margins of PMD is another approach investigated, but can be limited under long error bursts, which can originate from PMD in real link [175]. However, it has been demonstrated that FEC will provide a certain level of correction against PMD induced errors [176]. In [177] polarization scrambling was suggested as a valid method to avoid the long burst errors and allow for full FEC correction performance in the presence of PMD. An interesting combination is the use of FEC to control the electronic compensation using FFE and DFE techniques demonstrated in [178].

4.3.2 Optical PMD compensation by single fixed birefringence element

A PMD compensator has been implemented at Tellabs within the Master Thesis (collaboration between Tellabs and the Research Center COM) carried out by Thomas Tangaard Larsen [138]. The compensator is based on the *Fixed DGD* method described in the previous section, see Figure 4.11 b). It uses the measurement of the degree of polarization by a commercial component [179] to provide active feedback to control a Lithium Niobate based tunable polarization controller. The fixed DGD element is a PM fiber adjusted in length to the application being tested. The response time of the compensator was limited to 200 ms by the response time of the external power supplies used to control the different sections of the polarization controller. However the polarization controller by itself has a response time in the 100 ns scale and the sampling rate of the DOP is 5 KHz, which indicates that with an appropriate control circuit compensation could be done for the expected fast PMD changes in the 10 ms order [142].

The automatic control of the compensator was divided into two modes: scanning and tracking. In the scanning mode the polarization controller is tuned to cover all the possible states in order to find a total maximum DOP and in order to avoid being trapped in local maximums. Once the total maximum is found the compensator switches to the tracking mode, where each wave-plate of the

polarization controller is dithered to track any changes in the DOP observed and keep it at a maximum value. The scanning mode requires a period of time in which the PMD is stable for an optimum performance of the compensator.

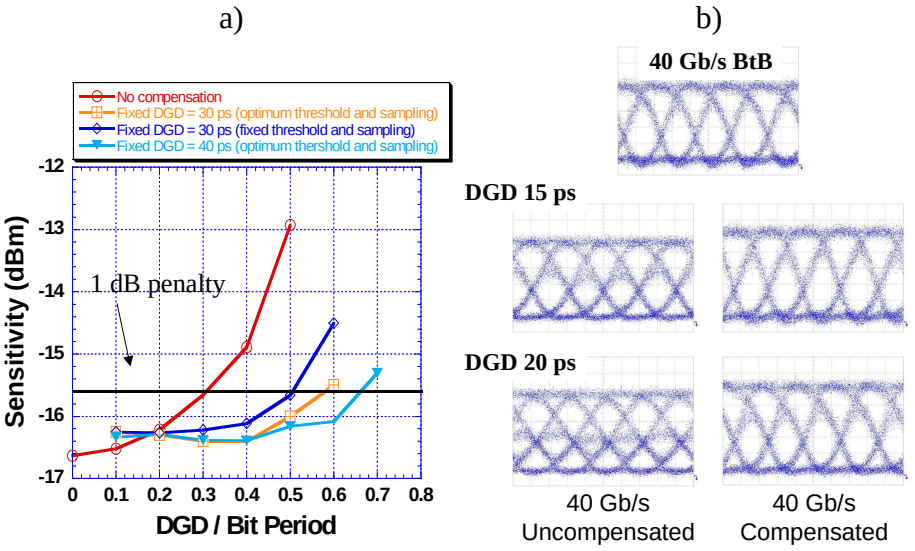

Figure 4.12: Experimental testing of Tellabs optical PMD compensator. a) Sensitivity measured at 10 Gb/s as a function of instantaneous DGD (expressed as a ratio over the bit period) under the following situations: 1) No PMD, 2) use of compensator with 30 ps and optimizing threshold and sampling, 3) use of compensator with 30 ps and no optimization in threshold and sampling, 4) use of compensator with 40 ps and optimizing threshold and sampling. b) Eye diagrams when used in a 40 Gb/s compensation set-up: horizontal scale 12.5 ps/div, vertical scale 165 $\mu W/div$.

The compensator has been tested using a first order PMD emulator following the principle described in Section 4.2.1, see Figure 4.4. Testing was conducted initially at 10 Gb/s where we could measure correctly sensitivity penalties in a commercial test-set. The transmitter is based on a chirp free Mach-Zehnder modulator (PRBS of $2^{31} - 1$) and a PIN based receiver with clock recovery circuit. The modulation format is NRZ and an EDFA was used in the system to compensate for insertion loss of the PMD emulator and compensator. Two different lengths of the PM fiber, corresponding to DGDs of 30 ps and 40 ps, were tested in order to verify simulated optimum lengths that could provide best performance. Testing results are presented in Figure 4.12. A sensitivity penalty of 1 dB has been taken as the success criteria in the analysis of the observed results. The emulator was tuned from 0 up to 70 ps of induced DGD with maximum distortion by tuning a polarization controller at the input and the

delay element. Without PMD compensator the maximum instantaneous DGD for 1 dB penalty was observed for 30 ps (0.3 DGD/Bit period). When using the 30 ps fixed DGD in the compensator the limit had shifted to 58 ps, which could be improved to 66 ps by setting the 40 ps fixed DGD element. A small penalty is observed at low DGD values (10 ps) when using the compensator, which might be induced by not setting the total polarization of the system totally aligned with the PSPs or by a slight OSNR degradation induced by the insertion of the compensator in the system. The total insertion loss of the compensator module was measured to be 6 dB induced mainly from a 3 dB coupler used as the splitter. A maximum instantaneous DGD accepted when using the PMD compensator relates to an average DGD of 22 ps if we want to ensure the $4 \cdot 10^{-5}$ ITU-T probability of obtaining the 1 dB penalty situation. These measurements were obtained for an optimized sampling and threshold point in each BER measurement. As mentioned in Section 4.2.1 it is interesting to evaluate the effect of no adjustment of the sampling and threshold at the receiver. The result is shown also in Figure 4.12 and reduced the allowed average DGD using a 30 ps DGD element from 58 ps to 51 ps even though a clock recovery circuit was used and should allow for certain sampling time optimization.

The compensator has also been tested at 40 Gb/s, but evaluation of the performance was here restricted to inspection of eye diagrams before and after compensation, see Figure 4.12 b). The fixed DGD element was now tuned to a PM fiber with a DGD of 9 ps. If we consider the eye-opening as the success criteria, we observed a reduction when using the PMD compensator to a 1 dB penalty (eye opening in the back to back operation is the 0 dB penalty point) for an instantaneous DGD of 17.5 ps. This value is equivalent to a 0.7 (DGD/Bit period) and fits the results obtained at 10 Gb/s. We would expect the PMD compensator to be able to compensate average PMD below 5.5 ps for a required $4 \cdot 10^{-5}$ probability of inducing a 1 dB penalty in a 40 Gb/s system. Figure 4.13 provides the design limitations in *span number* versus *fiber PMD coefficient* for the WDM system discussed in Section 4.2.2 when the maximum average DGD in the link has increased to the 5.5 ps limit allowed by the PMD compensator. A clear improvement is observed, however a five span system is still limited to fibers with PMD coefficients below 0.25 $ps/\sqrt{km}$.

Taking into account that the probability of having several channels of a WDM system observing a high instantaneous DGD in the link could be low we could share the use of the PMD compensator to reduce the overall outage time. A schematic of the proposed shared PMD compensation mechanism is presented in Figure 4.14. If one channel, C1, observes a high DGD (tracked by a performance monitor at the receiver side) it will be directed to the single wavelength compensator by tuning a wavelength add-drop multiplexer to the correct wave-

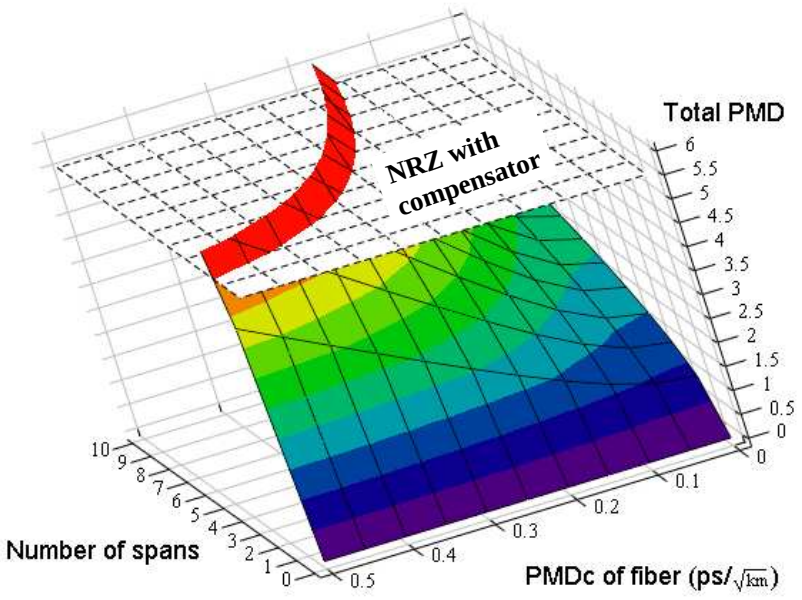

Figure 4.13: Design limitations induced by PMD in a 40 Gb/s WDM multi-span system when using a PMD compensator which allows a 5.5 ps average DGD in the link. We consider an average DGD in the EDFA of 0.5 ps and of 0.9 in the fiber based dispersion compensation modules.

length. When another channel, C2, observes a high DGD it will substitute C1 being compensated expecting that the instantaneous DGD of C1 has been reduced. Further work has to be done in estimating the probability functions for simultaneous multi-channel failure in a WDM system.

4.4 PMD tolerant modulation formats

Due to the complex mechanism of optical PMD compensation, it is interesting to evaluate tolerance to PMD of other modulation formats, which might allow to increase the margins in system design. Several articles have reviewed and compared the tolerance to PMD of NRZ, Return to Zero (RZ), Carrier Suppressed Return to Zero (CSRZ), Chirped Return to Zero (CRZ), Chirped Non Return to Zero (CNRZ) and optical duobinary [180, 181, 182, 183, 184].

The optical duobinary or PSBT modulation format provides a spectral reduction compared to NRZ and it is in this aspect where the improvement might arise from. It is however only under PMD compensation when this improvement

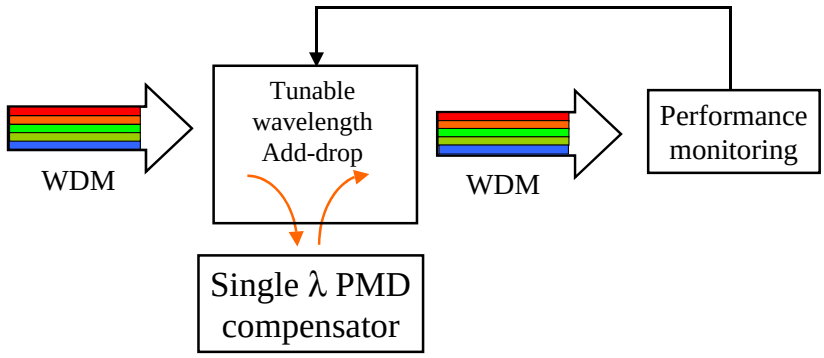

Figure 4.14: Schematic of proposed shared PMD compensator for a WDM transmission system.

is clearly observed [185]. RZ has been shown to provide increased tolerance with respect to NRZ [183]. Improvement is however dependent on the duty cycle of the optical pulses [180] and the design of the receiver used in the comparison [151]. Due to the asymmetry found in the chromatic dispersion tolerable margins, see Section 3.4.1 we do not consider chirped modulation formats. However they show an improvement in tolerance to PMD in comparison to their correspondent un-chirped formats [184]. CSRZ, which will be described in detailed in Chapter 6, has been shown to provide similar margins as traditional RZ [181]. We will keep the discussion in this section centered on the use of RZ modulation, presenting its practical implementation and PMD penalty margins.

4.4.1 Return to Zero modulation

We initiate this section by presenting practical implementation methods of a 40 Gb/s RZ transmitter. Following, tolerances of RZ to PMD will be discussed. In order to provide a fair comparison we also present chromatic dispersion compensation margins for RZ to provide a global picture of the advantages and disadvantages of the modulation format.

Implementation of an RZ transmitter

There are basically two methods of implementing a 40 Gb/s RZ transmitter, both are represented in Figure 4.15. The first method, a) in the figure, uses a 40 GHz pulsed laser directly as the light source to an electro-optical modulator, where information is added in a pulse per pulse basis. Promising 40 GHz pulse laser sources are actively mode-locked semiconductor lasers [186, 187] or

passively mode-locked laser based on saturable absorption [188]. The second method consists on carving pulses on a CW light source by using an electro-optical modulator while using a second modulator to add the information onto the pulses [126]. These two modulator based transmitter can be integrated into a single device and if Electro Absorption (EA) modulators are used it is possible to add a Semiconductor Optical Amplifier to compensate modulator loss [189].

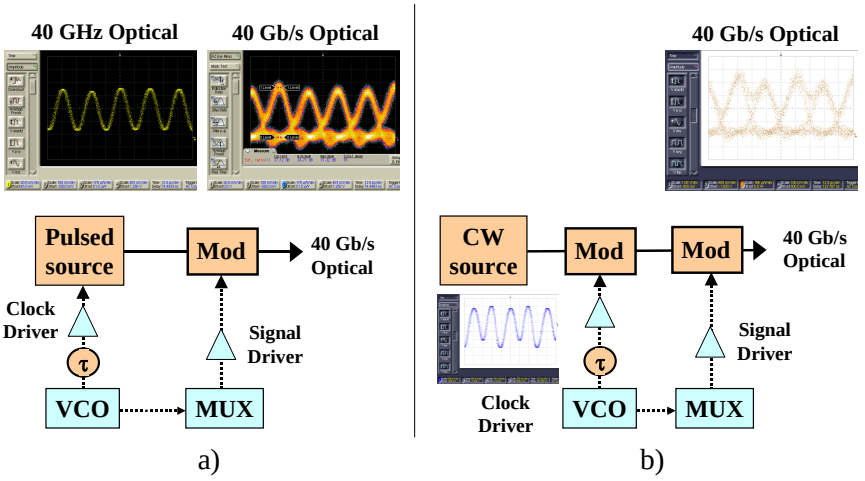

Figure 4.15: Illustration describing the two different methods which can be used as an RZ transmitter. a) Using a pulse source, eye diagrams are from a practical example using a passively mode-locked laser [188] . b) Using a CW laser source and a double stage modulation to create the pulses and modulate the data onto them. The example in b) is obtained from a tandem EA based modulator [189]. The difference observed in the time channels is directly related to the low quality 40 GHz signal generated experimentally.

The eye diagrams in Figure 4.15 show practical examples of RZ transmitters. In a) we use a device similar to the one described in [188] to generate a 40 Gb/s RZ signal. A main advantage of this device is its passive locking to the reference clock. High power, high frequency clock signals are complicated to generate and will introduce an additional cost in the transmitter. In b) we use a device similar to the one described in [189]. The quality of the 40 Gb/s optical signal is limited by the 40 GHz tone, which had to be implemented with frequency doublers and amplifiers from a 10 GHz tone. It is important to notice that there is a need to control the phase relation between the clock and the data signal in order to situate and keep the optical pulses at the right point in time in the modulation window.

Tolerance of RZ modulation to PMD

A main advantage of RZ over NRZ is its improvement in receiver sensitivity, usually in the order of 2 dB, induced by the higher powers in the "one" levels observed in RZ under an equal average power of the input signal to the receiver. However, sensitivity for RZ and NRZ are dependent on the bandwidth of the electrical filter placed at the receiver. In [180], where the electrical filter at the receiver was tuned for NRZ and RZ in order to provide optimum performance without PMD a clear advantage was observed when using RZ modulation. Average DGD acceptable with a 10^{-3} outage probability of having BER higher than 10^{-12} increased from a 16 to a 21 % of the bit period. However, a clear dependency on the duty cycle of the pulses was also observed. The tolerable average DGD increased from a 16 % of the bit period for a 20 % duty cycle to a 18 % of the bit period for a 40 % duty cycle. The probability density functions for the Q factor of NRZ and RZ modulation have been compared in [184, 190] showing both a reduction of the tails in the RZ PDFs and a higher average Q (related directly to the sensitivity improvement).

We follow a analysis similar to the one presented in Section 4.2.1 and results should be compared to those observed for NRZ in Figure 4.4. The transmitter used for experimental investigation uses a commercial PriTel fiber ring laser as the pulsed source and an optical filter to produce 9 ps FWHM pulses. The FWHM of the simulated optical pulses was 8 ps. First-order PMD is emulated both in simulations and experimentally by the polarization splitting and delay method explained previously.

The sensitivity penalty observed as a function of instantaneous DGD induced by the PMD emulator is show in Figure 4.16. Sensitivity improvement by use of RZ was 2.3 dB for a PIN diode and 2 dB for the EDFA preamplified receiver, see Figure B.4 for more details. A first observation of the results indicates that the penalty when using a PIN or an EDFA preamplified receiver is similar. The penalty when using a PIN receiver is worst than in the case of an NRZ signal, while better results are obtained for RZ when using a preamplified receiver. This might be explained [183] from the fact that higher ISI will be observed in NRZ for a similar DGD raising the level of the zeros. When using a preamplified receiver we must include noise from the zeros while the penalty for a PIN diode is simply related to the eye opening degradation. Relative eye opening degradation is higher in RZ than in NRZ while PMD induced ISI is lower in RZ than NRZ. We observed similar trends experimentally as with simulations, and we can estimate a 1 dB penalty for RZ for an instantaneous DGD in the order of 10 ps for a 32 % duty cycle generated pulse. We estimate from this margin that we can tolerate a 3.5 ps average DGD as the design limitation. If we apply this limitation to the WDM system analyzed in previous examples,

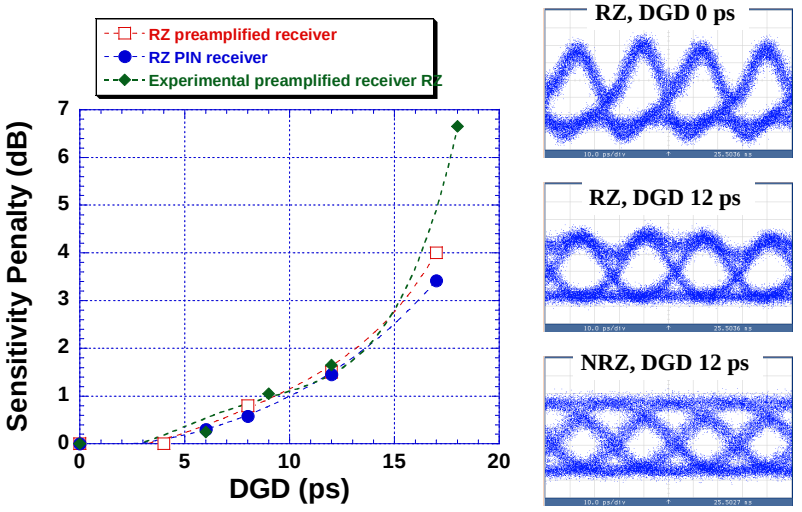

Figure 4.16: Analysis of penalty induced by first order PMD on a 40 Gb/s RZ signal. Sensitivity values are obtained for a BER of 10^{-10}. Optical eye diagrams are obtained from experimental investigation (time scale 10 ps/div).

we will observe limit in fiber coefficient around 0.15 $ps/\sqrt{km}$ for a 5 span system. Eye diagrams show in Figure 4.16 how the RZ signal evolves into an NRZ shaped, but eye diagrams are of higher quality than the NRZ case for the same applied DGD. However the improvement does not seem high enough to justify the introduction of RZ transmitter in a system just because of its PMD tolerance. An interesting effect to consider is that when using RZ modulation the optical PMD compensation methods described in the previous section are generally reduced in efficiency [138].

Tolerance of RZ modulation to chromatic dispersion

Shorter pulses need faster rise-fall time inducing a broadening in the spectrum of the optical signal generated. Broader spectrum will observe a higher delay between its components over a certain distance travelled in the fiber. This indicates first that RZ will have a reduced tolerance to dispersion and second that RZ signals generated with short low duty cycle pulses will even observe smaller tolerances. Simulated results are presented in Figure 4.17 for a PIN-preamplified receiver showing both effects. In a) we compare the dispersion margins of an NRZ to an 12 ps RZ signal. In b) Two different RZ signals, 9 ps and 5 ps, are compared. The 1 dB dispersion induced penalty is observed

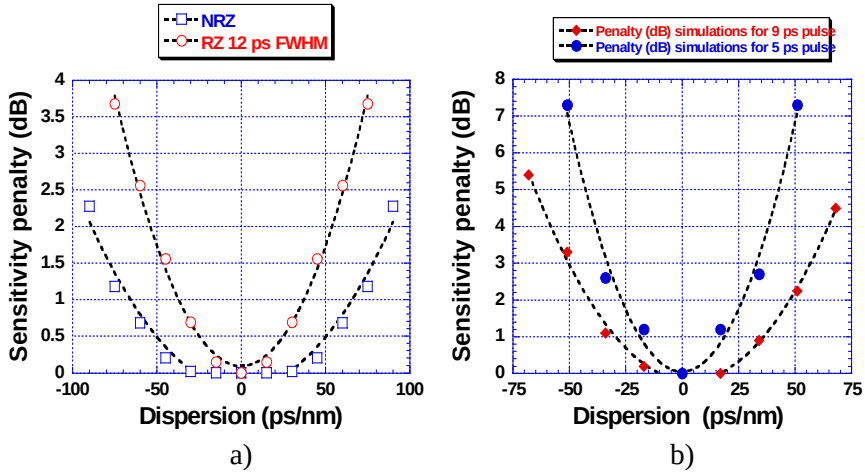

Figure 4.17: Tolerance of RZ modulation format to chromatic dispersion. a) Comparison of NRZ with 12 ps Gaussian pulses. b) Dependence of the duty cycle on the RZ dispersion tolerances. 9 ps and 5 ps Gaussian pulses are considered.

at ±38 ps for 12 ps pulses, at ±30 for the 9 ps pulses and at ±20 ps for the 5 ps pulses. If we recall the considerations presented in Sections 3.2.2 and 3.2.3 we can clearly understand that using RZ requires the use of tunable dispersion compensation even in the design of a short haul link.

4.5 Summary

In this chapter we have introduced the effect of polarization mode dispersion observed in optical fibers. We have briefly pointed out the main statistical parameters to consider in system design taking PMD into account. The effect of PMD can be separated into a first order and a second order approximation. While first order PMD in its worst situation can be easily emulated, second order PMD requires complex experimental set-ups or simulation models. The effect of PMD can only be considered completely by following a statistical approach, emulating a high number of fiber situations and observing the distribution of the BER or Q at the receiver to indicate an outage probability. We have shown how this outage probability will depend on the receiver characteristics, dispersion in the fiber or the margin allowed in the system.

If we consider 2.5 ps of average DGD in a link as the system design limitation we will not be able to comply even with a short haul application code for the allowed 0.5 $ps/\sqrt{km}$ fiber PMD coefficient in the ITU-T recommendations. A

four span WDM system will be limited for example to the use of fibers with PMD coefficients below 0.1 $ps/\sqrt{km}$.

These considerations indicate that there will be a need to have some kind of PMD compensation in the system if we want to be compliant with actual recommendations. We have reviewed optical and electronic methods of PMD compensation. A dynamic PMD compensator has been implemented following the method of fixed DGD element and tested at 10 Gb/s and 40 Gb/s. We estimated that average DGD allowed before compensation increases to 5.5 ps. This new margin will allow a five span WDM system to be implemented over fibers with PMD coefficients below 0.25 $ps/\sqrt{km}$.

PMD tolerant modualtion formats have been reviewed and RZ modulation has been introduced. We have investigated the PMD margins for this modulation format and found that we could allow for an average DGD of 3.5 ps for pulses with a 32 % duty cycle. The increased PMD tolerance does not seem to justify by itself the use of RZ as the modulation format.

Finally we have proposed a shared WDM PMD compensator as a practical way to reduce cost in the implementation of future 40 Gb/s systems.

Chapter 5

Optical power budget in 40 Gb/s single channel transmission

This chapter is dedicated to the investigation of optical power related limitations in the design of 40 Gb/s single channel transmission systems. We will analyze the limitations in multi-span systems by means of simulations and several experimental investigations. The goal of this analysis is to provide final parameters needed in the design of single wavelength application codes and to provide the guidelines for power budgets, which can be later used in WDM systems. In the simulation model we will consider a system free of residual chromatic dispersion and PMD. In the experimental verification we will refer when necessary to the design limitations induced by chromatic dispersion and PMD which have been presented in the previous chapters.

The chapter starts with a description of the main limitations we will observe in system design which are related to the power budgets: receiver sensitivity, optical signal to noise ratio limitations and self phase modulation induced distortion. In Section 5.2 we will investigate limitations for NRZ modulation in transmission over standard-SMF and NZDSF fibers. Section 5.3 is dedicated to RZ modulation. We will investigate performance of two different RZ transmitters in the same scenarios as used for the NRZ transmitter and compare their performance. Optical duobinary modulation is investigated in Section 5.4. Based on the simulated results obtained we propose in Section 5.5 simple design rules for estimating maximum span count in the design of a system. The chapter will finalize with a summary.

5.1 Optical power related limitations in a single channel system

Let us consider first a single channel/single span system where our goal will be to allow for longest link distance without the need to use any in-line optical amplifiers. We can reduce the design parameters related to the optical power budget to two: maximum power we can launch and minimum we can receive. Combinations of these parameters will provide different system performance.

Due to noise inherent in the optical to electrical conversion at the receiver a minimum optical power is needed at the input of the receiver to ensure a certain level of performance. *Receiver sensitivity*, recalling the definition presented in Chapter 3, is defined as the optical power needed at the input of the receiver to ensure a certain signal quality. Usually we will provide a value for the receiver sensitivity that ensures a specific BER, for example 10^{-12}.

The maximum power will seem to be limited only by the power we can achieve from the transmitter. Unfortunately the refractive index of the fiber is non-linear and induces a non-linear phase shift in the pulse for high power optical pulses. The varying phase can be considered as a varying instantaneous frequency across the pulse, also called chirp. This effect is known as Self Phase Modulation (SPM) and will be the limiting factor on the maximum optical power launched into the fiber in single channel transmission systems [191].

Let us now consider a multi-span system with optical in-line amplifiers. These amplifiers provide gain to compensate for the span loss, but add also a certain level of noise to the signal. The receiver will see this noise as an additional noise to the detection process and in order to observe the same 10^{-12} BER we will need to increase the optical power reaching the receiver. The difference between the power needed to reach the receiver in order to observe a certain BER and the receiver sensitivity is known as *sensitivity penalty* in this case induced by the increased noise level.

The power penalty observed in the receiver sensitivity is directly related to the Optical Signal to Noise Ratio (OSNR) when low optical power levels are launched into the transmission fiber. For high optical power levels launched into the transmission fiber the sensitivity penalty is related to the SPM, which also accumulates with the number of spans. We will traditionally see *bathtub* shaped curves when plotting the sensitivity penalty as a function of launched power into the transmission fiber. Figure 5.1 illustrates the reduction of the power margin as a function of the span number induced by the accumulation of OSNR and SPM induced effects.

In the following we present design rules and considerations in 40 Gb/s system design related to the receiver sensitivity, the optical signal to noise ratio and

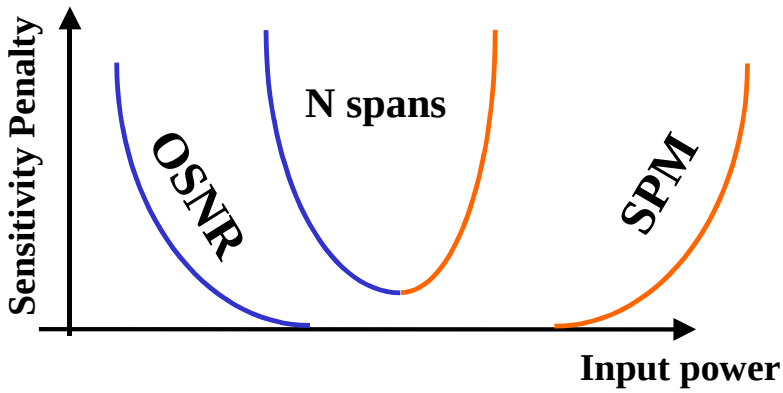

Figure 5.1: Illustration of the curves expected when plotting the sensitivity penalty versus the launched power into the transmission span for a multi-span system.

self phase modulation.

5.1.1 Sensitivity of 40 Gb/s receivers

Receiver characterization is a complex topic, depending not only on the receiver itself but also on the electronic circuits used for the clock recovery and decision gate that provides the BER. We provide an estimate of expected sensitivity values for different 40 Gb/s receiver configurations according to published examples. All sensitivities mentioned are for NRZ modulation.

For a PIN diode followed by an electrical preamplifier we would expect to reach sensitivities in the order of -12 dBm for BER of 10^{-10} [192]. However the state of the art commercial PIN-amplifier modules specify a sensitivity of -9 dBm for a BER of 10^{-10} [193].

It has only been recently that avalanche photodiodes (APD) have demonstrated a performance indicating that they can be used as 40 Gb/s receivers [194]. The device provided a sensitivity of -19 dBm for a BER of 10^{-10} and allowed multiplication factors of 10.

Optically preamplified receivers increase the complexity of the receiver design but allow for a substantial increase in sensitivity. Traditional EDFA based preamplified receivers followed by PIN-amplifier front-end can provide sensitivities in the order of -27 dBm [195]. A new trend at 40 Gb/s is to integrate a Semiconductor Optical Amplifier (SOA) with the PIN-amplifier front-end. This has been proven as an effective method to provide a compact device with

-17 dBm of receiver sensitivity for BER of 10^{-10} [196]. The main limitation of a SOA preamplified receiver is the higher noise figure compared to an EDFA preamplifier (traditionally 7 or 8 dB of noise figure for a SOA).

5.1.2 OSNR observed at the receiver

We can consider that the noise reaching the receiver in a multi-span system originates from the in-line optical amplifiers and that it accumulates linearly. The Amplified Spontaneous Emission from a single amplifier is given by [197]

$$P_{ASE} = 2 \cdot n_{sp} \cdot (G-1) \cdot h \cdot \nu \cdot B_o \tag{5.1}$$

where n_{sp} is the spontaneous emission factor of the amplifier, G is the gain, $h \cdot \nu$ the energy of a photon at frequency ν, and B_o the optical bandwidth considered, in Hertz. The noise figure of an optical amplifier, F is related to n_{sp} by

$$F = 2 \cdot n_{sp} \cdot (1 - \frac{1}{G}) + \frac{1}{G} \tag{5.2}$$

If we consider high gain values in the amplifiers and an average launched power into the transmission spans, P_L we can estimate the OSNR after a number N of spans to be

$$OSNR = \frac{P_L}{F \cdot G \cdot h \cdot \nu \cdot B_o \cdot N} \tag{5.3}$$

where the gain of the amplifiers will be equal to the span loss L, and all spans are considered to have equal span losses. Turning the expression into a logarithmic representation the OSNR evolution in a multi-span system can be described by the following expression [15]

$$OSNR(dB) = P_L(dBm) - L(dB) - F(dB) - 10 \cdot Log(N) - 10 \cdot Log(h \cdot \nu \cdot B_o) \tag{5.4}$$

where $10 \cdot Log(h \cdot \nu \cdot B_o)$ is -58 dBm in the 1.55 μm band and for 0.1 nm optical bandwidth.

The OSNR needed at the receiver to observe a Quality factor Q (in a linear scale), is related to the extinction ratio of the transmitted signal r, the optical (B_o) and the electrical bandwidth (B_e) at the receiver by [197]

$$OSNR_R = \frac{Q^2 \cdot B_e}{B_o} \cdot \frac{1+r}{(1-\sqrt{r})^2} \tag{5.5}$$

if we consider ASE the main source of noise. When increasing the bit rate by four from 10 Gb/s to 40 Gb/s we will traditionally increase the electrical bandwidth also by four. If we require the same Q for both systems we clearly

need a 6 dB higher OSNR at 40 Gb/s than at 10 Gb/s. We could compensate for the need of higher OSNR by launching higher optical powers, but this will increase on the other hand the SPM effect.

There are two methods that allow to avoid OSNR limitations in the system design: Forward Error Correction, which relaxes OSNR requirements, and distributed Raman amplification, which reduces the rate at which OSNR degenerates in the systems.

FEC was introduced in Section 2.3.2 as a way to reduce the Q needed at the receiver to provide a certain BER. If we consider Equation 5.5 in a logarithmic scale we can observe the direct relation between improvement of Q and the improvement in OSNR both measured in dB. For out-of-band FEC methods the coding gain obtained from FEC should include the bandwidth increase needed to accommodate for the coding, from 40 Gb/s to 42.8 Gb/s when using Reed-Salomon FEC for example, the parameter typically used is the *net coding gain*.

Distributed Raman amplification [198] uses the transmission fiber traditionally in a backwards pumping scheme to overcome the attenuation in the last part of the span and increase the minimum average power in the link. The final effect of Raman amplification is an improvement in OSNR observed at the receiver. This improvement is dependent on the gain obtained from the Raman amplifier and the effective noise figure of the amplifier. The gain is dependent on the type of fiber used as amplification media [199, 200]. The concept of effective noise figure of a Raman amplifier is presented in Appendix E. We use Raman amplification in an experimental set-up presented in Chapter 6 dedicated to WDM systems.

5.1.3 SPM induced limitations

The dependence of the refractive index of silica on the optical power can be expressed as

$$n = n_0 + n_2 \cdot \frac{P}{A_{eff}} \tag{5.6}$$

where n_2 is the nonlinear-index coefficient with an approximate value for silica fibers of $3 \cdot 10^{-20} m^2/W$ and A_{eff} is the Effective Area (EA) of the fiber considered and which depends on the design. Standard single mode fibers have an EA in the order of 80 μm^2 while NZDSF have a lower EA and become more sensitive to non-linear effects, see Table 3.1.

The nonlinear coefficient γ is defined as

$$\gamma = \frac{n_2 \cdot \omega_0}{c \cdot A_{eff}} \tag{5.7}$$

where ω_0 is the optical carrier frequency of the pulse.

The effective length, L_{eff} is defined as the length over which the power decreases by a factor of e in transmission fibers and related to the attenuation α and the total length L by

$$L_{eff} = \frac{1 - exp(-\alpha \cdot L)}{\alpha} \tag{5.8}$$

Self phase modulation can be understood as a broadening of the signal spectrum $\Delta\omega$ which is related to the nonlinear coefficient of the fiber, the shape of the pulse and the effective length by

$$\Delta\omega = -\gamma \cdot \frac{dP}{dt} \cdot L_{eff} \tag{5.9}$$

A first consideration from the last expression is that narrower pulses characteristic of higher bit rate systems will experience a higher spread of optical frequencies due to SPM. A second consideration, is that ideally if no chromatic dispersion is present in transmission and no optical filtering is included, there will be no SPM induced system degradation. Without dispersion it is not possible to obtain a conversion of the phase modulation into intensity modulation and pulses will not see any alteration in the time domain. At higher bit rates dispersion broadens the pulses faster reducing the peak power and the SPM effect. The interaction between SPM and dispersion is complex but we can estimate the dominant term by comparing two parameters; the *dispersion length* L_D and the *non-linear length* L_{NL}, these parameters are expressed as

$$L_D = \frac{T_0^2}{|\beta_2|} \tag{5.10}$$

$$L_{NL} = \frac{1}{\gamma \cdot P_0} \tag{5.11}$$

where T_0 is the half width at the $1/e$ intensity point and P_0 is peak power of the pulse.

SPM is the dominant effect when $L_{NL} << L_D$ while dispersion is the dominant effect when $L_D << L_{NL}$. These definitions fit directly for an RZ modulated signal as we always have the same pulse shape in transmission. For NRZ modulation we can consider them directly for single ones and for Gaussian fall/rise times. In long sequences of ones the effect of SPM will be observed in the first and last bit, in the rising and falling edges while no effect should be observed throughout the rest of ones. Let us take example related to a 40 Gb/s NRZ signal being transmitted over a standard-SMF fiber with dispersion of 17 $ps/nm \cdot km$, effective area of 80 μm^2 and attenuation of 0.2 dB/km. The pulse

has a FWHM of 20 ps and a peak power of 2 mW. L_D will be 7 km while L_{NL} will be 167 km, clearly the system is dominated by dispersion and we do not expect SPM to induce any significant distortion. If we consider now an increase in peak power to 20 mW, L_{NL} has been reduced to 17 km. Dispersion and SPM will interact throughout transmission. When both parameters are in the same order of magnitude the only way of investigating the evolution of the fiber is by solving numerically the nonlinear Schrödinger equation [201]. This is the approach followed in the simulated results presented in the following sections. The simulation tool used was VPI Transmission Maker^{TM} [155].

5.2 Multi-span transmission with NRZ modulation

In this section we present simulated and experimental results of a multi-span single wavelength transmission over standard-SMF and NZDSF fibers. All parameters used in the simulations have been kept as close as possible to those found in a practical case. However in terms of chromatic dispersion we compensate totally for dispersion and slope at each span. PMD in the fiber is not considered throughout simulations. For the experimental investigation we have also tried to implement system set-ups that resemble a practical situation. Unfortunately, we have been limited by the transmission and dispersion compensation fibers available and the practical implementation of the transmitter and receiver. All experimental work in this chapter has been conducted at AT&T Labs-Research. We use two different span length configurations: a 40 km span, which is aimed at a metro WDM network, and an 80 km span aimed at a traditional long haul WDM system.

5.2.1 Multi-span transmission over standard-SMF with NRZ modulation

Simulation model and results

The multi-span transmission system is modelled by a concatenation of fiber/EDFA spans. A schematic of the building blocks used in the 40 km and 80 km simulation set-ups is shown in Figure 5.2. Span attenuations follow maximum values of ITU standards, 11 dB and 22 dB for 40 km and 80 km respectively. In the 40 km span set-up, dispersion compensation fiber (DCF) is placed just after the transmission fiber before the in-line amplifier. In the 80 km span set-up, DCF is placed in between a two-stage amplifier ensuring that the input power into DCF is below -4 dBm to avoid non-linear effects. In all cases considered the DCF compensates totally for dispersion and dispersion slope after each span. All EDFAs considered have a noise figure of 5 dB and a gain that compensates

for the span losses. For NRZ modulation the rise/fall time is 8.3 ps (1/3 of of bit time-slot). Further details on simulation parameters are presented in Figure B.5. All simulations are performed by transmission of 1024 bits. Average power launched into the transmission fiber is varied in simulations from -3 dBm to 10 dBm for span counts from 1 to 10 of the different configurations described.

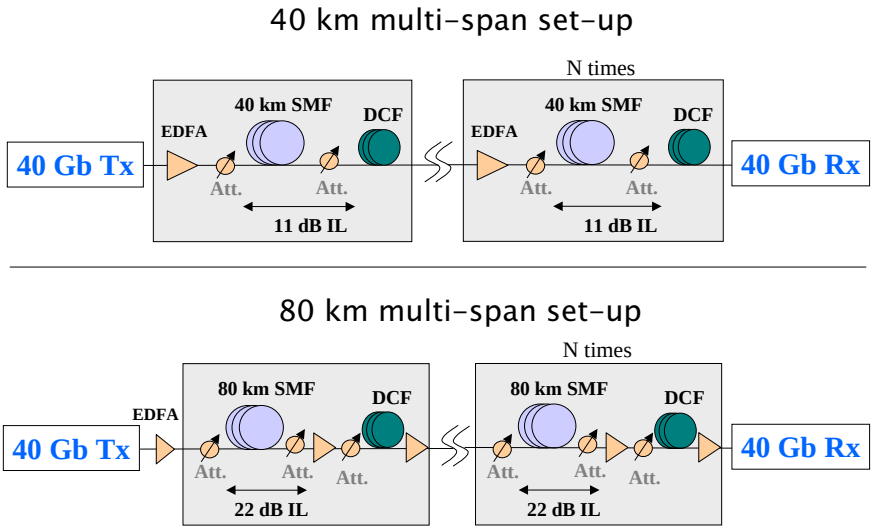

Figure 5.2: Schematic of building blocks used in the simulated multi-span set-up for 40 km and 80 km spans. IL: Insertion Loss.

Performance has been evaluated in simulations by the calculated receiver sensitivity penalty for a BER of 10^{-12} compared to a back-to-back situation. The back-to-back receiver sensitivity is the one measured or calculated when the transmitter is connected directly to the receiver without any transmission fiber, dispersion compensation modules or optical amplifiers. Results from the simulations are presented in Figure 5.3 for both situations a) 40 km and b) 80 km spans.

Results show how limited our margins become after a series of spans. For the 40 km span situation we could reach the 5 span for a penalty of 2 dB if we launched exactly 0 dBm into each span. However, we can clearly observe how sensitive to the launched power levels the system becomes. Penalty steeps sharply both for lower and higher power levels around the optimum point. We define the *power margin tolerance* as the difference between maximum and minimum optical power we can launch per span to observe a receiver sensitivity below a certain value. The power margin tolerance for a 3 dB sensitivity penalty is indicated in Figure 5.3 b) as an example. If we wanted to ensure a 4 dB power

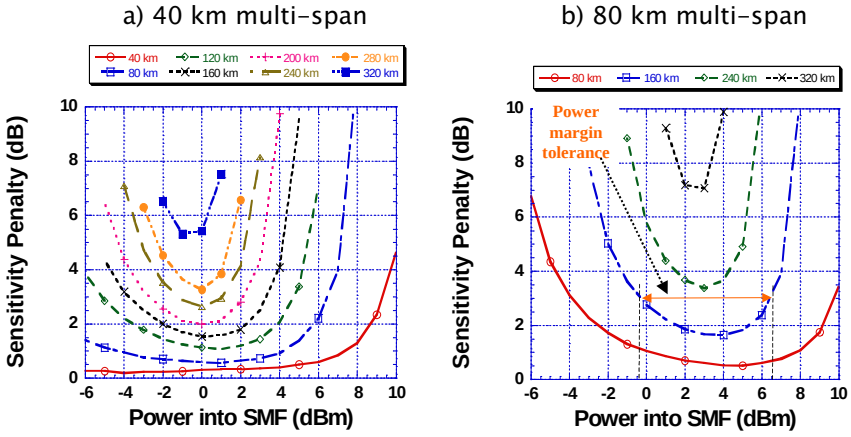

Figure 5.3: Simulated performance of a single channel at 40 Gb/s for multi-span transmission over standard-SMF using NRZ transmitter. a) 40 km spans, b) 80 km spans.

margin tolerance we should reduce the allowed number of spans to four.

For the 80 km case we are clearly limited to a two span system with a 4 dB power margin tolerance and 2 dB sensitivity penalty. We can observe how the optimum power has increased to 3 dBm in a three span system indicating that we are mainly limited by low OSNR reaching the receiver. This power level is higher than the optimum of 0 dBm observed for the 40 km span investigation. This indicates that we are actually compromising SPM distortion for increased OSNR. The OSNR margin could be clearly improved by use of FEC coding allowing to reduce launched power.

Experimental set-up and results

The experimental set-up consists of an ETDM based transmitter (4:1 multiplexer) and an electro-absorption modulator based demultiplexer, evaluating the performance at 10 Gb/s with a 2^{31-1} PRBS signal. Sensitivity measurements are done for the power of the 40 Gb signal at the input of an optical preamplifier for BER measurements of the 10 Gb/s signal reaching the test-set. A separate wavelength carrying the clock signal is multiplexed with a 10 dB power difference to the modulated signal. Differences in the 40 km and 80 km set-ups will be explained in detail.

In the 40 km set-up dispersion compensation fiber with slope compensation was not available. The dispersion for the different spans was measured, see Figure 5.4 a). A CW tunable laser is connected directly to the modulator

in order to try to tune the wavelength of the transmitted signal to a correct dispersion setting. The dispersion tolerance of the set-up was measured and is presented also in Figure 5.4 b). The transmitted signal is chirped and the optimum dispersion compensation is observed for 20 ps/nm. Unfortunately no tunable dispersion compensator was available during these multi-span experimental investigations. The narrow dispersion tolerance limits observed is believed to be induced mainly from the experimental set-up used based on Optical Time Domain Demultiplexing, see Appendix D for further details. The set-up for the several spans follows in all other aspects the one presented for simulations in Figure 5.2. Attenuators were tuned at the input of each span to control the power launched into the transmission fiber. Attenuators were included to emulate the 11 dB span loss in the standard-SMF. Including the DCF an average span loss was measured to be 16.8 dB. Noise figure of all EDFAs used was measured to be below 5 dB within the 1540 to 1565 nm window.

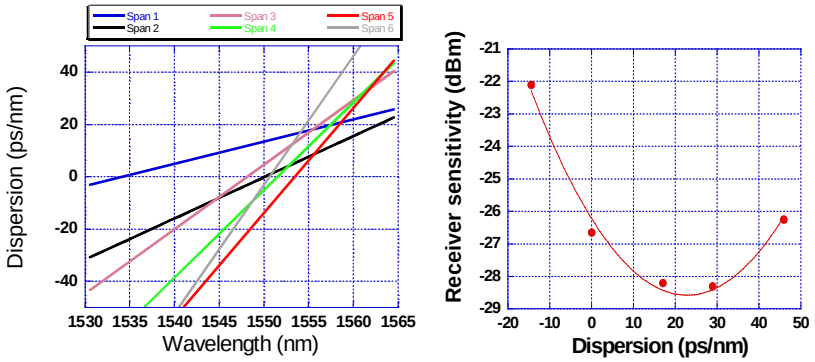

Figure 5.4: Dispersion characterization in the experimental investigation of 40 km multi-span transmission over standard-SMF. a) Measured dispersion for the implemented spans, b) Dispersion tolerance for the NRZ transmitter used.

Results for the 40 km spans are presented in Figure 5.5. They indicate that the optimum power launched per span is in the 0 dBm order in agreement with simulated results. The penalty is kept below 2.5 dB for a four span system comparable to the simulated results. The high penalty observed when moving from a one to two span system is believed to be induced by an incorrect dispersion compensation of the total length for the wavelength used in transmission. Measurements of the Q factor indicated a Q after four spans of 17.5 dB corresponding to BER ratios of 10^{-14}, 1.5 dB deteriorated in comparison with the back to back situation.

The experimental set-up for the investigation of transmission over 80 km

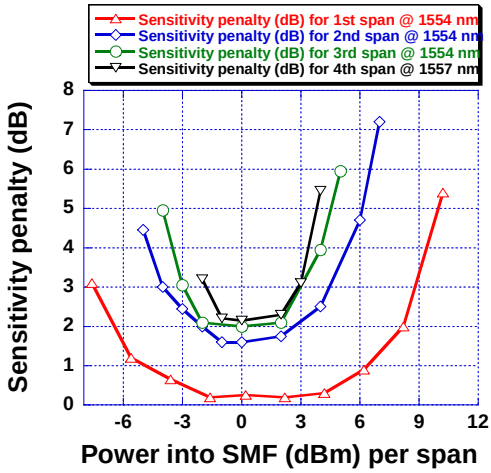

Figure 5.5: Sensitivity penalty as a function of launched power and number of spans observed in the experimental investigation of 40 km multi-span transmission over standard-SMF using a single channel 40 Gb/s NRZ transmitter.

spans is illustrated in Figure 5.6 a). In this case we were limited by the dispersion compensation modules which were designed to compensate for 100 km of standard-SMF and not 80 km. We placed two spans with 80 km of standard-SMF and a last span with 40 km standard-SMF. Two in-line double stage amplifiers were used with DCF in between the amplification sections. On the other hand the dispersion compensating modules available were 100 % slope compensating allowing to reduce the dispersion influence in the measurements observed in the 40 km situation. Figure 5.6 c) shows the dispersion observed as a function of wavelength, notice that dispersion is extremely flat over the whole C-band in the 200 km set-up we use for the NRZ investigation. Comparing these results with those obtained using standard DCF modules, see Figure 5.4, provides a feeling of the importance of using 100 % slope compensating modules in 40 Gb/s systems. Insertion loss was 18.5 dB for the 80 km standard-SMF modules and 9 dB for the DCF modules.

As chromatic dispersion was only compensated after the 200 km set-up we could not do a systematic investigation of the launched optical power into fiber per span. By keeping powers launched into standard-SMF below 1 dBm and power into dispersion compensating modules below -4 dBm we could obtain a Q factor of 16.9 dB (BER ratio below 10^{-12}) after 200 km transmission or a sensitivity penalty of 2 dB compared to back to back. We verified the deterioration of the system performance when changing the power level into

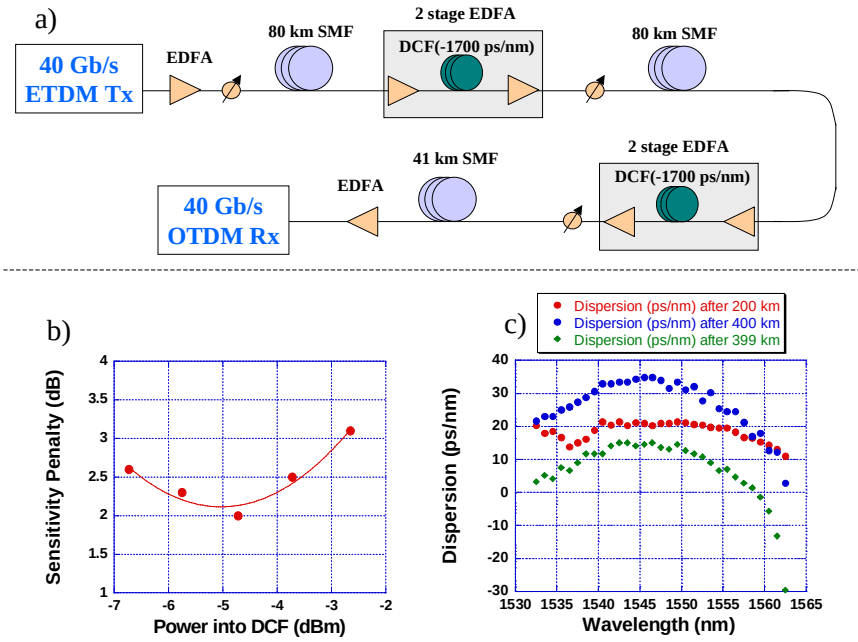

Figure 5.6: Experimental investigation of 80 km multi-span transmission over standard-SMF using single channel 40 Gb/s NRZ transmitter. a) Experimental set-up, b) Effect of power into DCF modules, c) Dispersion measured in the links.

the DCF modules while keeping power levels into the standard-SMF constant. The compromise between OSNR and SPM effect is again clearly observed in Figure 5.6 b). Optimum power levels launched into the slope compensation DCF modules was found to be around -5 dBm.

We should mention that the experimental set-up using 80 km spans differs in a main point from the simulated set-up. As dispersion is not compensated in a span per span basis, the signal will be completely dispersed in spans two and three. A dispersed signal will not have peak power levels in the same order as compensated signal and SPM effect will be different.

5.2.2 Multi-span transmission over NZDSF with NRZ modulation

Let us consider a possible case of NZDSF with chromatic dispersion of 4 $ps/nm \cdot km$, effective area of 62 μm^2 and increased attenuation to 0.25 dB/km. For a 40 Gb/s NRZ with FWHM pulse of 20 ps and peak power of 20 mW, the dispersion length is now 28 km while the nonlinear length is reduced to 13 km.

The difference indicates that we should be more influenced by SPM than when transmitting over standard-SMF, however the effective length is reduced by an increased attenuation characteristic of NZDSF. This inter-relation of SPM and chromatic dispersion is still complex in NZDSF and can only be investigated by means of numerical simulations or experimentally.

Simulation model and results

The simulation model used in the previous section was used with the exception of changing the transmission fiber to a NZDSF with effective area of 62 μm^2 and dispersion of 4 $ps/nm \cdot km$. The dispersion compensating fiber modules for NZDSF are modelled after [76]. Parameters used in the simulations for NZDSF transmission and dispersion compensation fibers are shown in Figure B.6. Results for the 40 km and 80 km span situations are presented in Figure 5.7.

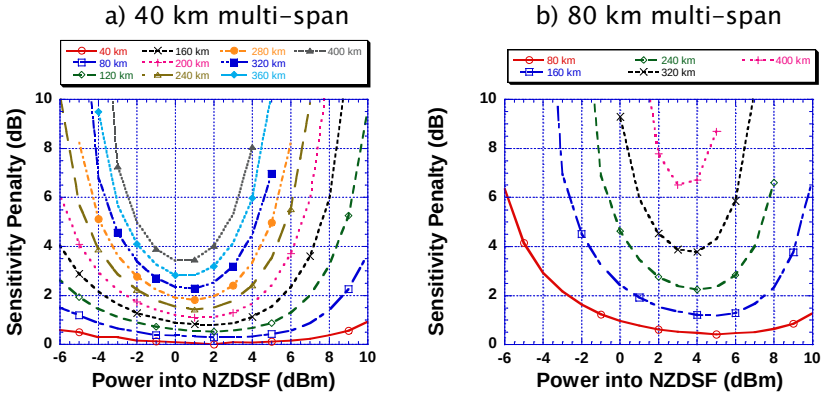

Figure 5.7: Simulated performance for the multi-span transmission over NZDSF using a single channel 40 Gb/s NRZ transmitter. a) 40 km spans, b) 80 km spans.

The accumulated chromatic dispersion per span is substantially smaller than in the standard-SMF case. We need 2.2 km of dispersion compensation fiber for NZDSF while we needed 6.8 km for standard-SMF. This induces a reduction in the total span attenuation for a fixed standard-SMF attenuation. Two positive effects are observed from this, first OSNR is improved and secondly, total SPM observed in the dispersion compensation fiber is reduced. The second effect can be noticed specially in the 40 km situation where the power launched into the DCF is directly related to the power launched into the transmission fiber and can reach -1 dBm for 10 dBm launched into the NZDSF. Even though the

effective area has been reduced we do not observe a significant reduction in the optimum power to be launched into NZDSF for a high number of spans. The total penalty is reduced compared to standard-SMF and transmission over a 6 span of 40 km could be reached with system penalties below 2 dB, ensuring a 4 dB power margin tolerance. For the 80 km span case we are still seriously limited and can not transmit over three spans with a reasonable power margin tolerance.

Experimental set-up and results

We are again limited in the experimental investigation by the available fiber. As we had no access to DCF modules for NZDSF we built a set-up consisting of three spans of 80 km NZDSF and a single dispersion compensation module, see Figure 5.8. The transmission fiber used is TrueWave Classic with lower dispersion within the C-band than the Reduced slope type presented in Table 3.1.

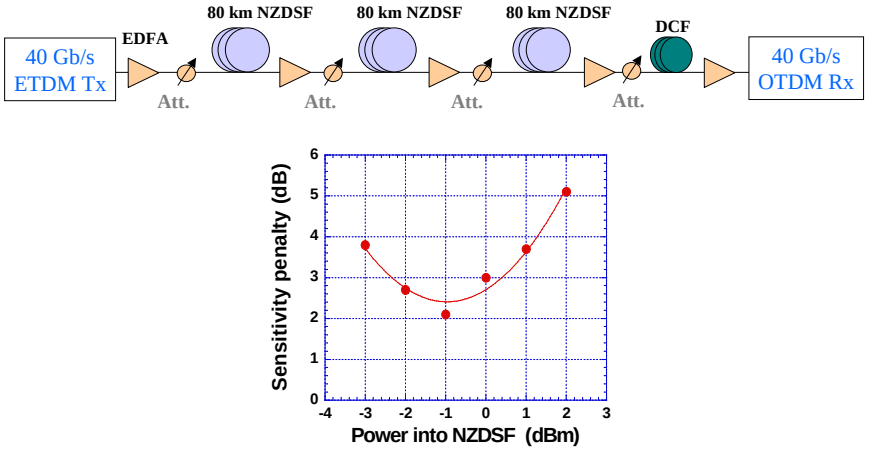

Figure 5.8: Experimental investigation of 80 km multi-span transmission over NZDSF using a single channel 40 Gb/s NRZ transmitter. Experimental set-up and sensitivity penalty after three spans of TrueWave Classic used as the NZDSF fiber.

We could only evaluate the signal performance after the three span plus DCF configuration. The total dispersion of the NZDSF fiber in the link was 600 ps/nm at 1550 nm and 760 ps/nm at 1560 nm. For this situation we evaluated the sensitivity penalty as a function of launched power into transmission fiber by tuning the attenuators placed after the EDFAs. The slope of dispersion was unmatched inducing a residual dispersion of -90 ps/nm at 1550 nm and of +60 ps/nm for 1560 nm. We tuned the transmitted wavelength to 1557 nm in

order to match best dispersion for the chirped transmitter. We could obtain a signal with Q value of 17 dB after the three span transmission with a launched power per span of -1 dBm. This power level is rather low if we compare it to the simulated results and could originate in the difference between simulated fibers and those used in the practical investigation. The effective area of the transmission fiber is thought to be 50 μm^2 compared to the 62 μm^2 used in the simulations.

5.3 Multi-span transmission with RZ modulation

Return to Zero has been suggested and investigated as an effective modulation format to increase transmission performance in multi-span 10 Gb/s [202, 203] and 40 Gb/s [204, 205, 206] transmission systems. The advantages of using RZ are originated by two characteristic properties of this modulation format. First, RZ provides an improved sensitivity compared to NRZ [205, 203], second RZ seems to be less affected by SPM than NRZ [207]. The sensitivity improvement is originated in the fact that for the same average power we will observe a higher peak power for the *ones* in RZ modulation. The higher extinction ratio, see Equation 5.5, directly allows for a lower OSNR needed to obtain a specific Q at the receiver. We have experimentally verified the OSNR versus Q relation for a NRZ signal and a 9 ps RZ. The set-up for the OSNR consisted of an attenuator and an EDFA, by tuning the attenuation at the input of the EDFA the OSNR was changed at the output of the EDFA. The set-up and results are presented in Figure 5.9 a). An improvement of close to 4 dB in OSNR was observed for a 16 dB Q value, for example. It must be mentioned that the OTDD receiver used in the experimental measurements might have induced an extra penalty due to the 12 ps rise/fall time of NRZ optical signal providing an extra benefit to RZ in the comparison, see Appendix D.

The SPM increased tolerance can be understood from the fact that the dispersion length is dependent on the square of the pulse-width while the nonlinear length is inverse proportional to the pulse peak power. Let us consider a reduction in the pulse width from 20 ps to 10 ps when using an NRZ or an RZ signal and consider that peak power has doubled for the RZ case, to 40 mW. If we consider transmission over standard-SMF the dispersion length is now 1.4 km while the non-linear length is 8.3 km. This can be considered as a substantial difference, the pulse will disperse fast in the fiber reducing the peak power and not allowing for the whole SPM effect to interact distorting the pulse. An example of 40 Gb/s NRZ and RZ signals being dispersed in standard-SMF is presented in Figure 5.9 b). The samples in both examples are taken every 0.5 km and the launched power into the fiber is -5 dBm. It is clearly observed the

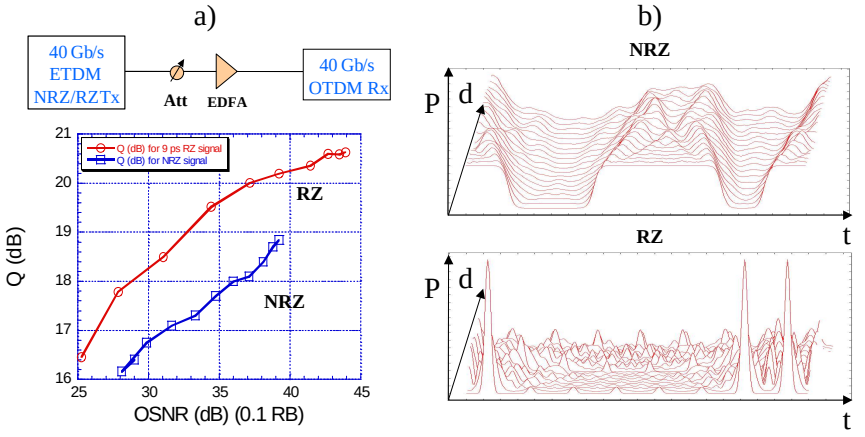

Figure 5.9: a) Experimental verification of the improvement in Q versus OSNR for NRZ versus RZ at 40 Gb/s. b) Example of 40 Gb/s NRZ (10011101) and RZ (1000001) signals being dispersed in the standard-SMF fiber, input power is -5 dBm, samples are take every 0.5 km. P: Power, d: distance, t: time.

rapid decay of the peak power of the RZ pulses while the NRZ keeps the peak power over a longer transmission length. This relation will be highly dependent on the duty cycle of the RZ pulses. Considering NZDSF the relation between dispersion length and non-linear length is close to unity if we consider the 9 ps pulses for 40 mW peak power, and the dispersion-SPM interaction will again follow a complex interaction.

5.3.1 Multi-span transmission over standard-SMF with RZ modulation

Simulation model and results

RZ modulation is implemented by using a Gaussian pulsed source as input to the Mach-Zehnder modulator at the transmitter. We have chosen two pulse widths, 8 ps and 4 ps FWHM to represent the influence of duty cycle. Launched power into the transmission fiber is characterized by the average power, being the peak power of the pulse related to the FWHM and pulse shape. Fiber and receiver settings are not changed from simulations described in Section 5.2.1. Simulated results for the 40 km and 80 km span cases are presented in Figures 5.10 and 5.11 respectively.

A clear improvement can be already observed when comparing the 8 ps RZ simulations over 40 km spans with the correspondent using NRZ, see Figure 5.3

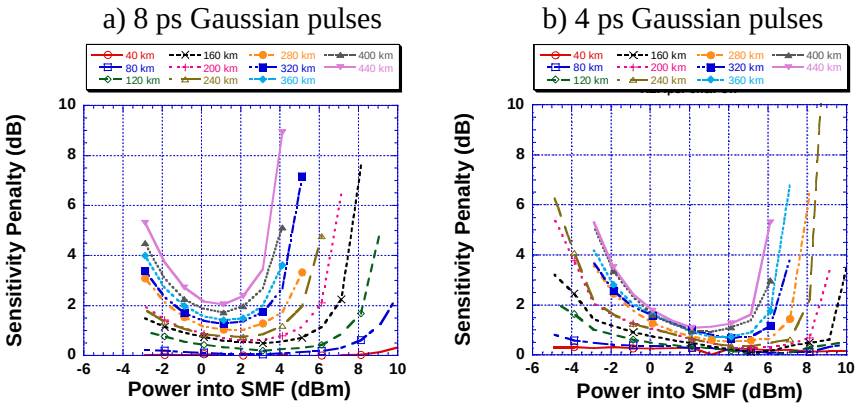

Figure 5.10: Simulated performance for the multi-span transmission over standard-SMF using a single channel 40 Gb/s RZ transmitter in 40 km spans. a) 8 ps pulses, b) 4 ps pulses.

a). Using 8 ps RZ we can transmit over 9 spans with a sensitivity penalty below 2 dB while keeping a reasonable 5 dB power margin tolerance. The improvement is even clearer when pulse width is reduced to 4 ps where transmission is possible over 11 spans with the same tolerance margins. The dispersion length for a 4 ps pulse transmitted over standard-SMF is below the 300 m while the non-linear length is 4 km if we consider an average launched power of 10 dBm. It is clear to observe that the optimum optical power which allows for a maximum number of spans in each case is increased from 0 dBm for NRZ to 1 dBm for 8 ps RZ and close to 3 dBm for the 4 ps RZ case. This is a clear indication of the increased SPM tolerance.

For the 80 km span case the launched power which allows a maximum number of spans has increased from 3 dBm for NRZ to 4 dBm for the RZ 8 ps transmitter and 5 dBm for the RZ 4 ps transmitter. The distortion observed for a given *power-span* setting is significantly reduced for the RZ transmitters compared to the NRZ case investigated previously, see Figures 5.11 and 5.3 b). We can reach 4 spans with 8 ps pulses and 5 spans with the 4 ps pulses while still keeping at least a 3 dB power margin tolerance. It is also possible to observe the improved tolerance to low power levels allowed by the improved sensitivity. In the NRZ case we reached 6 dB of penalty when launching -6 dBm and looking into one single span situation. The penalty is reduced below the 4 dB for the same power levels for the RZ modulation.

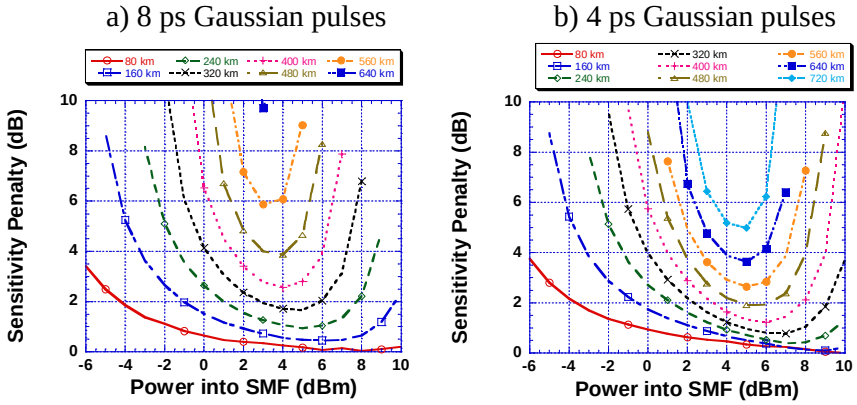

Figure 5.11: Simulated performance for the multi-span transmission over standard-SMF using a single channel 40 Gb/s RZ transmitter in 80 km spans. a) 8 ps pulses, b) 4 ps pulses.

Experimental set-up and results

The experimental implementation of the transmitter is the same as described previously in Section 4.4.1. We obtained optical pulses with 3 ps FWHM directly from the pulsed laser and could increase the pulse width to 9 ps by using a 0.6 nm optical filter. The quality factor Q was improved from 19 dB for NRZ to 20.5 dB for 3 ps RZ in a back to back situation. This is equivalent to a 2 dB improvement in the receiver sensitivity compared to the NRZ case. Q is measured for a high input power launched into the receiver of -14 dBm (optically preamplified receiver). In the 40 km per span case, we systematically changed the input power into the transmission fiber for all spans and recorded the sensitivity penalty. Results are presented in Figure 5.12 a) showing measured sensitivity penalty for one, four and six spans when using the 3 ps RZ transmitter.

We can clearly observe how the optimum average power has increased from 0 dBm to 4 dBm allowing for transmission over 6 spans with more than 4 dB power margin tolerance for a 2 dB sensitivity penalty. We were limited to a 6 span investigation by the availability of DCF modules. Figure 5.12 b) shows the influence of the pulse-width by comparing the 9 ps pulses to the 3 ps pulses in the six span situation and varying the launched optical power. We can observe a clear improvement in Q when using the 3 ps pulses while for the 9 ps pulses the optimum launched power was reduced to 2 dBm. The back-to-back Q value for the 9 ps RZ transmitter was 19.7 dB.

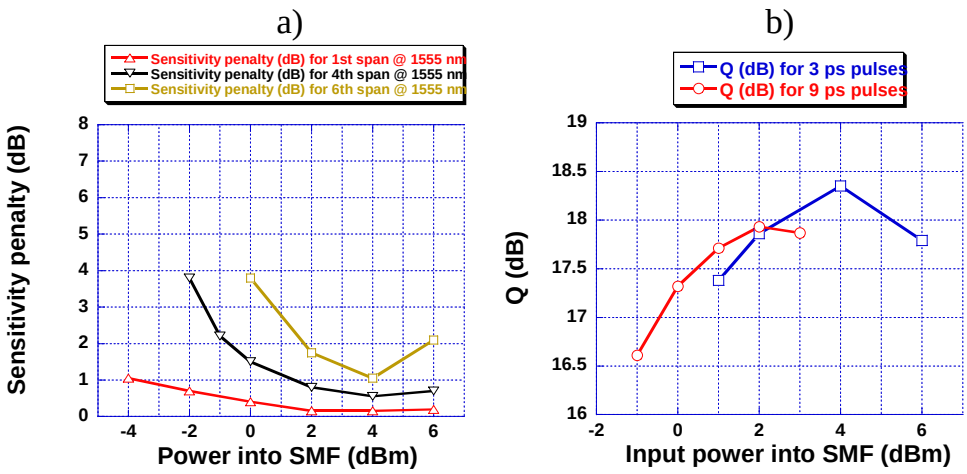

Figure 5.12: Experimental investigation of 40 km multi-span transmission over standard-SMF using single channel 40 Gb/s RZ transmitter. a) Sensitivity penalty as a function of launched average power and span number using 3 ps pulses. b) Pulse-width influence for a six span situation.

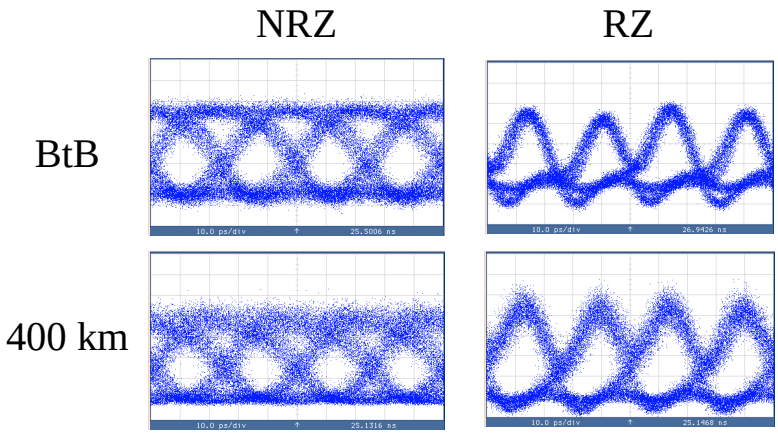

Figure 5.13: Comparison of eye diagrams for NRZ and 9 ps RZ modulation in a 400 km standard-SMF link. After transmission the Q factor for NRZ was 15 dB while for RZ 17.5 dB.

The experimental investigation for the 80 km span case was initiated by using the same 200 km transmission set-up as presented in Figure 5.6 and using the

9 ps RZ transmitter. By keeping powers launched into the standard-SMF at 2 dBm and power into dispersion compensating modules below -3 dBm we could obtain a Q factor of 18.8 dB after 200 km transmission. We could upgrade the set-up to a 400 km link by having 5 spans of 80 km standard-SMF while using 4 DCF modules each compensating the equivalent of 100 km standard-SMF. The measured residual dispersion of the 400 km link can be observed in Figure 5.6 c). As it was described in Section 4.4.1 the tolerance to chromatic dispersion is reduced for RZ compared to NRZ modulation. For 9 ps pulses we should expect 1 dB penalty already for $\pm 30\ ps/nm$ dispersion, see Figure 4.17. The residual dispersion was reduced to appropriate values within the dispersion tolerance of RZ modulation by reducing the standard-SMF length to 399 km, see also Figure 5.6 c). Keeping the same power levels as in the 200 km link we could obtain a Q factor for the 9 ps RZ transmitter of 17.5 dB.

For comparison the performance of NRZ in the 400 km link for optimized power levels showed a BER error floor of 10^{-8} equivalent to a Q of 15 dB. Eye diagrams in the back-to-back situation and after 400 km transmission are presented in Figure 5.13 for NRZ and 9 ps RZ.

5.3.2 Multi-span transmission over NZDSF with RZ modulation

No experimental results have been obtained for RZ modulation transmission over NZDSF. We have conducted simulations following the set-up presented previously where we combine the RZ transmitter with NZDSF fiber and DCF modules designed for dispersion compensation of NZDSF fiber. Simulated results are presented in Appendix F, see Figure F.1 and F.2. We observe the same trends as in Section 5.2 if we compare performance of the same RZ transmitter over standard-SMF and NZDSF. While keeping the same optimum power levels a higher number of spans can be reached when we transmit over NZDSF than over the standard-SMF. If we compare the two different RZ transmitters we can observe that as in Section 5.3.1 the optimum power level is higher for the 4 ps than for the 8 ps case. A maximum of 7 spans could be achieved for the 4 ps RZ transmitter for a 2 dB sensitivity penalty while keeping the power tolerance within a 3 dB margin. It is clear that for single channel transmission, a system designed considering the limitations observed in transmission over standard-SMF will perform in general better if transmission is done over NZDSF.

5.4 Multi-span transmission with optical duobinary modulation

Optical duobinary or PSBT was introduced in Section 3.4.2 as an effective format which would allow to relax the dispersion margins in 40 Gb/s system design. However, we mentioned as a disadvantage of this modulation format the reduction in receiver sensitivity due to an increased *zero* level and a reduction in the extinction ratio. On the other hand some of the dispersion tolerance is related to the phase changes which appear in consecutive *zeros* and *ones*. It would be expected that SPM will have a stronger influence in optical duobinary than in NRZ modulation where the phase in not used. However, it seems that the effect of SPM is similar for binary and optical duobinary modulation formats [208]. We have investigated the sensitivity degradation and the SPM effect by including a duobinary transmitter in the multi-span model described in the previous sections. The duobinary transmitter uses the parameters described previously in the chromatic dispersion investigation and are shown in Figure B.2.

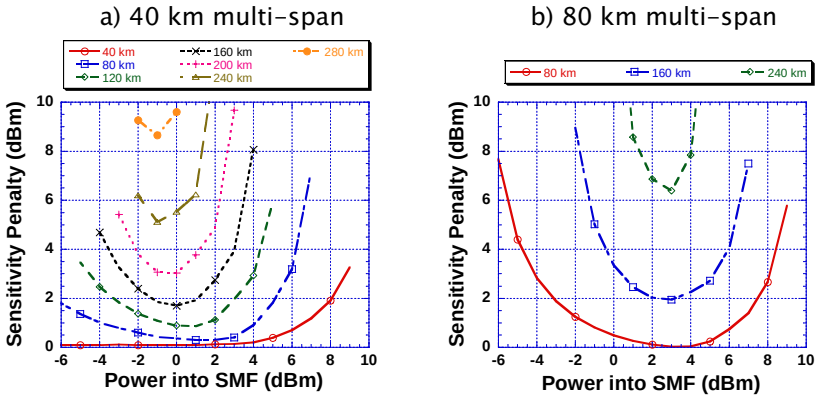

Figure 5.14: Simulated performance for the multi-span transmission over standard-SMF using optical duobinary modulation. a) Over 40 km spans. b) Over 80 km spans.

Results from simulations of duobinary modulation transmission over standard-SMF are presented in Figure 5.14. If we compare them with the results obtained for NRZ modulation, see Figure 5.3, we can observe a slightly worse performance for optical duobinary. For spans of 40 km we are limited to a four span system for a sensitivity penalty below 2 dB, with very tight power margin tolerances. For spans of 80 km we can just allow for a two span transmission for 2 dB penalty but with a power margin tolerance of 0 dB.

It is interesting however to observe a small improvement in performance for optical duobinary modulation when compared with NRZ in transmission over NZDSF fibers. Results for optical duobinary transmission over 80 km spans are presented in Figure 5.15 and should be compared to results presented in Figure 5.3 b). A thorough experimental investigation is required in order to verify these results.

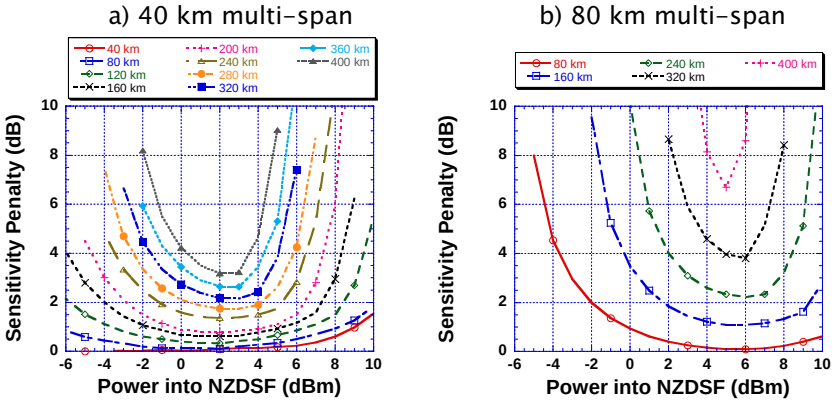

Figure 5.15: Simulated performance for the multi-span transmission over NZDSF using optical duobinary modulation. a) Over 40 km spans. b) Over 80 km spans.

5.5 Design rules based on analytical approximations of simulated results

In previous sections we have presented the limitations for a multi-span single channel system induced by OSNR and SPM in the transmission over standard-SMF and NZDSF for several modulation formats. The intention of this section is to provide rules by means of simple formulas that can provide the designer an idea of the limitations in the number of spans allowed for the different transmitter configurations.

The OSNR evolution in a multi-span system can be directly related, see Equation 5.4, to the insertion loss in the span, the amplifier noise figure, and the number of spans in the link. On the other hand we can relate the OSNR to the receiver sensitivity and estimate a necessary OSNR for a maximum admitted sensitivity penalty in the link. This way we can express the maximum number of spans allowed in a link N_{max} for a given sensitivity penalty as:

$$10 \cdot LogN_{max} = P_L - L - F + 58 - OSNR_{sens} \tag{5.12}$$

It has been suggested in [206] that under the influence of SPM the product of launched power into the transmission fiber and maximum number of spans able to transmit is constant. Our approach is to limit the maximum number of spans able to be reached at a certain launched power to those observed with a sensitivity penalty of 2 dB. If we plot the couples "power-maximum span for 2 dB penalty" obtained from the simulated results of previous sections in a logarithmic scale we observe a linear tendency which proves the suggested principle.

As an example we observe the results obtained from simulations in the 40 km span case in transmission over standard-SMF for NRZ and RZ. The same procedure can be applied to any other data set from the previous sections. We have estimated the need of 28 dB of OSNR to induce a penalty of 2 dB in an NRZ signal while for RZ it was 26 dB. We consider 17 dB of insertion loss in the span from standard-SMF and DCF modules. The noise figure is 5 dB as in simulations. Results can be observed in Figure 5.16.

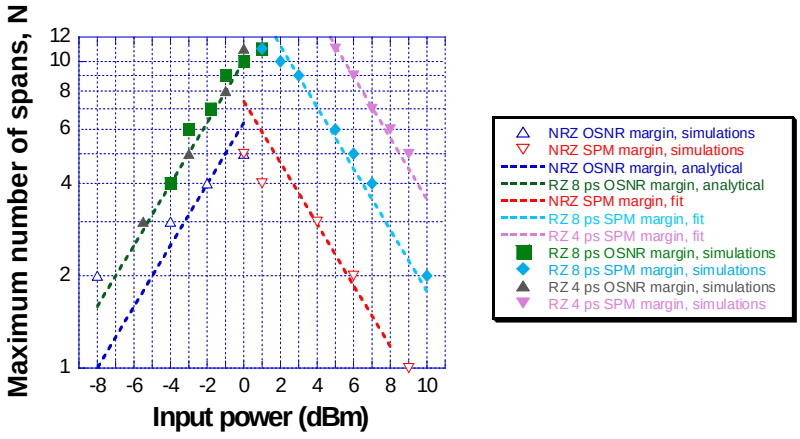

Figure 5.16: Design rules for 40 km transmission over standard-SMF for NRZ and RZ.

All samples in the graph are from simulated results. The OSNR analytical limitations are obtained following Equation 5.12. The SPM analytical limitations are obtained from a fit of the results obtained from simulated data to a linear relation between launched power and maximum number of spans. Please notice that simulated results and analytical formulas fit well in the flanks but not where OSNR and SPM predictions coincide providing an optimistic approximation. The equations which indicate the maximum number of spans for a certain launched power are:

for NRZ

$$10 \cdot LogN_{max} = 8.7 - P_L \tag{5.13}$$

for 8 ps RZ

$$10 \cdot LogN_{max} = 12.5 - P_L \tag{5.14}$$

for 4 ps RZ

$$10 \cdot LogN_{max} = 15.5 - P_L \tag{5.15}$$

Also as suggested in [206] the equations for RZ can be grouped into a single one dependent on the duty cycle DCy as

$$10 \cdot LogN_{max} = 18.5 - 18.75 \cdot DCy - P_L \tag{5.16}$$

which allows to evaluate performance of a general RZ transmitter.

Interpreting results from the 80 km span case in transmission over standard-SMF we have obtained very similar SPM analytical equations. For the OSNR we have to consider that the amplifier used in the simulations is a double stage EDFA with DCF as a middle section. In order to be able to use the same expression for the OSNR limitations we can estimate [197] an effective noise figure for this kind of amplifier F_{DC}, that can be expressed as

$$F_{DC} = F \cdot (1 + \frac{IL_{DCF} \cdot P_{in^A}}{P_{in}^{DCF}}) \tag{5.17}$$

dependent on the insertion loss of the DCF module IL_{DCF}, the power at the input of the first stage amplifier P_{in^A} and the power at the input of the DCF module $P_{in^{DCF}}$.

Following these recommendations simple rules can be obtained from the simulated results for all systems described in this chapter.

5.6 Summary

The optical power budget to be considered in the design of single channel transmission systems will be dependent on the receiver sensitivity, the OSNR at the receiver and the SPM induced distortion. The influence of OSNR and SPM have been introduced providing a practical view of their origins and effects. Their impact has been further investigated in a multi-span system by means of simulations and verification in several experimental set-ups. As a success criteria we allow systems to have a maximum sensitivity penalty of 2 dB. FEC or Raman amplification are not considered in the following results. Investigations have been carried out for NRZ, RZ and duobinary modulation formats, the transmission fiber considered was standard-SMF and a general case of NZDSF.

When considering NRZ as the modulation format and standard-SMF as the transmission fiber we are seriously limited in the number of spans over which we are able to transmit, simulations showed a maximum of 2 spans of 80 km and 4 spans of 40 km. Experimentally we have verified the feasibility of 4 spans of 40 km with sensitivity penalties below the 2.5 dB and of 2 spans of 80 km plus an additional 40 km with a sensitivity penalty of 2 dB. Transmission over NZDSF allows for a higher span count, simulations showed a maximum of 6 spans of 40 km and close to 3 spans of 80 km. Experimentally we were able to verify the feasibility of a 3 span system with 80 km transmission fiber per span with a penalty close to the 2 dB margin.

The increased tolerance of RZ modulation to SPM induced distortion has been thoroughly investigated. It has been observed that higher optical powers could be launched into the transmission fiber for RZ than for NRZ modulation. This increased launched power allowed for a higher span count in the transmission link. The reduction of SPM induced distortion is directly related to the duty cycle of the pulses originated in the RZ transmitter. Shorter pulses will disperse faster in the fiber inducing a reduction of their peak power and consequently SPM induced distortion.

For a simulated 8 ps RZ transmitter and transmission over standard-SMF fiber, we could reach 9 spans of 40 km or 4 spans of 80 km. Experimentally the transmitter implemented had a 9 ps FWHM and allowed for transmission in a 5 span system with 80 km standard-SMF with Q levels of 17.5 dB equivalent to BER in the 10^{-14} ratio. Optical power levels were kept at 2 dBm for launched power into the standard-SMF and -3 dBm into the DCF modules.

For a simulated 4 ps RZ transmitter and transmission over standard-SMF fiber we could achieve transmission over 11 spans of 40 km or 5 spans of 80 km for a sensitivity penalty below 2 dB. The transmitter implemented for experimental verification of the results used a 3 ps FWHM pulsed source. It was possible to transmit over a total of 6 spans of 40 km each with a penalty of 1 dB using higher optical power levels (4 dBm) than for NRZ modulation (0 dBm). Similar improvement has been observed for RZ in transmission over NZDSF fiber spans.

We have investigated the performance of optical duobinary in a multi-span system by means of simulations. When compared to NRZ modulation optical duobinary seems to perform slightly worse for transmission over standard-SMF while a slight improvement in performance can be observed for transmission over NZDSF.

Finally we have provided the system designer with a simple method to obtain analytical design rules for the influence of OSNR and SPM in the maximum number of spans allowed in the system for a certain launched optical power. The

method has been verified in the comparison of NRZ and RZ for transmission over standard-SMF over 40 km spans.

Chapter 6

40 Gb/s WDM system design and experimental investigations

It is the goal of this chapter to point out issues to be considered in the design of WDM systems which can limit the number of channels being transmitted or the distance over which we can transmit, other than those presented in the previous chapters. Furthermore, we will present practical examples of implementation of WDM systems analyzing their performance and limitations.

The chapter starts by investigating in Section 6.1 limitations induced by linear crosstalk in a 100 GHz channels spaced WDM system for the different modulation formats presented throughout the previous chapters: NRZ, RZ, and optical duobinary. Moreover, a new modulation format is introduced, Carrier Suppressed Return to Zero (CSRZ). We characterize CSRZ regarding linear crosstalk, dispersion tolerance and multi-span single channel transmission.

Section 6.2 introduces two non-linear effects characteristic of WDM systems, Cross Phase Modulation (XPM) and Four Wave Mixing (FWM). Their dependence on channel spacing and fiber used in transmission is reviewed. We present a practical investigation of their effects in a WDM system over standard-SMF and a particular NZDSF.

Section 6.3 is dedicated to practical examples for long haul WDM systems. We will describe a 400 km link consisting of 5 spans of 80 km standard-SMF, where Raman amplification is used to keep the OSNR reaching the receiver at the required level. We present a complete characterization of the set-up regarding dispersion, OSNR and Raman amplification. Transmission in the 400 km link has been investigated for a 16 channel WDM system with 200 GHz

channel spacing and a 32 channel with 100 GHz channel spacing providing an aggregate capacity of 1.28 Tb/s.

In Section 6.4 we present an experimental investigation of a 160 km link with 40 km spans of standard-SMF and using Semiconductor Optical Amplifiers (SOAs) as the in-line amplifiers. The span distance and use of SOAs are aimed at a possible Metro WDM network scenario.

6.1 Channel spacing, linear crosstalk and modulation formats in WDM systems

As it was introduced in Chapter 2 the main advantage of WDM system is the ability to transport a number of high capacity signals between two distant points over a single fiber. The limitations in the number of channels to be used in a WDM system is mainly dependent on the optical bandwidth available in the transmission link, the spacing between the channels and the optical bandwidth required by each channel. The last two factors are generally defined by a single parameter, the spectral efficiency S defined as:

$$S = \frac{B}{S_{ch}} \tag{6.1}$$

were B is the bit rate of the signal and S_{ch} the spacing between the channels. Traditional 10 Gb/s based WDM systems with 100 GHz channel spacing provide for example a 0.1 bit/s/Hz spectral efficiency. Increasing the bit rate to 40 Gb/s while keeping the channel spacing at 100 GHz will provide a 0.4 bits/s/Hz spectral efficiency. Figure 6.1 presents the relation between the total capacity of a WDM system, the channel spacing, the bit rate per channel and the total number of channels in the system. Clearly 40 Gb/s systems have the potential of providing higher capacity than 2.5 Gb/s or 10 Gb/s systems with a reduced number of channels.

Increasing the bit rate by four induces a proportional increase in the signal bandwidth and if channels are closely spaced optical filtering of each single channel from the WDM signal becomes more complicated. Figure 6.2 presents a comparison of the spectra observed for an 8 channel WDM signal using a 100 GHz grid channel spacing when transmitting either 40 Gb/s or 10 Gb/s per channel. Clearly, optical filtering at the receiver is a more demanding process in a 40 Gb/s WDM system than in a 10 Gb/s system.

Optimum filtering in a 100 GHz 40 Gb/s WDM system can be considered as a compromise between crosstalk allowed between neighboring channels and the effect of filtering out information contents of the signal. This compromise will be dependent on the amplitude frequency response of the filter considered.

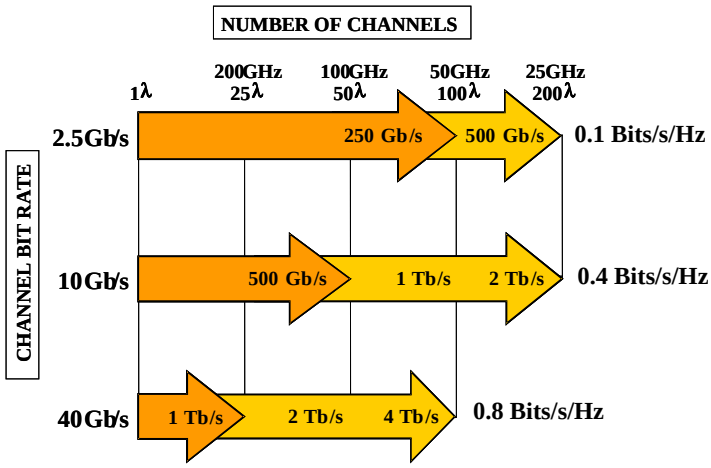

Figure 6.1: Illustration of the total capacity in a WDM system related to the bit-rate, the channel spacing and the number of channels. λ: Channel.

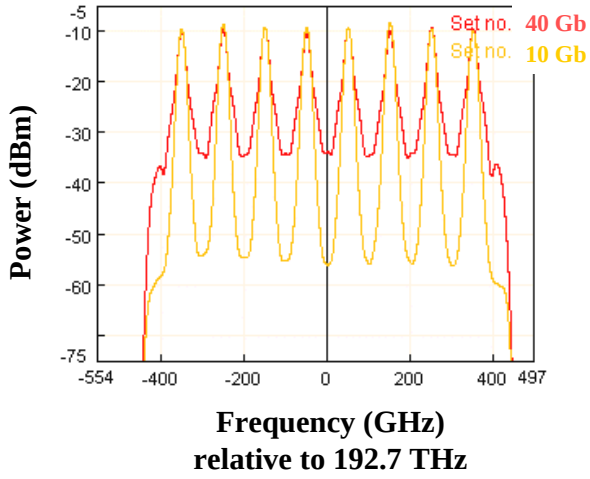

Figure 6.2: Comparison of spectrum observed for 100 GHz grid between 10 Gb/s and 40 Gb/s signals. Modulation format NRZ.

Furthermore, the dispersion tolerances for a 40 Gb/s signal have been shown to be small, in the order of ± 70 ps/nm for NRZ modulation. Optical filters can induce dispersion, reducing the effective optical pass-band or adding distortion and penalty in case of signal-filter center wavelength misadjustment [42, 43, 44].

The effect of dispersion in the bandpass of the filters is a clear limitation in the cascadability of these components in optical networks [209]. Dispersion induced in the filtering process has led to the characterization of filter performance not by their amplitude frequency response optical bandpass but by the penalty induced within the expected bandpass [210, 211].

Throughout the previous chapters we have introduced three modulation formats which are candidates to be used in 40 Gb/s transmission systems: NRZ, RZ and optical duobinary. Within this section we will characterize their performance in a 100 GHz channel spacing as a function of optical filtering. Furthermore, we introduce Carrier Suppressed Return to Zero (CSRZ) [212], a new modulation format which can overcome some of the disadvantages that traditional RZ presents in high spectral efficiency WDM systems.

6.1.1 NRZ, RZ and optical duobinary in dense WDM systems

We use a simple approach in the performance evaluation of high spectral efficiency systems using transmitters based on NRZ, RZ and optical duobinary modulation (PSBT) formats. A schematic for the modelled set-up is shown in Figure 6.3. Four channels are passively multiplexed at the desired frequency spacing, each channel carrying different data content. One of the middle channels is filtered and its performance evaluated by measuring the receiver sensitivity at a BER ratio of 10^{-12} in PIN based receiver. The electrical filter at the receiver is kept constant for all the modulation formats and equal to 28 GHz. The optical filter is modelled with an amplitude frequency response following first-order and second-order Gaussian shapes, also shown in Figure 6.3. These filtering functions can represent practical implementation of optical filters [211, 213]. The filter performance of each modulation format is evaluated as a function of the filter 3-dB bandwidth for both filter functions. The filter bandwidth obtained from the simulation model can be related to the desired dispersion-free bandwidth of a filter.

The results obtained when we use NRZ as the modulation format are presented in Figure 6.4. The four channel spectrum is shown as a reference for comparison with the other modulation formats. A penalty of 0.5 dB is observed in the optimum setting compared to the single channel performance. Even when we increase the channel spacing to 200 GHz this penalty is observed. There is a reasonable range of the filter bandwidth over which we obtain a penalty below 1 dB. The second-order filter has a steeper amplitude response function and its effect can clearly be felt as a fast increase in the sensitivity penalty in the narrow-bandwidth area. When we reach the 30 GHz bandwidth we observe a 4 dB penalty from filtering out part of the information of the signal. On the other hand the steep response of the second-order filter induces less distortion in the

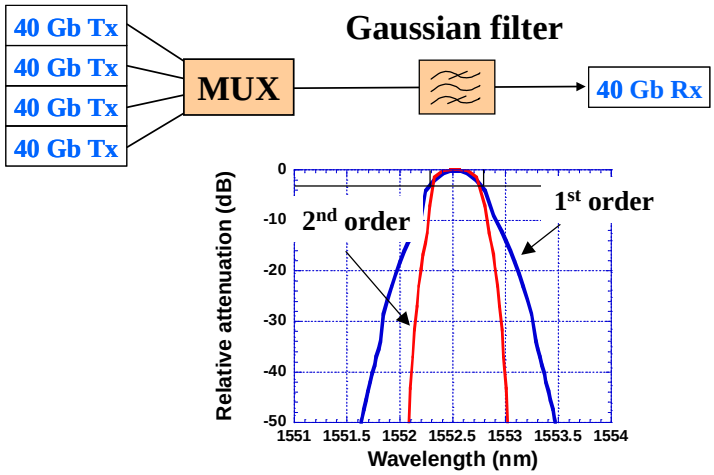

Figure 6.3: Schematic of set-up used in the simulations of four channel optical multiplexing for NRZ, RZ and optical duobinary. The two different filters used , first-order and second-order Gaussian shaped, are shown for reference (50 GHz 3 dB bandwidth).

broad-bandwidth area. The results indicate that filter designers are granted with high tolerances when we use NRZ as a modulation format in 100 GHz spacing 40 Gb/s WDM systems.

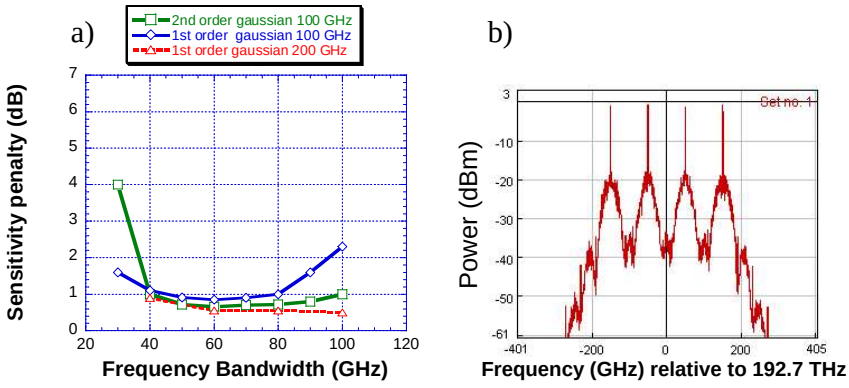

Figure 6.4: Filter bandwidth and shape influence in a 100 GHz spacing 40 Gb/s WDM system, NRZ modulation. a) Sensitivity penalty as a function of 3-dB filter bandwidth. b) Simulated frequency spectrum of the 4 channel WDM signal with NRZ modulation, Resolution bandwidth 0.1 nm.

The transmitter used for the RZ investigation uses an 8 ps pulsed source.

This transmitter proved to provide improved performance in the single span investigation presented in Chapter 5 compared to NRZ modulation. As the spectral-width of an RZ modulated signal is inverse proportional to the width of the pulses used we would expect that narrower pulses would perform even worse than the case under study. The sensitivity penalty as a function of filter bandwidth is shown in Figure 6.5. We observe a minimum penalty of 1.5 dB when using the second-order filter for a 70 GHz bandwidth in a 100 GHz channel spacing system. The penalty is increased to 2 dB when using the first-order type at an optimum bandwidth of 40 GHz. As with NRZ a residual penalty is observed even when we increase the channel spacing to 200 Ghz. There was a 2.5 dB sensitivity improvement for the 8 ps RZ transmitter when compared to NRZ, please notice that all sensitivity penalties are presented compared to the back-to-back performance of the transmitter being studied. The 4 channel spectrum is also included in Figure 6.5 and clearly shows how tight the channels are packed in comparison to the NRZ situation.

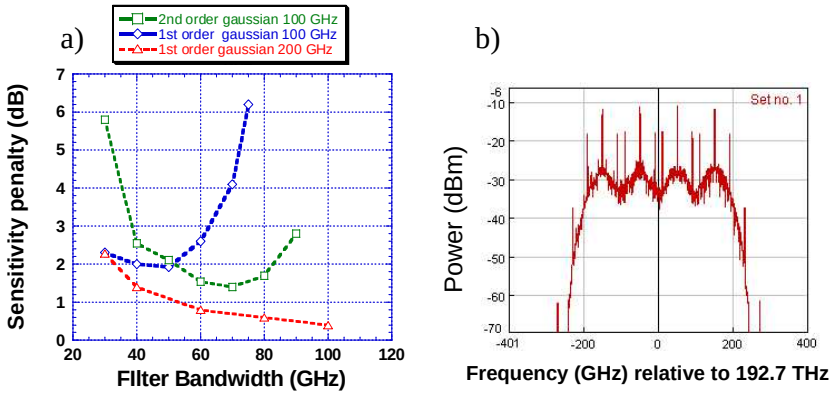

Figure 6.5: Filter bandwidth and shape influence in a 100 GHz spacing 40 Gb/s WDM system, 8 ps RZ modulation. a) Sensitivity penalty as a function of 3-dB filter bandwidth. b) Simulated frequency spectrum of the 4 channel WDM signal with RZ modulation, Resolution bandwidth 0.1 nm.

The PSBT transmitter follows the implementation described in Section 3.4.2. The receiver sensitivity in the back-to-back configuration of the PSBT transmitter is reduced by 1 dB compared to the sensitivity of the NRZ transmitter. The 4 channel spectrum can be observed in Figure 6.6 b). The PSBT modulation shows no carrier. The spectral reduction obtained in the PSBT transmitter can be clearly related to the reduced sensitivity penalty observed in the filtering results presented in Figure 6.6 a). A negative penalty is even observed for filter bandwidths within the 30 GHz to 80 GHz 3-dB bandwidth range. This

negative penalty induced in the filtering has been used in [214] for example to allow for an improvement in resistance of the PSBT modulation to SPM.

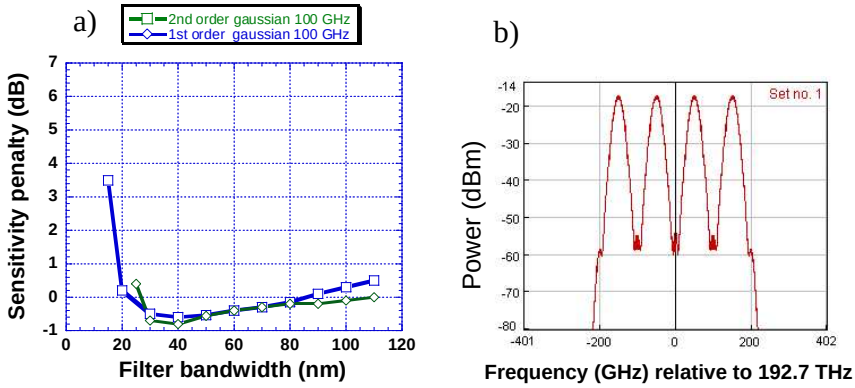

Figure 6.6: Filter bandwidth and shape influence in a 100 GHz spacing 40 Gb/s WDM system, PSBT modulation. a) Sensitivity penalty as a function of 3-dB filter bandwidth. b) Frequency spectrum of the 4 channel WDM signal with PSBT modulation, Resolution bandwidth 0.1 nm.

This proves the significant advantage of optical duobinary modulation in relation to the spectral efficiency which has allowed practical implementation of 75 GHz channel spaced 40 Gb/s WDM systems [215] providing a spectral efficiency of 0.53 bits/s/Hz. Demonstrations of higher spectral efficiency systems using other modulation formats make use of un-even channel spacing and vestigial side-band filtering [216] yielding 0.64 bits/s/Hz or optical pre-filtering followed by polarization multiplexing of odd/even channels [217, 218, 219] achieving 0.8 bits/s/Hz.

6.1.2 Carrier Suppressed Return to Zero

We have demonstrated, see Section 5.3, how RZ modulation is an effective modulation format regarding multi-span transmission. On the other hand, RZ modulation presents limitations regarding dispersion tolerance, see Section 4.4.1, and spectral efficiency. We present in this section a modulation format, CSRZ, that while maintaining the efficiency in multi-span transmission of RZ improves the spectral efficiency.

Implementation of a CSRZ transmitter

The CSRZ transmitter is generally implemented with a double stage Mach-Zehnder modulator. An illustration of the classical implementation is shown in Figure 6.7 a).

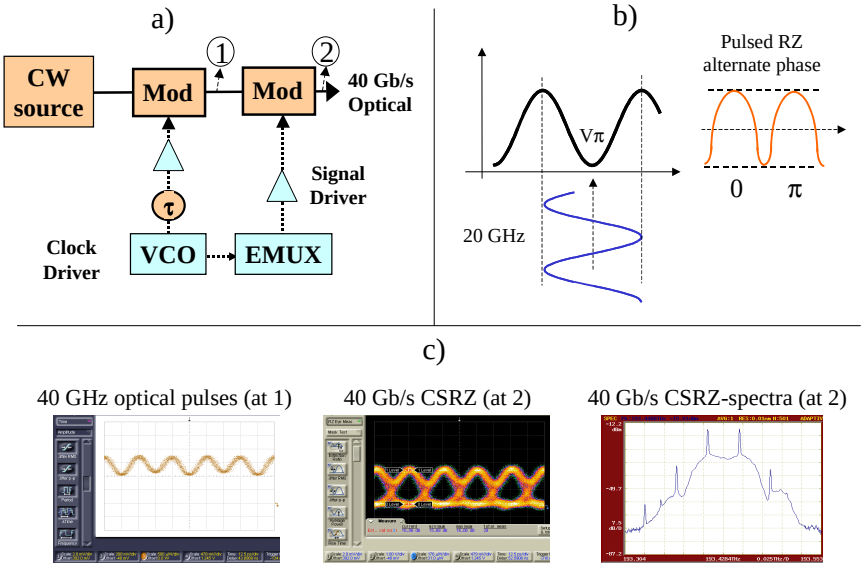

Figure 6.7: Illustration of the implementation of a CSRZ transmitter. a) Building blocks. b) Pulse generation from a 20 GHz electrical signal. c) Example from a practical implementation: 40 GHz pulse signal, 40 Gb/s CSRZ eye diagram and spectrum. EMUX: Electrical multiplexer.

The first stage generates the 40 GHz pulsed signal while the second modulator adds the information creating the 40 Gb/s CSRZ signal. The 40 GHz pulse signal is originated from a 20 GHz clock signal driving the modulator with $2 \cdot V_\pi$ voltage and bias at V_π as shown in Figure 6.7 b). The pulses have an alternate $0,\pi$ phase shift and duty cycle of 66 %. As an example we can observe in c) a typical eye diagram and spectrum from a practical implementation. The spectrum is very characteristic with two carriers separated 40 GHz, generated by the 20 GHz modulation. The signal presented in this example had an extinction ratio of 16 dB. A 40 Gb/s CSRZ integrated transmitter where CW laser source and the two stage modulator were included in the same package has been demonstrated in [220].

CSRZ in a 100 GHz channel spaced WDM system

We have modelled the CSRZ transmitter and used the same procedure as described in Section 6.1.1 to evaluate how CSRZ performs in a 100 GHz WDM system. Results of the investigation are shown in Figure 6.8. We can clearly keep the same penalty levels as when using NRZ modulation and even the same type of margins when using the second-order Gaussian filter. It is important to remember that we also obtain a sensitivity improvement with CSRZ in comparison to NRZ. For the simulations presented here it was a 2 dB improvement. The spectrum for the 4 channel WDM system with 100 GHz spacing clearly shows an improvement if it is compared to the one obtained from the RZ transmitter in Figure 6.5.

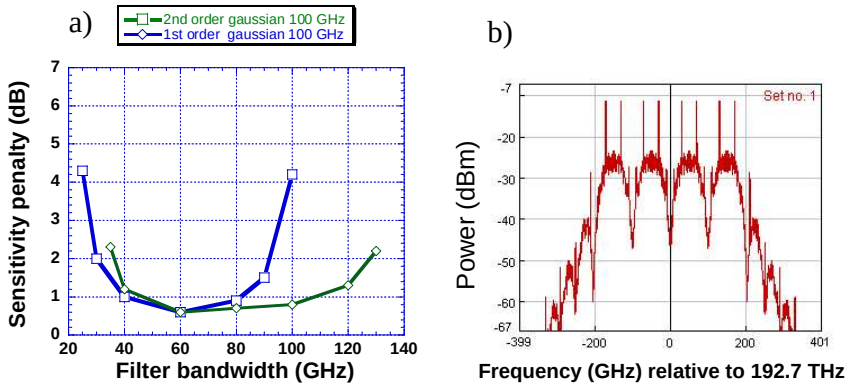

Figure 6.8: Filter bandwidth and shape influence in a 100 GHz spacing 40 Gb/s WDM system, CSRZ modulation. a) Sensitivity penalty as a function of 3-dB filter bandwidth. b) Simulated frequency spectrum of the 4 channel WDM signal with CSRZ modulation, Resolution bandwidth 0.1 nm.

Dispersion tolerance of a CSRZ transmitter

The dispersion tolerance of CSRZ modulation format has been compared by means of simulations to a 12 ps RZ transmitter. The sensitivity penalty as a function of dispersion for both modulation formats is shown in Figure 6.9. Results presented are after comparison to their respective back-to-back sensitivity and using a PIN based receiver.

The 1 dB penalty margin is slightly higher when using the CSRZ modulation format allowing for a tolerance of ±45 ps/nm. However the tolerance for CSRZ is still below the dispersion tolerance observed for PSBT or NRZ modulation.

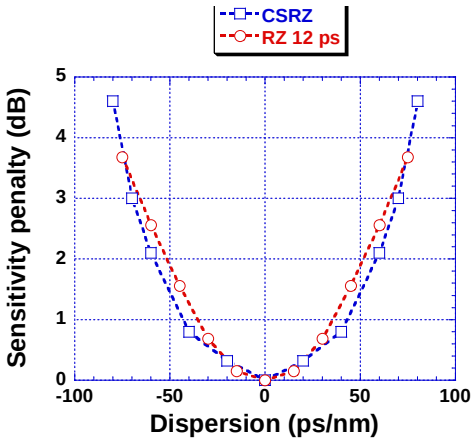

Figure 6.9: Comparison of dispersion tolerance for a a CSRZ transmitter and a 12 ps RZ transmitter.

CSRZ in a multi-span single wavelength system

We follow the single channel multi-span investigation presented in Chapter 5 to analyze the performance of CSRZ in comparison to RZ, NRZ and optical duobinary modulation formats. The results of the investigation of transmission over standard-SMF are presented in Figure 6.10.

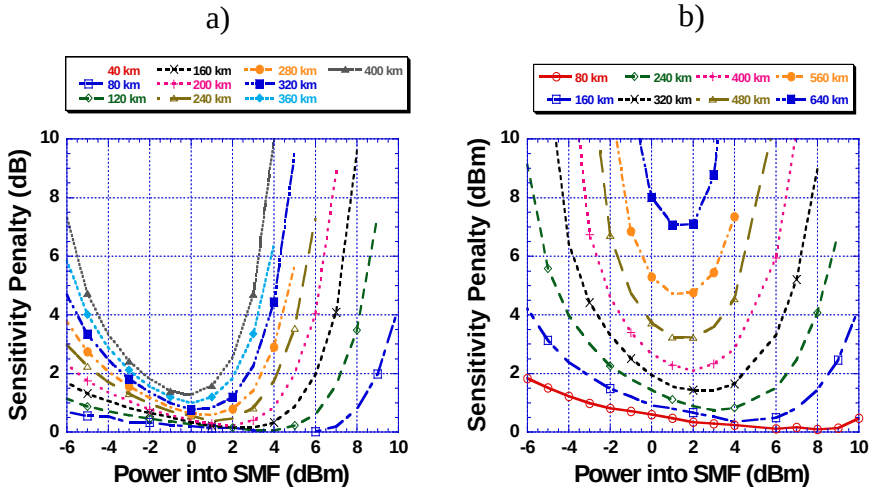

Figure 6.10: Simulated performance for the multi-span transmission over standard-SMF using CSRZ transmitter. a) 40 km spans, b) 80 km spans.

The performance of CSRZ over a multi-span system is comparable to the case of an 8 ps RZ transmitter, see Section 5.3. We are able to transmit over 10 spans of 40 km and 4 spans of 80 km standard-SMF with sensitivity penalties below 2 dB. The optimum launched power levels are lower for the CSRZ modulation, around 0 dBm in the 40 km span case and 2 dBm in the 80 km study.

6.2 Non-linear crosstalk in WDM systems

The goal of this section is not to provide a complete detailed insight into the complex topic of non-linearities in WDM systems but to illustrate with a few examples, their influence and characterization.[1] We will initiate this section by introducing briefly the two main sources of non-linear cross-talk in WDM systems; Cross-Phase Modulation (XPM) and Four Wave Mixing (FWM). The second part of the section will present a practical example of measurement of FWM and XPM effect in a WDM system.

6.2.1 Cross phase modulation and four wave mixing

Self Phase Modulation was defined, see Section 5.1.3, as the self-induced non-linear phase shift by a single channel at high power levels due to the non-linear refractive index. In a WDM system the nonlinear phase shift observed in a specific channel is dependent on the power of all the other channels. This effect is named Cross Phase Modulation. As with SPM, XPM is linked to dispersion in a complex way [222]. Dispersion induces signals at different wavelengths to travel at different speeds. In a WDM system, signals corresponding to different channels will be moving from each other in time, avoiding constant interaction of a fixed pattern over a long period. In addition, dispersion broadens the pulses reducing peak powers and consequently non-linear effects. On the other hand, dispersion is responsible for conversion of the phase modulation into amplitude distortion. XPM can be analyzed in the time domain using a pump-probe measurement set-up, where a modulated signal (pump) generates a copy of the information in the probe. The amplitude of the observed distortion is directly related to the XPM. It has been experimentally demonstrated that XPM is stronger in NZDSF than in standard-SMF fibers [57, 222] and that it is considerably reduced when using dispersion compensation [57, 223]. XPM is directly related to the channel spacing, generally the distortion induced by XPM increases for a reduced channel spacing. A final consideration is the fact that the intensity of the XPM distortion is dependent also on the relative

[1] The reader is suggested to look into reference [221] for a complete presentation of non-linear effects in WDM systems.

polarization of the signals, being maximum for co-polarized signals.

Four wave mixing originates from the beating between light at different frequencies and manifests itself by generation of new wave at new frequencies. If three components co-propagate at frequencies f_1, f_2 and f_3, nine new waves are generated at frequencies $[f_4..f_n..f_9]$ such that

$$f_n = f_i + f_j - f_k \tag{6.2}$$

where $i, j, k = 1, 2, 3$ with $j \neq k$ [201].

In an equally spaced WDM systems the generated wavelengths fall right in the frequencies allocated for other channels inducing crosstalk directly . The efficiency of the four wave mixing is directly related to the channel spacing, the dispersion of the fiber and the effective area (EA). Narrow channel spacing, and fibers with low dispersion and low effective areas will induce high power crosstalk levels. Following the description presented in [56] we have calculated the expected relative crosstalk levels for four different fiber types when two channels are transmitted with 1 mW over 100 km of fiber. Results are shown in Figure 6.11 using the following fiber parameters: dispersion 17 $ps/nm \cdot km$ and EA of 80 μm^2, dispersion 6 $ps/nm \cdot km$ and EA of 63 μm^2, dispersion 3 $ps/nm \cdot km$ and EA of 50 μm^2 and dispersion 1 $ps/nm \cdot km$ and EA of 50 μm^2. These results are intended to provide a reference for the influence of the dispersion, effective area and channel spacing in the FWM process.

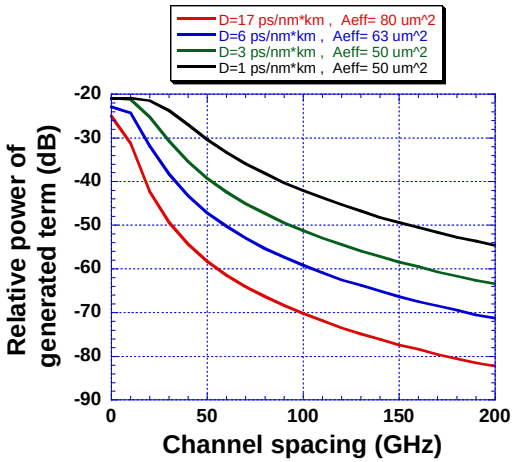

Figure 6.11: Crosstalk levels induced by FWM in different fiber configurations as a function of channel spacing. Following [56].

For example, crosstalk is increased by close to 10 dB when we change the

dispersion of the fiber from 17 to 6 $ps/nm \cdot km$ while keeping the same channel spacing for channel spacing above 50 GHz. It is important to consider that crosstalk terms will be added as a function of the number of channels in the WDM system. For example in a system with four channels we should observe already addition of three crosstalk terms in two of the channels. Crosstalk induced by FWM can be considered as interference crosstalk, a sensitivity penalty of 1 dB should be expected for a level of interference crosstalk of -20 dBm [224]. A method used to avoid crosstalk from FWM generated products and included in ITU standards [15] is to use a non-equal channel spacing between the transmitted signals inducing the crosstalk to fall at non-used frequencies. This method however reduces the spectral efficiency and increases the complexity of the system.

6.2.2 16 channel WDM system with 100 GHz channel spacing

The experimental transmission set-up presented in Figure 5.6 has been upgraded to a WDM system. Transmission fiber is standard-SMF, and DCF modules compensate for the slope of dispersion over a broad wavelength range. We multiplex passively 16 CW co-polarized sources placed in a 100 GHz grid. All channels are NRZ modulated at 40 Gb/s using a single Mach-Zehnder modulator. Channels are placed following the ITU grid [15] between 1548.51 nm to 1560.61 nm. Initially we set power levels for all channels at the input of standard-SMF and DCF modules within the optimum ranges obtained from the single wavelength investigation presented in Section, 5.2.1. The non-flat gain of the in-line amplifiers induces a spreading of the power levels which was tried to keep within small values to avoid OSNR limitations and SPM distortion. The range of power levels being transmitted at the different positions of the system are shown in Table 6.1.

Position in the systems	Maximum power [dBm]	Minimum power [dBm]
1^{st} span SMF	2	-1
1^{st} DCF	-4.6	-6.9
2^{nd} span SMF	1	-1.2
2^{nd} DCF	-4.4	-5.5
3^{rd} span SMF	0.15	-1

Table 6.1: Maximum and minimum optical power levels launched at the different positions of the 200 km standard-SMF link.

The in-line amplifiers induced a slight gain tilt which was corrected by pre-equalizing the power levels at the transmitter. Spectra at the input of the link

and after 200 km standard-SMF transmission are shown in Figure 6.12. We can observe at lower power levels the channel assigned for clock transmission and used at the receiver.

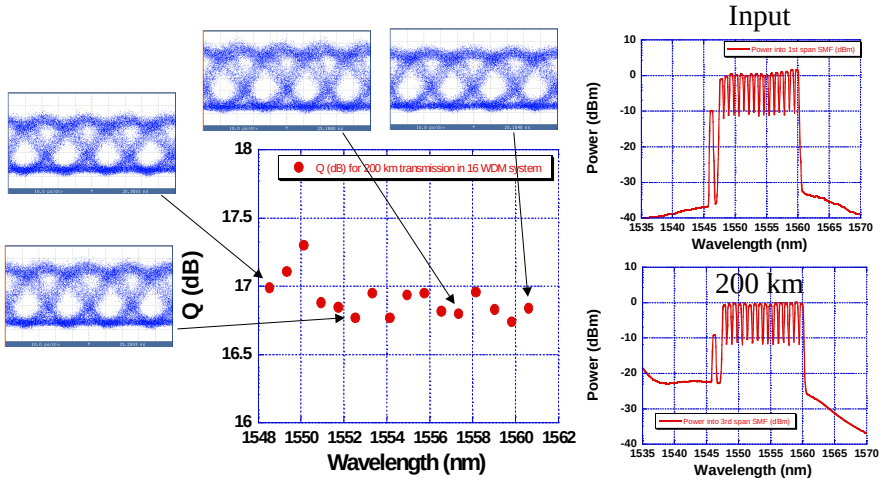

Figure 6.12: Results from the experimental investigation of transmission of 16 WDM channels over 200 km of standard-SMF for 100 GHz channel spacing and 40 Gb/s NRZ modulation. Q factor after transmission is evaluated for all 16 channels. Eye diagrams for four specific channels are shown. Optical spectra are observed at input to first span and output of the link. Spectra are taken with a 0.5 nm resolution bandwidth. Eye diagrams horizontal scale 10 ps/div.

The Q value was evaluated for all 16 channels with worst channel providing a Q of 16.74 dB equivalent to $3 \cdot 10^{-12}$. Eye diagrams are shown for some of the channels as a reference. Due to the slope compensating characteristics of the DCF modules, see Figure 5.6, there was no need for fine tuning dispersion for any channel at the receiver. We evaluated the presence of FWM terms by turning off channel number 9 and evaluated the spectrum at the output of the 200 km link, see Figure 6.13 a). No signs of FWM can be observed, however the FWM term could be buried within the ASE noise. In order to avoid ASE we observed the spectrum after transmission over the first 40 km standard-SMF, see Figure 6.13 b). We needed to increase the average power per channel to 4 dBm in order to observe a FWM term present -37.5 dB below the neighboring channels.

In order to evaluate the effect of XPM and FWM in a quantitative way the optical power level per channel launched into the standard-SMF fiber was increased and decreased simultaneously for all spans compared to the values presented in Table 6.1. Power levels launched into the slope compensating-DCF

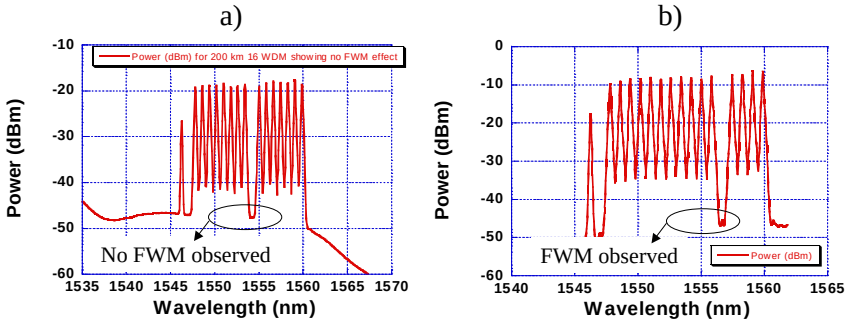

Figure 6.13: FWM in a 16 channel 100 GHz spacing WDM 40 Gb/s NRZ signal in transmission over standard-SMF. a) 200 km link, signal powers kept within -1 to 2 dBm into the standard-SMF and -4.5 to -7 dBm into the slope-DCF modules. b) Single 40 km span increasing power levels to 4 dBm per channel launched into the standard-SMF. Spectra are taken with a 0.1 nm resolution bandwidth.

are kept constant. If performance is limited by OSNR, increasing the power levels will provide an improved performance. If performance is deteriorated for increased power levels, distortion can be considered to be induced by SPM, XPM and FWM. Results from this investigation are presented in Figure 6.14.

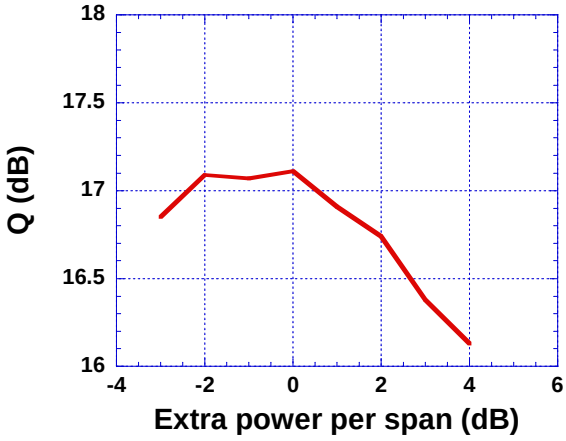

Figure 6.14: Investigation of the combined effect of XPM and FWM in a 16 channel 100 GHz spacing 40 Gb/s NRZ WDM signal in transmission over standard-SMF. The power launched into each standard-SMF transmission fiber is changed while keeping equal power levels at the slope compensating-DCF modules.

Optimum power levels are observed to be within the -2 to 0 dBm. If we consider that for single channel optimum power level was below 1 dBm, it seems that XPM and FWM do not induce serious additional distortion to the WDM system. We can conclude that expansion of a single channel using NRZ modulation to a 100 GHz spaced WDM system has been demonstrated and that power levels could be kept within the single channel optimum values without signs of XPM or FWM. It is important to underline that all channels launched into the transmission fiber in the experimental investigation are co-polarized which should emulate a worst case situation.

Finally as a reference we present a simple characterization using the NZDSF transmission fiber used in the experimental investigation of Section 5.2.2. This results should be compared to those shown in Figure 6.13. The dispersion of the NZDSF fiber was measured to be 3.5 $ps/nm \cdot km$ at 1550 nm. We use in this case only 8 channels at 100 GHz, and the optical power launched into the fiber is 4 dBm per channel. When channel 5 is switched off a FWM tone can be clearly observed, the power of the tone relative to the neighboring channels has now increased to -30 dB.

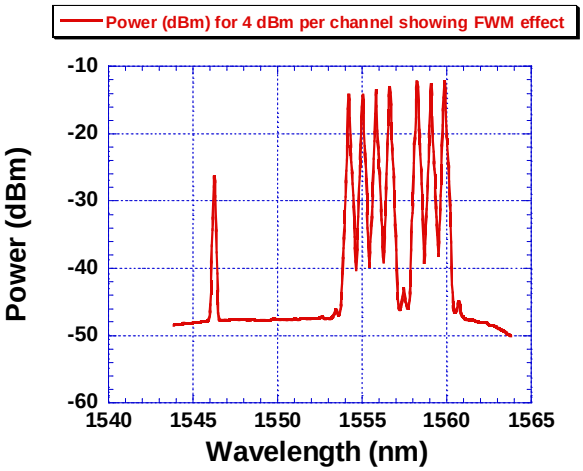

Figure 6.15: FWM in a 8 channel 100 GHz spacing 40 Gb/s NRZ WDM signal in transmission over NZDSF. Single 40 km span increasing power levels to 4 dBm per channel launched into the NZDSF. Spectra are taken with a 0.1 nm resolution bandwidth.

These results clearly demonstrate the expected increase in crosstalk levels in NZDSF due to FWM for high optical power launched per channel in a WDM system. The limitations will be different for each type of fiber and should be

carefully investigated for each case.

6.3 Long haul WDM transmission over 400 km standard-SMF

In this section we will present transmission characterization of different implementations of a 40 Gb/s WDM system in a 400 km link using standard-SMF. The first example will characterize a 16 channel system with 200 GHz channel spacing using CSRZ as the modulation format. The second one, will show an upgrade to a 32 channel system also using CSRZ. These transmission experiments have been carried out in collaboration with Quang Nghi Trong Le (Industrial Ph.D. with OFS Fitel Denmark I/S & Research Center COM).

6.3.1 16 channels at 200 GHz channel spacing using CSRZ

The 400 km link consisted of 5 spans of 80 km standard-SMF. Average insertion loss for an 80 km span was 17 dB. Slope compensation modules matched to the transmission fiber were used for chromatic dispersion compensation. Average insertion loss for the slope dispersion compensation modules is 6.5 dB. These modules are designed to compensate dispersion for 80 km standard-SMF. Moreover, Raman amplifiers were used every other span in order to keep an appropriate OSNR level reaching the 40 Gb/s receiver. The receiver is based on OTDD, further details on its implementation are presented in Appendix C. A schematic of the transmission set-up is presented in Figure 6.16. The total PMD of the link, calculated from data provided for the fiber spools, S-DCF and amplifiers was below 3 ps.

16 CW co-polarized lasers are multiplexed passively in a polarization maintaining combiner and amplified via a polarization maintaining EDFA. All channels keep the same polarization at the input of the first modulator of the 40 Gb/s CSRZ transmitter. The CSRZ transmitter is implemented following the method described in Section 6.1.2. The 16 channels are situated at the ITU grid defined in [15] between wavelengths 1535.82 nm and 1559.79 nm. The $LiNbO_3$ Mach-Zehnder modulator used for generating the 40 GHz pulsed signal is a single drive X-cut modulator, kindly provided by Corning-OTI. The modulator used for the data is a dual-drive Z-cut. Odd spans comprise a slope compensating DCF (S-DCF) module directly following the standard-SMF transmission fiber, a backwards Raman pumping scheme using the S-DCF as the gain medium and the first stage of a commercial Tellabs EDFA (MA-OFA). Even spans are build with the S-DCF in the middle section of a MA-OFA. Two of the Raman pumps used in the experimental investigation and the S-DCF

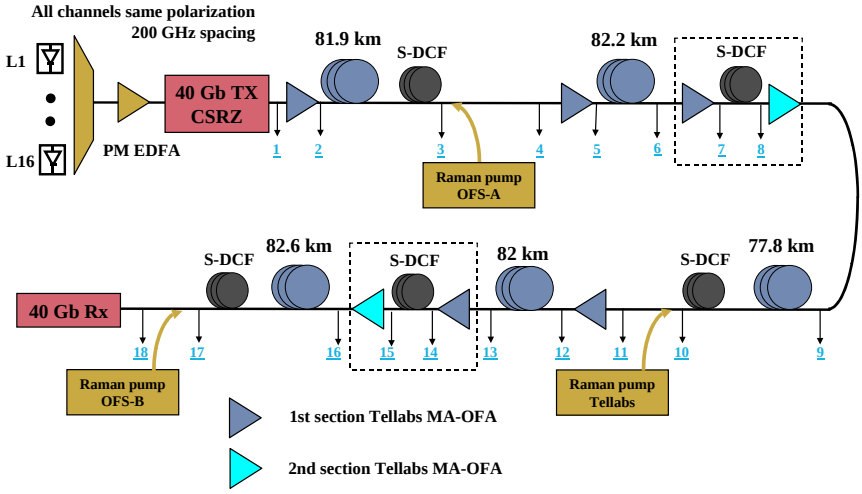

Figure 6.16: Schematic of the 40 Gb/s CSRZ WDM transmission set-up used in the 400 km standard-SMF link experimental investigations. PM: Polarization Maintaining, S-DCF: Slope Dispersion Compensation Fiber, MA-OFA: Mid Access Optical Fiber Amplifier. The 16 channels are situated at the ITU grid defined in [15] between wavelengths 1535.82 nm and 1559.79 nm. The 40 Gb/s Rx is based on OTDD.

modules were kindly provided by OFS-Fitel. Measured values of the chromatic dispersion of the different spools of standard-SMF and S-DCF modules used were provided by OFS-Fitel and allowed to calculate the chromatic dispersion throughout the link. In Figure 6.17 we can observe the calculated evolution of chromatic dispersion in the system as a function of wavelength, the length of the S-DCF modules is included in the distance calculation. We can clearly observe how the spreading of chromatic dispersion over wavelength after each 80 km of standard-SMF is effectively compensated by the slope of the dispersion in the S-DCF modules. The residual chromatic dispersion after the 400 km link varies from -15 ps/nm at 1530 nm to +40 ps/nm at 1565 nm.

We should recall now the discussion presented in Section 3.2.3. We can observe that in an experimental situation where we have specially designed the S-DCF modules to match the transmission fiber we still have a residual chromatic dispersion, which is very close for some channels to the tolerance limit for CSRZ presented in Figure 6.9. Any realistic case will without doubts introduce more uncertainties in the design than this experimental situation indicating that we would benefit very much from a tunable dispersion compensator for long haul WDM transmission.

Due to the smaller effective area of the dispersion compensation fiber which

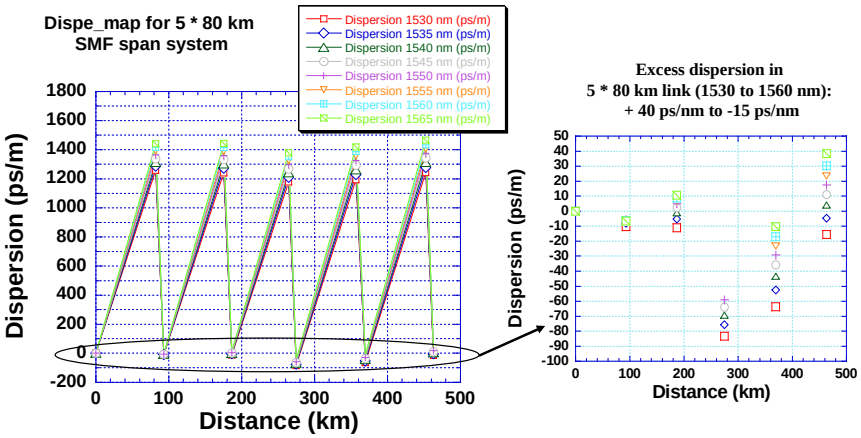

Figure 6.17: Calculated chromatic dispersion as a function of transmission distance and wavelength in the 400 km link using standard-SMF and slope compensating DCF modules. The length of the S-DCF modules is included in the distance calculation. Data for each 40 km standard-SMF and S-DCF modules were kindly provided by OFS-Fitel. The graph at the right shows the residual dispersion distribution over wavelength for each span.

induces a higher non-linear coefficient, see Equation 5.7, Raman amplification is more effective when using the S-DCF modules as the gain medium [199] than standard-SMF. Three different Raman pump configurations were used to provide Raman amplification in the S-DCF modules. The *Tellabs* module consisting of four pumps with 125 mW optical power per pump, wavelengths 1423 nm, 1435 nm, 1445 nm and 1455 nm.[2] The *OFS-A* consisted of two pumps, the first at 1465 nm providing 200 mW and the second one at 1436 nm providing 150 mW. The *OFS-B* consisted of three pumps with 250 mW optical power per pump, two placed at 1465 nm and one at 1437 nm. The amplification provided by the pumps when the S-DCF modules are used as the gain medium was characterized by the *on-off gain* and the effective noise figure F_{eff}. The effective noise figure of the Raman amplification process is a reference value, which indicates the noise figure of an EDFA that should be placed instead of the Raman amplifier to provide the same gain and ASE noise. The effective noise figure of a Raman amplifier can be directly calculated [225] by measuring the on-off gain G_{on-off}, and ASE level at the output of the Raman pump $P_{ASE_{out}}$ in a certain resolution bandwidth B_o, see Appendix E for details on the origin

[2]This module was designed and implemented by Ahmed Junaid Omer within the Master Thesis project "Multiwavelength backward pumped Raman optical amplifier" in a collaboration between Research Center COM and Tellabs.

of this expression.

$$F_{eff} = \frac{1}{G_{on-off}} \cdot \left(\frac{P_{ASE_{out}}}{h\nu B_o} + 1\right) \tag{6.3}$$

The experimental set-up used for the measurement of the on-off gain and the effective noise figure of the Raman amplifiers is presented in Figure 6.18 together with the measured spectra in *on* and *off* situations when using the OFS-B pump. We use a WDM signal consisting of 16 modulated signals as the input and we measure the on-off gain and ASE power in the first span of the 400 km link. In the presented example we could also measure that on-off gain induced in the S-DCF was 12 dB, while 8 dB were induced in the standard-SMF span, resulting in a total gain in the order of 20 dB. Measured on-off gain and F_{eff} for all the Raman pumps in the same characterization set-up are presented in Table 6.2 for channel 1 (1535.82 nm) and channel 16 (1559.79 nm).

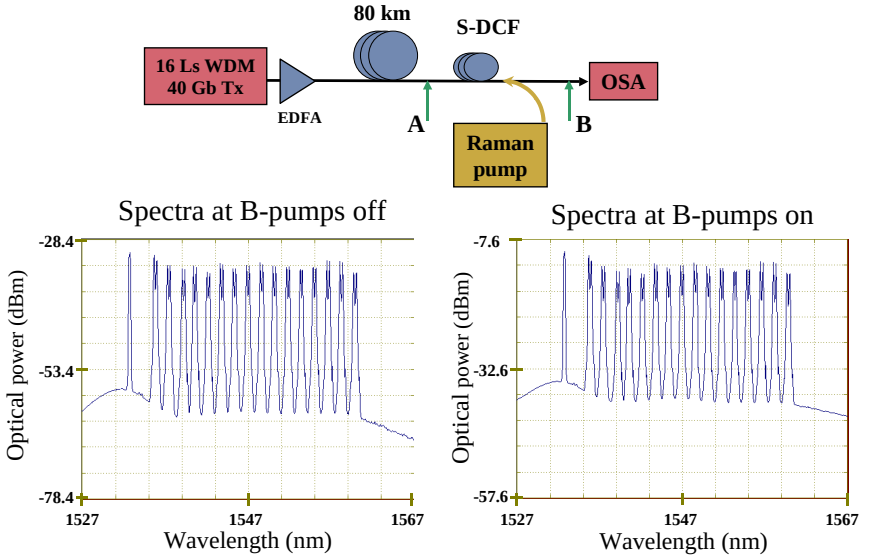

Figure 6.18: Illustration of experimental set-up used in the measurement of Raman on-off gain and effective noise figure. The example shows spectra with pumps on and off when using the OFS-B configuration. Resolution bandwidth 0.1 nm. The signal used in the characterization consists of 16 WDM channels with CSRZ as the modulation format.

Spectra at input to the first transmission span and output from last Raman pump, positions numbered 2 and 18 in Figure 6.16, are shown in Figure 6.19.

From the measured spectra we can deduce the optical signal to noise ratio at the input to the first span and output of the 400 km link, see Figure 6.20

Raman pump	On-Off gain (dB)		F_{eff} (dB)	
	1535.82 nm	1559.79 nm	1535.82 nm	1559.79 nm
Tellabs	13.1	12	0.8	0.3
OFS-A	13.1	14.4	0.2	-2.3
OFS-B	20.8	20.6	0.4	-1.3

Table 6.2: On-off gain and effective noise figure of Raman amplification provided by the different Raman pumps used.

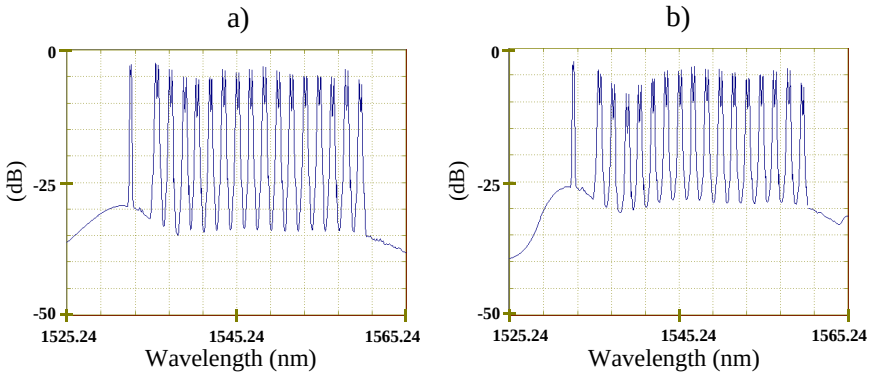

Figure 6.19: Spectra at input of first transmission span and output from the last span for a 16 wavelength WDM system in a 400 km standard-SMF link using 40 Gb/s CSRZ transmitters, at positions 2 and 18 respectively in Figure 6.16. CSRZ is the modulation format used. Resolution bandwidth 0.1 nm. Vertical scale: 5 dB/div.

b). The sensitivity penalty as a function of the OSNR degradation has been evaluated in a single channel CSRZ transmission set-up, see Figure 6.20 a). The OSNR is deteriorated by varying the input power into an EDFA. In a single channel situation we need to be above 28 dB of OSNR to avoid penalties higher than 2 dB.

Eye diagrams are shown in Figure 6.21 for four channels in two situations. First directly after the transmitter and second, after the 400 km standard-SMF link. Eye diagrams after transmission are open and show no clear signs of distortion.

Maximum and minimum optical power levels launched into the transmission fiber and the S-DCF modules (when placed in the MA-OFA) are presented in Table 6.3. These optical power levels were measured when optimum performance of the system was achieved. We can observe how the difference between maximum and minimum optical power within the 16 channels increases as a function of the spans passed in the link. This is mainly due to the fact that the

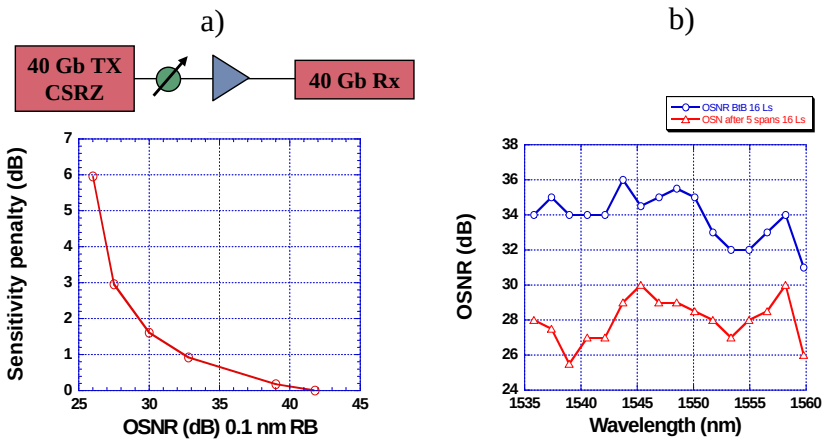

Figure 6.20: a) Set-up (upper schematic) and sensitivity penalty measured as a function of OSNR (lower graph) in a single channel 40 Gb/s CSRZ measurement set-up. The OSNR deterioration is induced by reducing the input power into an EDFA inducing high ASE. b) OSNR measured at input of first transmission span and output from the last span for a 16 wavelength WDM system in a 400 km standard-SMF link as presented in Figure 6.16.

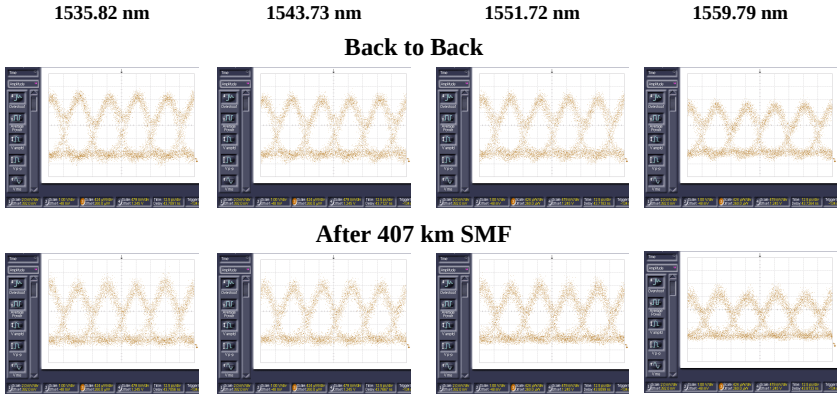

Figure 6.21: Eye diagrams observed directly at the input to the first span and after transmission over 400 km standard-SMF link. System comprises 16 channels at 40 Gb/s using CSRZ modulation, see Figure 6.16 for details. Vertical scale: 424 $\mu m/div$, Horizontal scale: 12.5 ps/div.

double stage amplifiers are designed with opposite gain tilt curves in the first and second sections of the MA-OFA. These gain curves cancel out when used combined providing a low Gain Non Uniformity (GNU). As we only used the

first section in three of the spans we obtained a higher GNU than we would have desired. Furthermore, Raman amplification induces also a wavelength dependent gain.

Span number	Optical power launched [dBm]			
	Standard-SMF		S-DCF	
	Maximum	Minimum	Maximum	Minimum
1	0.5	-2.5		
2	2.5	-1	0	-5
3	4.2	0.2		
4	3.7	0.2	1.6	-3.5
5	5.6	1.6		

Table 6.3: Maximum and minimum optical power levels launched into the transmission fibers in the 16 wavelength WDM system transmission experiment over a 400 km standard-SMF link, as presented in Figure 6.16.

Finally, the performance has been evaluated by measurements of BER and sensitivity penalty compared to the back to back WDM configuration. This means that we include in the reference measurement the 0.5 dB sensitivity penalty (compared to the single channel performance) induced by the filtering process. Figure 6.22 a) shows the BER as a function of the power at the receiver for the back-to-back WDM configuration, after 4 spans and after 5 spans in transmission over the full 400 km link. The channel measured is the one situated at 1550.12 nm. There is a 3 dB penalty observed after 5 spans at a BER of 10^{-10}. We can observe how the slope of the BER curves has tilted indicating a noise induced penalty.

Another way of evaluating the performance of an optical transmission system is by fixing a target BER and observing the variation of the power needed at the receiver to reach the target. Measurement of power needed at the receiver to reach a BER of 10^{-10} for the channel situated at 1550.12 nm is presented in Table 6.4 as a function of the position in the system. It should be observed how the relative increments in the required power grow with the number of spans transmitted. Sensitivity penalty has been evaluated after four spans and in the complete link for three other channels situated at wavelengths: 1545.27 nm, 1554.95 nm and 1559.79 nm. We are limited to measurements above 1545 nm by the experimental implementation of the OTDD based receiver, see Appendix C for further details. Measurements are presented in Figure 6.22 b). We can observe that average penalty within the wavelengths measured is in the order of 3 dB.

It is important to notice that even though some channels were launched with relatively high optical power levels into the transmission fiber we did not observe

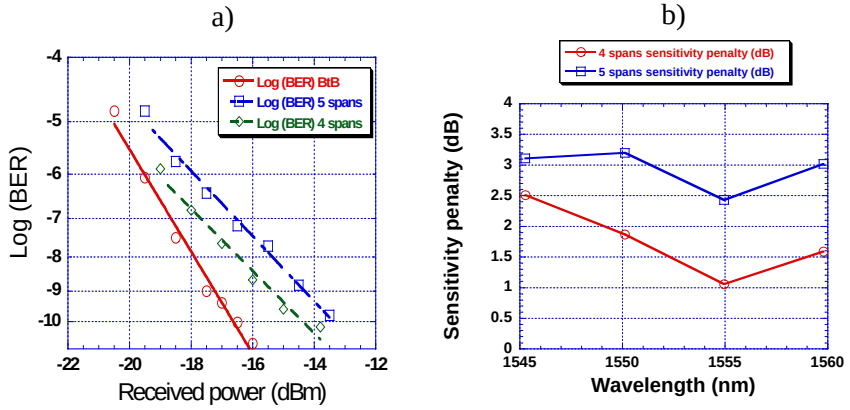

Figure 6.22: BER versus received power measured for the channel situated at 1550.12 nm in the 16 wavelength WDM system transmission experiment over a 400 km standard-SMF link, as presented in Figure 6.16. CSRZ is used as the modulation format. Measurements are shown for the back-to-back WDM situation, after four spans and for the full 400 km link. b) Sensitivity penalty measured for 4 channels.

Position in link	BER	Power at Rx [dBm]
BtB	$6.6 \cdot 10^{-11}$	-16.5
1^{st} span	$1.1 \cdot 10^{-10}$	-16.5
2^{nd} span	$1.7 \cdot 10^{-10}$	-16
3^{rd} span	$1.5 \cdot 10^{-10}$	-15.5
4^{th} span	$2 \cdot 10^{-10}$	-14.5
5^{th} span	$1.6 \cdot 10^{-10}$	-13.5

Table 6.4: Evolution of power needed at the receiver to keep a constant BER of 10^{-10} as a function of the spans travelled in the system in the 16 wavelength WDM system transmission experiment over a 400 km standard-SMF link. CSRZ is used as the modulation format.

signs of XPM or FWM in transmission. It has been indicated in [226] that CSRZ increases tolerances to XPM and FWM, optical power levels per channel as high as 3 dBm could be transmitted over NZDSF transmission fibers in an eight channel WDM experiment. This indicates that higher power levels than 3 dBm could be sent over standard-SMF. However, we also observed that in single channel multi-span transmission over standard-SMF, see Figure 6.10, the optimum power level was in the 2 dBm range.

6.3.2 32 channels at 100 GHz channel spacing using CSRZ

We double the number of channels by interleaving a second set of 16 CW co-polarized lasers. All 32 channels are modulated in a single CSRZ transmitter providing an aggregate capacity of 1.28 Tb/s. The 32 channels are situated at the ITU grid defined in [15] between wavelengths 1535.82 nm and 1560.60 nm. The implemented system provides a spectral efficiency of 0.4 bits/s/Hz. The transmission link set-up is kept as presented in Figure 6.16, and described in Section 6.3.1. Spectra at the input to the first span and output from the last span are shown in Figure 6.23. We can clearly observe in the output spectrum the effect of gain tilt and shaping from the first section MA-OFA. The OSNR ratio at the output of the last span is still kept within the 25 dB area for most of the channels.

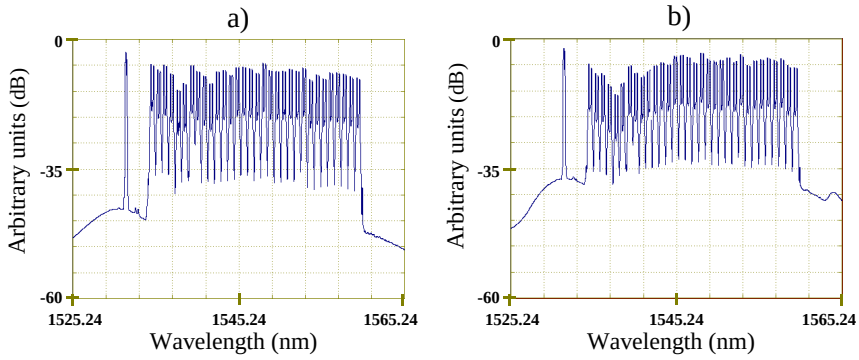

Figure 6.23: Spectra at the input of the first transmission span and output from the last span, positions 2 and 18 respectively in Figure 6.16, for a 32 wavelength WDM system in a 400 km standard-SMF link using CSRZ as the modulation format. Resolution bandwidth 0.1 nm.

Maximum and minimum optical power levels launched within the 32 channels are shown in Table 6.5. In some of the spans we were limited by the saturation power of the first section of the MA-OFA and maximum optical power levels per channel are generally reduced. We can also observe that the power spreading has increased mainly induced by the fact that channel number 4, placed at 1538.18 nm is placed at the minimum gain of the first section of a MA-OFA and is not compensated by the second section in three amplifiers.

The evolution of the average power throughout the link at the positions marked with numbers in Figure 6.16 is presented in Figure 6.24. We can clearly observe the reduction in span insertion loss allowed by the Raman amplifiers stages. When the Raman pumps were turned on the OSNR was improved by

Span number	Optical power launched [dBm]			
	Standard-SMF		S-DCF	
	Maximum	Minimum	Maximum	Minimum
1	1	-4.5		
2	2.3	-4	-0.5	-6
3	3.5	-3.5		
4	2	-5.7	1	-6.3
5	5	-2.7		

Table 6.5: Maximum and minimum optical power levels launched into the transmission fibers in the 32 channel 40 Gb/s CSRZ WDM system transmission experiment over a 400 km standard-SMF link, as presented in Figure 6.16.

3 to 5 dB (wavelength dependent) compared to the off situation.

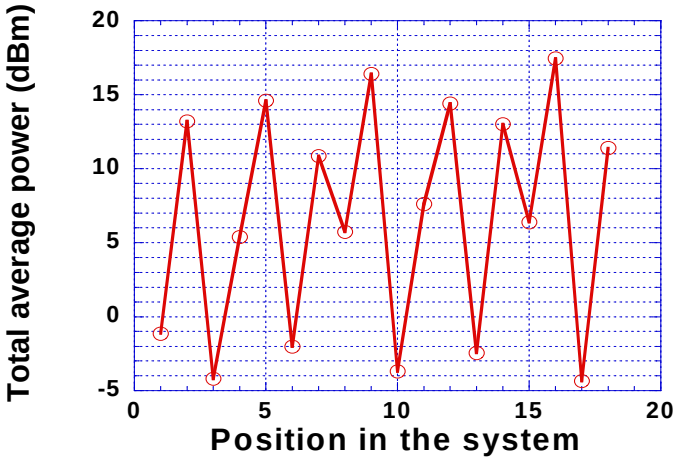

Figure 6.24: Evolution of the average power levels throughout the link at specific positions in the 32 channel 40 Gb/s CSRZ WDM transmission experiment over a 400 km standard-SMF link. Positions indicated correspond to those marked in Figure 6.16.

Eye diagrams for 12 channels out of the 32 are shown in Figure 6.25. We can observe a certain degradation in some of the eyes, for example channel 32 corresponding to wavelength 1560.61 nm, with signs of accumulated noise if we compare them to those presented in Figure 6.21.

An origin of the deterioration in the 32 channel set-up is the not optimized filtering at the receiver. The filter used at the receiver for channel selection has a 3 dB bandwidth of 0.55 nm and a 20 dB bandwidth of 1.54 nm, which indicates

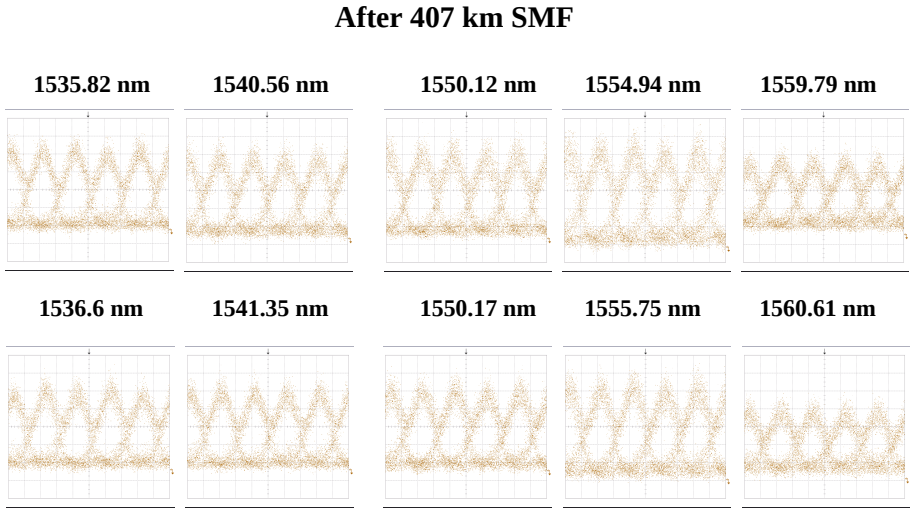

Figure 6.25: Eye diagrams observed directly in the 32 channel WDM experiment after transmission over 400 km standard-SMF link using CSRZ as the modulation format. Horizontal scale: 12.5 ps/div, vertical scale: dependent on wavelength.

a wider shape than a first order Gaussian filter. The crosstalk levels when filtering the 32 channel CSRZ WDM signal was as high as -15 dB introducing a penalty of 1.25 dB when comparing the back to back situation with the 16 channel CSRZ WDM signal. In Figure 6.26 we can observe the difference in crosstalk levels when filtering at the receiver a 100 GHz channel spaced NRZ (a) and CSRZ (b) WDM signal. For the NRZ signal, the crosstalk level is reduced below the -20 dB level. By proper design of the receiver filter we could obtain a reduction of the crosstalk levels and improvement in the CSRZ back-to-back sensitivity allowing for higher margins in the link.

Finally, performance has been evaluated by means of BER measurements. Figure 6.27 a) shows the BER as a function of power at the receiver for the back-to-back situation and after the 400 km transmission.

Sensitivity penalty after transmission over the 400 km link in the 32 channel WDM case has now increased to 3.5 dB for the measured channel at 1555.75 nm. Sensitivity penalty at BER of 10^{-10} is shown in b) for 7 other channels. An average penalty of 4 dB was observed with a minimum of 2.7 dB and a maximum of 4.9 dB. We are again limited by the receiver set-up to measurements above the 1545 nm channel, see Appendix D for further details. These penalty levels could be reduced if Raman amplification was used at each span, an optimized

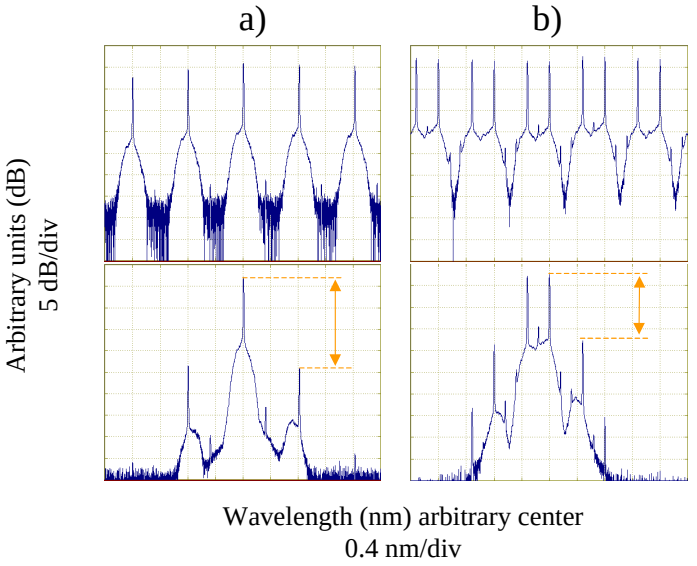

Figure 6.26: Experimental verification of the effect of filtering at the receiver in a 100 GHz channel spaced CSRZ WDM signal (b) compared to a 100 GHz NRZ WDM signal (a). The filter used at the receiver for channel selection has a 3 dB bandwidth of 0.55 nm and a 20 dB bandwidth of 1.54 nm

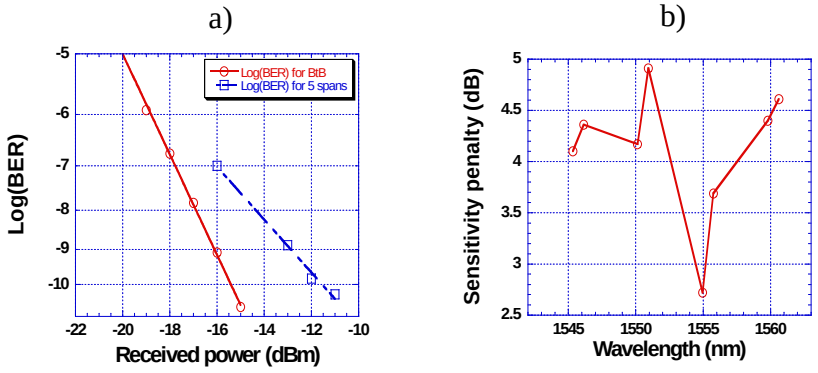

Figure 6.27: a) BER versus received power measured for the channel situated at 1555.75 nm in the 32 wavelength WDM system transmission experiment over a 400 km standard-SMF link using CSRZ as the modulation format. Measurements are shown for the back-to-back WDM situation and for the full 400 km link. b) Sensitivity penalty measured for 8 channels at a BER of 10^{-10}.

filter was used at the receiver, higher saturation powers were allowed from the EDFAs and GNU was reduced.

6.4 Metro WDM transmission over four spans of 40 km transmission fiber

Metro WDM networks cover typically spans with transmission distances below 50 km and wavelength grouping to avoid optical-electrical-optical conversion for all channels at all nodes. Amplification at each node might be done for each wavelength group and not for the full WDM signal. Moreover, Metro WDM equipment should minimize space usage as it will generally be placed in costly urban offices. The compactness and cost savings of Semiconductor Optical Amplifiers (SOAs) may be advantageous in Metro networks. A characteristic property of SOAs is their ability to follow fast variations in the gain, in the order of 100 ps. The fast gain response of SOAs makes them ideal to be used as gates [227] or as wavelength converters when used in saturation [228]. On the other hand, the fast gain induces crosstalk between channels in a WDM signal when the SOA is used in saturation, a phenomena known as Cross Gain Modulation (XGM). An illustration of the effect of XGM is presented in Figure 6.28 a) with an example of a 40 Gb/s eye diagram with high XGM distortion.

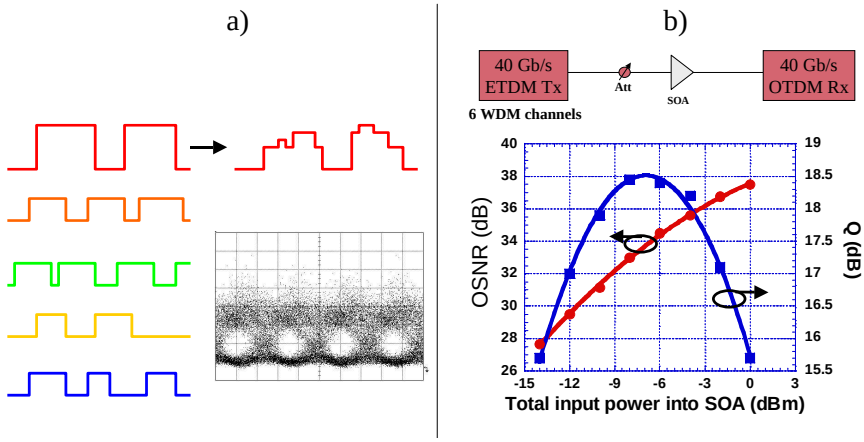

Figure 6.28: a) Illustration of the XGM effect observed in saturation of a SOA. The eye diagram of a 40 Gb/s NRZ signal shows clear traces from crosstalk on the *ones* level. Horizontal scale: 10 ps. b) Experimental verification of XGM, 6 NRZ channels at 40 Gb/s and 100 GHz spacing are launched into the SOA. An attenuator at the input determines the saturation level of the SOA.

The effect of XGM can be characterized by launching a WDM signal into

the SOA at different power levels and evaluate the performance of one of the channels as a function of the input power to the SOA. This has been done with a 6 channel 40 Gb/s WDM signal with 100 GHz channel separation and based on NRZ modulation format. The SOAs used were provided by JDS Uniphase, had a gain peak traditionally at 1520 nm of 20 dB, a gain at 1550 nm of 17 dB, noise figure within 8 to 10 dB, an output power within the 11 dBm range and a polarization dependent gain below 1.5 dB. The results of the XGM characterization are shown in Figure 6.28 b). We use measurement of the quality factor Q in dB for evaluating performance. The optimum working point is for a total optical power of -7 dBm input to the SOA or -15 dBm per channel. For power levels below this value we suffer from low OSNR, while for power levels above -7 dBm we observe a rapid decrease of Q due to the XGM, even though the OSNR continues increasing. Please notice that there is no fiber included and no other nonlinear effects should be observed.

There have been several methods proposed to avoid or control the XGM in SOAs; use of a *dummy* signal inverse in time of the modulated signal to trick the SOA to observe only a constant signal in time [229, 230], use of a high power reservoir channel which saturates the SOA and allows the individual modulated signals to avoid seeing gain variations [231] and use the SOA in a light saturation regime avoiding the XGM as much as possible [232]. We will follow the last method in the experimental work presented in this section. It is important to notice the recent introduction of the a Linear Optical Amplifier (LOA) in [233], which is designed to directly avoid any XGM and has a great potential for use in metro networks.

The experimental set-up is presented in Figure 6.29. It consisted of a 6 channel 40 Gb/s WDM NRZ transmitter followed by an attenuator and a polarization controller. These were adjusted to tune the first SOA situated at the transmitter to maximum gain and minimum XGM. Each span consisted of a 40 km standard-SMF spool and a dispersion compensation module (not slope compensating). The average attenuation per span was 14 dB. Between each span we placed a SOA as the in-line amplifier with no specific power or polarization control. Two isolators were included to avoid amplification of reflections in the link.

The spectra at the output of the first SOA situated at the transmitter and the last SOA in the link are shown in Figure 6.29 b). We can clearly observe a tilt caused by the characteristic gain shape of the SOAs. This tilt could be avoided for example by pre-equalizing the power levels at the transmitter. The OSNR observed at the receiver was higher than 28 dB if we consider a 0.1 nm resolution bandwidth. The quality factor was higher than 16 dB for all channels indicating bit error rates below 10^{-11}. There was no significant

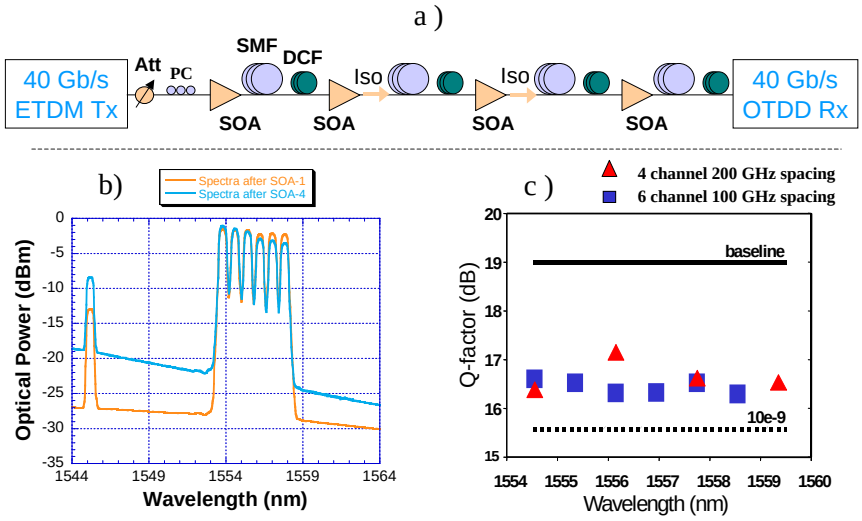

Figure 6.29: a) Illustration of the set-up used in the 4 times 40 km standard-SMF metro WDM experimental investigation. b) Spectra at the output of the first and last SOAs in the link. Resolution bandwidth of 0.5 nm. c) Quality factor performance for a 4 channel 200 GHz spacing and a 6 channel 100 GHz spacing situations.

difference observed between a 6 channel system in a 100 GHz spacing and a 4 channel system in a 200 GHz spacing. All power levels launched into the transmission fiber were in the order of 0 dBm per channel to avoid non-linear effects while keeping a high OSNR. The total power launched into all SOAs was kept below the -6 dBm range to avoid the XGM. We could vary the input power into the first SOA from -5 dBm to - 9 dBm and still keep a Q value above 16 dB for transmission through the full link. These results prove that SOAs could be used as in-line amplifiers for WDM systems at 40 Gb/s with low channel count and over span distances characteristic of Metro networks.

6.5 Summary

Linear crosstalk in a 100 GHz channel spaced WDM system has been investigated for different modulation formats: NRZ, RZ and optical duobinary. Optical duobinary is the modulation format which performs best in a dense WDM system providing even an improvement in sensitivity due to pulse re-shaping. Margins for NRZ are considerable and this modulation format is appropriate also for 100 GHz WDM systems. For RZ modulation we observe tight margins, steep filters with 3dB bandwidths between 60 and 80 GHz should be used in

order to avoid penalties above 2 dB.

We have introduced CSRZ as a new modulation format with improved performance compared to traditional RZ modulation in dense WDM systems. Furthermore, we have demonstrated that CSRZ performs well in a multi-span system allowing transmission over 4 spans of 80 km standard-SMF with penalties below 2 dB and high optical power level tolerances. CSRZ allows for a dispersion tolerance similar to a 12 ps RZ transmitter, estimated to be $\pm 45\ ps/nm$ by means of simulations.

XPM and FWM have been introduced as source of non-linear crosstalk in WDM system. We have demonstrated that in 16 channel WDM system using NRZ as the modulation format and in transmission over 200 km of standard-SMF we can avoid XPM and FWM if we keep launched optical power levels below 0 dBm. In a single 40 km span of standard-SMF we needed to set power levels per channel (15 channels) as high as 4 dBm to be able to observe FWM crosstalk levels in the order of -37.5 dBm. For a specific NZDSF fiber used and for only 7 channels, for the same power level of 4 dBm per channel the FWM crosstalk level had increase to -30 dBm.

We have presented a 400 km transmission link consisting of 5 spans of 80 km standard-SMF. Dispersion compensation was achieved using slope compensating DCF modules. Three Raman amplifiers were used to keep high OSNR levels reaching the receiver. The gain medium used in the Raman amplification were the slope compensating DCF modules with low effective area. CSRZ was used as the modulation format. Transmission of 16 channels at 200 GHz channel spacing was possible with sensitivity penalties of 3 dB. Transmission of 32 channels at 100 GHz channel spacing providing an aggregate capacity of 1.28 Tb/s and a spectral efficiency of 0.4 bits/s/Hz was achieved with sensitivity penalties of 4 dB. These penalty levels could be reduced if Raman amplification was used at each span, an optimized filter was used at the receiver, higher saturation powers were allowed from the EDFAs and GNU was reduced.

Finally we have demonstrated that Semiconductor Optical Amplifiers can be used as in-line amplifiers in 40 Gb/s WDM systems with span distances corresponding to those considered for Metro networks and with low channel count. Transmission avoiding Cross Gain Modulation has been demonstrated over four spans of 40 km standard-SMF for a WDM system consisting of 6 channels at 100 GHz spacing with measured Q above 16 dB for all channels. This level of performance could be maintained while the total input power into the first SOA varied from -5 dBm to -9 dBm.

Chapter 7

Proposal of 40 Gb/s systems

In this chapter we come back to the different optical transmission systems presented in Chapter 2 where 40 Gb/s technology could be used. We propose and define the implementation of single channel wavelength systems, long haul WDM systems and metro WDM systems.

In Section 7.1 we bring together the different modulation formats: NRZ, RZ, CSRZ and PSBT that have been evaluated throughout the thesis. We compare them in terms of chromatic dispersion, PMD, SPM, multi-span transmission, spectral efficiency and nonlinear crosstalk.

Section 7.2 presents proposals for system design of single wavelength systems, defining application codes for short, long and very long haul reach. Each proposed system implementation is described and the main parameters are discussed.

In Section 7.3 a proposal for a 32 channel WDM system will be presented. The defined WDM system will allow transmission over a maximum of 5 spans with typical lengths per span ranging between 40 and 80 km.

An example of a possible metro WDM network implementation for 40 Gb/s bit rate channels is presented in Section 7.4.

Section 7.5 will provide a review of the actual availability of the different components used in the proposed implementation of single wavelength, long haul WDM and metro WDM systems.

The chapter will end with a summary.

7.1 Comparison between modulation formats to be used in 40 Gb/s transmission systems

We have introduced and characterized throughout the previous chapters different modulation formats: NRZ, RZ, PSBT and CSRZ. In this section we provide a direct comparison of these modulation formats. This comparison will outline the modulation formats which best fit the different system applications.

The comparison of the modulation formats is done taking into account the following categories:

- Dispersion tolerance measured for a maximum penalty of 1 dB in a PIN receiver.
- Maximum total average DGD allowed in the link. We consider as a general case for comparison the average value that provides a probability of $4{\cdot}10^{-5}$ for reaching an instantaneous DGD which will induce a 1 dB penalty in a preamplified (EDFA or APD) receiver, see Chapter 4 for a background explanation. For NRZ and PSBT the penalty will be 0.5 dB in a PIN receiver while RZ and CSRZ will keep the 1 dB penalty still in a PIN receiver.
- Maximum optical power level which can be launched in a single standard-SMF dispersion compensated span resulting in a penalty below 1 dB in a preamplified receiver due to SPM distortion. We suppose that power levels into the DCF module are kept below values which induce SPM in these type of fibers.
- Maximum number of spans that can be reached with a total penalty below 2 dB in a preamplified receiver and that provide a power margin tolerance higher than 3 dB. The transmission fiber considered is standard-SMF.
- Expected end of life sensitivity to be available when using state of the art commercial PIN receivers.
- Channel spacing that is possible to guarantee with a sensitivity penalty below 1 dB.
- Relative performance expected for each modulation format regarding the non-linear crosstalk in NZDSF and DCF. NRZ is taken as the base for comparison.

Table 7.1 provides values for the different categories considering results from simulations, experimental work and literature that have been considered throughout the thesis.

Regarding dispersion it is clear to observe that PSBT is the modulation format with highest margin. It also provided the best results regarding spectral efficiency. On the other hand it has a low SPM limit and performs rather poorly in a multi-span system.

Regarding SPM limitations the low duty cycle RZ transmitter provides the highest margins and allows for transmission over 5 spans of 80 km without need of using FEC or Raman amplification. On the other hand low duty cycle RZ will not allow for channel spacing of 100 GHz making it not so attractive for a WDM system.

CSRZ provides a good overall performance, similar to moderate duty cycle RZ transmitters regarding SPM limitations and multi-span transmission while still able to be fitted in a 100 GHz channel spacing. Only regarding dispersion tolerance we can see a reduced margin compared to NRZ.

NRZ provides an acceptable overall performance regarding dispersion, channel spacing but is seriously limited by the SPM tolerance in a multi-span system.

Modulation format	Dispersion[1] tolerance [ps/nm]	PMD tolerance [ps]	Single span[4] SPM limit [dBm]	Max. spans[5] 40 km SMF single λ	Max. spans[5] 80 km SMF single λ	Sensitivity[6] [dBm]	Channel[7] spacing [GHz]
NRZ	$\pm$70	2.5[3]	8	4	2	-11	100
RZ moderate DCy[8]	$\pm$30	3.5[2]	12	9	4	-13	200
RZ low DCy[8]	$\pm$20	4[2]	14	> 11	5	-13.5	200
PSBT	$\pm$200	2.5[3]	7	4	1	-10	75
CSRZ	$\pm$45	3.5[2]	11	10	4	-13	100

Table 7.1: Comparison of NRZ, RZ, PSBT and CSRZ modulation formats regarding their performance in 40 Gb/s optical transmission systems. Notes: [1] For 1 dB sensitivity penalty in a PIN receiver. [2] Maximum average DGD allowed in the link resulting in a 1 dB sensitivity penalty in a noise dependent receiver. [3] 0.5 dB sensitivity penalty in a PIN receiver. [4] For a 1 dB sensitivity penalty in a preamplified receiver in transmission over standard-SMF. [5] For a 2 dB total sensitivity penalty with power margin tolerance higher than 3 dB in transmission over standard-SMF, no FEC or Raman amplification considered. [6] Expected sensitivity for a state of the art PIN receiver at end of life. [7] Possible channel spacing with a sensitivity penalty below 1 dB. [8] Moderate duty cycle corresponds to pulses of 8 to 11 ps, low duty cycle corresponds to pulses of 3 to 5 ps.

7.2 Proposal of single wavelength 40 Gb/s application codes

In this section we propose and define possible implementation of system configurations for short, long and very long haul applications. These proposals should be taken as an opinion from the author and are not related in any way to any Tellabs product definition.

The parameters used in the characterization of each proposed application code are directly related to the parameters defined and presented in Section 2.2.2 and can be better understood considering Figure 2.3.

We have followed the considerations presented throughout the thesis and resumed in the previous section regarding the decision over the limiting parameters and tried to provide a realistic approach to the proposals. When possible we have followed trends from STM-64 standardized application codes. No FEC is considered in the application codes defined. However, the use of FEC will improve the transmission performance and is recommended.

We do not discuss Intra-office or Very short reach applications as they can be implemented following ITU G.693 [27] and the OIF VSR-5 [28] recommendations.

The application codes are abbreviated following ITU notation. S, L or V regarding the span length and attenuation for Short, Long and Very long haul systems. *256* refers to the SDH capacity for Virtual Containers (VC) level 4 available in a 40 Gb/s signal. The fiber used for transmission is labelled *2* for standard-SMF and *5* for NZDSF. Finally the type of system defined will be referred to with letters *a,b,....*

7.2.1 Short haul application codes

Target transmission distances between 2 km and 40 km. We consider three possible implementations of a short haul system. Each proposal is defined for transmission over standard-SMF and NZDSF by consideration of chromatic dispersion limitations in each fiber type. The main optical parameters that specify each application code are presented in Table 7.2.

a) PSBT transmitter with PIN receiver

This method uses a PSBT based transmitter without any other method for chromatic dispersion compensation. The PIN receiver provides an end of life of -10 dBm. The maximum chromatic dispersion that the application code can tolerate is 200 ps/nm. This limits the distance over standard-SMF to links

below 10 km, if we consider maximum dispersion of standard-SMF to be 20 $ps/nm \cdot km$. For transmission over NZDSF the distance limitation is dependent on the actual chromatic dispersion of the fiber considered. For a dispersion below 5 $ps/nm \cdot km$ the maximum distance is 40 km. For the maximum dispersion of a standardized NZDSF 10 $ps/nm \cdot km$ the maximum link distance is 20 km. We indicate in the application codes the maximum PMD coefficient of the transmission fiber considering the maximum transmission length applicable. These PMD coefficient limits might be able to be reduced if we use some kind of electronic PMD compensation without additional changes in the optical link design. We do not consider optical PMD compensators in single channel application and believe that the network provider will choose adequate links with low PMD coefficient to be used for 40 Gb/s transmission.

Application code	S-256.2a S-256.5a	S-256.2b S-256.5b	S-256.2c S-256.5c
Operating wavelength [nm]	Any between 1530 and 1565		
Fiber type	Standard fiber G.652 or NZDSF G.655		
Max. IL of TDC [dB]	NA	4	4
Max PMD of TDC [ps]	NA	0.5	0.5
TDC tuning G.652 [ps/nm]	NA	0 to -800	0 to -800
TDC tuning G.655 [ps/nm]	NA	0 to -400	0 to -400
Mean launched power [dBm][1]	$2 < P < 4$	$2 < P < 4$	$-1 < P < 2$
Min. ER [dB]	10	10	10
Attenuation [dB]	$3 < A < 11$	$3 < A < 11$	$3 < A < 11$
D in G.652 [ps/nm]	< 200	< 800	< 800
D in G.655 [ps/nm]	< 200	< 400	< 400
Max. average DGD [ps][2]	2.5	2.5	2.5
Max. fiber PMD coefficient[3] $[ps/\sqrt{km}]$	0.4	0.31	0.31
Min. sensitivity (BER 10^{-12}) [dBm]	-10	-10	-18
Min. overload [dBm]	1	1	-1
Path penalty [dB]	1	1	2

Table 7.2: Proposal of application codes for short haul STM-256 optical interfaces. ER: Extinction Ratio, IL: Insertion loss, TDC: Tunable dispersion compensator, D: Chromatic dispersion, NA: Not Applicable, Max.: Maximum value, Min.: Minimum value. Notes: [1] Launched power into transmission fiber. [2] Maximum average DGD in the link including transmission fiber and other optical components that will result in 1 dB penalty in a preamplified receiver with a probability of $4 \cdot 10^{-5}$. [3] Maximum PMD coefficient of the transmission fiber considering the maximum link length.

b) NRZ modulation, TDC at the transmitter and PIN receiver

For this application code we suppose that we use a high power laser at the transmitter. The TDC is placed directly after the modulator and distorts the signal so that after transmission chromatic dispersion is zero. As the TDC is at the transmitter the tuning for optimum chromatic dispersion compensation will be done when setting up the system but no control of the TDC will be allowed as there is no feedback line between transmitter and receiver. We suppose that the TDC performance is not affected by high input powers up to 10 dBm.

c) NRZ modulation, TDC at the receiver and APD receiver

In this application code the TDC is placed at the receiver and allows for fast re-tuning if needed and even possibility for dynamical compensator. The APD considered at the receiver has an end of life sensitivity of -18 dBm for BER 10^{-12}. We can use a relatively low power transmitter.

7.2.2 Long haul application codes

Target transmission distances between 40 km and 80 km. We consider three possible implementations of a long haul system. Each proposal is defined for transmission over standard-SMF and NZDSF by consideration of chromatic dispersion limitations in each fiber type. The main optical parameters that specify each application code are presented in Table 7.2.2.

a) PSBT modulation, fixed dispersion compensation at receiver, optically preamplified receiver

In this application code we use the ±200 ps/nm chromatic dispersion tolerance of PSBT plus a selection of fixed dispersion compensation modules placed at the receiver to cover the full chromatic dispersion window. We consider minimum chromatic dispersion of standard-SMF to be 15 $ps/nm \cdot km$ and 2 $ps/nm \cdot km$ for NZDSF. For standard-SMF and chromatic dispersion between 600 and 1000 ps/nm we use a fixed dispersion module with -800 ps/nm. For dispersion between 1000 and 1400 ps/nm the fixed dispersion module should be -1200 ps/nm. For dispersion between 1400 and 1600 ps/nm the fixed dispersion module should be -1500 ps/nm. For NZDSF fixed dispersion compensation modules with -250 ps/nm and -625 ps/nm could cover the full range. We consider DCF modules for the fixed dispersion compensation in Table 7.2.2. The receiver uses an optical preamplifier that provides an end of life sensitivity of -27 dBm for a BER of 10^{-12}.

b) NRZ modulation, TDC at transmitter, APD receiver

We suppose that we can use a very high power source at the transmitter ($> 40mW$) as input to the optical modulator which allows to launch between 9 and 10 dBm into the TDC. The TDC will not induce distortions for such high optical powers. The receiver is based on an APD with an end of life sensitivity of -19 dBm for BER 10^{-12}.

c) NRZ modulation, TDC at receiver, optically preamplified receiver

We place the TDC at the receiver and relax the requirements of high power at transmitter compared to application code b). On the other hand we need an optically preamplified receiver with end of life sensitivity of -27 dBm as in application code a).

Application code	L-256.2a L-256.5a	L-256.2b L-256.5b	L-256.2c L-256.5c
Operating wavelength [nm]	Any between 1530 and 1565		
Fiber type	Standard fiber G.652 or NZDSF G.655		
Max. IL of TDC [dB]	NA	4	4
Max PMD of TDC [ps]	NA	0.5	0.5
TDC tuning G.652 [ps/nm]	NA	-600 to -1600	-600 to -1600
TDC tuning G.655 [ps/nm]	NA	-80 to -800	-80 to -800
Max. IL of DCF [dB]	6	NA	NA
Max PMD of DCF [dB]	0.8	NA	NA
Mean launched power [dBm][1]	$3 < P < 5$	$5 < P < 6$	$-1 < P < 2$
Min. ER [dB]	10	10	10
Attenuation [dB]	$11 < A < 22$	$11 < A < 22$	$11 < A < 22$
D in G.652 [ps/nm]	$600 < D < 1800$	$600 < D < 1800$	$600 < D < 1800$
D in G.655 [ps/nm]	$80 < D < 800$	$80 < D < 800$	$80 < D < 800$
Max. average DGD [ps][2]	2.5	2.5	2.5
Max. fiber PMD [3] $[ps/\sqrt{km}]$	0.26	0.27	0.27
Min. sensitivity [4] [dBm]	-27	-19	-27
Min. overload [dBm]	-7	-5	-9
Path penalty [dB]	2	2	2

Table 7.3: Proposal of application codes for long haul STM-256 optical interfaces. ER: Extinction Ratio, IL: Insertion loss, TDC: Tunable dispersion compensator, D: Chromatic dispersion, DCF: Dispersion Compensating Fiber. NA: Not Applicable, Max.: Maximum value, Min.: Minimum value. Notes: [1] Launched power into transmission fiber. [2] Maximum average DGD in the link including transmission fiber and other optical components that will result in 1 dB penalty in a preamplified receiver with a probability of $4 \cdot 10^{-5}$. [3] Maximum PMD coefficient of transmission fiber considering maximum link length. [4] Sensitivity penalty considered for BER at 10^{-12} and end of life of the system.

7.2.3 Very long haul application codes

Target transmission distances between 80 km and 120 km. We consider two possible implementations of a very long haul system. Each proposal is defined for transmission over standard-SMF and NZDSF by consideration of chromatic dispersion limitations in each fiber type. The main optical parameters that specify each application code are presented in Table 7.4.

a) CSRZ or RZ transmitter with TDC and booster amplifier, optically preamplified receiver

The transmitter should be using a modulation format that can tolerate high input powers into the transmission fiber, CSRZ or RZ. The TDC is placed at the transmitter and it is situated before a booster amplifier, see Figure 7.1. The output from the booster amplifier should be between 6 and 9 dBm if we use CSRZ. If a short duty cycle RZ transmitter is used higher power levels up to 13 dBm can be launched. At the receiver an optically preamplified receiver is used with an end of life sensitivity of -29 dBm (notice a 2 dB improvement compared to NRZ). The maximum DGD in the link is increased due to the use of RZ based signals.

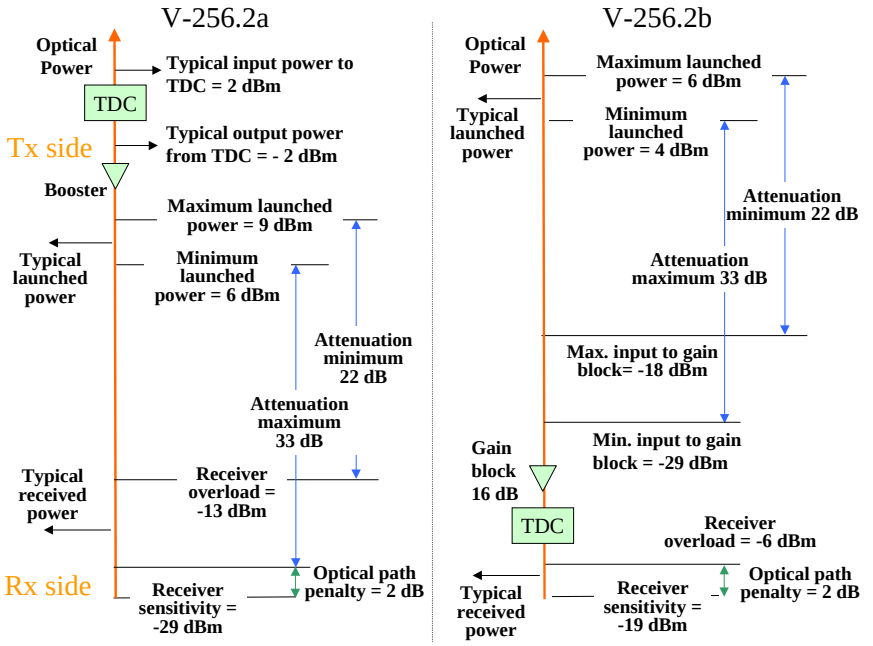

Figure 7.1: Relation between optical parameters used in the definition of V-256.a and V-256.b.

b) NRZ modulation, gain block, TDC and APD at receiver

We use a high power laser that should provide optical power levels after the modulator between 4 and 6 dBm. At the receiver, we place a gain block before the TDC and an APD receiver, see Figure 7.1. The gain block should have an optical filter incorporated to avoid excessive ASE noise to reach the APD

Application code	V-256.2a L-256.5a	V-256.2b L-256.5b
Operating wavelength [nm]	Any between 1530 and 1565	
Fiber type	Standard fiber G.652 or NZDSF G.655	
Max. IL of TDC [dB]	4	4
Max PMD of TDC [ps]	0.5	0.5
TDC tuning G.652 [ps/nm]	-1200 to -2400	-1200 to -2400
TDC tuning G.655 [ps/nm]	-160 to -1200	-160 to -1200
Mean launched power [dBm][1]	$6 < P < 9$	$4 < P < 6$
Min. ER [dB]	10	10
Attenuation [dB]	$22 < A < 33$	$22 < A < 33$
D in G.652 [ps/nm]	$1200 < D < 2400$	$1200 < D < 2400$
D in G.655 [ps/nm]	$160 < D < 1200$	$160 < D < 1200$
Max. average DGD [ps][2]	3.5	2.5
Max. fiber PMD coefficient[3] $[ps/\sqrt{km}]$	0.31	0.22
Gain block, target gain [dB]	NA	16
Noise figure of gain block [dB]	NA	< 6
Min. sensitivity (BER 10^{-12}) [dBm]	-29	-19
Min. overload [dBm]	-13	-6
Path penalty [dB]	2	2

Table 7.4: Proposal of application codes for very long haul STM-256 optical interfaces. ER: Extinction Ratio, IL: Insertion loss, TDC: Tunable dispersion compensator, D: Chromatic dispersion, DCF: Dispersion Compensating Fiber. NA: Not Applicable, Max.: Maximum value, Min.: Minimum value. Notes: [1] Launched power into transmission fiber. [2] Maximum average DGD in the link including transmission fiber and other optical components that will provide a 1 dB penalty in a preamplified receiver with a probability of $4 \cdot 10^{-5}$. [3] Maximum PMD coefficient of transmission fiber considering maximum link length.

receiver.

7.3 Proposal of a 40 Gb/s WDM transmission system

We present a proposal for a WDM system aimed at a long haul target distance between repeaters defined following approach of ITU standard G.692. The system should be able to support 32 channels and transmission over a maximum of 5 spans of standard-SMF or NZDSF, 32L5-256.2(5). We do not consider any wavelength add-drop modules in the system defined. We suppose that the following information regarding the link configuration is available:

- Fiber type used. Standard-SMF or NZDSF and an average value of dispersion at 1550 nm.
- Distance of each span in the link.
- PMD of each span in the link.

A schematic of the system implementation is shown in Figure 7.2. The transmitter modules will use CSRZ as the modulation format and should have a variable optical attenuator to allow for tuning the optical power levels at the input of the booster amplifier. Wavelength lockers will ensure a correct setting of the center frequency throughout the life-time of the system. Reed-Salomon FEC will be implemented at each transmitter requiring a bit rate of 42.8 Gb/s. Channels are spaced 100 GHz and are multiplexed in a device which does not induce any chromatic dispersion. A difference from the definitions presented in G.692 is that the multiplexer and demultiplexer building blocks do not include an optical amplifier in our description, the amplifier is considered an additional component.

The system should be able to accommodate for a maximum chromatic dispersion of 6800 ps/nm at 1550 nm. Chromatic dispersion compensation is achieved partially by fixed dispersion compensating modules at each link and by a final compensation with a tunable WDM dispersion compensator. The fixed dispersion compensating modules have to provide slope compensation. The value of dispersion compensation to be used at each repeater is dependent on the span length and the fiber type and can be found following Table 7.5. The residual chromatic dispersion from spans 1 to M-1 (where M is the total number of spans) and the chromatic dispersion of the last span (M) are compensated in a tunable dispersion compensator which also allows for tuning of the slope of the dispersion compensation. Tuning of the TDC will be done for each system installation. Dynamical compensation including slope could be done if a dispersion monitoring mechanism, see Section 3.3.4, were included in at least three receiver modules. The tuning range of the TDC should be from -220 to

-1820 ps/nm for standard-SMF. For NZDSF with dispersion at 1550 nm in the order of 4 $ps/nm \cdot km$ it should be from +100 to -616 ps/nm. For NZDSF with dispersion at 1550 nm in the order of 7 $ps/nm \cdot km$ it should be from 0 to -800 ps/nm.

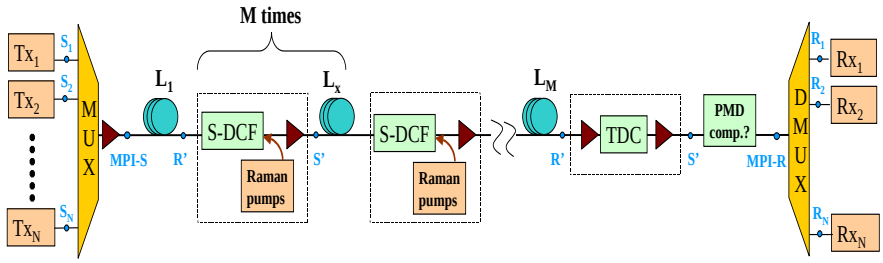

Figure 7.2: Schematic of building-blocks included in the proposed 32L5-256.2(5) WDM system. Reference points are indicated following ITU G.692 [15]. S-DCF: Slope dispersion compensating fiber. TDC: Tunable Dispersion compensator. PMD comp.: Polarization Mode Dispersion compensator.

Fiber type	Span length margins [km]	S-DCF dispersion at 1550 nm [ps/nm]
Standard-SMF	40 to 50	-765 ± 30
	50 to 60	-935 ± 30
	60 to 70	-1105 ± 30
	70 to 80	-1275 ± 30
NZDSF-a	40 to 60	-180 ± 6
	60 to 80	-300 ± 11
NZDSF-b	40 to 50	-300 ± 11
	50 to 65	-400 ± 11
	65 to 80	-500 ± 11

Table 7.5: Relation between span length and chromatic dispersion of DCF modules in the proposed WDM system implementation. Standard-SMF is considered to have dispersion of 17 $ps/nm \cdot km$ at 1550 nm. NZDSF-a has a chromatic dispersion in the order of 4 $ps/nm \cdot km$ at 1550 nm. NZDSF-b has a chromatic dispersion in the order of 7 $ps/nm \cdot km$ at 1550 nm.

Three types of amplifier configurations can be observed in Figure 7.2:

- A booster amplifier at the transmitter side, placed after the multiplexer.
- Combined Raman-EDFA as in-line amplifiers.

- A double stage EDFA with the TDC in the middle section at the receiver.

The booster amplifier will set the optical power per channel launched at point MPI-S (Multiple Path Interface at the transmitter) within 0 and + 2 dBm. Input power per channel is attenuated at each transmitter to ensure transmission within these limits. The Raman-EDFA in-line amplifier uses mainly the S-DCF modules as the gain medium for transmission over standard-SMF while for transmission over NZDSF the gain medium used are both the S-DCF and the NZDSF (this will be needed as the S-DCF modules will be relatively short). We should also consider that the reduced attenuation of the S-DCF in transmission over NZDSF provides a higher OSNR and the need of Raman gain is reduced compared to transmission over standard-SMF. The Raman gain will be in the order of 12 dB in an 80 km standard-SMF span, the rest of gain needed in the in-line amplifier will be provided by an EDFA section. Output power from the Raman-EDFA in-line amplifier should be between 0 and +2 dBm per channel, point S'. The gain variation in the combined Raman-EDFA amplifier should be below 1 dB for all channels in order to ensure optimum performance for all channels at the receiver.

The tunable chromatic dispersion compensator is situated in the middle section of a double stage EDFA. Introduction of a PMD compensator will be considered if fiber PMD coefficient per link is above 0.1 $ps/\sqrt{km}$, see Section 4.2.2. We suppose that the FEC can correct for certain amount of PMD. The optical demultiplexer at the receiver will not introduce any significant chromatic dispersion and will provide effective filtering without adding significant crosstalk from neighboring channels.

The receiver is based on an APD which provides a receiver sensitivity for end of life of -19 dBm for a BER of 10^{-12} when FEC is turned off. The Reed-Salomon FEC coding used provides a BER correction from 10^{-5} to 10^{-12} and should allow for signals with an OSNR of 21 dB (measured in a 0.1 nm resolution bandwidth) to be received error free.

Application code: 32L5-256.2 and 32L5-256.5	Value	Units
Number of channels	32	
Bit Rate/Format of channels	42.8/CSRZ	[Gb/s]
Individual transmitter outputs at points S_n		
Spectral characteristics		
- Maximum -20 dB width	0.6	[nm]
- Minimum SMSR	30	dB
Extinction ratio	> 10	[dB]
Channel frequencies	G.692	
	Appendix III	
Channel spacing	100	[GHz]
Central frequency deviation	± 3	[GHz]
Optical interfaces at point MPI-S		
Crosstalk from neighboring channel	< -30	[dB]
Channel output power	0 to +2	[dBm]
Channel signal-to-noise[1]	> 35	[dB]
Maximum channel power difference	< 1	[dB]
Optical line amplifier		
Multi channel gain variation	< 1	[dB]
Total received power maximum[2]	+6	[dBm]
Total received power minimum[3]	-7	[dBm]
Total launched power maximum[4]	+17	[dBm]
Signal spontaneous noise figure[5]	< 6	[dB]
Optical interfaces at points S'		
Crosstalk from neighboring channel	< -30	[dB]
Channel output power	0 to +2	[dBm]
Total launched power maximum	+17	[dBm]
Maximum channel power difference (i=1,..,5)	$1 + i$	[dB]
Optical path		
Attenuation	5 spans	[dB]
	$11 < Att./span < 22$	
Chromatic dispersion	Up to 6800	[ps/nm]
	at 1550 nm	
Maximum discrete reflectance	-27	dB
Minimum return loss	24	dB
Maximum PMD coefficient per span[6]	0.1	$[ps/\sqrt{km}]$
Optical interfaces at points R'		
Mean channel input power		

Table 7.6: Proposal of 32L5-256.2 and 32L5-256.5 WDM systems.

Table 7.6: Proposal of 32L5-256.2 and 32L5-256.5 WDM systems....continued. Notes: i: Number of spans. [1] OSNR measured always in a 0.1 nm resolution bandwidth. [2] Considering a 32 channel load and 11 dB span. [3] Considering 1 channel load and 22 dB span. [4] Considering 32 channel load. [5] Noise figure of EDFA gain block of the in-line Raman-EDFA amplifiers. [6] For a PMD of EDFA <0.5 ps and a PMD for S-DFC modules <0.9 ps. [7] Minimum OSNR to be observed at input of last amplifier to ensure an OSNR > 21 dB at the individual receivers.[8] If we consider a PMD compensator. [9] Path penalty with FEC on. [10] Dependent on the channels chosen and the amplifier design.

Application code: 32L5-256.2 and 32L5-256.5	Value	Units
- Maximum	-9	[dBm]
- Minimum	-22	[dBm]
Mean total input power		
- Maximum	+6	[dBm]
Channel signal-to-noise ratio[7]	> 22	[dB]
Optical signal crosstalk	< -30	[dB]
Maximum channel power difference (i=1,..,5)	$1 + (i - 1)$	[dB]
Optical interfaces at point MPI-R		
Mean channel input power		
- Maximum	+2	[dBm]
- Minimum[8]	-9	[dBm]
Mean total input power		
- Maximum	+17	[dBm]
Channel signal-to-noise ratio	> 21	[dB]
Optical signal crosstalk	< -30	[dB]
Maximum channel power difference	6	[dB]
Individual receiver inputs at points R_n		
Receiver sensitivity	-19	[dBm]
Receiver overload	-4	[dBm]
Optical path penalty[9]	2	[dB]
Receiver reflectance	-27	[dB]
Optical signal to noise ratio	> 21	[dB]
Minimum receiver wavelength[10]	1530	[nm]
Maximum receiver wavelength[10]	1565	[nm]

7.4 Proposal of a 40 Gb/s metro WDM network system architecture

The proposed metro WDM network uses assigned wavelength groups to communicate between specific nodes in order to reduce the number of transmitter-receiver modules needed at each node. The example presented, see Figure 7.3, is an application to a six node ring network, connection between each node is duplex (one fiber for each direction). Communication between nodes is done by using the assigned wavelength groups. The logical connectivity is equivalent to a full mesh where all nodes can communicate with all others in the ring without any optical-to-electrical conversion at a node. For this full connectivity we need 6 wavelength groups. If we allowed one optical-to-electrical conversion in a communication between nodes the wavelength groups needed in a 6 node example would be reduced to 3.

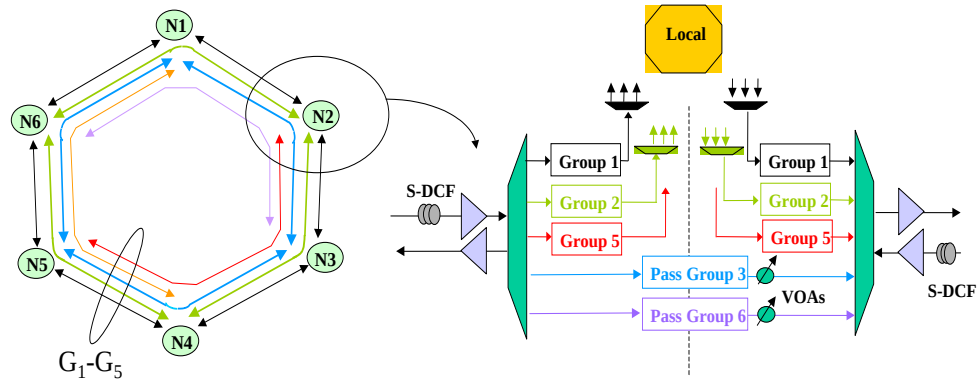

	N1	N2	N 3	N4	N5	N6
N1	x	G_1	G_3	G_4	G_3	G_1
N2	G_1	x	G_1	G_2	G_5	G_2
N3	G_3	G_1	x	G_1	G_3	G_6
N4	G_4	G_2	G_1	x	G_1	G_2
N5	G_3	G_5	G_3	G_1	x	G_1
N6	G_1	G_2	G_6	G_2	G_1	x

Figure 7.3: Schematic of metro WDM network architecture. The example proposed is for a 6 node network and full mesh connectivity indicating which wavelength groups connect each node. A detailed schematic of the optical building blocks of a node in the network is included, the node shows only the optical path in the West to East transmission.

An interesting point to observe from the example is that the maximum number of spans a wavelength group passes through is 3. For an ring-network with 8 nodes and following the same scenario the maximum number of spans travelled

without optical-to-electrical conversion will be 4. If we consider that traditionally metro WDM span lengths are below the 50 km range we can realize that requirements regarding optical transmission will be seriously relaxed when compared to a long haul WDM system. For example in a 6 node ring-network and maximum 3 spans optical transmission of a group wavelength the PMD coefficient of the fiber could reach 0.2 $ps/\sqrt{km}$, refer to Section 4.2.2 Figure 4.10.

We suppose that the following information regarding the fiber connecting the nodes is available:

- Fiber type used. Standard-SMF or NZDSF and an average value of dispersion at 1550 nm.
- Distance of each span in the link.
- PMD of each span in the link.

A proposal for a node architecture is shown in Figure 7.3, the example shows the optical path in West to East transmission at node N_2. The WDM signal reaching the network node is separated into the different wavelength groups by an optical demultiplexer. The wavelength groups not aimed at the node are by-passed and connected directly to the output optical multiplexer. For this latter case VOAs are tuned to provide equalization of the WDM signal at the output of the multiplexer. Chromatic dispersion compensation is achieved partially by S-DCF modules situated at the input of each node and partially by a TDC for each wavelength group. The relation between span length and chromatic dispersion of the DCF modules in the proposed metro WDM network are presented in Table 7.7. The TDC should also allow for controlled slope compensation within the wavelength group. The TDC should provide for tunable chromatic dispersion compensation for -255 to +255 ps/nm in the 6 node network example presented. Please notice that the maximum number of TDCs to be included at each node considering both directions for transmission is 5. The different channels within a wavelength group are finally separated by a second optical demultiplexer and arrive at the corresponding receiver at the local node. Notice that it is also possible to re-direct a single channel to the following node for example by setting a channel by channel optical by-pass. However, this would require further study of optical transmission limitations. All the optical multiplexers and demultiplexers used both for wavelength groups and individual channels are supposed to be free of chromatic dispersion.

Limitations in the maximum attenuation per spans allowed will be dependent on the insertion loss of optical multiplexers, demultiplexers, TDC and the S-DCF modules. We believe however that for the network example depicted in

this section we should be able to allow for at least a maximum span attenuation of 14 dB. The transmitter modules could use NRZ modulation with FEC coding and the receivers should include an APD.

Fiber type	Span length margins [km]	S-DCF dispersion at 1550 nm [ps/nm]
Standard-SMF	0 to 10	-85 ± 6
	10 to 20	-255 ± 11
	20 to 30	-425 ± 16
	30 to 40	-595 ± 16
	40 to 50	-765 ± 21
NZDSF-a	0 to 20	None
	20 to 50	-140 ± 6
NZDSF-b	0 to 10	None
	10 to 30	-140 ± 6
	30 to 50	-280 ± 11

Table 7.7: Relation between span length and chromatic dispersion of DCF modules in the proposed metro WDM system implementation using NRZ modulation at the transmitter. Standard-SMF is considered to have dispersion of 17 $ps/nm \cdot km$ at 1550 nm. NZDSF-a has a chromatic dispersion in the order of 4 $ps/nm \cdot km$ at 1550 nm. NZDSF-b has a chromatic dispersion in the order of 7 $ps/nm \cdot km$ at 1550 nm.

7.5 Availability of components used in the 40 Gb/s system designs

In this section we review the availability of the components which have been proposed to be used in the single wavelength and WDM systems defined in the previous sections. This review allows to provide a prediction in the time frame over which 40 Gb/s optical transmission systems could become a product reality.

If the component is available we will specify at which *stage*: Research, prototype or a product. The table should be considered as a gradual description were most of the components described in the single wavelength application codes will be also used in the implementation of WDM systems. Please be aware that the data for this section is valid as of February 2003 and component availability will evolve, strongly dependent on the need of 40 Gb/s optical transmission systems.

Looking into the availability of components it seems clear that 40 Gb/s single

Component	Availability stage
Single wavelength application codes	
2.5 Gb/s to 40 Gb/s (16:1) electronic multiplexer	Product
40 Gb/s CDR and electronic demultiplexer to 2.5 Gb/s (1:16)	Product
CW laser 40 mW	Product
40 Gb/s driver amplifier	Product
40 Gb/s modulator	Product
Single wavelength TDC	Product
PIN receiver	Product
APD receiver	Prototype [194]
PSBT pre-coder	Prototype [130]
CSRZ transmitter	Prototype [220]
Long haul WDM system	
Optical Mux-Demux low chromatic dispersion	Product
S-DCF	Product
Raman pump	Product
32 channel WDM TDC with slope compensation	Research [103]
PMD compensator	Research[1]
Metro WDM system	
Low channel count TDC	Research/Prototype [234, 106, 235]

Table 7.8: Availability of components used in the definition of the different 40 Gb/s systems. CDR: Clock and Data Recovery. [1] Products are available at 10 Gb/s [236, 114]. 40 Gb/s optical PMD compensators are available but the question is their practical use in a product due to their size, insertion loss and no availability of a WDM PMD compensator. An interesting option is electronic PMD compensation. This table should be considered as for February 2003.

wavelength systems should be possible to develop within the near future. WDM metro networks will probably follow as tunable dispersion compensation devices for a few channels could be available soon. For Long haul WDM systems to become a product reality we have to provide a solution to the low PMD allowed in the fiber and large channel count WDM TDCs have to be available with a certain degree of slope compensation tunability.

7.6 Summary

We have presented a comparison of the advantages and disadvantages of the different modulation formats which have been introduced and investigated throughout the thesis. PSBT can relax the tight chromatic dispersion tolerances observed for NRZ, RZ and CSRZ. On the other hand, the resistance of PSBT to SPM induced distortion is low and reduces the effectiveness of this modulation format in a long haul multi-span transmission. CSRZ provides a good overall performance allowing for 100 GHz channel spacing and long haul multi-span transmission while keeping higher chromatic dispersion tolerances than RZ modulation.

We have proposed different possible implementations of short, long and very long haul single wavelength transmission systems. It is clear that the actual maximum fiber PMD coefficient of 0.5 $ps/\sqrt{km}$ defined for ITU application codes aimed at 10 Gb/s systems is too relaxed to allow for installation of 40 Gb/s standardized commercial systems. To ensure reliable performance some kind of PMD compensation will be required. We define the maximum PMD coefficient of the fiber in the link allowed for the different application codes and suppose that the network operator will have detailed information of the links which can tolerate the PMD requirements. Use of tunable chromatic dispersion compensators is necessary in most of the defined implementations. It is believed that CSRZ or RZ modulation will be needed for the implementation of very long haul transmission systems.

We have presented a proposal for a long haul 40 Gb/s WDM system which should fit within ITU application code 32L5.256.2(5). Chromatic dispersion is partially compensated by fixed S-DCF modules and partially by a WDM tunable dispersion compensator placed at the receiver side able to correct also for the slope of dispersion. The in-line amplifier are based on a combination of Raman pumps and EDFA. The Raman pumps will use the S-DCF modules and the transmission fiber as the gain media. The transmitter modules are based on CSRZ modulation format and the receiver on an APD. The fiber PMD coefficient is limited to 0.1 $ps/\sqrt{km}$ for a 5 span system.

An example of a six node ring architecture metro WDM network at 40 Gb/s has been proposed using wavelength grouping. Chromatic dispersion compensation is partially achieved by fixed S-DCF and partially by a low count multi-channel TDC with ability for slope compensation within these channels. The transmitter is based on NRZ modulation and the receiver on an APD. Due to the ring architecture a maximum of three nodes are travelled by a wavelength group without optical-to-electrical conversion in the six node example presented. This reduces the transmission requirements considerably compared

to the long haul WDM system. Fibers in the link could have a PMD coefficient up to 0.2 $ps/\sqrt{km}$ for example.

Finally we have reviewed the availability of the different components needed for the implementation of the proposed 40 Gb/s systems. We can conclude that single wavelength 40 Gb/s transmission systems could be implemented today or in a very near future. Metro 40 Gb/s WDM might be implemented in a nearer future than long haul 40 Gb/s WDM systems. The later mainly dependent on the development of high count channel tunable chromatic dispersion compensators which allow for slope compensation and multi-channel PMD compensators.

Chapter 8

Conclusion

This thesis has presented investigations of the main limitations in the design and implementation of potentially commercial 40 Gb/s single channel and Wavelength Division Multiplexed (WDM) systems. Furthermore, alternative modulation formats that can provide increased design tolerances and practical compensation methods of distortion effects such as chromatic dispersion or Polarization Mode Dispersion (PMD) have been analyzed and investigated.

Regarding chromatic dispersion, the traditional Non Return to Zero (NRZ) modulation format, provides a tolerance margin at 40 Gb/s within ± 70 ps/nm for a 1 dB sensitivity penalty (measured in a PIN receiver). The tolerance margin observed at 10 Gb/s for NRZ of ± 1200 ps/nm provides an idea of the tight limitations in 40 Gb/s system design induced by chromatic dispersion. We have investigated the tolerance of chirped NRZ modulation format to chromatic dispersion and found that it provides increased tolerance to over-compensation while reduced tolerance to under-compensation. This asymmetric performance is not desirable in a system that will need some fixed chromatic dispersion compensation. Optical duobinary modulation format on the other hand does provide a symmetric performance with extended tolerance to chromatic dispersion up to ± 200 ps/nm. In a practical implementation of an optical duobinary transmitter we could observe open and clear eye diagrams after 12 km of transmission over standard Single Mode Fiber (SMF). Return to Zero (RZ) modulation provides a reduced chromatic dispersion tolerance compared to NRZ. The tolerance is reduced to ± 30 ps/nm for a 33 % duty cycle transmitter. Carrier Suppressed RZ (CSRZ) modulation format provides also a reduced tolerance of ± 45 ps/nm compared to NRZ.

The most used commercially available fixed dispersion compensation methods have been reviewed. As an example of the tight design margins observed in single channel transmission regarding chromatic dispersion, we present a prac-

tical scenario for the use of Dispersion Compensating Fiber (DCF) modules in a 40 km or 80 km link for a single channel 40 Gb/s system. If we consider the uncertainty in chromatic dispersion of the transmission fiber and the DCF modules and add the temperature fluctuations we can observe that using NRZ modulation we are not able to ensure transmission even for an 80 km link.

The performance of two different methods of single wavelength tunable dispersion compensators based on chirped fiber Bragg gratings have been investigated experimentally at 40 Gb/s using an NRZ based transmitter. The first method uses control of the temperature gradient induced on the Bragg grating to tune the dispersion. The device could be tuned to minimize system penalty in a series of different transmission spans ranging from 21.5 km to 41 km of standard-SMF. Tuning within this range provided a maximum sensitivity penalty of 0.8 dB (PIN receiver). The second method uses controlled stretching of a non-linearly chirped fiber Bragg grating as the dispersion tuning mechanism. The performance of the device has been investigated in a series of unrepeatered transmission spans ranging from 45.8 km to 103.8 km with a maximum sensitivity penalty of 2 dB (PIN receiver), observed for the longest span.

Another very important parameter to consider in the design of 40 Gb/s WDM systems is the compensation of the slope of the chromatic dispersion of the transmission fiber. In an ideal case we need to ensure that the slope is compensated by more than 85 % per span if we want to ensure transmission within a 35 nm optical bandwidth in a 5 span link with 80 km per span. However if we consider the uncertainty in the dispersion and dispersion slope of the transmission fiber and the DCF modules and add the expected temperature induced fluctuations we observe that already for a single 40 km span we will be close to reach the maximum tolerance of an NRZ transmitter for those channels situated in the edges of the spectrum.

A tunable dispersion compensator intended for WDM application has been tested. The device is based on a combination of a Virtually Imaged Phased Array (VIPA) and a three dimensional mirror which allows for the tuning of dispersion within ± 700 ps/nm for 25 WDM channels spaced 200 GHz apart. The performance of the device is mainly limited by the lack of slope compensation which can clearly be observed if the residual dispersion overcomes the dispersion margin. Tunability of the dispersion slope is clearly a necessary function of a WDM tunable dispersion compensator if it should compete against a channel by channel compensator technique.

PMD is an effect variable in time and frequency. In order to avoid high levels of distortion induced by PMD we need to design systems so that a worst case situation will occur with a very low probability. The International Telecommu-

nications Union, Telecommunications sector (ITU-T) recommendations, only consider first-order PMD and limit the maximum PMD in a link to 10 % of the bit period. This is equivalent to a 2.5 ps limit for a 40 Gb/s system. The penalty observed for NRZ modulation is extremely dependent on the receiver design. RZ modulation provides an increased tolerance for a preamplified receiver allowing for a maximum PMD of 3.5 ps in the link for a 33 % duty cycle transmitter.

Taking into account PMD originated in the DCF modules and the Erbium Doped Fiber Amplifiers (EDFA), using a Root Mean Square (RMS) addition and considering a maximum of 2.5 ps PMD in the link, we are limited to a PMD coefficient of the transmission fiber below 0.4 $ps/\sqrt{km}$ for a 40 km link. This is already below the maximum PMD coefficient of 0.5 $ps/\sqrt{km}$ allowed in ITU recommendations for transmission fibers . For a multi-span transmission, limitations in the PMD coefficient of the fiber are significantly higher. For example, in an 80 km per span system we will be limited to a four span system with fibers with a PMD coefficient as low as 0.1 $ps/\sqrt{km}$.

The different methods proposed in the literature for first-order PMD compensation have been presented and evaluated. We have implemented a PMD compensator based on a fixed birefringent element with dynamical adjustment to optimum compensation. An improvement which at least doubles the traditional limitation for NRZ signals at 40 Gb/s has been demonstrated, allowing for a maximum PMD in the link of 5.5 ps when using the PMD compensator. This would increase the limits in the PMD coefficient of the fiber close to 0.3 $ps/\sqrt{km}$ in the previously aforementioned four span example.

An interesting way of observing the combined effect of first- and second-order PMD is by evaluating the Probability Density Function (PDF) of the Quality factor (Q) or the Bit Error Rate (BER) observed at the receiver. Following this analysis it is estimated for example, that a precise decision timing is more important than a threshold adjustment at the receiver for a system under the influence of PMD.

Limitations in multi-span transmission over standard-SMF and Non Zero Dispersion Shifted Fiber (NZDSF) have been investigated when using NRZ, RZ, optical duobinary and Carrier Suppressed RZ (CSRZ) as the modulation formats for a single channel 40 Gb/s system. We can observe a significant advantage of using RZ or CSRZ modulation formats compared to NRZ, while optical duobinary modulation provides a performance very close to NRZ. RZ and CSRZ provide higher tolerances to Self Phase Modulation (SPM) and an improved receiver sensitivity. For example considering simulation results for span length of 80 km and transmission over standard-SMF we could achieve transmission only over two spans when using NRZ modulation while for RZ or

CSRZ we were able to reach transmission over four spans. These results are obtained without considering the use of Forward Error Correction (FEC) or Raman amplification.

Experimentally, in a transmission set-up consisting of 40 km spans of standard-SMF, we have demonstrated that considering NRZ we could transmit over four spans with a sensitivity penalty slightly higher than 2 dB (preamplified receiver). When we used a 3 ps pulsed RZ transmitter we could reach transmission over six spans with a sensitivity penalty slightly higher than 1 dB (preamplified receiver).

Finally, the system designer has been provided with a simple method to obtain analytical design rules for the influence of Optical Signal to Noise Ratio (OSNR) and SPM in the maximum number of spans allowed in a system for a certain launched optical power. The method has been verified in the comparison of NRZ and RZ for transmission over standard-SMF over 40 km spans.

The influence of linear crosstalk in a 100 GHz channel spaced 40 Gb/s WDM system has been investigated for NRZ, RZ, optical duobinary and CSRZ modulation formats. The optical duobinary format provides the best performance indicating that even narrower channel spacing (75 GHz) could be achieved using this modulation format. NRZ and CSRZ provide considerable margins to the filter shape and bandwidth included in the optical multiplexer or demultiplexer to be used in a WDM system. Penalties below 1 dB (measured in a PIN receiver) are observed in simulated results both for NRZ and CSRZ modulation formats over a broad filter bandwidth range. RZ modulation is apparently not suited for 100 GHz channel spaced WDM systems as penalties above 1.5 dB and narrow tolerances to the filter shape and bandwidth are observed.

Regarding nonlinear cross-talk, an experimental investigation has shown that optimum launched power levels in transmission over a 200 km standard-SMF link for a 100 GHz spaced 16 channel 40 Gb/s WDM system using NRZ modulation are very close to the optimum power levels in single channel transmission. Launched optical power levels per channel into the standard-SMF were kept between -1 and 2 dBm while optical power levels launched into the DCF modules were between -4 and -7 dBm. No significant FWM crosstalk could be observed at these power levels. Launched power per channel into the fiber had to be increased to an average of 4 dBm in order to observe a crosstalk level of -37.5 dBm for a center channel in transmission over standard-SMF. For transmission over NZDSF and for a 100 GHz spaced 8 channel WDM system using NRZ modulation the crosstalk level had increased to -30 dBm for a center channel.

We have experimentally investigated 40 Gb/s WDM systems using the CSRZ modulation format in transmission over standard-SMF. Aided by Raman amplification every other span and using the DCF modules as the gain media

we could achieve transmission over 5 spans of 80 km. For a 16 channel 200 GHz spaced WDM system we observed sensitivity penalties after transmission in the order of 3 dB (measured in a PIN receiver) while for a 32 channel 100 GHz spaced WDM system the average sensitivity penalty increased to 4 dB (measured in a PIN receiver). These penalties could be reduced significantly if; Raman amplification were used for each span, an optimized optical demultiplexer were used at the receiver, the gain non uniformity of the in-line amplifiers were reduced and FEC were used in the transmitter-receiver modules.

The possibility of using Semiconductor Optical Amplifiers (SOA) has been demonstrated in a low channel count 40 Gb/s WDM system with NRZ modulation format and over distances corresponding to those that commercial metro systems target. Transmission over four spans of 40 km standard-SMF could be achieved with Q values higher than 16 dB for all channels when keeping the SOAs slightly under the saturation regime.

Finally, we have proposed and described possible implementation of single channel and WDM 40 Gb/s systems. Furthermore, we have investigated the availability of components needed for the implementation of the different proposals. It seems that commercial single channel 40 Gb/s systems could be built within the near future with state of the art components, among others; TDCs, Avalanche Photodiodes (APD) receivers, optical duobinary pre-coders or CSRZ transmitters.

We believe that 40 Gb/s WDM systems aiming at distances characteristic of metro networks will be the next products to be seen as commercially available. A low channel count TDC could allow these systems to be installed over links containing fibers with PMD coefficients up to 0.2 $ps/\sqrt{km}$ without the need of any PMD compensation and using traditional NRZ modulation format.

A long haul 40 Gb/s WDM system has been proposed making use of Raman amplification and CSRZ as the modulation format. A main limitation for a practical implementation of a commercial 40 Gb/s WDM system today is the need for a WDM-TDC that can allow also for the tuning of the slope of chromatic dispersion in the compensation process. A second limitation is observed regarding PMD, for a 5 span 80 km link one will need to ensure that all fibers installed have a PMD coefficient below 0.1 $ps/\sqrt{km}$

Two topics that might provide a competitive advantage in the implementation of 40 Gb/s transmission systems should be considered for future investigation . First, electronic chromatic dispersion and PMD compensation for each channel used in combination with FEC for performance monitoring, will allow to avoid complicated slope compensating TDCs in a WDM system and increase transmission margins considerably. Second, investigation of PMD statistics in a WDM system, in order to find out how many PMD compensators will allow for

an acceptable statistical performance by using the shared PMD compensator approach proposed in this thesis.

Bibliography

[1] F.P.Kapron, D.B.Keck, and R.D.Maurer, "Radiation losses in glass optical waveguides," *Applied Physics Letters*, vol. 17, no. 10, pp. 423–425, 1970.

[2] I.Hayashi, M.B.Panish, P.W.Foy, and S.Sumski, "Junction lasers which operate continuosulsy at Room-Temperature," *Applied Physics Letters*, vol. 17, no. 3, 1970.

[3] T. D. Telecom moderator, "First laser phone call zips the Atlantic! Isaac Asimov dedicates TAT-8; makes first call," *Telecom Digest, Web access the 22-2-2003 at: http://digest.textfiles.com/TELECOMDIGEST/vol08.iss0190-0213.txt*, vol. 8, December 1988.

[4] H.Ishio, J.Minowa, and K.Nosu, "Review and status of wavelength-division-multiplexing technology ans its application," *Journal of Lightwave Technology*, vol. LT-2, pp. 448–463, August 1984.

[5] S.B.Poole, D.N.Payne, R.J.Mears, M.E.Fermann, and R.I.Laming, "Fabrication and characterization of low-loss optical fibers containing rare-earth ions," *Journal of Lightwave Technology*, vol. LT-6, pp. 870–876, July 1986.

[6] C.R.Giles, E.Desurvire, J.R.Talman, J.R.Simpson, and P.C.Becker, "2-Gbit/s signal amplification at $\lambda = 1.53\ \mu m$ in an Erbium-doped single mode fiber amplifier," *Journal of Lightwave Technology*, vol. 7, pp. 651–656, April 1989.

[7] W.Weiershausen, H.Schol, F.Kuppers, R.Leppla, G.Hein, H.Burkhard, E.Lach, and G.Veith, "40 Gb/s field trial test on an installed fiber link wiht high PMD and investigation of differential group delay impact on the transmission performance," *in Technical Digest of OFC'99*, vol. Paper ThI5, pp. 125–127.

[8] P. release from PhotnoEx, "Deutsche Telekom first in the world with a 40 Gb/s R&D field trial using PhotonEx core optical transport system and EMS," *Downloaded the 22-2-2003 from : http://www.photonex.com/news_events/newsentry_view.cfm?post=35*, June 2002.

[9] P. R. from Lucent Technologies, "LambdasXtreme^{TM} succesfully completes field trial in Deutsche Telekom netowork," *Downloaded the 22-2-2003 from : http://www.lucent.com/press/0702/020729.nsa.html*, July 2002.

[10] The GSM association, "Subscribers forecast," *Downloaded the 22-2-2003 from: http://www.gsmworld.com/news/statistics/subforecasts.shtml*, January 2003.

[11] K. G.Koffman and A. M.Odlyzko, *Optical Fiber Telecommunications IV, Chapter 2: Growth of the Internet*, vol. B. Academic Press, 2002, ISBN: 0-12-395173-9.

[12] P.A.Saiz, "Germany looks beyond core communications-for now," *Lightwave Europe*, pp. 32–35, September 2002.

[13] Telecommunications Standardization Sector, International Telecommunications Union, "Recommendation G.691, Optical interfaces for single channel STM-64, STM-256 systems and other SDH systems with optical amplifiers," 2002.

[14] Telecommunications Standardization Sector, International Telecommunications Union, "Recommendation G.957, Optical interfaces for equipments and systems relating to the synchronous digital hierarchy, Chapter 3: Transport Network Architecture," 1999.

[15] Telecommunications Standardization Sector, International Telecommunications Union, "Recommendation G.692, Optical interfaces for multichannel systems with optical amplifiers," 1998.

[16] Telecommunications Standardization Sector, International Telecommunications Union, "Recommendation G.957.1, Optical transport network physical layer interfaces," 2003.

[17] M. Sexton and A. Reid, *Broadband Networking: ATM, SDH and SONET*. Artech House, 1997, ISBN: 0-89006-578-0.

[18] N. Ghani, J.-Y. Pan, and X. Cheng, *Optical Fiber Telecommunications IV, Chapter 8: Metropolitan Optical Networks*, vol. B. Academic Press, 2002, ISBN: 0-12-395173-9.

[19] F.Ruhl and T.Anderson, "Cost-effective metro WDM network architectures," *Technical Digest of OFC'2001*, vol. 3, March 2001. Paper WL1.

[20] P.A.Humblet, "The direction of optical technology in the metro area," *in Technical Digest of OFC'2001*, vol. 3, Paper WBB1, 2001.

[21] N.Madamopoulos, C.Friedman, I.Tomkos, and A.Boskovic, "Study of transparent and reconfigurable metropolitan area network," *in Technical digest of LEOS'2001*, vol. 2, pp. 427–428, 2001.

[22] Products and Services, Tellabs Web page, "Tellabs Switch Node 6350," *Downloaded 8-1-2003 from http://www.tellabs.com/products/6000/tellabs6350.shtml.*

[23] Products and Services, Tellabs Web page, "Tellabs 7200 Optical transport system," *Downloaded 8-1-2003 from http://www.tellabs.com/products/7000/tellabs7200.shtml.*

[24] Products and Services, Tellabs Web page, "Tellabs 7100 Optical transport series," *Downloaded 8-1-2003 from http://www.tellabs.com/reference/bro/tellabs7100br.pdf.*

[25] J.J.Ojha, "OIF Very Short Reach (VSR) interface implementation agreements," *White paper of the OIF, downloaded the 9-1-2002 from http://www.oiforum.com/public/documents/VSRWhitePaper.pdf.*

[26] A. Iguchi and R. Tuckk, "Very short reach (VSR) OC-192/STM-64 interface based on parallel optics," *Implementation agreement OIF-VSR4-01.0*, May 2000.

[27] Telecommunications Standardization Sector, International Telecommunications Union, "Recommendation G.693, Optical interfaces for intra-office systems," 2001.

[28] K.Gass, M.Lerer, K.L.Chen, M.Laha, and P.Dartnell, "Very short reach interface level 5 (VSR-5):Sonet/SDH OC-768 interface for verys short reach (VSR) applications," *Contribution number OIF2001.643.08*, May 2002.

[29] A. Amstrong, S.Killmeyer, J.Yee, G.Uscategui, R.Deming, T.Jung, R.Heilam, H. Patterson, D. Y.Ro, L.Mack, and X.Mu, "Design trends and challenges for parallel optical interconnect," *in Technical Digest of LEOS'2001*, vol. 1, pp. 44–45, 2001.

[30] 300 pin multi source agreement group, "Reference document for 300 pin 40 gb transponder," *Downloaded the 10-1-2003 from: http://www.300pinmsa.org/document/40Gb.pdf*, May 2002.

[31] R.H.Walders, *High-speed circuits for lightwave communications. Chapter titled: A review of recent progress in InP-based optoelectronic integrated circuit receiver front-ends*, vol. 13 of *Selected topics in electronics and systems*. World Scientific, 1999, ISBN: 981-02-3536-4.

[32] P.Fray, W.Wohlmuth, A.Mahajan, C.Caneau, S.Chandrasekhar, and I. Adesida, "Low-noise performance of monolithically integrated 12 Gb/s p-i-n/HEMT photoreceiver for long-wavelength transmission systems," *IEEE Photonic Technology Letters*, vol. 10, pp. 713–715, May 1998.

[33] A.H.Gnauck, S.K.Korotky, J.J.Veselk, J.Nagel, C.T.Kemmerer, W.J.Minford, and D.T.Moser, "Dispersion penalty reduction using an optical modulator with adjustable chirp," *IEEE Photonic Technology Letters*, vol. 3, pp. 916–918, October 1991.

[34] S.K.Kim, O.Mizuhara, Y.K.Park, L.D.Tzeng, Y.S.Kim, and J. Jeong, "Theorethical and experimental study of 10 Gb/s transmission performance using 1.55 μm $LiNbO_3$ based transmitters with adjustable extinction ratio and chirp," *Journal of Lightwave Technology*, vol. 17, pp. 1320–1325, August 1999.

[35] A. E. Willner and B. Hoanca, *Optical Fiber Telecommunications IV, Chapter 14: Fixed and tunable management of fiber chromatic dispersion*, vol. B. Academic Press, 2002, ISBN: 0-12-395173-9.

[36] K.Sato, T.Hosoda, T. Watanabe, S.Wada, Y.Iriguchi, K.Makita, J.Shimizu, K.Sakamoto, I.Watanabe, K.Mitamura, and M.Yamaguchi, "Record highest sensitivity of -28.0 dBm at 10 Gb/s achieved by newly developed extremely-compact superlattice-APD module with TIA-IC," *in Technical Digest of OFC'2002*, vol. Postdeadline papers, FB11, 2002.

[37] BaySpec Inc., "White paper: Optical Channel Performance Monitor," *Downloaded the 10-1-2003 from: http://www.bayspec.com/pdf/OCPM-OCM.pdf*, November 2002.

[38] S.Aisawa, T.Sakamoto, M.Fukui, M.Jimno, and K.Oguchi, "Ultra-wideband, long distance WDM demonstration of 1 Tbit/s (50x20 Gbit/s) 600 km transmission using 1550 and 1580 nm wavelength bands," *Electronic Letters*, vol. 34, no. 11, pp. 1127–1129, 1998.

[39] H.Ono, M.Yamada, and Y.Ohishi, "Gain flattened Er^{3+} doped fiber amplifier for WDM signal in the 1.57-1.60 μm wavelength region," *IEEE Photonic Technology Letters*, vol. 9, no. 5, pp. 596–598, 1997.

[40] A. Ellison and J. Minelly, *Optical Fiber Telecommunications IV, Chapter 3: New materials for Optical Amplifiers*, vol. A. Academic Press, 2002, ISBN: 0-12-395173-9.

[41] P.F.Wysocki, J.B.Judkins, R.P.Espindola, M.Andrejco, and A.W.Vengsarkar, "Broad-band Erbium-doped fiber amplifier flattened beyond 40 nm using long-period gating filter," *IEEE Photonic Technology Letters*, vol. 9, pp. 1343–1345, October 1997.

[42] R.M.Forthenberry, M.E.Wescott, L. Ghislain, and M.A.Scobery, "Low chromatic dispersion thin film DWDM filters for 40 Gb/s transmission systems," *in Technical Digest of OFC'2002*, vol. 1, paper WS2, pp. 319–320, 2002.

[43] G.Lenz, B.J.Eggleton, C.K.Madsen, C.R.Giles, and G.Nykolak, "Optimal dispersion of optical filters for WDM systems," *IEEE Photonic Technology Letters*, vol. 10, pp. 567–569, April 1998.

[44] M.Kusnestov, N.M.Froberg, S.Henion, and K.Rauschenbach, "Power penalty for optical signals due to dispersion slope in WDM filter cascades," *IEEE Photonic Technology Letters*, vol. 11, pp. 1411–1413, November 1999.

[45] Y.Yokoyama, H.Hatakeyama, K. Naniwae, K. Satoh, and M.Yamaguchi, "94-channel wavelength-selectable light source module with intragrated multi-wavelength locker," *in Technical Digest of OFC'2002*, vol. 1, Paper WF3, pp. 206–207, 2002.

[46] G.Vareille, O. Sab, G. Bassier, J. Collet, B. Julien, D.Dufournet, F.Pitel, and J.F.Marcerou, "1.5 terabit submarine 4000 km system validation over a deployed line with industrial margins usign 25 GHz channel spacing and NRZ format over NZDSF," *in Technical Digest of OFC'2002*, vol. 1, Paper WP5, pp. 293–294, 2002.

[47] N. S.Bergano, *Optical Fiber Telecommunications IV, Chapter 4: Undersea Communication Systems*, vol. B. Academic Press, 2002, ISBN: 0-12-395173-9.

[48] H.Kidorf, N. Ramanujam, I. Hayee, M. Nissov, J.X.Cai, B.Pedersen, A.Puc, and C.Rivers, "Perfomance improvement in high capacity, ultra-

long distance, WDM systems using forward error correction codes," *in Technical Digest of OFC'2000*, vol. 3, paper ThS3-1, pp. 274–276, 2000.

[49] O.A.Sab, "FEC techniques in submarine transmission systems," *in Technical Digest of OFC'2001*, vol. 1, paper TuF1-1, 2001.

[50] P. Kumar, M. Z. Win, H.-F. Lu, and C. N. Georghiades, *Optical Fiber Telecommunications IV, Chapter 17: Error-Control Coding Techniques and Applications*, vol. B. Academic Press, 2002, ISBN: 0-12-395173-9.

[51] Telecommunications Standardization Sector, International Telecommunications Union, "Recommendation G.709, Interfaces for optical transport network (OTN)," 2003.

[52] Telecommunications Standardization Sector, International Telecommunications Union, "Recommendation G.975, Forward error correction for submarine systems," 2000.

[53] G. P. Agrawal, *Fiber-Optic Communication Systems, Chapter 2: Optical Fibers*. John Wiley and Sons, 2nd ed., 1997, ISBN: 0-471-17540-4.

[54] Telecommunications Standardization Sector, International Telecommunications Union, "Recommendation G.652, Characteristics of a single-mode optical fibre cable," 2000.

[55] Telecommunications Standardization Sector, International Telecommunications Union, "Recommendation G.653, Characteristics of a dispersion shifted single-mode optical fibre cable," 2000.

[56] R. Tkach, A. Chraplyvy, F. Forghieri, A. Gnauck, and R. Derosier, "Four-photon mixing and high speed WDM systems," *Journal of Lightwave Technology*, vol. 13, pp. 841–849, May 1995.

[57] S. Bigo, G. Belloti, and M. W. Chbat, "Investigation of cross-phase modulation limitation over various types of fiber infrastructure," *IEEE Photonic Technology Letters*, vol. 11, pp. 605–607, May 1999.

[58] Telecommunications Standardization Sector, International Telecommunications Union, "Recommendation G.655, Characteristics of a non-zero dispersion-shifted single-mode optical fiber cable," 2000.

[59] OFS Marketing Communications, "TrueWave® RS Fiber, Nonzero Dispersion Optical Fiber," *Downloaded the 16-1-2003 from: http://www.ofsoptics.com/simages/pdfs/fiber/brochure/truewaversweb.pdf*, 2002.

[60] Corning Incorporated, "Corning® LEAF® Optical Fiber, Product information," *Downloaded the 19-1-2003 from: http://www.corning.com/...../pi1107Dec2002.pdf*, 2002.

[61] Alcatel, "Alcatel 6911, TeraLight^{TM} Metro Fiber," *Downloaded the 16-1-2003 from: http://www.alcatel.com/opticalfiber/...../teralightmetro.pdf*, 2001.

[62] Sumitomo Electric, "Optical Cable: Optical fiber for general purpose," *Downloaded the 16-1-2003 from: http://www.sei.co.jp/SUMIOFCAS/english/index.html*.

[63] G.Ghosh, M. Endo, and T. Iwasaki, "Temperature-dependent Sellmeier coefficients and chromatic dispersions for some optical fiber glasses," *Journal of Lightwave Technology*, vol. 12, pp. 1338–1342, August 1994.

[64] M.J.Hamp, J.Wright, M.Hubbard, and B.Brimacombe, "Investigation into the temperature dependence of cromatic dispersion in optical fiber," *IEEE Photonic Technology Letters*, vol. 14, number =, 2002.

[65] T. Kato, Y. Koyano, and M. Nishimura, "Temperature dependence of chromatic dispersion in various types of optical fibers," *in Technical Digest of OFC'2000*, vol. 1, Paper TuG7, pp. 104–106, March 2000.

[66] W.H.Hatton, "Temperature dependence of chromatic dispersion in single mode fibers," *Journal of Lightwave Technology*, vol. 4, pp. 1552–1555, October 1986.

[67] D.Penninckx, M.Chbat, L.Pierre, and J.P.Thiery, "The phase-shaped binary transmission (PSBT): A new technique to transmit far beyond the chromatic dispersion limit," *IEEE Photonic Technology Letters*, vol. 9, pp. 259–261, February 1997.

[68] K. Yonenaga and S. Kuwano, "Dispersion-tolerant optical transmission system using duobinary transmitter and binary receiver," *Journal of Ligtwave Technology*, vol. 15, pp. 1530–1537, August 1997.

[69] T. Wuth, W. Kaiser, W. Rosenkranz, G. Mohs, R. Neuhauser, and C. Glingener, "200 km repeaterless 10 Gb/s transmission on standard single mode fiber with single side band (SSB) modulation and Raman amplification," *in Technical Digest of OECC/IOOC*, pp. 8–9, July 2001.

[70] M. Sieben, J. Conradi, and D. E. Dodds, "Optical single sideband transmission at 10 Gb/s using only electrical dispersion compensation," *Journal of Lightwave technology*, vol. 17, pp. 1742–1749, October 1999.

[71] A.Hodzic, B.Konrad, and K. Petermann, "Alternative modulation formats in N x 40 Gb/s WDM standard fiber RZ transmission systems," *Journal of Lightwave Technology*, vol. 20, pp. 598–607, April 2002.

[72] S.Watanabe and M.Shirasaki, "Exact compensation for both chromatic dispersion and Kerr effect in a transmission fiber using optical phase conjugation," *Journal of Lightwave Technology*, vol. 14, pp. 243–248, March 1996.

[73] M.F.C.Stephens, D.Nesset, K.A.Williams, R.V.Penty, I.H.White, and M.J.fice, "Dispersion compensation at 40 Gbit/s over 100 km of standard fibre via mid-span spectral inversion in semiconductor optical amplifier with integrated pump laser," *Electronic Letters*, vol. 35, pp. 1359–1361, August 1999.

[74] L.G.Nielsen, S.N.Knudsen, T.Veng, B.Edvold, and C.C.Larsen, "Design and manufacture of dispersion compensating fibre for simultaneous compensation of dispersion and dispersion slope," *in Technical Digest of OFC'99*, vol. 2, Paper WM13-1, pp. 232–234, 1999.

[75] L.G.Nielsen, T.Veng, S.N.Knudsen, C.C.Larsen, and B.Edvold, "New dispersion compensating fibres for simultaneous compensation of dispersion and dispersion slope of non-zero fispershion shifted fibres in the C or L band," *in Technical Digest of OFC'2000*, vol. 2, Paper TuG6-1, pp. 101–103, 2000.

[76] Q. N.T., T.Veng, and L.G.Nielsen, "New dispersion compensating module for compensation of dispersion and dispersion slope of non-zero dispersion fibres in the C-band," *in Technical Digest of OFC'2001*, vol. 1, Paper TuH5-1, 2001.

[77] OFS Marketing Communications, "Wbdk-C Wide Band Dispersion Compensating Modules (C-band)," *Downloaded the 16-1-2003 from: http://www.ofs-fitel.dk/upload/2001112115031074-WBDK_C_0111_ofs.pdf*, 2002.

[78] M.Tur, E.Herman, and Y.Danziger, "Nonlinear properties of dispersion management modules employing high-order mode fibers," *in Technical Digest of OFC'2001*, vol. 2, Paper TuS5-T1-3, 2001.

[79] LaserComm, "HiMode^{TM} Dispersion Management Device," *Downloaded the 17-1-2003 from: http://www.lasercomm-inc.com/media/DMD_Brochure.pdf*, 2001.

[80] A.H.Gnauck, L.D.Garrett, Y.Danziger, U.Levy, and M.Tur, "Dispersion and dispersion-slope compensation of NZDSF over the entire C band using higher-order-mode fibre," *Electronic Letters*, vol. 36, November 2000.

[81] T. A.Strasser and T. Erdogan, *Optical Fiber Telecommunications IV, Chapter 10: Fiber Grating Devices*, vol. A. Academic Press, 2002, ISBN: 0-12-395173-9.

[82] R. Kashyap, *Fiber Bragg Gratings*. Academic Press, 1999, ISBN: 0-12-400560-8.

[83] W.H.Loh, R.I.Laming, N.Robinson, A.Cavaciuti, F.Vaninetti, C.J.Anderson, M.N.Zervas, and M.J.Cole, "Dispersion compensation over diatances in excess of 500 km for 10-Gb/s systems using chirped fiber gratings," *IEEE Photonic Technology Letters*, vol. 8, pp. 944–946, July 1996.

[84] L.D.Garret, A.H.Gnauck, R.W.Tkach, B.Aglogliati, L.Arcangeli, D.Scarano, V.Gusmeroli, C.Tosetti, G. Maio, and F.Forghieri, "Cascaded chirped fiber gratings for 18-nm-bandwidth dispersion compensation," *IEEE Photonic Technology Letters*, vol. 12, pp. 356–358, March 2000.

[85] J. III, E.Hernandez, J.A.Valenti, P.G.Sinha, M.R.Matthews, D.E.Elder, G.A.Beauchesne, and C.H.Byrd, "Dispersion and dispersion-slope correction with a fiber Bragg rating over the full C-band," *in Technical Digest of OFC'2001*, vol. Postdeadline papers, Paper PD12, 2001.

[86] M.Ibsen, M.K.Durkin, M.J.Cole, and R.I.Laming, "Sinc-sampled fiber Bragg gratings for identical multiple wavelength operation," *IEEE Photonic Technology Letters*, vol. 10, pp. 842–844, June 1998.

[87] Y.Painchaud, A.Mailloux, H.Chotard, E.Pelletier, and M.Guy, "Multichannel fiber Bragg gratings for dispersion compensation and slope compensation," *in Technical Digest of OFC'2002*, pp. 581–582, March 2002.

[88] K.Ennser, R.I.Laming, and M.N.Zervas, "Analysis of 40 Gb/s TDM-Transmission over embeded standard fiber employing chirped fiber grating dispersion compensators," *Journal of Lightwave Technology*, vol. 16, pp. 807–811, May 1998.

[89] T.N.Nielsen, B.J.Eggleton, and T.A.Strasser, "Penalties associated with group delay imperfections for NRZ, RZ and duo-binary encoded optical signals," *Prodeedings of ECOC'99*, vol. 1, pp. 388–389, September 1999.

[90] R.Khosravani and B.Hoanca, "Tolerance to amplitude and group delay ripple for systems using chirped fiber Bragg gratings," *in Technical Digest of LEOS'2001*, vol. 1, pp. 22–23, 2001.

[91] Corning Incorporated, "Corning® PureForm^{TM} DCM® Modules for LEAF® Fiber," *Downloaded the 16-1-2003 from: http://www.corning.com/...../pi1380_08-02.pdf*, 2002.

[92] Nettest, "Specifications of S19 tunable laser chromatic dispersion measurement system," *Values of specifications appearing the 18-1-2003 at: http://www.nettest.com/products/s19/specifications.php*, 2003.

[93] T.Sugihara, K.Shimomura, K.Shimizu, Y.Kobayashi, K.Matsuoka, M.Hashimoto, T.Hashimoto, T.HIrai, S.Matsumoto, T.Ohira, M.Takabayashi, K.Yoshiara, and T.Mizuochi, "Automatically tracked dispersion compensation with penalty-free tunable dispersion equalizer for 40 Gbit/s system," *in Technical Digest of OFC'2002*, pp. 577–578, 2002. Paper ThAA2.

[94] K.M.Feng, J.-X.Cai, V.Grubsky, D.S.Starodubov, M.I.Hayee, S.Lee, X.Jiang, A.E.Willner, and J.Feinberg, "Dynamic dispersion compensation in a 10 Gb/s optical system using a novel voltage tuned nonlinearly chirped fiber grating," *IEEE Photonic Technology Letters*, vol. 11, pp. 373–375, March 1999.

[95] J. Uniphase, "Product Bulletin: Fiber grating tunable dispersion compensator (FTDC)," *Downloaded the 18-1-2003 at: http://www.nettest.com/products/s19/specifications.php.*

[96] B.J.Eggleton, A.Ahuja, P.S.Westbrook, J.A.Rogers, P.Kuo, T.N.Nielsen, and B.Mikkelsen, "Integrated Tunable Fiber Gratings for Dispersion Management in High-Bit Rate Systems," *Journal of Lightwave Technology*, vol. 18, pp. 1418–1432, October 2000.

[97] B.J.Eggleton, B.Mikkelsen, G.Raybon, A.Ahuja, J.A.Rogers, P.S.Westbrook, T.N.Nielsen, S.Sultz, and K.Dreyer, "Tunable dispersion compensation in a 160-Gb/s TDM system by a voltage controlled chirped fiber Bragg grating," *IEEE Photonic Technology Letters*, vol. 12, pp. 1022–1024, August 2000.

[98] M.M.Ohn, A.T.Alavie, R.Maaskant, M.G.Xu, F.Bilodeau, and K.O.Hill, "Tunable fiber grating dispersion using a piezoelectric stack," *in Technical Digest of OFC'1997*, vol. 6, Paper WJ3, pp. 155–156, 1997.

[99] J.A.J.Fells, P.J.Bennett, R.Feced, P.Ayliffe, J.Wakefield, H.F.M.Priddle, V.Baker, S.E.Kanellopoulos, C.Boylan, S.Sahil, W.S.Lee, S.J.Clements, and A. Hadjifotiou, "Widely tunable twin fiber grating dispersion compensator for 80 Gbit/s," *in Technical Digest of OFC'2001*, vol. Post Deadline, Paper PD11, 2001.

[100] "Private communication. Specifications of sample provided by Phaethon Communications," June 2002.

[101] M.Shirasaki, "Chromatic-Dispersion Compensator Using Vitually Imaged Phased Array," *IEEE Photonic Technology Letters*, vol. 9, pp. 1598–1600, December 1997.

[102] M.Shirasaki, A.N.Akhter, and C.Lin, "Virtually imaged phased array with graded reflectivity," *IEEE Photonic Technology Letters*, vol. 11, pp. 1443–1445, November 1999.

[103] M.Shirasaki, "Compensation fo chromatic dispersion and dispersion slope using a virtually imaged phased array," *in Technical Digest OFC'2001*, vol. 2, Paper TuS1, 2001.

[104] L.D.Garret, A.H.Gnauck, M.H.Eiselt, and R.W.Tkach, "Demonstration of virtually-imaged phased array device for tunable dispersion compensation in 16x10 Gb/s WDM transmission over 480 km standard fiber," *in Technical Digest of OFC'2000*, vol. Post Deadline Paper, Paper PD7, 2000.

[105] H.Ooi, K.Nakamura, Y.Akiyama, T.Takahara, J.Kumasako, J.C.Rasmusen, T.Terahara, Y.Kawahata, H.Isono, G.Ishikawa, and N.Yamaguchi, "3.5 Tbit/s (43 Gbit/s x 88 ch) transmission over 600-km NZDSF with VIPA variable dispersion compensators," *in Technical Digest of OFC'2002*, pp. 555–556, 2002. Paper ThX3.

[106] C.K.Madsen, G.Lenz, A.J.Bruce, M.A.Capuzzo, L.T.Gomez, and R.E.Scotti, "Integrated all-pass filters for tunable dispersion and dispersion slope compensation," *IEEE Photonic Technology Letters*, vol. 11, pp. 1623–1624, December 1999.

[107] C.K.Madsen, S.Chandraeskhar, E.J.Laskowski, K.Bogart, M.A.Capuzzo, A.Paunescu, L.W.Stulz, and L.T.Gomez, "Compact integrated tunable chromatic dispersion compensator with a 4000 ps/nm tuning range," *in Technical Digest of OFC'2001*, vol. Post Deadline Paper PD9, 2001.

[108] D.J.Moss, S.McLaughlin, G.Randall, M.Lamont, M.Ardenaki, and P.Colbourne, "Multichannel tunable dispersion compensation using allpass multicavity etalons," *in Technical Digest of OFC'2002*, pp. 132–133, 2002. Paper TuT2.

[109] L.M.Lunardi, D.J.Moss, S.Chandrasekhar, and L.L.Buhl, "An etalon-based tunable dispersion compensator (TDC) device for 40-Gbit/s applications," *in Proceedings of ECOC'2002*, 2002. Paper Tu6.4.2.

[110] C.K.Madsen and G.Lenz, "A multi-channel dispersion slope compensating optical allpass filter," *in Technical Digest of OFC'2000*, vol. 2, Paper WF5, 2000.

[111] J.-X.Cai, K.-M.Feng, A.E.Willner, V.Grubsky, D.S.Starodubov, and J.Feinberg, "Simultaneous tunable dispersion compensation of many WDM channels using a sampled nonliarely chirped fiber Bragg grating," *IEEE Phtonic Technology Letteres*, vol. 11, pp. 1455–1457, Novemeber 1999.

[112] F.Buchali, H.Bulow, W.Baumert, R.Ballentin, and T.Wehren, "Reduction of the chromatic dispersion penalty at 10 Gbit/s by integrated electronic equalisers," *Tehcnical Digest of OFC'2000*, vol. 3, Paper ThS1, pp. 268–270, 2000.

[113] Santel Networks Inc., "Electronic dispersion compensation," *Downloaded the 20-1-2003 from: http://www.santelnet.com/Whitepaper1.pdf*, 2002.

[114] Santel Networks Inc., "Preliminary product brief: S44501/S44003 Electronic dispersion compensator/CDR-D chip set," *Downloaded the 20-1-2003 from: http://www.santelnet.com/S44501_003%20Product%20Brief.pdf*, 2002.

[115] M.Tomizawa, A.Sano, Y. Yamabayashi, and K.Hagimoto, "Automatic dispersion equalization for installing high-speed optical transmission systems," *Journal of Lightwave Technology*, vol. 16, pp. 184–190, February 1998.

[116] M.N.Petersen, Z.Pan, S.Lee, S.A.Havstad, and A.E.Willner, "Online chromatic dispersion monitoring and compensation using a single inband subacarrier tone," *IEEE Photonic Technology Letters*, vol. 14, pp. 570–572, April 2002.

[117] Z.Pan, Q.Yu, Y.Xie, S.A.Havstad, A.E.Willner, D.S.Starodubov, and J.Feinberg, "Chromatic dispersion monitoring and automated compensation for NRZ and RZ data using clock regeneration and fading without

adding signaling," *in Technical Digest of OFC'2001*, vol. 3, Paper WH5, 2001.

[118] Q.Yu L.-S.Yan and A.E.Willner, "Chromatic dispersion monitor for WDM systems using vestigial-sideband optical filtering," *Tehcnical Digest of OFC'2002*, pp. 197–199, 2002.

[119] M. N. Petersen, "Dispersion monitoring," *Research Center COM, Master Science final thesis*, November 2001.

[120] S.Kuwahara, A.Sano, K.Yonenaga, Y.Miyamoto, and Y.Yamabayashi, "Adaptive dispersion equalisation by detecting dispersion fluctuations using PM-AM conversion," *Electronic Letters*, vol. 34, pp. 1956–1958, October 1998.

[121] G.Ishikawa and H.Ooi, "Demonstration of automatic dispersion equalization in 40 Gbit/s OTDM transmission," *in Proceedings of ECOC'98*, vol. 1, pp. 519–520, 1998.

[122] S.Walklin and J.Conradi, "Multilevel signaling for increasing the reach of 10 Gb/s lightwave systems," *Journal of Lightwave Technology*, vol. 17, pp. 2235–2247, Novemeber 1999.

[123] K.Yonenaga, Y.Miyamoto, H.Toba, K.Murata, M.Yoneyama, Y.Yamane, and H.MIyazawa, "320 Gbit/s WDM repeaterless transmission using fully encoded 40 Gbit/s optical duobinary channels with dispersion tolerance of 380 ps/nm," *Electronic Letters*, vol. 37, pp. 109–110, January 2001.

[124] G.Wenke and M.Klimmek, "Considerations on the α-factor of nonideal, external optical Mach-Zehnder modulators," *Journal of Optical Communications*, vol. 17, no. 2, pp. 42–48, 1996.

[125] B. L.Kasper, O. Mizuhara, and Y.-K. Chen, *Optical Fiber Telecommunications IV, Chapter 16: High bit-rate receivers, transmitters and electronics*, vol. A. Academic Press, 2002, ISBN: 0-12-395173-9.

[126] Y.Zhu, W.S.Lee, G.Pettitt, M.Jones, and A.Hajifotiou, "Eight-channel 40 Gb/s RZ transmission over four 80 km spans (328 km) of NDSF wiht net dispersion tolerance in excess of 180 ps/nm," *in Technical Digest of OFC'2000*, vol. 1, Paper TuD4, pp. 51–55, 2000.

[127] A. Carlson, *Communication systems: An introduction to Signals and Noise in Electrical Communication.* McGraw-Hill Book Company, third ed., 1986, ISBN: 0-07-Y100560-9.

[128] A.Røyset and D.R.Hjelme, "Symmetry requirements for 10-Gb/s optical duobinary transmitters," *IEEE Photonic Technology Letters*, vol. 10, pp. 273–274, February 1998.

[129] W.Kaiser, T.Wuth, M.Wichers, and W.Rosenkranz, "Reduced complexity optical duobinary 10 Gbit/s transmitter setup resulting in an increased transmission distance," *IEEE Photonic Technology Letters*, vol. 13, pp. 884–886, August 2001.

[130] K.Murata, K.Yonenaga, Y.Miyamoto, and Y.Yamane, "Parallel precoder IC module for 40 Gbit/s optical duobinary transmission system," *Electronic Letters*, vol. 36, pp. 1571–1572, August 2000.

[131] D.Peninckx, G.Vendrome, M.Maignan, and J.C.Jacquinot, "Experimental verification of the phase-shaped binary transmission (PSBT) effect," *IEEE Photonic Technology Letters*, vol. 10, pp. 612–614, April 1998.

[132] D.Penninckx, "Effect of electrical filtering of duobinary signals on the chromatic dispersion transmission limitatins," *in Proceedings of ECOC'98*, pp. 537–538, September 1998.

[133] J.M.Gene, R.Nieves, A.Buxens, C.Peucheret, J.Prat, and P.Jeppesen, "Reduced driving voltage optical duobinary transmitter and its impact on transmission performance over standard single-mode fiber," *IEEE Photonic Technology Letters*, vol. 14, pp. 843–845, June 2002.

[134] X.Zheng, F.Liu, and P.Jeppesen, "Receiver optimization for 40-Gb/s optical duobinary signal," *IEEE Photonic Technology Letters*, vol. 13, pp. 744–746, July 2001.

[135] T.Frank, T.N.Nielsen, and A.Stentz, "Experimental verification of SBS suppression by duobinary modulation," *in Proceedings of ECOC'1997*, pp. 71–74, 1997.

[136] J. Mills, "Cash-strapped carriers cread 40 Gbit/s roadblocks," *FibreSystems, Europe*, pp. 30–33, 2001. Special issue: ECOC 2001.

[137] H. Kogelnik, R. M. Jopson, and L. E. Nelson, *Optical Fiber Telecommunications IV, Chapter 15: Polarization-mode dispersion*, vol. B. Academic Press, 2002.

[138] T. T. Larsen, "Dynamic compensation polarization-mode dispersion in high-speed optical systems," *Research Center COM, Master Science final thesis*, February 2002.

[139] N.Gisin, J. der Weid, and J.P.Pellaux, "Polarization mode dispersion of short and long single mode fibers," *Journal of Lightwave Technology*, vol. 9, pp. 821–827, July 1991.

[140] A.F.Judy, W.T.Greene, and J.B.Haber, "PMD characterization of production cables for critical lightwave systems," *in Proceedings of International Wire and Cable Symposium 1993*, pp. 630–634, 1993.

[141] G.J.Foschini, L.E.Nelson, R.M.Jopson, and H.Kogelnik, "Probability densities of second order polarization mode dispersion including polarization dependent chromatic fiber dispersion," *IEEE Photonic Technology Letters*, vol. 12, pp. 293–295, March 2000.

[142] H.Bulow, W.Baumert, H.Schmuck, T.Mohr, T.Schulz, F.Kuppers, and W.Weisershausen, "Measurement of the maxium speed of PMD fluctuation in installed field fiber," *in Technical Digest of OFC'99*, vol. 2, Paper WE4-1, pp. 83–85, 1999.

[143] J.Cameron, L.Chen, X.Bao, and J.Stears, "Time evolution of polarization mode dispersion in optical fibers," *IEEE Photonic Technology Letters*, vol. 10, pp. 1265–1267, September 1998.

[144] M.Karlsson, J.Brentel, and P.A.Andrekson, "Long-term measurement of PMD and polarization drift in installed fibers," *Journal of Lightwave Technology*, vol. 18, pp. 941–951, July 2000.

[145] M.Brodsky, P.D.Magill, and N.J.Frigo, "Evidence of parametric dependence of PMD on temperature in installed 0.05 $ps/km_{1/2}$ fiber," *in Proceedings of ECOC'2002*, vol. 4, Paper 9.3.2, 2002.

[146] L.E.Nelson, R.M.Jopson, and H.Kogelnik, "Measurement of depolarization and scaling associated with second-order polarization mode dispersion in optical fibers," *IEEE Photonic Technology Letters*, vol. 11, pp. 1614–1616, December 1999.

[147] G.J.Foschini, L.E.Nelson, R.M.Jopson, and H.Kogelnik, "Statistics of second-order PMD depolarization," *Journal of Lightwave Technology*, vol. 19, pp. 1882–1886, December 2001.

[148] G.J.Foschini, L.E.Nelson, R.M.Jopson, and H.Kogelnik, "Probability densities of second-order polarization mode dispersion including polarization dependent chromatic fiber dispersion," *IEEE Photonic Technology Letters*, vol. 12, pp. 293–295, March 2000.

[149] D.Penninkx and F.Bruyere, "Impact of the statistics of second-order polarization dispersion on system performance," *in Technical Digest of OFC'1998*, pp. 340–342, 1998. Paper ThR2.

[150] L.E.Nelson, R.M.Jopson, and H.Kogelnik, "Polarization mode dispersion penalties associated with rotation of principal states of polarization in optical fibers," *in Technical Digest of OFC'2000*, vol. 3, Paper ThB2, pp. 25–27, 2000.

[151] P.J.Winzer, H.Kogelnik, C.H.Kim, H.Kim, R.M.Jopson, and L.E.Nelson, "Effect of receiver design on PMD outage for RZ and NRZ," *in Technical Digest of OFC'2002*, pp. 46–48, 2002. Paper TuL1.

[152] A. Forno, A.Paradisi, R.Passy, and J. der Weid, "Experimental and theorethical modelling of polarization-mode dispersion in single-mode fibers," *IEEE Photonics Technology Letters*, vol. 12, pp. 296–298, March 2000.

[153] W.Wiershausen, R.Leppla, F.Kuppers, and H.Scholl, "Polarization-mode dispersion in fibre transmission: Theoretical approach, impact on systems, and suppresion of signal degradation effects," *in Proceedings of ECOC'99*, vol. 2, pp. 130–133, 1999.

[154] J.P.Elbers, C.Glingener, M.Duser, and E.Voges, "Modelling of polarisation mode-dispersion in singlemode fibres," *Electronic Letters*, vol. 33, pp. 1894–1895, October 1997.

[155] A. J. Lowery, *Optical Fiber Telecommunications IV, Chapter 12: Photonic Simulation Tools*, vol. B. Academic Press, 2002, ISNB: 0-12-395173-9.

[156] R.Khosravani, I.T.Lima, P.Ebrahimi, E.Ibragimov, A.E.Willner, and C.R.Meyuk, "Time and frequency domain characteristics of polarization-mode dispersion emulators," *IEEE Photonic Technology Letters*, vol. 13, pp. 127–129, February 2001.

[157] D.Beltrame, F.Matera, M.Settembre, A.Galrarossa, A.Pizzinat, F.Favre, D.LeGuen, and M.Henry, "Statistical behaviour of the Q-factor in optical transmission systesm due to the polarization mode dispersion," *in Proceedings of ECOC'2000*, 2000. Paper 5.2.3.

[158] H.Bulow, "Operation of digital optical transmission system with minimal degradation due to polarisation mode dispersion," *Electronic Letters*, vol. 31, pp. 214–215, February 1995.

[159] M.Karlsson, "Probability density functions of the differential group delay in optical fiber communication systems," *Journal of Lightwave Technology*, vol. 19, pp. 324–331, March 2001.

[160] B. Technology, "OA2000 Advance product information: C-band Erbium Doped Fiber Amplifier," *Downloaded the 27-1-2003 from : http : //www.bookham.com/opticalsolutions/optproducts/OA2000df*, 2002.

[161] S.Sarkimukka, A.Djupsjobacka, A.Gavler, and G.Jacobsen, "Mitigation of polarization-mode dispersion in optical multichannel systems," *Journal of Lightwave Technology*, vol. 18, pp. 1374–1380, October 2000.

[162] T.Ono, Y.Yano, L.D.Garret, J.A.Nagel, M.J.Dickerson, and M.Cvijetic, "10 Gb/s PMD compensation field experiment over 452 km using principal state transmission method," *in Technical Digest OCF'2000*, vol. Post Dadline Paper, PD-44, 2000.

[163] T.Takahashi, T.Imai, and M.Aiki, "Automatic compensation technique for timewise fluctuatin polarisation mode dispersion in in-line amplifier system," *Electronic Letters*, vol. 30, pp. 348–349, February 1994.

[164] H.Ooi, Y.Akiyama, and G.Ishikawa, "Automatic polarization-mode dispersion compensation in 40-Gbit/s transmission," *in Technical Digest of OFC'99*, vol. 2, Paper WE5, pp. 86–88, 1999.

[165] J.A.Nagel, M.W.Chbat, L.D.Garret, J.P.Soigne, N.A.Weaver, B.M.Desthieux, H.Bulow, A.R.McCornick, and R.M.Derosier, "Long-term PMD mitigation at 10 Gb/s and time dynamics over high-PMD installed fiber," *in Proceedings of ECOC'2000*, 2000. Paper 4.2.1 (Invited).

[166] C.Francia, F.Bruyere, J.P.Thiery, and D.Pennincks, "Simple dynamic polarisation mode dispersion compensation," *Electronic Letters*, vol. 35, March 1999.

[167] M.H.Smith and R.A.Chipman, "Comparison of different PMD compensator configurations base on outage probability," *in Technical Digest of OFC'2002*, 2002. Paper Wi2.

[168] M.Karlsson, "A comparison of different PMD-compensation techniques," *in Proceedings of ECOC'2000*, 2000. Paper 4.2.2.

[169] D.Sandel, M.Yoshida-Dierolf, R.Noe, A.Schopflin, E.Gottwald, and G.Fischer, "Automatic polarisation mode dispersion compensation in 40 Gbit/s optical transmission system," *Electronic Letters*, vol. 34, pp. 2258–2259, November 1998.

[170] W.Shieh, H.Haunstein, B.Mckay, D.Fishman, A.Golubchik, J.Diubaldi, C.Martell, V.Arya, R.Lee, and H.Choudhury, "Dynamic polarization-mode-dispersion compensation in WDM systems," *in Proceedings of ECOC'2000*, 2000. Paper 4.2.5.

[171] H.Rosenfeldt, R.Ulrich, U.Feiste, R.Ludwig, H.G.Weber, and A.Erhrhardt, "PMD compensation in 10 Gbit/s NRZ field experiment using polarimetric error signal," *Electronic Letters*, vol. 36, pp. 448–450, March 2000.

[172] H.Sunnerud, C.Xie, M.Karlsson, R.Samuelsson, and P.A.Andrekson, "A comparison between different PMD compensation techniques," *Journal of Lightwave Technology*, vol. 20, pp. 368–378, March 2002.

[173] H.Bulow, F.Buchali, and G.Thielecke, "Electronically enhanced optical PMD compensation," *in Proceedings of ECOC'2000*, vol. 2, pp. 39–40, 2000.

[174] D.Schlump, B.wedding, and H.Bulow, "Electronic equalisation of PMD and chromatic dispersion induced distortion after 100 km standard fibre at 10 Gbit/s," *in Proceedings of ECOC'98*, vol. 1, pp. 535–536, 1998.

[175] K.Ho and C.Lin, "Performance analysis of optical transmission system with polarization mode dispersion and forward error correction," *IEEE Photonic Technology Letters*, vol. 9, pp. 1288–1290, September 1997.

[176] M.Tomizawa, Y.Kisaka, T.Ono, Y.Miyamoto, and Y.Tada, "FEC performance in PMD limited high-speed optical transmission systems," *in Proceedings of ECOC'2000*, vol. 2, Paper 5.2.4, 2000.

[177] B.Wedding and C.N.Haslach, "Enhanced PMD mitigation by polarization scrambling and forward error correction," *in Technical Digest of OFC'2001*, vol. 2, Paper WAA1, 2001.

[178] H.F.Haunstein, K.Sticht, and R.Schlenk, "Control of 3-tap electrical feed-forward equalizer by conditional error counts from FEC in the presence of PMD," *in Technical Digest of OFC'2002*, pp. 307–308, 2002.

[179] S. Corporation, "Santec Optical Instruments, Polarization Analysis Module PAM-10," *Downloaded the 29-1-2003 from : http://www.santec.com/pdf/components/PAM-10.pdf*, 2002.

[180] H.Sunnerud, M.Karlsson, and P.A.Andrekson, "A comparison between NRZ and RZ data formats with respect to PMD-induced system degradation," *IEEE Photonic Technology Letters*, vol. 13, pp. 448–450, May 2001.

[181] D.Dahan and G.Eisentein, "Numerical comparison between distributed and discrete amplification in a point-to-point 40-Gb/s 40-WDM-based transmission system with three different modulation formats," *Journal of Lightwave Technology*, vol. 20, pp. 379–388, March 2002.

[182] R.Khosravani and A.E.Willner, "System performance evaluation in terrestrial systems with high polarization mode dispersion and the effect of chirping," *IEEE Photonic Technology Letters*, vol. 13, no. 4, pp. 296–298, 2001.

[183] R.M.Jopson, L.E.Nelson, G.J.Pendock, and A.H.Gnauck, "Polarization-mode dispersion impairment in return-to-zero and nonreturn-to-zero systems," *in Technical Digest of OFC'1999*, vol. 2, Paper WE3-1, pp. 80–82, 1999.

[184] S.Lee, Y.Xie, O.H.Adamczyk, and A.E.Willner, "Penalty distribution comparison for different data formats under high PMD values," *in Proceedings of ECOC'2000*, 2000. Paper 5.2.2.

[185] S.Lanne, D.Penninckx, J.P.thiery, and J.P.Hamaide, "Extension of polarization-mode dispersion limit using optical mitigation and phase-shaped binary transmission," *in Technical Digest of OFC'2000*, vol. 3, Paper ThH3, pp. 116–118, 2000.

[186] M.Dulk, W.Hunziker, L.Tallone, and H.Melchior, "40 GHz actively mode-locked semiconductor laser with hybrid external fiber Bragg grating cavity," *in Proceedings of ECOC'2000*, 2000. Paper 6.3.6.

[187] Y.Hashimoto, H.Yamada, R.Kuribayashi, and H.Yokoyama, "40-GHz tunable optical pulse generation from a highly external cavity mode locked semiconductor laser module," *in Technical Digest of OFC'2002*, pp. 342–343, 2002. Paper WV5.

[188] G.J.Spuhler, M.Dymott, I.Klimov, G.Luntz, L. Baraldi, I.Kilburn, P.Crosby, S.Thomas, O.Zehnder, C.Y.Teisset, M.Brownell, K.J.Weingarten, R.Dangel, B.J.Offrein, G.L.Bona, O.Boccafusca, Y.Kaneko, L.Krainer, R.Paschotta, and U.Keller, "40 GHz pulse generation source with less than 350 fs timing jitter," *Electronic Letters*, vol. 38, pp. 1031–1033, August 2002.

[189] A.Ougazzaden, C.W.Lentz, T.G.B.Mason, K.G.Glogovsky, C.L.Reynolds, G.J.Przybylek, R.E.Leibenguth, T.L.Kercher, J.W.Boardman, M.T.Rader, J.M.Geary, F.S.Walters, L.J.Peticolas, J.M.Freund, S.N.G.Chu, A.Sirenko, R.J.Jurchenko, M.S.Hybertsen,

L.J.PKeetelsen, and G.Raybon, "40 Gb/s tandem electro-absoption modulator," *in Technical Digest of OFC'2001*, vol. PostDeadline paper PD14, 2001.

[190] R.Khosravani and A.E.Willner, "Comparison of different modulation formats in terrestrial systems with high polarization mode dispersion," *in Technical Digest of OFC'2000*, vol. 2, Paper WL5, 2000.

[191] S.Bigo, D.Penninckx, and M.W.Chbat, "Investigation of self-phase modulation limitation on 10 Gbit/s transmission over different types of fiber," *in Technical Digest of OFC'98*, vol. 2, Paper FC2, 1998.

[192] D.Huber, R.Bauknecht, C.Bergamaschi, M.Bitter, A.Huber, T.Morf, A.Neiger, M.Rohner, I.Schnyder, V.Schwarz, and H.Jackel, "InP-InGaAs Single HBT technology for photoreceiver OEIC's at 40 Gb/s and beyond," *Journal of Lightwave Technology*, vol. 18, pp. 992–1000, July 2000.

[193] OptoSpeed, "RX40D0-530 50 Gb/s Optical Front-End, Rev 2.0 preliminary data sheet," *Downloaded the 2-1-2003 from: http://www.optospeed.ch/en/products/optical_front_ends_receivers/RX40D0-530_R20.pdf.*

[194] T.Nakata, T.Takeuchi, K.Makita, Y.Amamiya, T.Kato, Y.Suzuki, and T.Torikai, "High-sensitivity 40-Gb/s receiver with a wideband InAlAs waveguide avalanche photodiode," *in Proceedings of ECOC'2002*, vol. 4, Paper 10.5.1, 2002.

[195] A.Farbert, G.Mohs, S.Spalter, J.P.Elbers, C.Furst, A.Schopflin, E.Gottwald, C.Scheerer, and C.Glingener, "7 Tb/s (176x40 Gb/s) Bidirectional interleaved transmission with 50 GHz channel spacing," *in Proceedings of ECOC'2001*, vol. Post Deadline Paper-3, 2001.

[196] B.Mason, J.M.Geary, J.M.Freund, A.Ougazzaden, C.Lentz, K.Glovsky, G.Prybylek, L.Peticolas, F.Walters, L.Reyonolds, J.Boardman, T.Kercher, M.Rader, D.Monroe, and L.Ketelsen, "40Gb/s photonic integrated receiver sith -17 dBm sensitivity," *in Technical Digest of OFC'2002*, vol. Post Deadline Paper FB10, 2002.

[197] R.-J. Essiambre, G. Raybon, and B. Mikkelsen, *Optical Fiber Telecommunications IV, Chapter 6: Pseudo-linear transmission of high-speed signals*, vol. B. Academic Press, 2002, ISBN: 0-12-395173-9.

[198] K.Rottwitt, J.Bromage, M.Du, and A.Stentz, "Design of distributed Raman amplifiers," *in Proceedings of ECOC'2000*, 2000. Invited paper, 4.4.1.

[199] M.H.Eiselt and L.D.Garrett, "Optical SNR versus Q-factor improvement with distributed Raman amplification in long amplifier chains," *in Proceedings of ECOC'2000*, 2000. Paper 4.4.4.

[200] C.Fludger, A.Maroney, N.Jolley, and R.Mears, "An analysis of the improvement in OSNR from distributed Raman amplifiers using modern transmission fibres," *in Technical Digest of OFC'2000*, vol. 4, Paper FF2, pp. 100–102, 2000.

[201] G. P. Agrawal, *Nonlinear fiber optics*. Academic Press, second ed., 1995, ISBN: 0-12-0455142-5.

[202] B.Bakhshi, M.Vaa, E.A.Golovchenko, W.W.Patterson, R.L.Maybach, and N.S.Bergano, "Comparison of CRZ, RZ and NRZ modulation formats in a 64 x 12.3 Gb/s WDM transmission experiment over 9000 km," *in Technical Digest of OFC'2001*, vol. 3, Paper WF4, 2001.

[203] C.Caspar, H-M.Foisel, A.Gladisch, N.Hanik, F.Kupers, R.Ludwig, A.Mattheus, W.Pieper, B.Strebel, and H.G.Weber, "RZ versus NRZ modulation format for dispersion compensated SMF-based 10 Gb/s transmission wiht more than 100 km amplifier spacing," *IEEE Photonic Technology Letters*, vol. 11, pp. 481–483, April 1999.

[204] S.G.Park, A.H.Gnauck, J.M.Wisenfeld, and L.D.Garret, "40-Gb/s transmission over multiple 120-km spans of conventional single-mode fiber using highly dispersed," *IEEE Photonic Technology Letters*, vol. 12, pp. 1085–1087, August 2000.

[205] R.Ludwig, U.Feiste, E.Dietrich, H.G.Weber, D.Breuer, M.Martin, and F.Kupers, "Experimental comparison of 40 Gbit/s RZ and NRZ transmission over standard singlemode fibre," *Electronic Letters*, vol. 35, pp. 2216–2218, December 1999.

[206] C.Furst, G.Mohns, H.Geiger, and G.Fischer, "Performance limits of nonlinear RZ and NRZ coded transmission at 10 and 40 Gb/s on different fibers," *in Technical Digest of OFC'2000*, vol. 2, Paper WM3, pp. 302–304, 2000.

[207] D.Breuer and K.Petermann, "Comparison of nrz- and rz-modulation format for 40 gb/s tdm standard-fiber systems," *IEEE Photonic Technology Letters*, vol. 9, pp. 398–400, March 1997.

[208] T.Wuth, W.Kaiser, and W.Rosenkranz, "Impact of self-phase modulation on bandwidth efficient modulation formats," *in Technical Digest of OFC'2001*, vol. 1, Paper MM6, 2001.

[209] C.Peucheret, A.Buxens, T.Rasmussen, C.F.Pedersen, and P.Jeppesen, "Cascadability investigation of fibre Bragg gratings for narrow channel spacing systems," *in Proceedings of OECC/IOOC 2001*, pp. 266–267, 2001. Paper WA4.

[210] K.H.Yla-Jarkko, M.K.Durkin, M.N.Zervas, I.Barry, P.Skull, R.Wixey, S.Pillay, and D.Steel, "8-channel 200 GHz-spacing OADM with 50 GHz linear-phase FBGs," *in Proceedings of ECOC'2002*, vol. 4, paper 10.4.3, 2002.

[211] G.Nykolak, B.J.Eggleton, G.Lenz, and T.A.Strasser, "Dispersion penalty measurement of narrow fiber Bragg gratings at 10 Gb/s," *IEEE Photonic Technology Letters*, vol. 10, pp. 1319–1321, September 1998.

[212] Y.Miyamoto, "40Gbit-s Transport system: Its WDM upgrade," *in Technical Digest OFC'2000*, vol. 3, Paper ThW4, 2000.

[213] H. Takahashi, K.Oda, H.Toba, and Y.Inoue, "Transmission characteristic of arrayed waveguide NxN wavelenght multiplexer," *Journal of Lightwave Technology*, vol. 13, pp. 447–455, March 1995.

[214] G.Charlet, J.-C.Antona, S.Lanne, P.Tran, W.Idler, M.Gorlier, S.Borne, A.Klekamp, C.Simonneau, L.Pierre, Y.Frignac, F.Beaumont, J.-P.Hamaide, and S.Bigo, "6.4 Tb/s (159x42.7 Gb/s) capacity over 21x100 km using bandwidth-limited phase-shaped binary transmission," *in Proceedings of ECOC'2002*, vol. Post Deadline Papers, PD4.1, 2002.

[215] K.Yonenaga and Y.Miyamoto, "Dispersion-managed high-capacity WDM systems using zero-dispersion-flattened transmission line," *in Technical Digest of OFC'1999*, vol. 4, Paper FD4, pp. 71–73, 1999.

[216] S.Bigo, A.Bertaina, Y.Frignac, S.Borne, L.Lorcy, D.Hamoir, D.Bayart, J.Hamaide, W.Idler, E.Lach, B.Franz, and G.Veith, "5.12 Tbit/s (128x40 Gbit/s WDM) transmission over 3x100 of $TeraLight^{TM}$ Fibre," *in Proceedings of ECOC'2000*, vol. Post Deadline Papers, Paper 1.2, 2000.

[217] T.Ito, K. Fukuchi, D. Ogasahara, R.Ohhira, and T.Ono, "6.4 Tb/s (160x40 Gb/s) WDM transmission experiment with 0.8 bits/Hz spectral efficiency," *in Proceedings of ECOC'2000*, vol. Post Deadline papers, Paper 1.1, 2000.

[218] K.Tanaka, I.Morita, and N.Edagawa, "50 GHz spaced 40 Gbit/s x 25 WDM transmission over 480 km using bandlimited RZ signals," *Electronic Letters*, vol. 37, pp. 775–777, June 2001.

[219] D.F.Grosz, A.Agarwal, S.Banerjee, A.P.Kung, D.N.Maywar, A.Grevich, T.H.Wood, C.R.Lima, B.Faer, J.Black, and C.Hwu, "5.12 Tb/s (128x42.7 Gb/s) transmission with 0.8 bits/s/Hz spectral efficiency over 1280 km of standard single-mode fiber using all-Raman amplification and strong signal filtering," *in Proceedings of ECOC'2002*, vol. Post Deadline Papers, Paper 4.3, 2002.

[220] R.A.Griffin, R.G.Walker, B.J.Buck, R.Powell, L.N.Langley, J.Hall, and A.C.Carter, "40 Gb/s RZ GaAs transmitter with integrated waveform monitoring," *in Proceedings of ECOC'2002*, vol. 4, Paper 10.5.4, 2002.

[221] P. Bayvel and R. Killey, *Optical Fiber Telecommunications IV, Chapter 13: Nonlinear Optical effects in WDM transmission*, vol. B. Academic Press, 2002, ISBN: 0-12-395173-9.

[222] M.Staif, M.Eiselt, and L.D.Garret, "Cross-phase modulation distortion measurements in multi-span WDM systems," *IEEE Photonic Technology Letters*, vol. 12, pp. 88–90, January 2000.

[223] H.J.Thiele, R.I.Killey, and P.Bayvel, "Investigation of XPM distortion in transmission over installed fiber," *IEEE Photonic Technology Letters*, vol. 12, pp. 669–671, June 2000.

[224] C. J. Videcrantz, *LD 124, Optical amplificatioin and processing in high capacity photonic networks*. PhD thesis, Technical University of Denmark, Department of Electromagnetic Systems, March 1997.

[225] P.B.Hansen, L.Eskildsen, A.J.Stentz, T.A.Strasser, J.Judkins, J.J.DeMarco, R.Pedrazzani, and D.J.DiGiovanni, "Rayleigh scattering limitations in distributed Raman pre-amplifiers," *IEEE Photonic Technology Letters*, vol. 10, pp. 159–161, January 1998.

[226] Y.Miyamoto, S.kuwahara, A.Hirano, Y.Tada, Y.Yamane, and H.Miyazawa, "Reduction of nonlinear cross-talk by carrier-suppresed RZ format for 100 GHz-spaced Nx43 Gbit/s WDM in non-zero dispersion shifted band," *in Proceedings of ECOC'2001*, vol. 4, pp. 528–529, 2001.

[227] N.Sahri, D.Prieto, S.Silvestre, D.Keller, F.Pommerau, M.Reanaud, O.Rofidal, A.Dupas, F.Dorguille, and D.Chiaroni, "A highly integrated 32-SOA gates optoelectronic module suitable for IP multi-terabit optical routers," *in Technical Digest of OFC'2001*, vol. Post Deadline Papers, PD32, 2001.

[228] J.W.Wisenfeld, B.Glance, J.S.Perino, and A.H.Gnauck, "Wavelength conversion at 10 Gb/s using a Semiconductor Optical Amplifier," *IEEE Photonics Technology Letters*, vol. 5, pp. 1300–1303, Novemeber 1993.

[229] H.K.Kim and S.Chandrasekhar, "Reduction of Cross-Gain Modulation in the Semiconductor Optical Amplifier by using wavelength modulated signal," *IEEE Photonic Technology Letters*, vol. 12, pp. 1412–1414, October 2000.

[230] A.K.Srivastava, S.Banerjee, B.R.Eichenbaum, C.Wolf, Y.Sun, J.W.Sulhoff, and A.R.Chraplyvy, "A polarization multiplexing technique to mitigate WDM crosstalk in SOAs," *IEEE Photonic Technology Letters*, vol. 12, pp. 1415–1416, October 2000.

[231] S.Banerjee, A.K.Srivastava, Y.Sun, J.W.Sulhoff, K.Kantor, and C.Wolf, "Cascaded semiconductor optical amplifiers for transmission of 32 DWDM channels over 315 km," *in Technical Digest of OFC'2000*, vol. 2, Paper WM32, pp. 305–307, 2000.

[232] L.H.Spiekman, J.M.Wiesenfeld, A.H.Gnauck, L.D.Garret, G. den Hoven, T. Dongen, M.J.H.Sander-Jochem, and J.J.M.Binsma, "8x10 Gb/s DWDM transmission over 240 km of standard fiber using cascade of semiconductor optical amplifiers," *IEEE Photonic Technology Letters*, vol. 12, pp. 1082–1084, August 2000.

[233] D.A.Francis, S.P.DiJaili, and J.D.Walker, "A single-chip linear optical amplifier," *in Technical Digest of OFC'2001*, vol. Post Deadline Papers, PD13, 2001.

[234] Y.Xie, S.Lee, Z.Pan, J.-X.Cai, A.E.Willner, V.Grubsky, D.S.Starodubov, E.Salik, and J.Feinberg, "Tunable compensation of the dispersion slope mismarch in dispersion manraged systems using a sampled nonlinearly chirped FBG," *IEEE Photonic Technology Letters*, vol. 12, pp. 1417–1419, October 2000.

[235] Teraxion Inc., "TH-MTDC, Multi-channel Tunable Dispersion Compensator," *Downloaded 20-2-2003 from http://www.teraxion.com/en/pdf/products/TH-MTDC_092002.pdf.*

[236] Teraxion Networks, "The Yafo 10, Polarization Mode Dispersion Compensator 10 Gbit/sec," *Downloaded 20-2-2003 from http://www.yafonet.com/pages/pdf/Yafo10Datasheet.pdf.*

[237] G. P. Agrawal, *Fiber-Optic Communication Systems, Chapter 4: Optical receivers*. John Wiley and Sons, 2nd ed., 1997. ISBN: 0-471-17540-4.

[238] N.S.Bergano, F.W.Kerfoot, and C.R.Davidson, "Margin measurements in optical amplifier systems," *IEEE Photonic Technology Letters*, vol. 5, pp. 304–306, March 1993.

[239] P.S.Andre, J.L.Pinto, A.L.J.Teixeira, J. Rocha, T. Almeida, and M.Pousa, "Optical-signal-quality monitor for bit-error-ratio assesment in transparent DWDM networks based on asynchronous sampled amplitude hitograms," *Journal of Optical Networking*, vol. 1, pp. 118–128, March 2002.

[240] J. Seoane, "Clock recovery for 40 gb/s optical transmission systems," *Research Center COM, Master Science final thesis*, Novemeber 2000.

[241] L. K. Oxenløwe, *Optical signal processing with semiconductor components*. PhD thesis, Technical University of Denmark, Research Center COM, March 2002.

[242] K. S. Jepsen, *LD 140, High Speed Optical Signal Processing for High Capacity Optical Networks*. PhD thesis, Technical University of Denmark, Department of Electromagnetic Systems, February 1999.

[243] K. Rottwitt and A. J.Stentz, *Optical Fiber Telecommunications IV, Chapter 5: Raman amplification in lightwave communication systems*, vol. A. Academic Press, 2002, ISBN: 0-12-395173-9.

Appendix A

Analysis of multi span performance

In this Appendix we will cover the concept of Quality factor Q, and its measurement technique. Moreover, we develop an analytical solution for the evolution of Q in a multi span transmission system, which allows to estimate performance in the linear regime.

A.1 Quality factor and Bit Error Ratio

The Bit Error Rate (BER) is obtained by comparing the sampled value at the receiver with the expected value over a large amount of transmitted data. An error will occur if we detect a zero when expecting a one, $P_{1/0}$, or when we detect a one expecting a zero, $P_{0/1}$, see Figure A.1. If there is equal probability to receive ones and zeros the BER can be written as:

$$BER = \frac{1}{2} \cdot [P_{1/0} + P_{0/1}] \tag{A.1}$$

If we assume Gaussian distributions at a specific sampling time for the "ones", mean value μ_1 and standard deviation σ_1, and for the "zeros", mean value μ_0 and standard deviation σ_0, and a decision threshold, I_d we can write the BER [237] as

$$BER = \frac{1}{4} \cdot [erfc(\frac{\mu_1 - I_d}{\sigma_1\sqrt{2}}) + erfc(\frac{I_d - \mu_0}{\sigma_0\sqrt{2}})] \tag{A.2}$$

The quality factor Q refers to the optimum performance which requires the

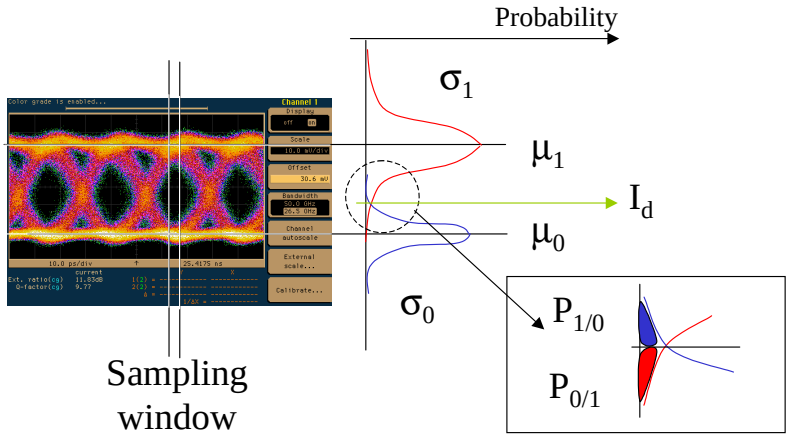

Figure A.1: Measured 40 Gb eye diagram and concepts required for the understanding of Q and BER

lowest BER, this occurs when

$$\frac{\mu_1 - I_d}{\sigma_1} = \frac{I_d - \mu_0}{\sigma_0} = Q \tag{A.3}$$

where Q is usually expressed as

$$Q = \frac{\mu_1 - \mu_0}{\sigma_0 + \sigma_1} \tag{A.4}$$

and is related to the BER for optimum setting of the decision threshold by

$$BER = \frac{1}{2} \cdot erfc(\frac{Q}{\sqrt{2}}) \approx \frac{exp(-Q^2/2)}{Q \cdot \sqrt{2 \cdot \pi}} \tag{A.5}$$

The approximation in Equation A.5 is reasonably accurate for $Q > 3$ [237]. A common way of expressing Q when working on system design is in decibels $Q(dB) = 20 \cdot Log(Q)$. Figure A.2 shows the relation between BER and Q (linear) following the approximation of A.5. The relation between Q (linear) and Q (dB) is shown as a reference for the reader.

A.2 Practical measurement of Q

When BER is very low, measuring times can be extremely long. An accurate method to evaluate the system performance for low BER is the decision-circuit

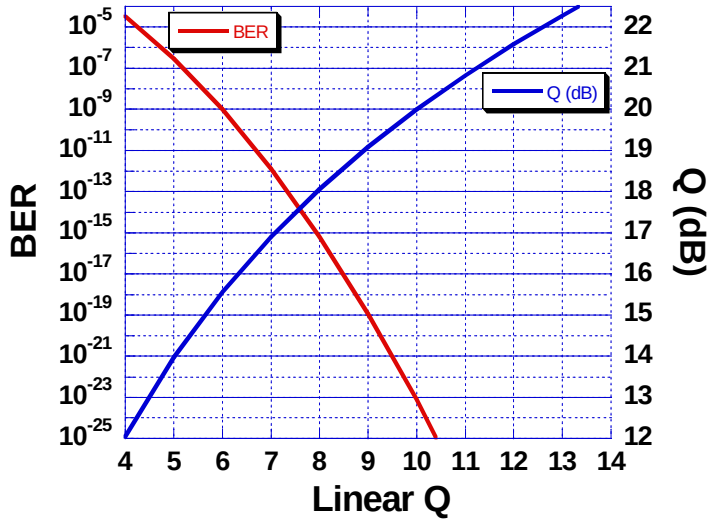

Figure A.2: Relation between the BER, Q (linear) and between Q and Q expressed in dB for reference.

method of Q measurement [238], which includes the effect of inter symbol interference originated in the system from EDFAs, dispersion or nonlinearities [47]. The method consists, see example in Figure A.3, on measuring the BER as a function of the decision threshold of the receiver. Two distinctive set of data appear which can be fitted to a polynomial function [238]. The intersection of these curve fits will indicate a best BER directly related to Q.

Other methods of measuring Q use direct measurement of the gaussian approximation of distribution functions of the eye diagram observed in an oscilloscope [239] however this will not include the performance of the receiver in the measurement. For example the direct measurement of the same signal shown in Figure A.3 in an oscilloscope was of 19.8 dB while Q measurements using the decision-circuit were reduced to 18.2 dB as they included for example an optical demultiplexer at the receiver to convert the measuring signal to 10 Gb/s.

A.3 Analytical investigation of Q in a multi span WDM system

In this section we present an analytical model for the investigation of the performance of a multi-span WDM system. The model includes transmitter and

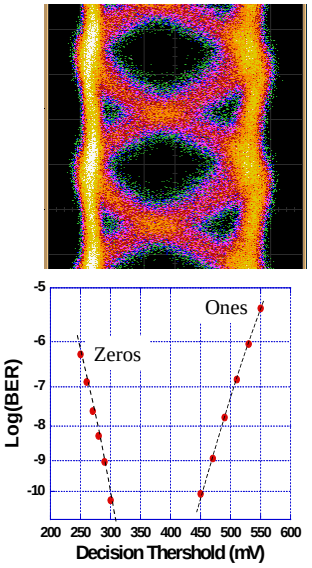

Figure A.3: Practical example of the measurement of Q for a 40 Gb/s NRZ signal.

receiver configurations for NRZ and RZ modulation. The analysis is gradual and is divided into two subsections, the first one looks into a simple model based on fiber-amplifier sections, the second one includes a two stage amplifier with a dispersion compensation module placed in the middle section.

A.3.1 Evolution of Q in a fiber-amplifier simple chain

The analysis has its origins in Equation A.4 which can be written as a function of the variances in the photocurrent observed at the receiver, $\sigma^2(i_{noise1})$ and $\sigma^2(i_{noise1})$, the difference between the power for a one and a zero $(P_{sig1} - P_{sig0})$ and the responsivity of the photodiode, R_d as [224]

$$Q = \frac{R_d \cdot (P_{sig1} - P_{sig0})}{\sqrt{\sigma^2(i_{noise1})} + \sqrt{\sigma^2(i_{noise0})}} \tag{A.6}$$

We consider the spontaneous-signal beat noise, with variance $\sigma^2 i_{s-sp}$ and the thermal noise, variance $\sigma^2 i_{th}$ as dominant noise contributions of a chain of amplifiers where the signal-spontaneous beat noise only affects the receiver when there is a one and can be written as

$$\sigma^2 i_{s-sp} = \frac{2R_d^2 P_{sig1} P_{sp} B_e}{B_o} \tag{A.7}$$

where B_e is the electrical bandwidth of the receiver, B_o is the bandwidth of the optical signal reaching the receiver (it should have been filtered in order to discard the spontaneous-spontaneous beat noise contribution) and P_{sp} is the power of the spontaneous emission expressed as

$$P_{sp} = F \cdot (G-1) \cdot h \cdot v \cdot B_o \tag{A.8}$$

where F and G are the noise figure and the gain of the amplifiers respectively and $h \cdot v$ is the photon energy.

The thermal noise can be directly related to the sensitivity of the receiver, R_{sens} (average received power for a given BER or Q) if we consider that it is measured without any amplifiers and the noise contribution is dominated by the thermal noise. For example if we take the sensitivity to be -16 dBm for a 10 Gb/s PIN diode for a BER of 10^{-12} (a Q of 7) we can write from A.6

$$7 = Q = \frac{2 \cdot R_{sens}}{\sqrt{\sigma^2 i_{th}} + \sqrt{\sigma^2 i_{th}}} \tag{A.9}$$

the variance of the thermal noise can be written as a function of the Q measured for the receiver sensitivity described

$$\sigma^2 i_{th} = (\frac{R_{sens}}{7})^2 \tag{A.10}$$

The power difference between the power in the ones and zeros, $(P_{sig1} - P_{sig0})$, can be expressed as a function of the average power P_a, the extinction ratio R, the duty cycle of the signal DC and the photodiode responsivity R_d as

$$(P_{sig1} - P_{sig0}) = 2 \cdot (\frac{P_a \cdot R_d}{DC}) \cdot (\frac{R-1}{R}) \tag{A.11}$$

The duty cycle allows to include in the analysis an RZ signal with the desired pulse width, for an NRZ signal the duty cycle will be unity. We consider a 3dB electrical bandwidth of the receiver B_e related to the bit rate B_r by $B_e = 0.7 \cdot B_r$. In addition we consider the amplifier gain to be equal to the span loss.

With all these considerations and taking into account equations A.6 to A.10 we can write the evolution of the quality factor Q in dBs function of the number of spans N as

$$Q_{dB}(N) = 20 \cdot Log \left[\frac{2 \cdot (\frac{P_a \cdot R_d}{DC}) \cdot (\frac{R-1}{R})}{\sqrt{2N \cdot R_d^2 (FG-1) \cdot hv \cdot (\frac{2P_a}{DC}) \cdot B_e + (\frac{R_{sens}}{7})^2} + \sqrt{(\frac{R_{sens}}{7})^2}} \right] \tag{A.12}$$

where a linear accumulation of the spontaneous noise and no changes in the amplifier gain are supposed.

A.4 Evolution of Q in a repeatered system with 2 stage optical amplifiers

In this subsection we estimate the evolution of Q in a repeatered system where the optical amplifiers are designed to accommodate for a dispersion compensation module. The amplifier is usually designed in a two stage model with the gain of the first section limited to the level where optical non-linear effects will distort transmission in the dispersion compensation fiber. The total sum gain of both amplifiers compensates for the loss of the span and the dispersion compensation module. The analytical model is found by estimating the variance of the signal-spontaneous contribution of a chain of amplifiers-transmission spans as depicted in Figure A.4

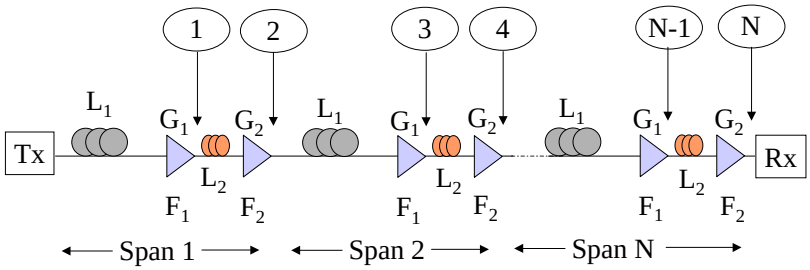

Figure A.4: Model followed in the analytical modelling of a repeatered system including 2 stage amplifier and dispersion compensation modules.

Following an iterative process; the total power at the output of the amplifiers, the signal-spontaneous noise contribution and the variance for points 1,2,3 and 4 in Figure A.4 are evaluated analytically, see Figure A.5.

Following the iterative process an expression for the variance of the signal-spontaneous emission after a certain number of spans N, can be obtained. This expression is a function of the amplifiers gain and noise figure, $G1$ and $F1$ for first section, $G2$ and $F2$ for second section, the attenuation of span, $L1$ and attenuation of the dispersion compensation module, $L2$

$$\sigma^2 i_{s-sp} = 2 \cdot R_d^2 \cdot P_a \left[N \cdot \left(\frac{G2}{L2} \cdot Psp_1 + Psp_2 \right) \right] \cdot \frac{B_e}{B_o} \tag{A.13}$$

where

$$Psp_1 = (F1 \cdot G1 - 1) \cdot h \cdot v \cdot B_o \tag{A.14}$$

and

$$Psp_2 = (F2 \cdot G2 - 1) \cdot h \cdot v \cdot B_o \tag{A.15}$$

Finally knowing the variance of the signal-spontaneous emission and following the approach described in Section A.3.1 we can reach an expression for Q as a function of the span number

$$Q_{dB}(N) = 20{\cdot}Log\left[\frac{2\cdot(\frac{P_a\cdot R_d}{DC})\cdot(\frac{R-1}{R})}{\sqrt{2N\cdot R_d^2\cdot(\frac{2P_a}{DC})\cdot(Psp_2+Psp_1\cdot\frac{G2}{L2})\cdot\frac{B_e}{B_o}+(\frac{R_{sens}}{7})^2}+\sqrt{(\frac{R_{sens}}{7})^2}}\right] \tag{A.16}$$

1

$$Pout_{\underline{1}} \equiv \left(\frac{G1}{L1}\right)\cdot Pa + Psp_{\underline{1}} \qquad Psp_{\underline{1}} \equiv (F1\cdot G1 - \underline{1})E\cdot Bo$$

$$Var\left(i_{s-sp}\right) \equiv \underline{2}Rd^{\underline{2}}\left(Pa\cdot\frac{G1}{L1}\right)\cdot Psp_{\underline{1}}\cdot\frac{Be}{Bo}$$

2

$$Pout_{\underline{2}} \equiv \left(\frac{G2}{L2}\right)\cdot Pout_{\underline{1}} + Psps_{\underline{2}} \qquad Psp_{\underline{2}} \equiv (F2G2 - \underline{1})E\cdot Bo$$

$$Pout_{\underline{2}} \equiv Pa + \left(\frac{G2}{L2}\right)\cdot Psp_{\underline{1}} + Psp_{\underline{2}}$$

$$var\left(i_{s-sp}\right) \equiv \underline{2}Rd^{\underline{2}}\cdot Pa\cdot\left[\left(\frac{G2}{L2}\right)\cdot Psp_{\underline{1}} + Psp_{\underline{2}}\right]\frac{Be}{Bo}$$

3

$$Pout_{\underline{3}} \equiv \left(\frac{G1}{L1}\right)\cdot Pout_{\underline{2}} + Psp_{\underline{1}}$$

$$Pout_{\underline{2}} \equiv \left(\frac{G1}{L1}\right)\cdot Pa + \underline{2}\cdot Psp_{\underline{1}} + \left(\frac{G1}{L1}\right)\cdot Psp_{\underline{2}}$$

$$var\left(i_{s-sp}\right) \equiv \underline{2}\cdot Rd^{\underline{2}}\left(Pa\cdot\frac{G1}{L1}\right)\cdot\left[\underline{2}\cdot Psp_{\underline{1}} + \left(\frac{G1}{L1}\right)\cdot Psp_{\underline{2}}\right]\cdot\frac{Be}{Bo}$$

4

$$Pout_{\underline{4}} \equiv \left(\frac{G2}{L2}\right)\cdot Pout_{\underline{3}} + Psps_{\underline{2}}$$

$$Pout_{\underline{4}} \equiv Pa + \underline{2}\left[\left(\frac{G2}{L2}\right)\cdot Psp_{\underline{1}} + Psp_{\underline{2}}\right]^{|}$$

$$var\left(i_{s-sp}\right) \equiv \underline{2}\cdot Rd^{\underline{2}}\cdot Pa\cdot\left[\underline{2}\cdot\left[\left(\frac{G2}{L2}\right)\cdot Psp_{\underline{1}} + Psp_{\underline{2}}\right]\right]\cdot\frac{Be}{Bo}$$

Figure A.5: Iteration for the two stage amplifier repeatered system. Presentation of iterative process for estimating the total power at the output of the amplifiers, the signal-spontaneous noise contribution and the variance of this noise contribution.

Appendix B

Simulation parameters

In this Appendix we present the main parameters used in the different results shown throughout the thesis obtained from simulations using the photonic simulation tool VPI Transmission Maker^{TM} [155]. Each set of parameters is represented in a figure containing the table of parameters used.

Parameter	Bit rate	
	10 Gb	40 Gb
Transmitter type	Mach-Zehnder	Mach-Zehnder
Chirp	No	No
Extinction ratio	12 dB	12 dB
Rise/fall time	1/4 Bit period	1/3 Bit period
Receiver type	PIN	PIN
Sensitivity BER 10^{-10}	-19 dBm	-12.48 dBm
Receiver Bessel filter	7 GHz	28 GHz
Simulation bits	1024	1024
PRBS	2^{10}-1	2^{10}-1
Non-linear coefficient	Off	Off

Figure B.1: Simulation parameters used in the simulation of penalty versus dispersion for 10 Gb/s and 40 Gb/s single wavelength transmission. Chapter 3.

Parameter	Modulation format		
	40 Gb Chirped NRZ	40 Gb Duobinary	40 Gb NRZ
Transmitter type	Mach-Zehnder	Mach-Zehnder	Mach-Zehnder
Chirp	α= –0.7 / +0.7	0	0
Extinction ratio	13 dB	13 dB	12 dB
Rise/fall time	1/4 Bit period	n.a	1/3 Bit period
Bessel filter (5^{th} order)	n.a	11.2 GHz	n.a
Receiver type	PIN/preamp.	PIN/preamp	PIN/preamp.
EDFA gain	25 dB		
Noise figure	5 dB		
Filter after EDFA	160 GHz		
Sensitivity BER 10^{-10} PIN receiver	-12.9 dBm	-11.6 dBm	-12.48 dBm
Sensitivity BER 10^{-10} Preamp. receiver	-30.3 dBm	-27.7 dBm	-29.5 dBm
Receiver Bessel filter	28 GHz		
Simulation bits	1024	256	1024
PRBS	2^{10}-1	2^{8}-1	2^{10}-1
Non-linear coefficient	Off		

Figure B.2: Simulation parameters used in the simulation of dispersion margins for chirped-NRZ and duobinary modulation comparing them with NRZ modulation. Chapter 3.

General Parameters	
PRBS order	**2^8-1 (Fixed starting point all simulations**
Number of bits	**256**
Number of simulations per case	**1000**
Bit rate	**40 Gb/s**
Others	**No non-linear effects & no dispersion in fibre**
Transmitter Parameters	
Wavelength	**1552.52 nm**
Mach-Zehnder extinction ratio	**30 dB**
Rise time	**8.33 ps**
Fiber parameters	
Length	**40 km**
Correlation length	**50 m**
Receiver Parameters	
PIN diode responsivity	**0.52 A/W**
Thermal noise	**24.1* 10^{-12} A/Hz$^{1/2}$**
Electrical filter	**7 GHz**
Sensitivity (no PMD) @ BER=10^{-12}	**-12 dBm**

Figure B.3: Simulation parameters used in the simulation of PMD in fiber throughout Chapter 4.

Parameter	Modulation format	
	40 Gb RZ	40 Gb NRZ
Transmitter type	Mach-Zehnder	Mach-Zehnder
Chirp	0	0
Extinction ratio	12 dB	12 dB
Rise/fall time	1/3 Bit period	1/3 Bit period
Pulse shpae	Gaussian	n.a
Pulsewidth (FWHM)	8 ps	n.a
Receiver type	PIN/preamp.	PIN/preamp.
EDFA gain	25 dB	
Noise figure	5 dB	
Filter after EDFA	160 GHz	
Sensitivity BER 10^{-10} PIN receiver	-14.7 dBm	-12.48 dBm
Sensitivity BER 10^{-10} Preamp. receiver	-31.5 dBm	-29.5 dBm
Receiver Bessel filter	28 GHz	
Simulation bits	1024	
PRBS	2^{10}-1	
Non-linear coefficient	Off	

Figure B.4: Simulation parameters used in the simulation of PMD in fiber for NRZ versus RZ in Chapter 4.

	40 km	80 km
Bits simulated	1024	
Samples per bit	32	
PRBS	2^{10}-1	
Transmitter type	Mach-Zehnder	
Chirp	No	
Extinction ratio	13 dB	
Rise-fall time	1/3 Bit period	
Dispersion SMF	17 ps/nm*km	
Attenuation SMF	0.2 dB/km	
SMF IL	11 dB	22 dB
EA SMF	80 μm^2	
EA DCF	20 μm^2	
Dispersion DCF	-100 ps/nm*km	
DCF IL	6 dB	8 dB
Attenuation DCF	0.5 dB/km	
Power into DCF	< -1 dBm	-4 dBm
Slope compensation	Yes	
EDFAs noise figure	5 dB	
Receiver type	EDFA preamplified	
Optical filter	160 GHz	
Receiver Bessel filter	28 GHz	
Receiver sensitivity BER 10^{-12}	-28.5	

Figure B.5: Simulation parameters used in the simulation of multi-span NRZ over standard-SMF in Chapter 5.

	40 km	80 km
Dispersion in NZDSF	4 ps/nm*km	
Attenuation in NZDSF	0.25dB/km	
NZDSF	11 dB	22 dB
EA NZDSF	62 μm^2	
EA DCF	15 μm^2	
Dispersion NZDSF	-144 ps/nm*km	
DCF IL	4 dB	5.5 dB
Attenuation DCF	0.55 dB/km	
Power into DCF	< -1 dBm	-4 dBm
Slope compensation	Yes	

Figure B.6: Simulation parameters used in the simulation of multi-span over NZDSF in Chapter 5.

Appendix C

Implementation and characterization of Tellabs 40 Gb/s test-bed

In this Appendix we will describe the 40 Gb/s test-bed implemented at the Tellabs laboratories in Denmark and which has been used in all the experimental characterizations performed except for the work done during the period at AT&T Research Labs. The set-up has been limited mainly by the budget available for this project and also by the quality of components and instruments available at the point in time were a choice had to be made on which implementation path would be followed. It is clear that the ideal test-bed should count with a 40 Gb/s test-set able to measure directly Bit Error Rate (BER) performance for Pseudo Random Binary Sequence (PRBS) signals at that bit rate. However back in March 2001 when we had to decide which system we should implement there was only one manufacturer of 40 Gb/s test sets available and unfortunately the price was way beyond the budget of this project. The choice which was followed was a combination of an Electrical Time Domain Multiplexing (ETDM) from four 10 Gb/s to create the 40 Gb/s signal for the transmitter (which allowed for Non Return to Zero (NRZ) transmission) and of Optical Time Domain Demultiplexing (OTDD) at the receiver of one of the 10 Gb/s channels from the 40 Gb/s signal. This approach allowed to use available 10 Gb/s test-set equipment reducing total cost considerably compared to the use of a 40 Gb test set. The decision also allows to complete the receiver part in the future with a full electrical demultiplexing unit, unfortunately this upgrade has not been possible within the time frame of the project. Section C.1 will describe the actual implementation of the test-bed while Section C.2 will provide a detailed characterization of its performance.

C.1 Implementation of Tellabs 40 Gb/s test-bed

A high level block diagram of the test-bed is shown in Figure C.1, as mentioned previously the transmitter is based on the multiplexing of four 10 Gb/s signals (channels A,B,C and D) in a SHF 4005 40 Gb/s electrical multiplexing, the four 10 Gb/s channels are provided by a splitter with delays of 2 ns, 4 ns and 6 ns from channels B, C and D to A respectively. These delays allow enough time mixing to provide a quality testing signal. However, the testing signal is not a true 40 Gb/s PRBS sequence and we will refer to the PRBS of the 10 Gb/s signals when describing the experimental work. Figure C.2 shows the main blocks of the 40 Gb/s ETDM transmitter together with the most important signals. In the electrical domain the 20 Gb/s AxC and BxD test outputs and 40 Gb/s Data. In the optical domain the 40 Gb/s optical signal at the output of the transmitter, the typical extinction ration obtained is in the order of 12 dB.

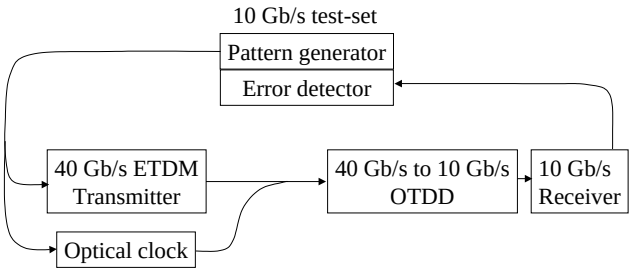

Figure C.1: Overview block diagram of 40 Gb/s test-bed.

At the point when the set-up was designed there were no clock recovery modules available for 40 Gb/s transmission which could be used both for NRZ and RZ transmission [1]. The implemented method for clock recovery uses the transmission of a 10 GHz reference clock through the same optical channel as the 40 Gb/s signal and its extraction at the receiver. The clock generator set-up is shown in Figure C.3, a typical WDM spectra is shown where the first channel is the transmitted clock. In the time domain the clock is send as a pulsed signal, this is used to improve the switching window of the OTDD. The principle of operation of the OTDD is shown in Figure C.4, the EA creates a time switching window allowing only one every four pulses to be observed, providing one of the 10 Gb/s original channels into the ETDM multiplexer

[1] At the Research Center COM and as a result of the work within the Master Thesis project "Clock recovery for 40 Gb/s optical transmission systems" [240] a clock recovery is available now for use with RZ transmission

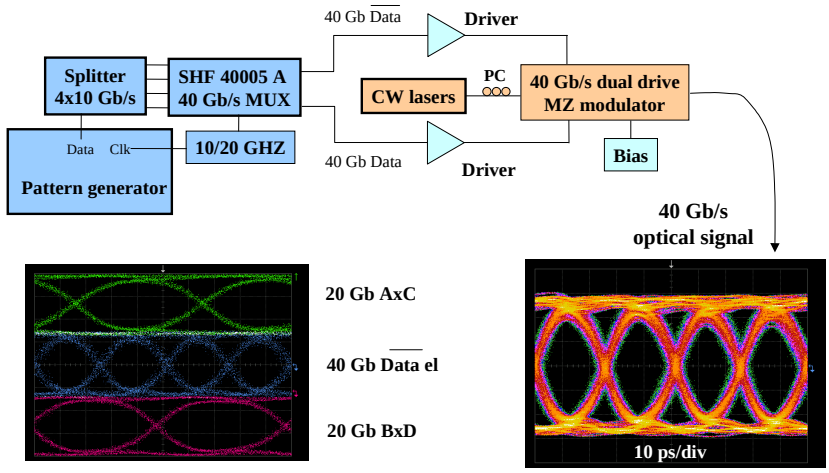

Figure C.2: Experimental set-up of 40 Gb/s ETDM transmitter. Example of main electrical signals and final optical 40 Gb/s output by means of eye diagrams.

of the transmitter. The signal which drives the EA is directly obtained from the transmitted clock, when using a pulsed clock we could obtain a significant reduction of the switching window. The effect of the pulsed clock is such that when driving the Electro Absorption (EA) modulator with a sinusoidal clock we obtained an error floor at 10^{-6} which was reduced to error free using the pulsed driving signal. The pulsed clock requires that the photodiode and the amplifier placed before the EA have a broad bandwidth and are able to amplify correctly a short pulsed signal. Typical switching windows obtained using this technique are in the order of 20 ps. The optical transmitted clock is used both for the switching window of the EA modulator and for the error detector.

A main limitation of the OTDD technique is the attenuation induced by the EA modulator, which needs to be compensated by the use of optical amplifiers. The first EA modulator used in the test-bed had an insertion loss higher than 18 dB. In later versions of the set-up this parameter has been reduced down to 12 dB improving the receiver performance.

Finally the 10 Gb/s RZ signal obtained at the output of the EA modulator passes through a 10 Gb/s receiver, see Figure C.5, consisting of an automatic controlled filter and attenuator followed by electrical amplifiers and filters. The final amplifier is a limiting amplifier which reduces the need for threshold tuning at the error detector of the 10 Gb/s test-set. Figure C.6 shows a component based set-up for the receiver, it includes four signal monitoring points which are inputs to an optical switch. The output of this switch is connected to an

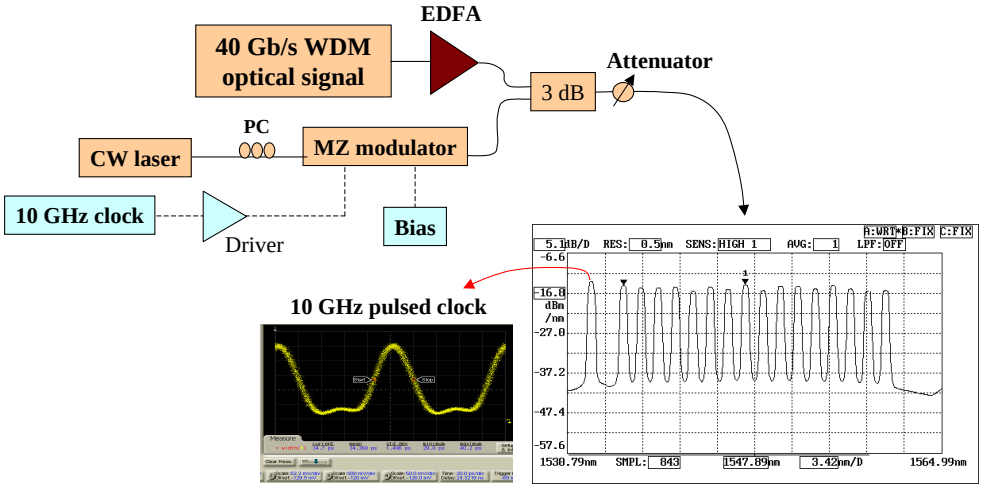

Figure C.3: Experimental set-up of pulsed clock generation in Tellabs 40 Gb/s test-bed. A typical WDM spectrum is shown with the first channel as the clock. A typical trace for the clock signal is also shown as a reference.

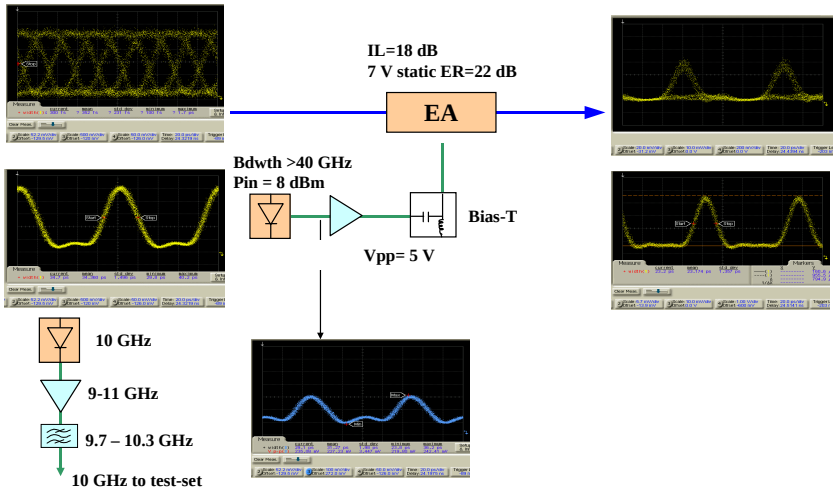

Figure C.4: Operation principle of the Optical Time Domain Demultiplexing (OTDD) technique. Short pulses are used as the driving signal for the Electro Absorption (EA) modulator reducing considerably the optical switching window. The pulsed signal is used also to provide the clock to the 10 Gb/s error detector.

oscilloscope, a power meter and an OSA. Monitoring these four signals allows to

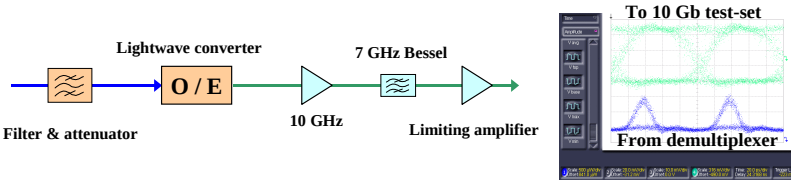

Figure C.5: Experimental set-up for the 10 Gb/s receiver used in Tellabs 40 Gb/s test-bed.

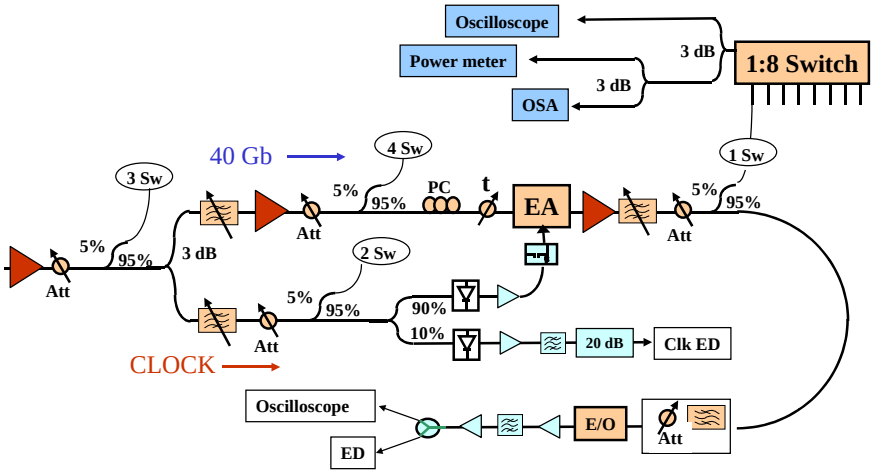

Figure C.6: Component set-up used in the receiver implementation at the Tellabs 40 Gb/s Test-bed.

set the OTDD receiver at optimum performance without the need to disconnect any optical fibers.

Figure C.7 shows a picture of the test-bed. It has been implemented in a single rack and has been used for over a year in a series of different experiments described throughout this thesis.

C.2 Performance of Tellabs 40 Gb/s test-bed

Initially the performance was evaluated comparing the 40 Gb/s performance to a 10 Gb/s back-to-back system were no ETDM multiplexing or OTDM demultiplexer were included. For the 100 Gb/s system we used the same optical transmitter as for 40 Gb/s, driven now by a 10 Gb/s signal directly from the

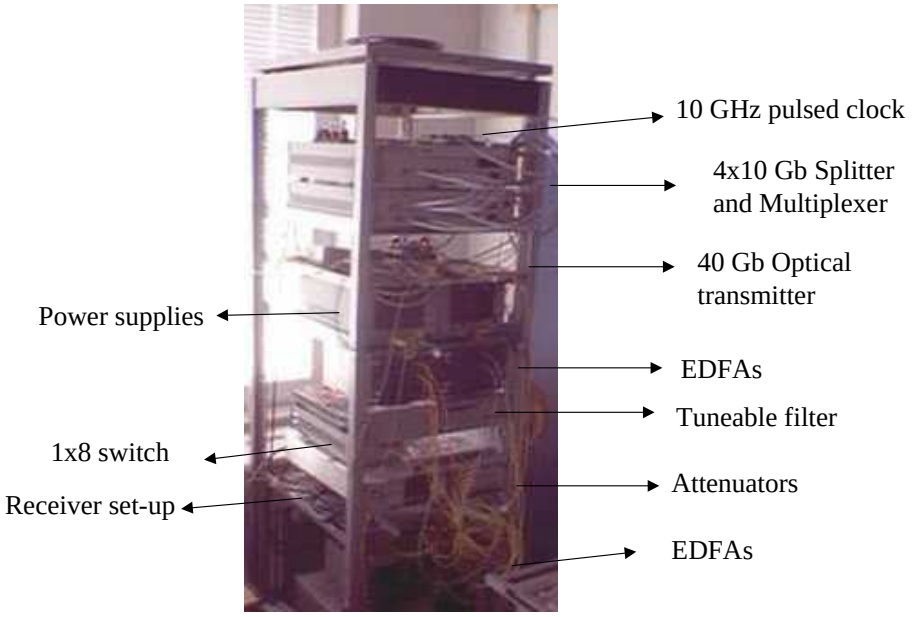

Figure C.7: Picture of the Tellabs 40 Gb/s test-bed indicating where the different blocks are physically situated in the rack.

test-set, and the same 10 Gb/s receiver set-up. The BER characterization comparison is shown in Figure C.8. In the order of 1 dB penalty is observed comparing both curves at a BER of 10^{-10} and no signs of error floor were observed allowing for stable measurements down to 10^{-12} BER ratios.

The performance of the test-bed has been also evaluated as a function of the length of the 10 Gb/s PRBS sequence used as input to the ETDM multiplexer at the transmitter. We can observe close to a 1dB difference in receiver sensitivity (measured for a BER of 10^{-10} from a $2^7 - 1$ to a $2^{31} - 1$ PRBS sequences, results are shown in Table C.1.

10 Gb/s PRBS order	Sensitivity (dBm) (BER 10^{-10})
31	-15.8
15	-16.42
7	-16.92

Table C.1: Sensitivity dependence of Tellabs test-bed on the 10 Gb/s PRBS sequence length.

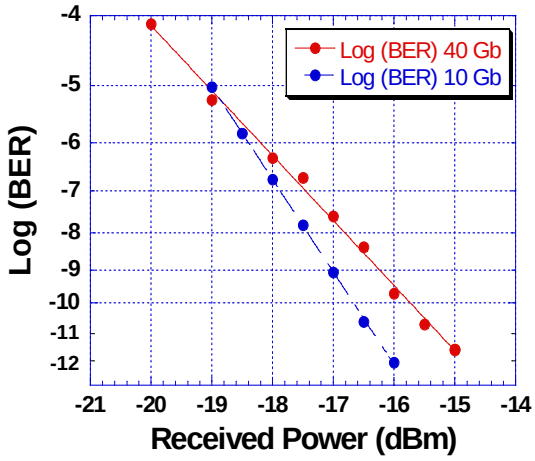

Figure C.8: Characterization of Tellabs 40 Gb/s test-bed performance. The BER obtained directly from a 10 Gb/s NRZ signal with no Optical Time Domain Multiplexing (OTDD) using the same 10 Gb/s receiver is compared to the performance of a 40 Gb/s NRZ signal.

Furthermore, the sensitivity penalty has been also evaluated in a 40 Gb/s back-to-back case for the four 10 GB/s time channels which form the 40 Gb/s signal. The different channels can be chosen by tuning an optical time delay at the receiver. The results for the four time channels are presented in Table C.2, a sensitivity difference of 0.8 dB can be observed between the best and worse channel.

Channel	Sensitivity (dBm)(BER 10^{-10})
A	-16.06
B	-15.24
C	-15.27
D	-15.86

Table C.2: Sensitivity dependence of Tellabs test-bed on the 10 Gb/s time domain channel demultiplexed.

The final characterization described in this section is the wavelength dependence of the test-bed performance. Unfortunately this is directly dependent on the EA modulator used as these are inherently wavelength dependent [241]. As an example Figure C.9 shows the static characterization (extinction ratio and insertion loss) of an EA used at the receiver and the penalty in sensitivity

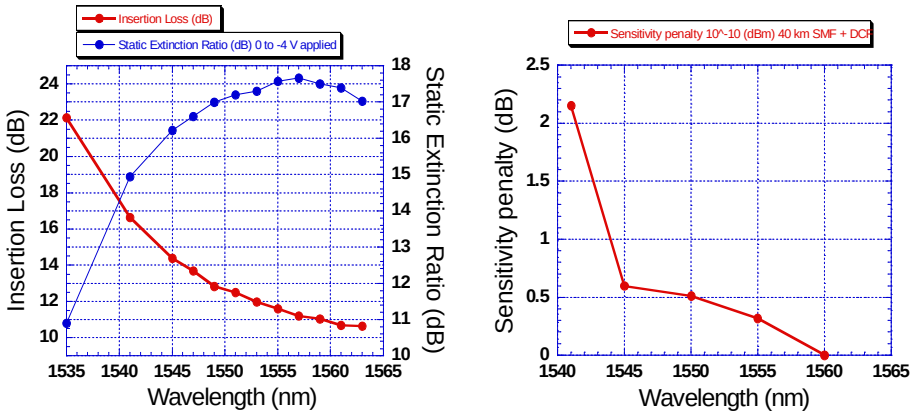

Figure C.9: Characterization of Tellabs 40 Gb/s test-bed as a function of wavelength. The static performance of the EA is provided as a function of wavelength.

(BER of 10^{-10}) observed as a function of wavelength.

It is clearly observed that there is a direct relation between EA characteristics and test-bed performance. This effect has reduced in some of the WDM experiments the ability to use the receiver to evaluate the performance of channels within the 1530 to 1545 nm range.

Appendix D

Effect of the use of OTDD in penalty measurements of NRZ signals

In this Appendix we analyze the discrepancy between simulated and experimental dispersion margins observed for NRZ signals and suggest an explanation by means of simulations. It is believed that there is a direct relation between the switching window created by the Electro Absorption (EA) modulator in the Optical Time Domain Demultiplexing (OTDD) process and the observed penalty, which differs from that expected for Non Return to Zero (NRZ) if it would be analyzed by a direct 40 Gb/s receiver. The set-up used in simulations is shown in Figure D.1, the quality of the original NRZ signal is evaluated both by a 40 Gb/s Electrical Time Domain Multiplexing (ETDM) based receiver and a 40 Gb/s OTDD based receiver (with a 10 Gb/s ETDM based receiver after optical demultiplexing). The switching window of the EA modulator based OTDD is controlled by changing the electrical pulsed signal applied (Gaussian shaped). We consider two cases, the first one where an electrical driving signal of 30 ps produces an optical 20 ps switching window (similar to the experimental set-up). In the second case the switching window is reduced to 13 ps by changing the electrical driving pulses to 20 ps. The EA transfer function used in the simulations corresponds to a measured sample and used in the experimental set-up.

Moreover, we use the same model to analyze the sensitivity penalty observed using OTDD in the measurement of the performance of modulators with low rise-fall times and the penalty induced by first order Polarization mode dispersion (PMD).

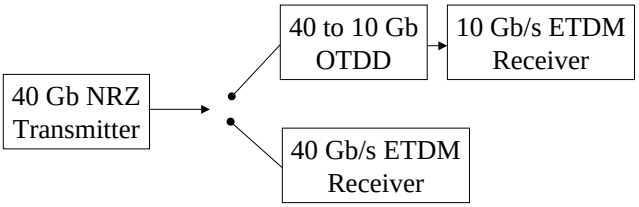

Figure D.1: Overview block diagram of simulation set-up for analysis of OTDD influence on penalty measurements.

D.1 Influence of OTDD on the measured dispersion margins for NRZ

In Figure D.2 we can observe the optical and electrical eye diagrams for different values of dispersion and for the three cases described previously, 40 Gb/s ETDM receiver, 20 ps and 13 ps switching windows. Electrical filtering is always 70% of the bit period, 28 GHz for 40 Gb/s receiver and 7 GHz for the 10 Gb/s receiver.

For the back to back case and looking at the eye diagrams we can observe for the OTDD receiver case the influence of the not perfect demultiplexer suppression ratio which allows for crosstalk from neighboring channels to be present in the decision at the receiver, this effect has been previously analyzed for RZ signals and OTDD based receiver in [242]. As a reference a 0.6 dB sensitivity penalty is observed when comparing the 20 ps to the 13 ps switching window case. When we include dispersion the crosstalk effect is enhanced due to the broadening of the pulses and the level of crosstalk observed is directly dependent on the switching window. For a dispersion of 50 ps/nm for example we observe eye openings of 7.5 dB, 7.5 dB and 5.8 dB for the direct ETDM, 13 ps and 20 ps switching window cases respectively. In order to evaluate the performance difference, sensitivity penalty (for BER 10^{-10}) has been evaluated for the three cases as a function of dispersion. The penalty is calculated for each case related to the equivalent back-to-back situation as in the experimental work. The results are shown in Figure D.3. They show a clear reduction of the dispersion margin when measured with an OTDD receiver and how this influence is directly related to the switching window of the receiver configuration. Following these results we would expect the 1 dB dispersion margin to be measured for a dispersion $\pm 40 ps/nm$ when using OTDD receivers rather than the margin of $\pm 70 ps/nm$ observed in the simulations and confirmed experimentally in Section 3.1.2 for using an ETDM receiver.

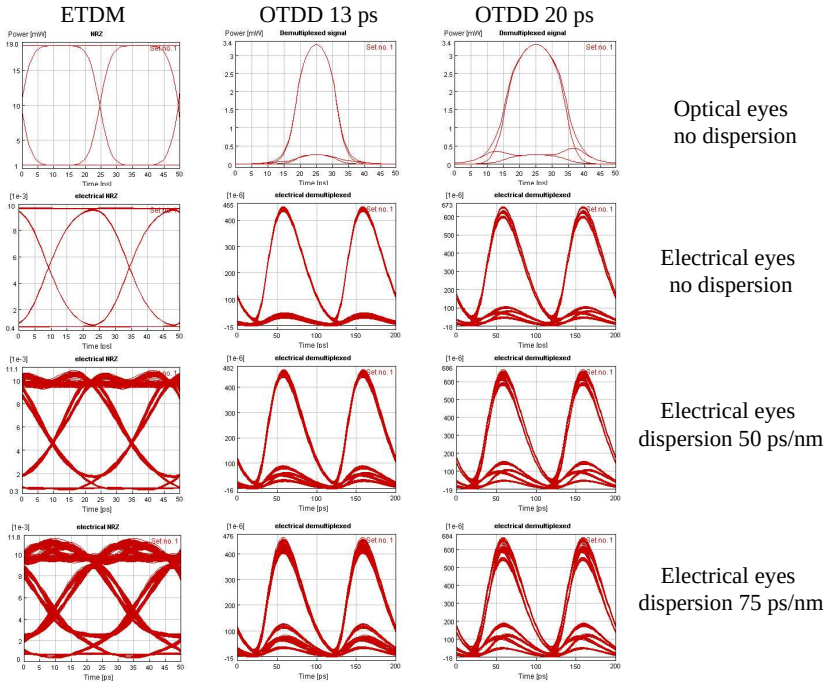

Figure D.2: Comparison of eye diagrams observed in the simulated dispersion margin measurements measured with ETDM versus OTDD receivers. Please observe that different time scales are used.

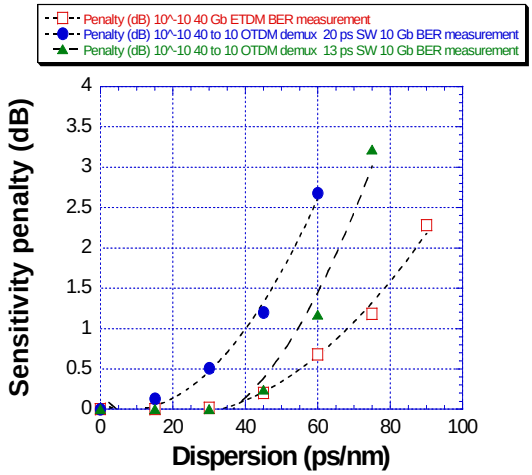

Figure D.3: Sensitivity penalty curves of performance analysis under the effect of dispersion when measured with ETDM versus OTDD receivers.

D.2 Influence of OTDD on the characterization of modulators

It has been observed in several occasions that we could not measure BER performance using Tellabs test-bed when using EA modulators as transmitters. In this Section we analyze the influence of an OTDD based receiver on the sensitivity penalty measured for a $LiNbO_3$ with 11 dB of ER as a function of the rise/fall of the electrical driving signal applied to the modulator (full V_π modulation). Optical eye diagrams, see Figure D.4 show clearly the rising crosstalk for slower rise-fall times in the modulator, which affects the performance strongly in the case of OTDD receiver set-up.

We compare the sensitivity penalty curves (reference back-to-back situation for each case) for 40 Gb/s ETDM and the OTDD based receiver with a 20 ps switching window, see Figure D.5. We can observe a steeper penalty curve for the OTDD demultiplexing. This is believed to be the reason why we could not measure BER when characterizing some EA samples in the Tellabs test-bed.

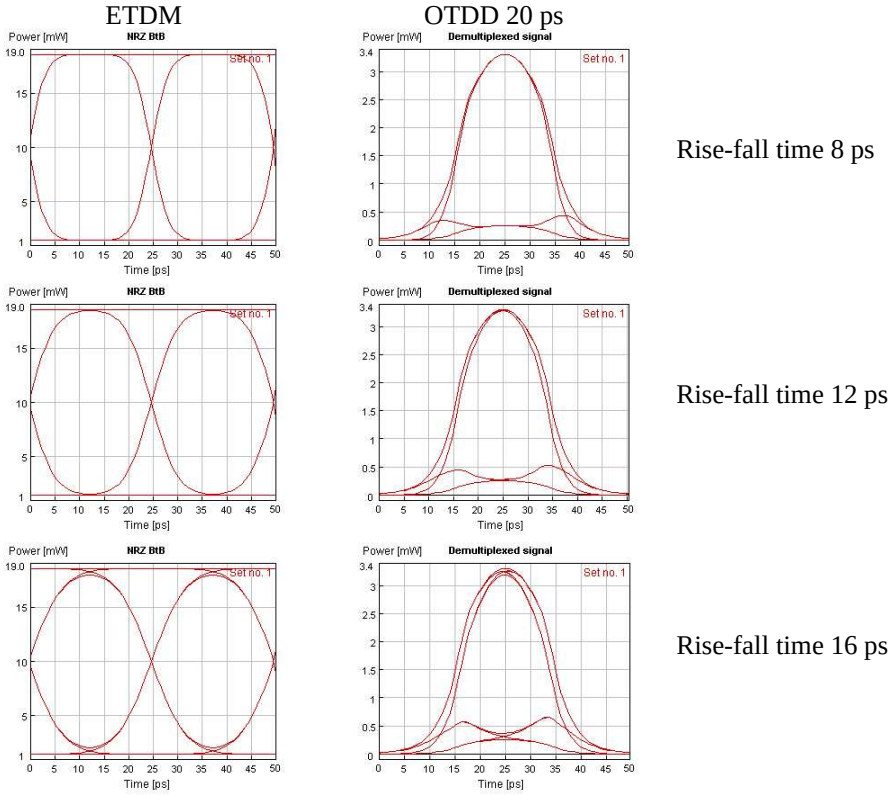

Figure D.4: Comparison of eye diagrams observed for different electrical rise/fall times measured with ETDM versus OTDD receivers.

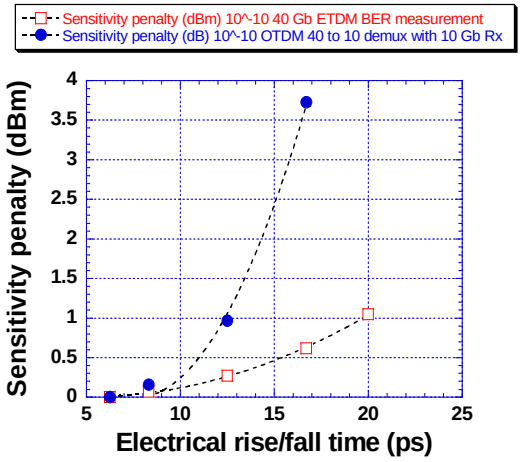

Figure D.5: Sensitivity penalty curves of performance analysis as a function of rise/fall time when measured with ETDM versus OTDD receivers.

D.3 Influence of OTDD on the measurement of 1st order PMD penalties

A similar effect has been as described in the previous sections has been observed in the measurement of penalties induced by first order PMD. We have analyzed the effect of OTDD by applying the modelled OTDD receiver and comparing the sensitivity penalty (PIN receiver) to those obtained with and ETDM. In Figure D.6 we can observe the significant difference observed between the penalties as a function of first order PMD generated with a simple polarization splitter-optical delay set-up.

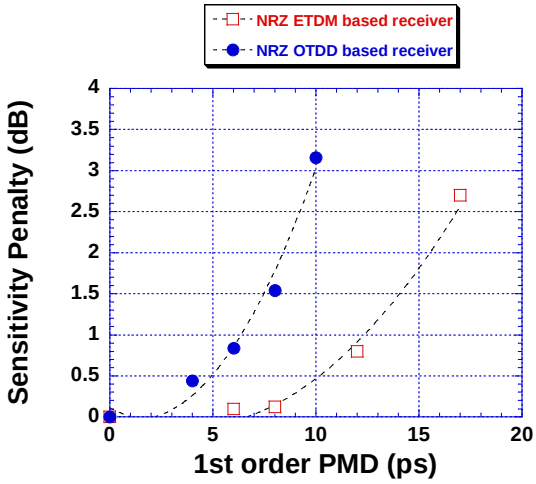

Figure D.6: Sensitivity penalty curves of performance analysis as a function of first order PMD when measured with ETDM versus OTDD receivers.

Appendix E

Effective noise figure of a Raman amplifier

In this Appendix we will review the concept of effective noise figure of a Raman amplifier. A schematic of the model followed is shown in Figure E.1. The main idea is to find an equivalent EDFA with gain equal to the On-Off gain of the Raman amplifier and with a noise figure which introduces the same ASE level as the Raman ampllifier. Using this model it is possible to define an effective noise figure of the Raman amplifier by measuring the ASE power at the output of the Raman amplifier and the On-Off gain.
The gain relations can be written as

$$G_{AC} = G_{AB} \cdot G_{BC} \tag{E.1}$$

The noise figure of the link considering the lumped EDFA model can be written as

$$F_{AC} = F_{AB} + \frac{F_{BC} - 1}{G_{AB}} \tag{E.2}$$

The noise figure of a passive fiber includes the degradation of the signal to noise ration due to shot noise

$$F_{AB} = \frac{1}{e^{-\alpha \cdot L}} \tag{E.3}$$

by including E.3 in E.2 and considering that the negative gain observed in the fiber is directly the loss we rewrite E.2 as

$$F_{AC} = \frac{1}{e^{-\alpha \cdot L}} + \frac{F_{BC} - 1}{e^{-\alpha \cdot L}} = \frac{F_{BC}}{e^{-\alpha \cdot L}} = \frac{F_{BC}}{G_{AB}} \tag{E.4}$$

If we now consider the segment AC as a black box model with a gain, G_{AC}, a noise figure, F_{AC} and an observed ASE level at point C of E.1 we can write

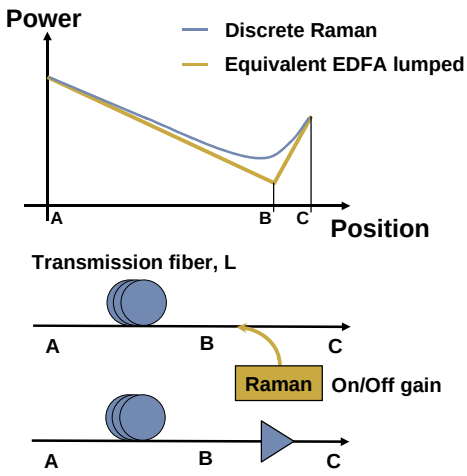

Figure E.1: Schematic of power levels through a transmission link when using a distributed Raman amplifier and its equivalent EDFA model from which we define the effective noise figure.

this observed ASE as [243]

$$P_{ASE_C} = (G_{AC} \cdot F_{AC} - 1) \cdot h\nu B_o \tag{E.5}$$

By substituting E.1 and E.4 in E.5 we obtain

$$P_{ASE_C} = (G_{AB} \cdot G_{BC} \cdot \frac{F_{BC}}{G_{AB}} - 1) \cdot h\nu B_o \tag{E.6}$$

which solved for the noise figure of the EDFA, F_{BC} to which we refer as effective noise figure, provides the final expression

$$F_{BC} = \frac{1}{G_{BC}} \cdot (\frac{P_{ASE_C}}{h\nu B_o} + 1) \tag{E.7}$$

where G_{BC} is the On-Off gain of the Raman amplifier.

Appendix F

Additional results

In this Appendix we include results from the multi-span simulations not included in Chapter 5.

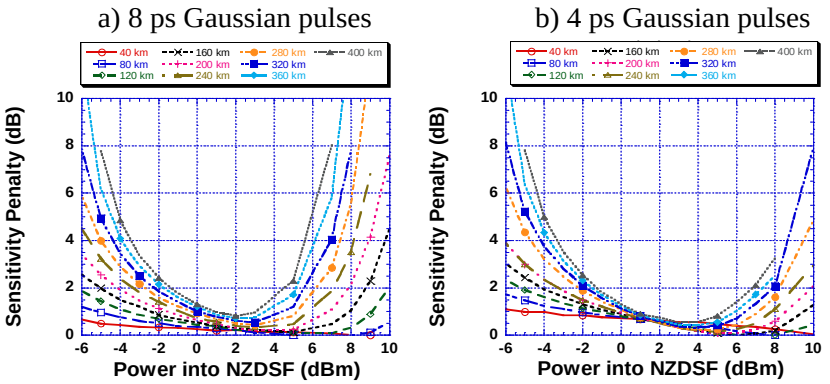

Figure F.1: Simulated performance for the multi-span transmission over NZDSF using RZ transmitter in 40 km spans. a) 8 ps pulses, b) 4 ps pulses.

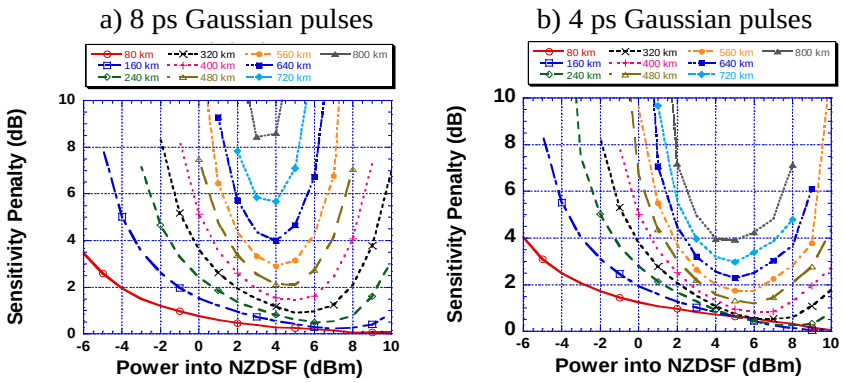

Figure F.2: Simulated performance for the multi-span transmission over NZDSF using RZ transmitter in 80 km spans. a) 8 ps pulses, b) 4 ps pulses.

List of publications

Articles in refereed journals and refereed international monographs

1. A.T. Clausen, K.S. Jepsen, H.N. Poulsen, A. Buxens, B. Mikkelsen and K.E. Stubkjaer, "Interface for 10 Gbit/s bit synchronization, format and wavelength conversion with 3R regeneration capabilities", Electronic Letters, Vol. 34, No. 16, August 1998.

2. K.S. Jepsen, A. Buxens, A.T. Clausen, H.N. Poulsen, B. Mikkelsen and K. E. Stubkjaer, "20 Gbit/s optical 3R regeneration using polarization-independent monolithically integrated Michelson interferometer", Electronic Letters, Vol 34, No. 5, march 1998.

3. Stubkjaer, K.E. Kloch, A.; Bukhave Hansen, P.; Poulsen, H.N.; Wolfson, D.; Stockholm Jepsen, K.; Clausen, A.T.; Limal, E.; Buxens, A., IEICE Transactions on communications , "Wavelength converter technology", Vol.E82-B Issue.2, pp. 338-48, 1999.

4. C. Peucheret, I. Munoz, A. Buxens, F. Liu and S.N. Knudsen, "L-band transmission over 1000 km using standard and dispersion-compensating fibres in pre-compensation scheme optimized at 1550 nm", Electronics Letters, 1999, vol. 35, no. 20, pp. 1759-1761.

5. S. Bischoff, A. Buxens, H. N. Poulsen, A. T. Clausen and J. Mørk, "Bidirectional four-wave mixing in semiconductor optical amplifiers: theory and experiment", Journal of Lightwave Technology, 1999, vol. 17, no. 9, pp. 1617-1625.

6. S.Bouchoule, R. Lefevre, E. Legros, F. Devaux, H. Melchior, M. Dülk, R. Hess, E. Lach, H. Blow, G. Veith, J. R. Burie, J. F. Cadiou, F. Brillouet, J. Hourany, D. Hoffman, B. Sartorius, K. S. Jepsen, A. T. Clausen, A. Buxens, H. N. Poulsen, K. E. Stubkjaer, H. Burkhard, H.-J. Schll, D. Nesset, A. E. Kelly, D. Marcenac, R. V. Penty and I. H. White, "Photonic

technologies for ultra-high-speed information highways, I. 40 Gbit/s TDM components and subsystems", (Invited paper), Optical Fiber Technology, 1999, vol. 5, no. 3, pp. 275-300.

7. X. Zheng, F. Liu, A. Clausen and A. Buxens, "High Performance Wavelength Converter Based on Semiconductor Optical Amplifier and Mach-Zehnder Interferometer Optical add/drop Multiplexer", in 10th Optical Amplifiers and Their Applications, OSA Technical Digest (Optical Socity Of America, Wasshington DC, 1999), p132-134.

8. K. Stubkjaer, A. Kloch, P.B. Hansen, H.N. Poulsen, D. Wolfson, K.S. Jepsen, A.T. Clausen, E. Limal, A.Buxens", Wavelength Converter Technology", IEICE Transactions on Electronics, Joint Special Issue on Photonics in Switching: Systems and Devices - INVITED PAPER - Photonic WDM Devices -, Vol.82 Issue.2, pp. 338-348, 1999.

9. A. Buxens, A. T. Clausen, H. N. Poulsen, P. Jeppesen, "10 Gb/s bidirectional gating in semiconductor optical amplifiers for optical cross-connects exploiting network connection-symmetry", Trends in Optics and Photonics Series (TOPS), Photonics in Switching, Volume 32, pp. 127-131.

10. J. Yu, A. Buxens, A. Clausen and P. Jeppesen, "16x10 Gb/s WDM bidirectional gating in a semiconductor optical amplifier for oftical cross-connects exploiting network connection symmetry", IEEE Photonic Technology Letters, Vol. 12, No. 6, pp. 702-704, June 2000.

11. F. Liu, X. Zheng, R. J. S. Pedersen, P. Varming, A. Buxens, Y. Qian and P. Jeppesen, "Cost-effective wavelength selectable light source using DFB fibre laser array", Electronics Letters, 2000, vol. 36, no. 7, pp. 620-621.

12. St. Fischer, M. Dülk, E. Gamper, W. Vogt, W. Hunziker, E. Gini, H. Melchior, A. Buxens, H. N. Poulsen and A. T. Clausen, "All optical regenerative OTDM add-drop multiplexing at 40 Gbit/s using monolithic InP Mach-Zehnder interferometer", IEEE Photonics Technology Letters, 2000, vol. 12, no. 3, pp. 335-337.

13. M. Dülk, St. Fischer, E. Gamper, W. Vogt, E. Gini, H. Melchior, W. Hunziker, H. N. Poulsen, A. T. Clausen, A. Buxens and P. Jeppesen, "Efficient regenerative wavelength conversion at 10 Gbit/s over C- and L-band (80 nm span) using a Mach-Zehnder interferometer with monolithically integrated semiconductor optical amplifiers", Electronics Letters, 2000, vol. 36, no. 3, pp. 241-243.

14. A. Buxens, H. N. Poulsen, A. T. Clausen and P. Jeppesen, "All-optical OTDM to WDM signal-format translation and OTDM add-drop functionality using bidirectional four wave mixing in semiconductor optical amplifier", Electronics Letters, 2000, vol. 36, no. 2, pp. 156-158.

15. A. Buxens, H.N. Poulsen, A.T. Clausen and P. Jeppesen, "Gain flattened L-band EDFA based on upgraded C-band EDFA using forward ASE pumping in an EDF section", Electronic Letters, Vol. 36, No. 9, April 2000, pp.821-823.

16. J.M. Gene, R. Nieves, A. Buxens, C. Peucheret, J. Prat and P. Jeppesen, "Reduced driving voltage optical duobinary transmitter and its impact on transmission performance over standard single-mode fiber", IEEE Photonic Technology Letters, Vol. 14, No. 6, June 2002, pp. 843-845

17. S. Bischoff, A. Buxens, St. Fischer, M. Dülk, A. T. Clausen, H. N. Poulsen and J. Mrk, "Comparison of all-optical co- and counter-propagating high-speed signal processing in SOA-based Mach-Zehnder interferometers", Optical and Quantum Electronics, 2001, vol. 33, pp. 907-926

18. M. Dülk, St. Fischer, M. Bitter, M. Caraccia, W. Vogt, E. Gini, H. Melchior, W. Hunziker, A. Buxens, H. N. Poulsen and A. T. Clausen, "Ultrafast all-optical demultiplexer based on monolithic Mach-Zehnder interferometer with integrated semiconductor optical amplifiers", Optical and Quantum Electronics, 2001, vol. 33, pp. 899-906.

Conference contributions

1. A.T. Clausen, A. Buxens, K. S: Jepsen, H. N. Poulsen, K. E. Stubkjer, "Polarisation-independent 3R regenerator at 20 Gbit/s using a monolithically integrated semiconductor optical amplifier", in Technical Digest OECC98, pp 12, Chiba, Japan, July 1998.

2. A. Buxens, G. Soule, J. H. Povlsen, R. J. Pedersen, B. Mikkelsen, J. Farre, K. E. Stubkjaer, "Influence of optical amplification on Optical Time Domain Reflectometry", in Technical Digest OECC98, pp 72, Chiba, Japan, July 1998.

3. K. E. Stubkjr, S. L. Danielsen, A. Kloch, P. B. Hansen, K. S. Jepsen, H. N. Poulsen, D. Wolfson, A. T. Clausen, E. Limal, A. Buxens, "All-Optical Wavelength Converters", In Technical Digest OECC98, pp 464, Chiba, Japan, July 1998.

4. H. N. Poulsen, K. S. Jepsen, A. T. Clausen, A. Buxens, K. E. Stubkjaer, R. Hess, M. Dülk, H. Melchior, "Fast Optical Signal Processing in High Bit Rate OTDM Systems", in Proc. of LEOS'98, vol. 1, Invited paper, pp. 67-68, Orlando, Florida, December 1998,

5. A. Buxens, A.T. Clausen, H. N. Poulsen, K. S. Jepsen , K. E. Stubkjaer, C. Bornholdt, O. Brox, B. Sartorius,"40 to 10 Gbit/s demultiplexing using a self-pulsating DFB laser for clock recovery", in Proceedings of ECOC98, Vol. 1, pp. 507-508, Madrid, Spain, September 1998

6. K.S. Jepsen, H. N. Poulsen, A. T. Clausen, A. Buxens, K. E. Stubkjr, "Investigation of cascadability of add-drop multiplexers in OTDM systems", in Proceedings of ECOC98, Vol. 1, pp. 619-620, Madrid, Spain, September 1998

7. A. Buxens, H. N. Poulsen, A.T. Clausen, K. S. Jepsen , K. E. Stubkjaer, "New Bi-directional Mid Span Spectral Inversion using Bi-directional Four Wave Mixing in Semiconductor Optical Amplifiers", in Proceedings of ECOC98, post deadline paper,Vol. 3, pp 97-98, Madrid, Spain, September 1998.

8. S. Bischoff, A. Buxens, H. N. Poulsen, A. T. Clausen, J. Mrk, "Bi-directional four wave mixing in semiconductor amplifiers for mid span spectral inversion: Theory and experiments", CLEO99. Baltimore, USA, Paper CtuW3, May 1999.

9. X. Zheng, F. Liu, A. Clausen and A. Buxens, "High performance wavelength converter based on semiconductor optical amplifier and Mach-Zehnder interferometer optical add/drop multiplexer", in Technical Digest of Optical Amplifiers and their Applications, OAA'99, Nara, Japan, pp. 132-134.

10. A. Buxens, A. T. Clausen, H. N. Poulsen, P. Jeppesen, "10 Gb/s bi-directional gating in semiconductor optical amplifiers for optical cross-connects exploiting network connection-symmetry",in Technical Digest of Photonic in Switching99, Santa Barbara, California, pp. 85-87, July 1999.

11. A. T. Clausen, A. Buxens, H. N. Poulsen, L. Oxenloewe and P. Jeppesen, "Polarisation independent bi-directional four wave mixing for mid span spectral inversion", in Proceedings of ECOC'99, Nice, France, vol. 1, pp. 146-147, September 1999.

12. H. N. Poulsen, P. Varming, A. Buxens, A. T. Clausen, I. Munoz, P. Jeppesen, C. V. Poulsen, J. E. Pedersen and L. Eskildsen, "1607 nm DFB

fibre laser for optical communications in the L-band", in Proceedings of ECOC'99, Nice, France, vol. 1, pp. 70-71, September 1999.

13. A. Buxens, H. N. Poulsen, A. T. Clausen, K. S. Jepsen and P. Jeppesen, "Simultaneous all-optical add-drop multiplexing functionality using bi-directional four wave mixing in a semiconductor optical amplifier", in Proceedings of ECOC'99, Nice, France, vol. 1, pp. 248-249, September 1999.

14. St. Fischer, M. Dülk, M. Bitter, M. Caraccia, W. Vogt, E. Gini, H. Melchior, W. Hunzkier, A. Buxens, H. N. Poulsen and A.T. Clausen, "Ultrafast all-optical demultiplexer based on monolithic Mach-Zehnder interferometer with integrated semiconductor optical amplifiers", in Proceedings of Optoelectronics and Communications Conference (OECC), Chiba, Japan, Paper 13C-3, July 2000.

15. H. N. Poulsen, A. Buxens, A.T. Clausen, P. Jeppesen, M. Dülk, St. Fischer, E. Gamper, W. Vogt, W. Hunziker, E. Gini and H. Melchior, "Wavelength conversion from C- to L- band at 10 Gbit/s including transmission over 80 km of SSMF", in Technical Digest of CLEO2000, paper CWI2, San Francisco, California, May 2000.

16. A. Buxens, H. N. Poulsen, A.T. Clausen, P. Jeppesen, M. Dülk, St. Fischer, E. Gamper, W. Vogt, W. Hunziker, E. Gini and H. Melchior, "All-optical regenerative OTDM add/drop multiplexing at 40 Gb/s using InP Mach Zehnder interferometer", in Technical Digest of CLEO2000, paper CWD3 (Invited Paper), San Francisco, California, May 2000.

17. M. Dülk, St. Fischer, M. Bitter, M. Caraccia, W. Vogt, E. Gini, H. Melchior, W. Hunzkier, A. Buxens, H. N. Poulsen and A.T. Clausen, "Efficient and robust regenerative all-optical wavelength converter for C- and L- band (80 nm span) and for data rates up to 40 Gb/s", in Technical Digest of CLEO2000, paper CtuG7, San Francisco, California, May 2000.

18. C. Peucheret, A. Buxens, T. Rasmussen, C. F. Pedersen and P. Jeppesen, "Cascadability of fibre Bragg gratings for narrow channel spacing systems using NRZ and duobinary modulation", in Proceedings OECC/IOOC 2001, paper TUA3, pp. 92-93, Sydney, Australia, July 2001.

19. A. Buxens, D. Olesen, L. Ellegård, M. Birk, M. Brodsky, N. Frigo and P. Jeppesen, "Detailed modeling and experimental investigation of 40 Gb/s multi-span transmission systems in standard SMF for NRZ and RZ modulation", in Proceedings European Conference on Optical Communication, ECOC'2002, paper P3.25, vol. 3, Copenhagen, Denmark, September 2002.

20. A. Buxens, T. Tokle, C. Peucheret and P. Jeppesen, "Influence of optical time domain demultiplexing in chromatic dispersion and PMD induced penalty measurements at 40 Gb/s", in Proceedings European Conference on Optical Communication, ECOC'2003, paper We 4.P.121, vol. 3, Rimini, Italy, September 2003.

21. B. Zsigri, C. Peucheret, A. Buxens and P. Jeppesen, "Performance comparison of optical singel side band generation techniques", in Proceedings European Conference on Optical Communication, ECOC'2003, paper We 3.5.3, vol. 3, Rimini, Italy, September 2003.

Workshop contributions

1. A. T. Clausen, A. Buxens, K. S. Jepsen, H. N. Poulsen, K. E. Stubkjaer,"3R regeneration at 20 Gbit/s using a monolithically integrated Semiconductor Optical Amplifier based Michelson Interferometer", in Proc. of The Rank Prize Funds, Mini-Symposium on Ultrafast Photonic Processing and Networks, Grasmere, Cumbria, April 1998.

2. K. E. Stubkjaer, K. S. Jepsen, A. T. Clausen, H. N. Poulsen, A. Buxens, S. L. Danielsen, P. B. Hansen, A. Kloch, D. Wolfson, "High-speed photonic processing", in Proc. of The Rank Prize Funds, Mini-Symposium on Ultrafast Photonic Processing and Networks, Invited paper, Grasmere, Cumbria, April 1998.

3. S. Bischoff, A. Buxens, H.N. Poulsen, A.T. Clausen and J. Moerk, "Bidirectional four-wave mixing in semiconductor optical amplifiers", in Proc. of COST 267 Workshop, Rome, April. 1999.

4. H.N. Poulsen, A.T. Clausen, A. Buxens, L.Oxenløwe, A. Kloch, D. Wolfson, T. Fjelde and P. Jeppesen, "All-optical signal processing with semiconductor amplifiers", Workshop at OFC'2000, Baltimore, Maryland, March 2000.

5. A.Buxens, L. Ellegård, D. Olesen, "New modulation formats to be used in 40 Gb/s systems", Tellabs Current Practice Seminar 2001, Chicago, Illinois, Session two, June 2001.

6. A.Buxens, L. Ellegård, D. Olesen, "New modulation formats to be used in 40 Gb/s systems", Tellabs Current Practice Seminar 2001, Copenhagen, Denmark, Track A, September 2001.

7. A. Buxens, "40 Gb transmission systems", Invited presentation at the Danish Optical Society meeting, Ballerup, Denmark, February 2002.